Ice injected up to the tropical tropopause layer by deep convection

Iris-Amata Dion

THÈSE

En vue de l'obtention du

DOCTORAT DE L'UNIVERSITÉ DE TOULOUSE

Délivré par : *l'Université Toulouse 3 Paul Sabatier (UT3 Paul Sabatier)*

Présentée et soutenue le *25 Octobre 2019* **par :**

DION IRIS-AMATA

Glace injectée dans la Tropopause Tropicale par Convection Profonde

---

JURY

ATTIE JEAN-LUC	Professeur d'Université	Président du Jury
CLAUD CHANTAL	Directrice de Recherche	Rapporteure
SANTEE MICHELLE	Directrice de Recherche	Rapporteure
RICAUD PHILIPPE	Directeur de Recherche	Directeur de Thèse
HAYNES PETER	Professeur	Directeur de Thèse
CARMINATI FABIEN	Ingénieur de Recherche	Examinateur
RIVIERE EMMANUEL	Maître de Conférences	Examinateur

École doctorale et spécialité :
SDU2E : Océan, Atmosphère, Climat

Unité de Recherche :
Centre National de Recherches Météorologiques (CNRM), Météo-France – CNRS (UMR 3589)

Directeur de Thèse :
RICAUD Philippe, HAYNES Peter

Rapporteur :
CLAUD Chantal, SANTEE Michelle

Ice injected up to the Tropical Tropopause Layer by Deep Convection

Author: Iris-Amata DION

Thesis supervisor: Philippe RICAUD

Co-supervisor of the thesis: Peter HAYNES

Thesis of the Toulouse III University - Paul Sabatier

Defended 25/10/2019 at Météo-france, Toulouse, France

– August 26, 2019 –

– Storm cell on the Amazon River, June 2016, Chantal Michelet –

*À **mon grand frère**, mon inspiration !*

*À **mes parents**, ces aventuriers, qui m'ont toujours écoutée et encouragée à faire ce qui m'inspire.*

*À **Gaël**, pour tant et pour tout.*

« Ooh mais elle est Trop-po-pausée cette thèse ! », « Une thèse sur la glace ? Tu veux dire, sur la glace à la vanille, à la framboise ou au chocolat? » Quelques perles entendues.

REMERCIEMENTS

A l'issue de la rédaction de ce manuscrit, j'aimerais exprimer ma gratitude envers toutes celles et ceux qui m'ont accompagnée, conseillée, écoutée, encouragée et soutenue durant ma thèse. Merci à vous.

Mes **directeurs de thèse et l'équipe TEASAO**. Merci à Philippe et Peter, pour m'avoir accueillie et fait confiance dans l'élaboration de cette thèse. Ce fut pour moi une expérience enrichissante. J'ai pu découvrir différentes facettes du monde de la recherche, aussi bien les opportunités que les difficultés. Plus particulièrement, merci Philippe pour m'avoir donné la possibilité de participer à des conférences et à une école d'été. Ce furent des voyages très enrichissant. Merci aussi pour les nombreuses relectures de mes travaux. Peter, merci beaucoup pour ton accueil à Cambridge ! J'en garde un excellent souvenir. Merci aussi à l'équipe TEASAO pour m'avoir permis de faire cette thèse et pour m'avoir accompagnée tout au long de celle-ci.

Les membres du jury, **Michelle Santee, Chantal Claud, Fabien Carminati, Emmanuel Rivière, Yves Morel et Jean-Luc Attié**. Merci d'avoir accepté de lire et d'échanger autour de mes travaux. I would especially like to thank Michelle for her many and helpful feedback.

Claire Doubremelle. Sincèrement merci pour votre soutien et votre écoute et pour avoir su adoucir certaines situations avec beaucoup d'empathie.

L'équipe COMETS et en particulier **Béatrice Josse., Virginie Marécal. et Sophie Belamari.**, merci pour vos conseils, votre bienveillance, et votre soutien. Merci d'être régulièrement venues me rappeler votre présence en cas de doutes. **Béa**, merci de m'avoir consacré du temps avec beaucoup de douceur lors des moments plus difficiles. Merci beaucoup aussi pour tes conseils sur mes travaux

et sur les différents jeux de données pouvant être intéressants! **Virginie**, merci beaucoup d'avoir relu une partie de mes travaux et merci beaucoup pour tes encouragements! **Laaziz El Amraoui.**, merci d'avoir veillé au bon déroulement de ma thèse et d'avoir été membre de mon comité de thèse.

Jean-Pierre Chaboureau, merci pour m'avoir fourni des données du modèle Meso-NH et merci pour ta confiance.

Fabien Carminati, merci pour tes retours enrichissants sur mes travaux. Merci aussi pour l'agréable accueil à Exeter et pour avoir organisé à mon intention ce séminaire, qui, au cours de ma deuxième année de thèse, m'a fait gagner confiance en moi et en mes travaux!

Thibaut Dauhut, un grand merci pour tes conseils dès le début de ma thèse et tout au long de celle-ci. Merci pour ton écoute, tes explications et pour nos discussions sur les divers processus dans la tropopause tropicale, tout en traversant King's College! Tu as été un modèle (sans jeu de mot ..) et un ami.

Samuel Q., Valentin P. et Cyrille D., un grand merci pour m'avoir consacré du temps et de l'énergie dans l'apprentissage d'un nouveau langage informatique.

Merci aussi à toutes les très chouettes personnes rencontrées lors de conférences et durant l'école d'été à Cape Town. Je pense notamment à **Suneeth K V** et **Moha Diallo** mais aussi à bien d'autres.

Les amies du CNRM, dans le désordre, merci à vous: **Maxence Descheemaecker**, mon co-bureau, merci pour avoir été toi-même, drôle, touchant et enthousiaste. Une bienveillance "co-bureautale" plus qu'apréciée ! **Damien Specq**, merci pour ton amitié, les chouettes moments partagés et ces joies de nous voir progresser aux cours d"équi"! **Yann Cohen**, merci pour ton écoute, ton amitié et ces fiestas toulousaines qui nous ont fait sortir la tête de l'eau (H_2O)!

Martin Cussac, merci pour ta "positive attitude" quelle que soit la situation. **Clément Strauss**, merci pour ces grands questionnements philosophiques qui nous ont obligés à faire des pauses. **Matteo Ponzano, Thomas Drugé et Léo Ducongé**, merci pour votre jolie cohésion très vivante. **Quentin Fumiere**, merci pour avoir partagé ces années de thèse dans une atmosphère humoristique bien à toi :-) **César Sauvage**, merci pour ces moments de guitare, saxo et chant. **Hugo Marchal**, merci pour m'avoir laissée gagner au ping-pong! **Yannick et Nizar**, merci pour vos encouragements, et vos longs débats avec Maxence. **Valentin Petiot** merci pour nos partages et pour nos découvertes de toutes sortes de thés lors de discussions sur les Pyrénées. Merci pour ton amitié. **Guillaume Bigeard Kurt**, merci pour tes conseils de post-doc, les couchers de soleil sur les Pyrénées depuis le CNRM et tout plein d'autres moments très sympas. **Gab Lellouche**, merci pour ta super belle énergie! **P-A J.**, merci pour tes partages de musique qui ont accompagné certains moments de ma thèse. **Marie Mazoyer**, un très grand merci pour ce coup de pouce, ce "boost" de confiance en soi, que tu m'as offert juste avant ma soutenance !! **Alexane Lovat**, pour ton rire qui se propage si vite! **Sabine Radanovics**, pour le chant et tes encouragements de dernière minute qui m'ont été si précieux !! merci aux joueurs de ping-pong de 13h00, et à tant d'autres, Claire Lamotte, Zied Sassi, Nicolas Maury, la chorale, le tissu aérien, la capoera, ...

Mes colocs, qui ont accompagné cette thèse avec du soleil: **Étienne** qui m'a inspirée et impressionnée par son énergie, sa vitalité et sa grande curiosité. Merci pour ces énormes fêtes que tu sais incroyablement préparer. **Brice** qui m'a fait rêver, chanter et danser. **Hugo**, qui a été et est toujours un bijou de sagesse et d'amour, merci pour cela. Des amitiés précieuses.

Judith, merci d'avoir été ce petit ange. Merci à mon Amie bienveillante pour

ton fort soutien, tes conseils de doctorante, pour ta Folie qui éveille, élève et émerveille. Merci d'être une Perle précieuse de bonheur.

Merci aux pétillantes **copines de Paris, Fleur, Alice, Rim** et **Mathilde**! Merci d'être venues me voir sur Toulouse. Vos fascinants projets, débordant d'aventure, m'ont inspirée et permis de prendre un dernier bol d'air chaud et doux avant la grande ligne droite de la fin de thèse. J'aimerais en profiter pour remercier plus spécifiquement ma grande Amie **Mathilde** : savions-nous déjà au lycée que nous serions toujours toutes les deux étudiantes plus de 10 ans plus tard ? Merci pour ta bienveillance, tous tes encouragements, pour avoir toujours cru en moi, pour ta complicité, et ton amitié !

Merci à **toute ma famille**. Merci Paulette pour tes encouragements. Merci à **ma grand mère**, qui du haut de ses 92 ans, m'a toujours félicitée et encouragée! Et bien sûr, par dessus tout, merci à **mes parents** et à **Camille**, merci pour tout !

Merci beaucoup aussi à tous les amis et la famille qui sont, pour certains, venus de loin assister à ma soutenance : **Séverine, Jean-Marc et Valérie, Pierre et Louise, Mathilde, Fleur, Alice, Faustine, Marion et Jérémie**! Séverine, merci aussi pour la relecture de dernière minute très précieuse !

Enfin et surtout, **Gaël**, merci d'être présent et de rayonner à mes côtés depuis le début de nos années d'études. Merci d'avoir nourri de nombreux rêves et d'avoir partagé cette curiosité et cette sensibilité au vaste domaine des sciences de la Terre et de l'Univers. Tout cela nous a transportés depuis les roches terrestres jusqu'à, pour ma part, la Tropopause et toi, toujours plus haut, jusqu'à la planète Mars! Toute ma tendresse et ma reconnaissance pour le soutien et l'aide que tu m'as apportés, pour m'avoir relue plusieurs fois, conseillée, écoutée et finalement pour avoir grandement partagé cette aventure! Merci pour tout.

Abstract

Key words: Tropical Tropopause Layer, Maritime Continent, upper troposphere, lower stratosphere, ice, precipitation, flashes, water vapour, MJO, ENSO, MLS, TRMM

The tropical tropopause layer (TTL) defined by the layer surrounding the cold point, delimiting the troposphere to the stratosphere, controls the vertical distribution of temperature, clouds, water vapour and ice. However, water vapour and cirrus clouds (clouds composed of ice) have a significant radiative effect on climate. Furthermore, the way in which water vapour and ice are transported up to the TTL and even higher into the lower stratosphere is still not well understood. Among the main processes identified to control the humidity of the TTL, this thesis focuses on the rapid (diurnal-scale) deep convective processes to estimate its impact on the amount of ice injected (ΔIWC) into the TTL.

The Microwave Limb Sounder (MLS) instrument on board the Aura satellite have measured the ice water content (IWC) and water vapour mixing ratio in the upper tropophere (at 146 hPa) and near the cold point of the TTL (at 100 hPa) from 2004 to 2017 with measurements at a low temporal resolution of two local times per day: at 01:30 and 13:30 local times in the tropics. Instruments on-board the Tropical Rainfall Measuring Mission (TRMM) satellite have measured precipitation (Prec) and number of flashes during thunderstorm events (Flash) from 2004 to 2015 in the tropics, with a much better temporal resolution than MLS allowing to study diurnal cycles with a 1-hour temporal resolution and a horizontal resolution of $2^\circ \times 2^\circ$ ($\sim 200 \times 200$ km). Our studies focus on the austral convective season of December, January and February (DJF).

The thesis proposes a model relating Prec and Flash from TRMM, used as

a proxy of deep convection and the two daily MLS IWC measurements to estimate ΔIWC in the TTL. The model has been validated using the Superconducting Submillimeter-Wave Limb-Emission Sounder (SMILES) space-borne instrument, which was able to provide IWC in the TTL with a 1-hour temporal resolution from December 2009 to February 2010. ΔIWC in the TTL has been estimated over several oceanic and continental regions of the tropics (South America, South Africa, Indian Ocean, Pacific Ocean and Maritime Continent (MariCont, including Indonesia)), highlighting the highest values of ΔIWC over the MariCont. ΔIWC estimated from Flash and Prec have been compared to ΔIWC calculated from IWC provided by ERA5 meteorological reanalyses averaged from 2005 to 2016, over the MariCont. Over land, ΔIWC calculated from the different datasets (found from 4 to 10 and from 0.5 to 3.5 mg m^{-3} at 146 and 100 hPa, respectively) are larger than over sea (found from 0.2 to 4.0 and from 0.0 to 0.7 mg m^{-3} at 146 and 100 hPa, respectively). The Java island, composed of high mountains (> 2000 m) abruptly reaching the sea, reveals the largest ΔIWC whatever of the dataset used ($\sim$ 1.5 and $\sim$ 8.5 mg m^{-3} at 146 and 100 hPa, respectively). Finally, the impact of large-scale intra-seasonal oscillations (Madden-Julian Oscillation (MJO) and La Niña) on ΔIWC in the TTL over the MariCont has been studied. During La Niña, ΔIWC tends to increase over land (from $\sim$ +4 mg m^{-3} per pixel) and to decrease over the sea (from $\sim$ -4 mg m^{-3} per pixel) compared to ΔIWC estimated during DJF. During the active phase of the MJO, small differences (< 1 mg m^{-3} per pixel) in ΔIWC are observed compared to ΔIWC obtained in DJF. The impact of the MJO in active and suppressed phases on ΔIWC are studied using ice provided by the meso-scale model Meso-NH. A complementary study has been drawn, applying the model proposed in this thesis to the Asian monsoon area, known for its strong transport of air masses up to the stratosphere.

Résumé

Mots clés : Tropopause tropicale, teneur en eau glacée, Continent Maritime, précipitation, nombre d'éclairs, haute troposphère, basse stratosphère, vapeur d'eau, MJO, ENSO, MLS, TRMM.

La tropopause tropicale (TTL), définie par la couche autour du point froid, délimitant la troposphère de la stratosphère, contrôle la distribution verticale de la température, des nuages, de la vapeur d'eau et de la glace. Or la vapeur d'eau ainsi que les cirrus (nuages composés de glace) ont un effet radiatif important sur le climat. Cependant, la façon dont la vapeur d'eau et la glace sont transportées jusqu'à la TTL et même au-delà jusqu'à la stratosphère est encore mal connue. Parmi les processus majeurs identifiés pour contrôler l'humidité de la TTL, cette thèse se focalise sur les processus rapides (à l'échelle diurne) de convection profonde dans le but d'estimer les quantités de glace injectées (ΔIWC) dans la TTL.

L'instrument MLS (Microwave Limb Sounder) à bord du satellite Aura a mesuré la teneur en eau glacée (IWC) et le rapport de mélange en vapeur d'eau dans la haute troposphère (146 hPa) et proche du point froid de la TTL (100 hPa), de 2004 à 2017 mais avec des mesures à faible résolution temporelle de deux heures locales par jour : à 01h30 et 13h30 en heures locales dans les tropiques. Les instruments du satellite TRMM (Tropical Rainfall Measuring Mission) ont mesuré les précipitations (Prec) et le nombre d'éclairs lors d'évènements orageux (Flash) dans les tropiques de 2004 à 2015 avec une bien meilleure résolution temporelle que MLS permettant d'établir le cycle diurne avec une résolution d'une heure et une résolution horizontale de $2^\circ \times 2^\circ$ ($\sim 200 \times 200$ km). Nos études se focalisent sur la saison convective australe de décembre, janvier et février (DJF).

La thèse propose un modèle reliant les observations de Prec et de Flash de TRMM, utilisées comme approximation de la convection profonde, et les deux

mesures journalières de IWC de MLS pour estimer ΔIWC dans la TTL. Le modèle a été validé à l'aide de l'instrument spatial SMILES (Superconducting Submillimeter-Wave Limb-Emission Sounder), capable de fournir IWC dans la TTL avec une résolution temporelle d'une heure de décembre 2009 à février 2010. ΔIWC a été estimé sur plusieurs régions océaniques et continentales des tropiques (Amérique du Sud, Afrique du Sud, Océan Pacifique, Océan Indien et le Continent Maritime (MariCont, incluant l'Indonésie)), montrant les plus fortes valeurs de ΔIWC dans la TTL au-dessus du MariCont. Sur le MariCont, ΔIWC estimé à partir de Flash et Prec ont été comparés à ΔIWC estimé à partir des données de IWC fournis par les réanalyses météorologiques de ERA5 moyennées de 2005 à 2016. Sur les terres, ΔIWC calculés à partir des différents ensembles de données (trouvé de 4 à 10 et de 0,5 à 3,5 mg m^{-3} respectivement à 146 et 100 hPa) sont plus grands que sur les mers (de 0,2 à 4,0 et de 0,0 à 0,7 mg m^{-3} respectivement à 146 et 100 hPa). L'île de Java, composée de hauts reliefs (> 2000 m) se jetant dans la mer, révèle les plus importantes valeurs de ΔIWC quel que soit le jeu de données utilisé ($\sim$ 8.5 et $\sim$ 1.5 mg m^{-3} respectivement à 146 et 100 hPa). Enfin, l'impact des oscillations intra-saisonnières à grande échelle (Madden Julian Oscillation (oscillation de Madden-Julian (MJO) et La Niña) sur ΔIWC dans la TTL a été étudié sur le MariCont. Durant La Niña, ΔIWC tend à augmenter sur les terres (de $\sim$ + 4 mg m^{-3} par pixel) et diminuer sur les mers (de $\sim$ - 4 mg m^{-3} par pixel) par rapport à ΔIWC estimé durant DJF. Pendant la phase active de la MJO, de faibles différences (< 1 mg m^{-3} par pixel) de ΔIWC sont observées par rapport à ΔIWC obtenu en DJF. L'impact de la MJO en phases actives et inhibées sur ΔIWC est étudié en utilisant la glace fournie par le modèle de méso-échelle Meso-NH. Une étude complémentaire a été réalisée, appliquant le modèle proposé dans cette thèse à la région de la mousson asiatique, connue pour son fort transport des masses d'air jusqu'à la stratosphère.

Contents

Main acronyms

ACP: Atmospheric Chemistry and Physics journal

AMA: Asian monsoon anticyclone

CAPE: Convective available potential energy

CIN: Convective inhibition

CNRM: Centre National de Recherches Météorologiques

CPT: Cold Point Tropopause

ΔIWC: Amount of ice injected

ΔIWC^{ERA5}: Amount of ice injected estimated from IWC^{ERA5}

$\left\langle \Delta IWC_{z_0}^{ERA5} \right\rangle$: Amount of ice injected estimated from $\left\langle IWC_{z_0}^{ERA5} \right\rangle$ (at zo = 146 or 100 hPa)

ΔIWC^{Flash}: Amount of ice injected estimated from IWC^{MLS} and Flash

$\Delta\text{IWC}^{Meso-NH}$: Amount of ice injected estimated from MRI from Meso-NH

ΔIWC^{Prec}: Amount of ice injected estimated from IWC^{MLS} and Prec

DJF: December, January, February

DJF (chapter 6): DJF period excluding MJO and La Nina periods

DJF_Clim (chapter 6): DJF period including MJO and La Nina periods

ENSO: El Nino Southern Oscillation

Flash: Number of flashes from lightning measured by TRMM-LIS

GMT: Greenwich Mean Time

IndOc: Indian Ocean

ITCZ: Inter-Tropical Convergence Zone

IWC: Ice Water Content

IWC^{MLS}: Ice Water Content from MLS

IWC^{ERA5}: Ice Water Content from ERA5

$\left\langle IWC_{z_0}^{ERA5} \right\rangle$: the convolved IWC^{ERA5} following eq. 5.4

JJA: June, July, August

LFC: Level of the Free Convection

LNB: Level of Neutral Buoyancy

LS: Lower Stratosphere

LZRH: Level of Zero Radiative Heat

La Nina: La Nina period excluding MJO and DJF periods

MariCont: Maritime Continent

MariCont_L: Lands of the Maritime Continent

MariCont_O: Oceans of the Maritime Continent

MCS: Mesoscale Convective Systems

MJO: Madden-Juilan Oscillation

MJO (chapter 6): MJO period excluding DJF and La Nina periods

MLS: Microwave Limb Sounder

MRI: Mixing ratio of ice

NAuSea: Seas in North of Australia

NCAR : National Center for Atmospheric Research

NCEP: National Center for Environmental Prediction

NE_India: North East of India study zone

NOAA: National Oceanic and Atmospheric Administration

PacOc: Pacific Ocean

pIWP: Partial ice water path

PR: Precipitation radar

Prec: Precipitation from TRMM-3B42

PV: Potential vorticity

PVU: Potential vorticity unit

RHI: Relative humidity with respect to ice

RMMM: Real-time Multivariate MJO

SE_China: South East of China study zone

SMILES: Submillimeter-Wave Limn-Emission Sounder

SouthAm: South America

SouthAfr: South Africa

SPCZ: South Pacific Convergence Zone

S_Vietnam : South of Vietnam study zone

TEMP: Temperature

TL: Tropopause level

TRMM: Tropical Rainfall Measuring Mission

TRMM-LIS: TRMM Lightning Imagining Sensor

TRMM-3B42: TRMM algorithm 3B42

TST: Troposphere to stratosphere transport

TTL: Tropical Tropopause Layer

UT: Upper Troposphère

UV: Utra violet

WSumSea: Sea in the West of Sumatra

WV: Water Vapour

Chapter 1

Introduction

1.1 Introduction (English)

Tropical deep convection is the main process in the transport of air from the surface to the upper tropical troposphere and even to the lower stratosphere (Folkins et al., 2006; Fueglistaler et al., 2009). This vertical transport plays a rôle on the global atmosphere composition and dynamics. It is known that this transport is impacted by the surface proprieties that the diurnal cycle of deep convection differs over tropical land and ocean (Liu and Zipser, 2005). The altitude reached by the tropical deep convection cloud is crucial in the understanding of the atmospheric air masses distribution. When the convection does not reach the stratosphere, air masses are impacted by radiative cooling and subside. However, when the tropical deep convection reaches the stratosphere, the air masses can be distributed toward high latitudes by the Brewer-Dobson circulation (Brewer, 1949; Holton et al., 1995; Butchart, 2014). The transition between the troposphere and the stratosphere, called the **tropopause**, is a key atmospheric area controlling the vertical distribution of air masses temperature, clouds, water vapour and ice. The tropopause is subject to many studies because of its particularity to

be the area where the temperature gradient changes to the point named the cold point tropopause (CPT). The tropopause can be considered as a level (as defined by the World Meteorological Organization (WMO)) or as a layer (Gettelman and Fothers, 2002; Mehta et al., 2008; Birner and Charlesworth, 2017). In this thesis, we consider the tropical tropopause as an intermediate layer around the tropical CPT, between 14 and 18.5 km above sea level (150 and 70 hPa, respectively) Fueglistaler et al. (2009a) named the TTL as tropical tropopause layer. Figure 1.1 from Fueglistaler et al. (2009a) illustrates the tropospheric cloud processes and zonal mean circulation in the tropics during deep convective activity.

The main atmospheric component transported by air masses during deep convective activity is water (through the vapour, liquid and solid phases as a function of the pressure and temperature reached). **Water vapour** (**WV**) is one of the main greenhouse gases and has an important impact on the radiative balance of the troposphere, the stratospheric ozone, and thus on the climate, particularly in the tropics. The WV distribution in the tropical upper troposphere (UT) (Soden et al., 2008) and stratosphere (Solomon et al., 2010) is strongly coupled to the distribution of thin cirrus clouds composed of ice crystals, known as having a significant effect on the overall thermal balance of the troposphere (Zhou et al., 2014). However, the way in which WV and ice travel from the troposphere to the lower stratosphere in the tropics is still poorly understood.

At the surface, evaporation and evapotranspiration release water vapour in the atmosphere. Warm air masses become lighter than the environment and start to rise up in the troposphere. With the ascent and the decrease of pressure and temperature, the water vapour contained in the air masses can start to condensate. Water particles continue to rise up as long as the particles are light enough. Otherwise, condensed water particles fall down to the surface. Near the TTL, WV and ice concentrations are controlled by temperature which regulate the satura-

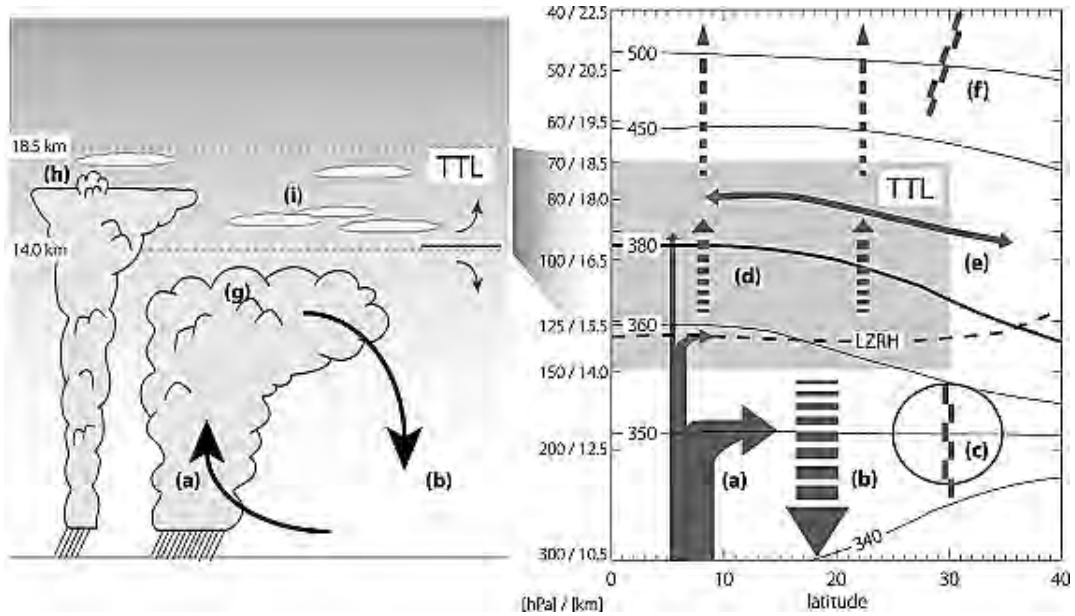

Figure 1.1 – Schematic (left) of cloud processes and transport and (right) of zonal mean circulation. Arrows indicate circulation, black dashed line is clear-sky level of zero net radiative heating (LZRH), and black solid lines show isentropes (in K, based on European Centre for Medium Range Weather Forecasts 40-year reanalysis (ERA-40)). The letter a indicates deep convection: main outflow around 200 hPa, rapid decay of outflow with height in tropical tropopause layer (TTL), and rare penetrations of tropopause. Fast vertical transport of tracers from boundary layer into the TTL. The letter b indicates radiative cooling (subsidence). The letter c indicates subtropical jets, which limit quasi-isentropic exchange between troposphere and stratosphere (transport barrier). The letter d indicates radiative heating, which balances forced diabatic ascent. The letter e indicates rapid meridional transport of tracers and mixing. The letter f indicates the edge of the "tropical pipe," relative isolation of tropics, and stirring over extratropics ("the surf zone"). The letter g indicates deep convective cloud. The letter h indicates the convective core overshooting its level of neutral buoyancy. The letter i indicates ubiquitous optically (and geometrically) thin, horizontally extensive cirrus clouds, often formed in situ. Note that the height-pressure-potential temperature relations shown are based on tropical annual mean temperature fields, with height values rounded to the nearest 0.5 km. Figure 1 from Fueglistaler et al. (2009a)

tion mixing ratio in air masses (Hartmann et al., 2001; Fueglistaler et al., 2009a; Khaykin et al., 2013), decreasing the WV concentration and increasing ice particles. Thus, the ratio between WV and ice crystals in convective clouds strongly

varies with altitude. However, the vertical distribution of WV over ice ratio is still not well understood, particularly in the upper troposphere and close to the TTL where i) the cold point effect plays on the water budget phase changes with micro-physics processes and ii) the troposphere to stratosphere air masses exchanges impact the water budget in the TTL (Gettelman and Fothers, 2002; Corti et al., 2006; Dauhut, 2016).

Two major processes have been identified to control the humidification of TTL. Firstly, a slow and large-scale process, controlled by the radiative heating of the air masses, allowing to gain buoyancy and cross the cold point by about 300 m per month (Corti et al., 2006). This transport contributes to the circulation of Brewer-Dobson (Corti et al., 2006). Secondly, a rapid (1 day) and small scale process of the deep convection, named overshoots, is defined by the direct transport of air masses from the top of the deep convective cloud to the lower stratosphere (Adler and Mack, 1986; Danielsen, 1982; Dessler, 2002; Fueglistaler et al., 2009a). Overshoot can have a significant impact on the composition of the stratosphere. However, it has been shown that only a small part ($\sim 18\%$) of water mass flux from cloud overshoot are irreversibly transported in the stratosphere (Dauhut et al., 2015), the remaining falls back into the troposphere because of the stratification.

The goal of this thesis is to improve our knowledge on the **water budget in the TTL**. Ice and water vapour in the upper troposphere and near the CPT are studied separately in relation with the deep convective activity in the tropics to provide information on the impact of the deep convection on the vertical and horizontal distribution of the water budget in the TTL. This thesis focuses more particularly on the solid phase of water and on the processes at the **diurnal time scale** in order

to estimate the amount of **ice injected** by deep convection up to the TTL over tropical convective areas and during convective seasons. To achieve this objective, the thesis uses firstly observational datasets from satellites, and then complete the study with meteorological reanalysis and meso-scale model datasets.

Ice water content (**IWC**), WV, temperature and relative humidity with respect to ice, are provided from the **Microwave Limb Sounder** (**MLS**) instrument on board the Aura satellite in the upper tropopshere and near the CPT (146 hPa, 100 hPa) during 2004-2017. One of the main drawbacks of the MLS observations where studying the diurnal cycle is its low temporal resolution. Crossing the tropics at two fixed times, MLS provides IWC and WV at 01:30 local time (LT) and 13:30 LT. IWC from MLS will also be compared to IWC measured at high (1-hour) temporal resolution from the Superconducting Submillimeter-Wave Limb-Emission Sounder (SMILES) during the short period provided by the instrument (April 2009 to October 2010). In order to study the impact of deep convection on ice and WV up to TTL, firstly precipitation from the **Tropical Rainfall Measuring Mission** (**TRMM**) 3B42 algorithm (TRMM-3B42), averaged at high (1-hour) temporal resolution during the same study period as MLS and over the all tropical band (30°S, 30°N), is used and combined with the MLS datasets. Secondly, the deep convective activity is also studied by considering the number of flashes from lightnings provided from the Lightning Imaging Sensor (LIS) instrument on TRMM, from 2004 to 2015 at 1-hour resolution. Finally, IWC from the ERA5 meteorological reanalysis and the non-precipitating ice (MRI) from Meso-NH mesoscale model are compared to observation datasets to evaluate the capacity of the model of the meteorological analysis to reproduce the measured amount of ice injected up to the TTL from deep convection.

This study takes place within the TEASAO (Turbulence Effects on Active Species in Atmosphere, `http://www.legos.obs-mip.fr/projets/`

`axes-transverses-processus/teasao`, last access: June 2019) project lead by Dr Yves Morel and Professor Peter Haynes. The goal of the project is the preparation of the next generation of prediction and climate systems for both the atmosphere and the ocean. The challenge of this project is to answer societal problems of water resources, air and water pollution by improving models and knowledges regarding small-scale turbulences and vertical mixing of chemical and biological species in atmosphere and ocean. Theoretical and applied studies compose the project. The project is based on four teams from the LEGOS (Laboratoire d'Etudes en Géophysique et Océanographie Spatiales), the LA (Laboratoire d'Aerologie) and the CNRM (Centre National de Recherches Météorologiques) and welcomes for four years Professor Peter Haynes (from University of Cambridge (UK)) who is an international expert on atmospheric and oceanic dynamics and on transport and mixing of trace species.

The manuscript is separated in several chapters.

• Chapter 2 provides an overview on the tropospheric and stratospheric structure and composition. **Tropical atmospheric dynamical processes** are detailed and deep convective activity processes are presented. A focus on the water budget in the tropical troposphere and tropopause layer is drawn.

• Chapter 3 introduces some backgrounds on **remote sensing observations** and presents the instruments and the reanalysis and meso-scale model used in this thesis to estimate the amount of ice injected in the TTL during the austral convective season of December, January and February (DJF) over the tropics (chapter 4) and over the named Maritime Continent region (chapter 5) and considering the Madden-Julian Oscillations (MJO) and the El Nino Southern Oscillation (ENSO) periods (chapter 6).

• Chapter 4 is based on the article published in Atmospheric Chemistry and

Physics (ACP) (Dion et al., 2019). It evaluates the mechanisms affecting the diurnal cycle of water budget in the TTL over the tropics. A **method is developed** combining MLS and TRMM observations to estimate the **amount of ice injected** (Δ**IWC**) by deep convection up to the TTL. Precipitation is shown to be a good proxy of deep convection over convective regions and during the convective period. The model is validated using IWC from the SMILES instrument providing the diurnal cycle of IWC in the troposphere and tropopause layer during less than one year (October 2009 to April 2010). Finally, ΔIWC is estimated over several convective tropical oceanic and continental regions at 146 hPa in the UT and at 100 hPa in the tropopause layer (renamed TL).

• Chapter 5 is based on the article submitted and revised in ACPD (Dion et al, 2020), focusses on the tropical region where ΔIWC is the highest namely the **Maritime Continent** [15°S – 10°N; 90°W – 150°W] that includes Indonesia. ΔIWC is studied at high horizontal resolution (2° $\times$ 2° which represent $\sim$ 200 $\times$ 200 km) separating ΔIWC over islands and seas of the Maritime Continent. Combined with precipitation from TRMM, we also use another proxy of deep convection, the number of flashes from TRMM-LIS. The observed ΔIWC over island and seas of the Maritime Continent. Finally, the observational range of ΔIWC is finally compared to ΔIWC estimated from ice provided by ERA5 meteorological reanalyses.

• Chapter 6 shows ΔIWC estimated over the Maritime Continent during convective periods governed by the Madden Julian Oscillation (MJO) and the Southern El Nino Oscillations (ENSO) in order to identify processes related to **intraseasonal oscillations** on the amount of ice injected from deep convection in the TTL. Observed ΔIWC during MJO is compared to ΔIWC estimated from the Meso-NH MRI datasets simulated for an MJO episodes of November 2011.

• Chapter 7 presents a study of the ice injected up to the TTL from deep con-

vection over an extra-tropical region known to be efficient for injecting air masses in the UTLS, namely Asia, during the **Asian Monsoon** from June to August (JJA). The study is based on the model developed in the thesis with precipitation and the number of flashes from TRMM as proxies of deep convection and IWC from MLS. This work has been done in parallel to the present thesis within the framework of the Cyrille Dallet's Master 2 internship, supervised by Philippe Ricaud and myself.

• Conclusions are finally drawn and present some perspectives based on the results obtained with the PhD studies.

Introduction (Français)

1.2 Introduction (Français)

La **convection profonde tropicale** est le principal processus de transport des masses d'air de la surface vers la haute troposphère et même jusqu'à la basse stratosphère dans les tropiques (Folkins et al., 2006; Fueglistaler et al., 2009a). Ce transport vertical joue un rôle sur la composition et la dynamique de l'atmosphère globale. On sait que ce transport est influencé par les propriétés de surface et que le cycle diurne de la convection profonde diffère sur les terres de sur les océans tropicaux (Liu and Zipser, 2005). L'altitude atteinte par le nuage tropical de convection profonde est crucial pour la compréhension de la distribution des masses d'air atmosphériques. Lorsque la convection n'atteint pas la stratosphère, les masses d'air sont affectées par le refroidissement radiatif et s'abaissent. Cependant, lorsque la convection profonde tropicale atteint la stratosphère, les masses d'air peuvent être réparties vers les hautes latitudes suivant la circulation de Brewer-Dobson (Brewer, 1949; Holton et al., 1995; Butchart, 2014). La transition entre la troposphère et la stratosphère, appelée tropopause, est une zone atmosphérique clé qui contrôle la distribution verticale de la température des masses d'air, des nuages, de la vapeur d'eau et de la glace. La tropopause fait l'objet de nombreuses études en raison de sa particularité d'être la zone où le gradient de température change au point appelé le point froid de la tropopause (CPT

pour "cold point tropopause"). La tropopause peut être considérée comme un niveau (tel que défini par l'Organisation météorologique mondiale (WMO)) ou comme une couche atmospherique (Gettelman and Fothers, 2002; Mehta et al., 2008; Birner and Charlesworth, 2017). Dans cette thèse, nous considérons la tropopause tropicale comme une couche intermédiaire autour du CPT tropical, entre 14 et 18,5 km au-dessus du niveau de la mer (respectivement entre 150 et 70 hPa), (Fueglistaler et al., 2009a), désignée par le terme générique TTL pour "Tropical Tropopause Layer". La Figure 1.2 de Fueglistaler et al. (2009a) illustre les processus des nuages troposphériques et la circulation moyenne zonale dans les tropiques au cours des périodes suivant une activité convective profonde.

Le principal composant atmosphérique transporté par les masses d'air pendant l'activité convective profonde est l'eau à travers les phases vapeur, liquide et solide en fonction de la pression et de la température atteinte. La **vapeur d'eau** (**WV** pour "water vapour") est l'un des principaux gaz à effet de serre et a un impact important sur l'équilibre radiatif de la troposphère, mais aussi sur l'ozone stratosphérique et donc sur le climat, en particulier sous les tropiques. La distribution de la WV dans la haute troposphère tropicale (UT pour "upper troposphere") (Soden et al., 2008) et dans la stratosphère (Solomon et al., 2010) est fortement liée à la distribution spatiale des fins nuages composés de cristaux de glace (les cirrus), connus pour avoir un effet significatif sur le bilan radiatif global de la troposphère (Zhou et al., 2014). Cependant, la façon dont la WV et la glace sont transportées de l'UT dans la basse stratosphère (LS pour "lower stratosphere") sous les tropiques est toujours mal comprise.

En surface, l'évaporation et l'évapotranspiration libèrent de la vapeur d'eau dans l'atmosphère. Les masses d'air chaudes deviennent plus légères que l'environnement et commencent à s'élever dans la troposphère. Avec la montée en altitude et la baisse de la pression et de la température, la vapeur d'eau contenue

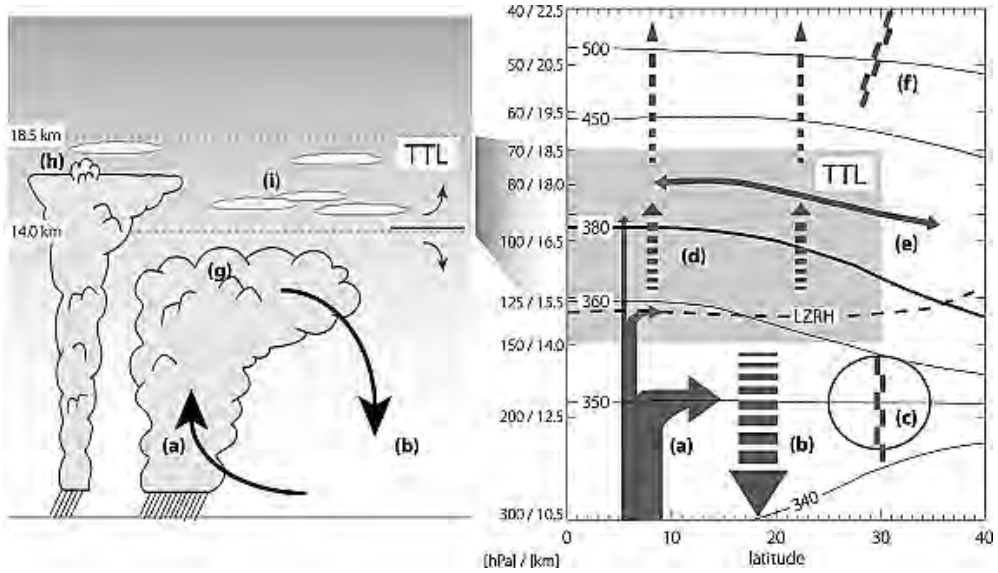

Figure 1.2 – Schéma (à gauche) des processus et du transport des nuages et (à droite) de la circulation moyenne zonale. Les flèches indiquent la circulation, la ligne pointillée noire correspond au niveau de chauffage radiatif nul en ciel clair (LZRH) et les lignes pleines noires indiquent les isentropes (en K, basée sur la réanalyse sur 40 ans du Centre européen pour les prévisions météorologiques à moyenne portée (ERA-40)). La lettre a indique le processus de convection profonde : son écoulement principal est autour de 200 hPa, une décroissance rapide de l'écoulement se produit avec la hauteur dans la couche tropicale de la tropopause (TTL), laissant apparaitre de rares pénétrations de la tropopause. Dans la tropopause, on retrouve de rapide transports verticaux des masses d'air depuis la couche limite jusqu'à la TTL. La lettre b indique le refroidissement radiatif (affaissement). La lettre c indique les jets subtropicaux, qui limitent les échanges quasi-ontropiques entre la troposphère et la stratosphère (barrière de transport). La lettre (d) indique l'ascension diabatique forcée, équilibrée par le chauffage radiatif. La lettre (e) indique un transport méridien rapide des traceurs et du mélange. La lettre f indique "la zone de surf", la zone où se produit l'isolement relatif des tropiques face à l'agitation des extratropics. La lettre (g) indique un nuage convectif profond. La lettre (h) indique que le noyau convectif a dépassé son niveau de flottabilité neutre. La lettre (i) indique des cirrus omniprésents, optiquement et géométriquement fins, étendus horizontalement, souvent formés *in situ*. Notez que les relations hauteur-pression-température potentielle sont basées sur les moyenne annuelle tropicale de température, les altitudes étant arrondies au 0,5 km le plus proche. Figure 1 d'après Fueglistaler et al. (2009a)

dans les masses d'air ascendantes peut commencer à condenser. Les particules d'eau continuent de monter tant qu'elles sont suffisamment légères. Sinon, des particules d'eau condensées tombent à la surface par gravité. Près de la TTL, les concentrations de WV et de glace sont contrôlées par les très faibles température qui régulent le rapport de mélange de saturation dans les masses d'air (Hartmann et al. 2001 ; Fueglistaler et al., 2009 ; Khaykin et al., 2013), réduisant la concentration de WV et augmentant les particules de glace. Ainsi, le rapport entre la WV et les cristaux de glace dans les nuages convectifs varie fortement avec l'altitude. Cependant, la distribution verticale du rapport WV sur glace n'est pas encore bien comprise, en particulier dans la haute troposphère et à proximité du TTL où i) l'effet du point froid joue sur les changements de phase du bilan hydrique avec la microphysique et ii) les échanges entre la troposphère et les masses d'air de la stratosphère ont un impact sur le bilan hydrique dans la TTL (Gettelman et Fothers, 2002 ; Corti et al., 2006 ; Dauhut, 2016).

Deux processus majeurs ont été identifiés pour contrôler l'humidification de la TTL. Tout d'abord, un processus lent et à grande échelle, contrôlé par le réchauffement radiatif des masses d'air, et permettant aux masses d'air de franchir le point froid à une vitesse d'environ 300 m par mois (Corti et al., 2006). Ce transport contribue à la circulation de Brewer-Dobson (Corti et al., 2006). Deuxièmement, un processus rapide ($\sim$ 1 jour) et à petite échelle de la convection profonde, appelé percées nuageuses (*overshoots* en anglais), est défini par le transport direct des masses d'air du sommet du nuage convectif profond vers la basse stratosphère (Adler and Mack, 1986; Danielsen, 1982; Dessler, 2002; Fueglistaler et al., 2009a). Le dépassement peut avoir un impact significatif sur la composition de la stratosphère. Cependant, il a été démontré que seule une petite partie ($\sim$ 18%) du flux massique d'eau provenant de la surabondance des nuages est transportée de façon irréversible dans la stratosphère (Dauhut et al., 2015), le reste

retombe dans la troposphère en raison de la stratification.

Le but de cette thèse est d'améliorer nos connaissances sur le **bilan hydrique dans la TTL**. La glace et la vapeur d'eau dans la haute troposphère et à proximité du CPT sont étudiées séparément en relation avec l'activité convective profonde dans les tropiques pour fournir des informations sur l'impact de la convection profonde sur la distribution verticale et horizontale du bilan en eau dans le TTL. Cette thèse porte plus particulièrement sur la phase solide de l'eau et sur les processus **à l'échelle diurne** afin d'estimer la quantité de **glace injectée par convection profonde jusqu'à la TTL** sur les zones tropicales convectives et pendant les saisons convectives. Pour atteindre cet objectif, la thèse utilise d'abord des jeux de données d'**observation** provenant de satellites, et complète l'étude par des données de **réanalyse météorologique** et des données de **modèle** de méso-échelle.

La **teneur en eau glacée** (**IWC** pour "ice water content" en anglais), la WV, la température et l'humidité relative par rapport à la glace sont fournies par l'instrument **MLS** (**Microwave Limb Sonder**) à bord du satellite Aura dans la haute troposphère (146 hPa) et près du CPT (100 hPa) durant la période d'étude de 2004 à 2017. L'un des principaux inconvénients des observations MLS lorsque l'on étudie le cycle diurne d'un élément est sa faible résolution temporelle. Survolant les tropiques à deux heures locales fixes, MLS fournit IWC et WV à 01:30 heure locale (LT pour local time en anglais) et 13:30 LT. IWC fournie par MLS sera également comparée à IWC mesurée à une résolution temporelle élevée (1 heure) par l'instrument SMILES (Superconducting Submillimeter-Wave Limb-Emission Sounder) à bord de la station spatiale internationale pendant la courte période de mesure fournie par l'instrument (d'avril 2009 à octobre 2010). Afin d'étudier l'impact de la convection profonde sur la glace et la WV jusqu'à la TTL, on utilise d'abord les précipitations fournies à partir des mesures du satellite **TRMM** (**Tropical Rainfall Measuring Mission**) et de l'algorithme 3B42

(TRMM-3B42), dont la résolution temporelle moyenne est élevée (1 heure). TRMM-3B42 est utilisé pendant la même période d'étude que MLS et sur toute la bande tropicale (30°S – 30°N). Les données sont ensuite combinées aux jeux de données MLS. Deuxièmement, l'activité convective profonde est également étudiée en considérant le nombre d'éclairs durant les événements orgareux fournis par l'instrument LIS (Lightning Imaging Sensor) à bord de la plateforme TRMM, de 2004 à 2015 avec une résolution d'une heure. Enfin, IWC fournie par les réanalyses météorologiques de ERA5 et la glace non précipitante (MRI pour "mixing ratio ice") fournie par le modèle de méso-échelle, Méso-NH, sont comparées aux jeux de données d'observation afin d'évaluer la capacité du modèle et des analyses météorologiques à reproduire la quantité mesurée de glace injectée jusqu'à la TTL par convection profonde.

Cette étude a lieu dans le cadre du projet TEASAO (Turbulence Effects on Active Species in Atmosphere, http://www.legos.obs-mip.fr/projets/axes-transverses-processus/teasao, dernier accès : juin 2019) dirigé par le Dr Yves Morel (LEGOS, France) et le Professeur Peter Haynes (DAMTP, Cambridge, G-B). Le but du projet est de préparer la prochaine génération de systèmes de prévision et de systèmes climatiques pour l'atmosphère et l'océan. Le défi de ce projet est de répondre aux problèmes sociétaux de ressources en eau, de pollution de l'air et de l'eau en améliorant les modèles et les connaissances concernant les turbulences à petite échelle et le mélange vertical des espèces chimiques et biologiques dans l'atmosphère et l'océan. Quatre projets basés sur des études théoriques et appliquées composent le projet et s'appuient sur quatre équipes du LEGOS (Laboratoire d'Etudes en Géophysique et Océanographie Spatiales), du LA (Laboratoire d'Aerologie) et du CNRM (Centre National de Recherches Meteorologiques). Il vise aussi à s'appuyer sur l'expertise internationale du Professeur Peter Haynes (Université de Cambridge) dans les domaines de la dynamique atmosphérique et

océanique et du transport et mélange des éléments traces en l'accueillant pendant quatre ans à l'OMP à Toulouse.

Le manuscrit est séparé en plusieurs chapitres.

• Le chapitre 2 donne un aperçu de la structure et de la composition troposphériques et stratosphériques. Les **processus dynamiques atmosphériques tropicaux** sont détaillés et les processus d'activité convective profonde sont présentés. L'accent est mis sur le bilan hydrique dans la troposphère et la tropopause tropicale.

• Le chapitre 3 présente les observations de télédétection ainsi que les **instruments** et les réanalyses meteorologiques et le modèle de méso-échelle utilisés dans cette thèse afin d'estimer la quantité de glace injectée dans le TTL pendant la saison convective australe de décembre, janvier et février (DJF) sur les tropiques (chapitre 4) et sur la région dénommée Continent Maritime (chapitre 5) en considérant aussi les oscillations à large échelle: Oscillations Madden-Julian (MJO) et El Niño Southern Oscillation (ENSO) (chapitre 6).

• Le chapitre 4 est basé sur l'article publié dans Atmospheric Chemistry and Physics (ACP) (Dion et al., 2019). Il évalue les mécanismes affectant le cycle diurne du bilan hydrique dans le TTL sous les tropiques. Une **méthode est mise au point** combinant les observations MLS et TRMM pour estimer la **quantité de glace injectée** (ΔIWC) par convection profonde jusqu'à la TTL. Les précipitations se révèlent être un bon indicateur de la convection profonde dans les régions convectives et pendant la période convective. Le modèle est validé à l'aide de IWC mesurée par l'instrument SMILES qui fournit le cycle diurne de IWC dans la troposphère et la tropopause avec un pas de temps de 1 heure d'octobre 2009 à avril 2010. Enfin, ΔIWC est estimée sur plusieurs régions convectives océaniques et continentales dans les tropiques dans l'UT à 146 hPa et dans la tropopause (nommé TL) à 100 hPa.

• Le chapitre 5 est basé sur l'article soumis et révisé à ACPD (Dion et al., 2020), se concentre sur la région tropicale où on a montré que ΔIWC était la plus élevée, à savoir le **Continent Maritime** [15°S – 10°N ; 90°W – 150°W] qui inclut l'Indonésie. ΔIWC est étudiée à haute résolution horizontale (2° × 2° ce qui représente ∼ 200 × 200 km) en distinguant les îles et mers du Continent Maritime. En complément des précipitations fournies par TRMM, nous utilisons également une autre approximation de la convection profonde, le nombre d'éclairs durant les évènements orageux fourni par l'instrument LIS du satellite TRMM pour caractériser ΔIWC au-dessus des îles et mers du Continent Maritime. Enfin, ΔIWC estimée à partir des données d'observations satellitaires est comparée à ΔIWC estimée à partir des données de teneur en eau glacée fournies par les réanalyses météorologiques ERA5.

• Le chapitre 6 est composé de l'étude de ΔIWC estimée sur le Continent Maritime pendant les périodes convectives régies par l'oscillation Madden-Julian (MJO) et les oscillations La Nina afin d'identifier l'impact des processus liés aux **oscillations intra-saisonnières** et **inter-annuelles** sur la quantité de glace injectée dans la TTL. ΔIWC estimée à partir des observations pendant la MJO est comparée à ΔIWC estimée à partir des jeux de données de glace fournis par le modèle de meso-échelle Meso-NH, simulée pour un épisode de MJO de novembre 2011.

• Le chapitre 7 présente l'étude de la quantité de glace injectée jusqu'à la TTL par convection profonde sur une région extra-tropicale connue pour son efficacité à injecter des masses d'air dans l'UTLS, notamment en Asie, pendant la **mousson asiatique** de juin à août (JJA). L'étude est basée sur le modèle développé dans la thèse utilisant les précipitations et le nombre d'éclairs fournis par TRMM comme approximations de la convection profonde et IWC fournie par MLS. Ce travail a été réalisé en parallèle à la présente thèse dans le cadre du stage de Master 2 de

Cyrille Dallet, encadré par Philippe Ricaud et moi-même.

• Des conclusions sont enfin tirées et quelques perspectives basées sur les résultats obtenus avec les études de cette thèse sont présentées.

Chapter 2

Fundamentals in atmospheric physics and chemistry

This chapter provides an overview on the tropospheric and stratospheric structure and composition. Transport and processes controlling tropical deep convection and its internal structure, mechanism and impacts are detailed. A focus on the definition of tropopause and on the tropical troposphere to stratosphere exchanges as well as on the water budget in these atmospheric layers is overviewed. Some basic meteorological concepts and terminology specific to the study of tropical deep convection are recalled.

2.1 Structure of the atmosphere and tropopause definitions

2.1.1 Global atmospheric structure

The atmosphere is an envelope of gas surrounding the Earth. Because of gravity, the density of the atmosphere is higher at the surface than in altitude, meaning

that pressure decreasing with altitude. Figure 2.1 presents the atmospheric structure and temperature profile: each altitude of temperature inversion defines the separation between two layers. Because of the chemical composition of the atmosphere, the temperature profile changes with altitude. The layer extending from the surface to 7-15 km is called the Troposphere. This layer is the thinnest layer but contains about 80 % of atmosphere's total mass and about 99% of the atmosphere's total water vapour. Temperature decreases by about -3 to -10 K km^{-1} with altitude according do the Ideal Gas Law because pressure decrease with altitude. Vertical turbulent mixing is relatively frequent in this layer. The top of the troposphere is called the tropopause where temperature reaches a minimum, called the cold point tropopause (CPT). Then, temperature increases with altitude in the layer above the tropopause, called the Stratosphere. Thus, the tropopause is the level of transition between the two layers and will be defined precisely in sections 2.1.2 and 2.1.3. In the stratosphere, the temperature increases from 1 to 3 K km^{-1}, and the layer can be defined between 10 and 50 km of altitude. This layer has got the particularity of containing the greatest part of the ozone (O_3), in a intra-layer (called the ozonophere, with a maximum around 25 km of altitude). The amount of O_3 in the stratosphere is an important for the protection of living organisms, by absorbing most of the sun's ultraviolet radiation. Higher than the stratosphere, the mesosphere is found between 50 and 80 km, with temperature decreasing with height up to the mesopause where temperature is the lowest in atmosphere. Above, the thermosphere reaches an altitude up to 620 km. This layer accommodates boreal aurora and the International Space Station.

2.1.2 Tropopause, a level: thermal and dynamical definitions

The tropopause can be considered as a level or a layer. This section present the definition of the tropopause level. The level of the tropopause is defined by a

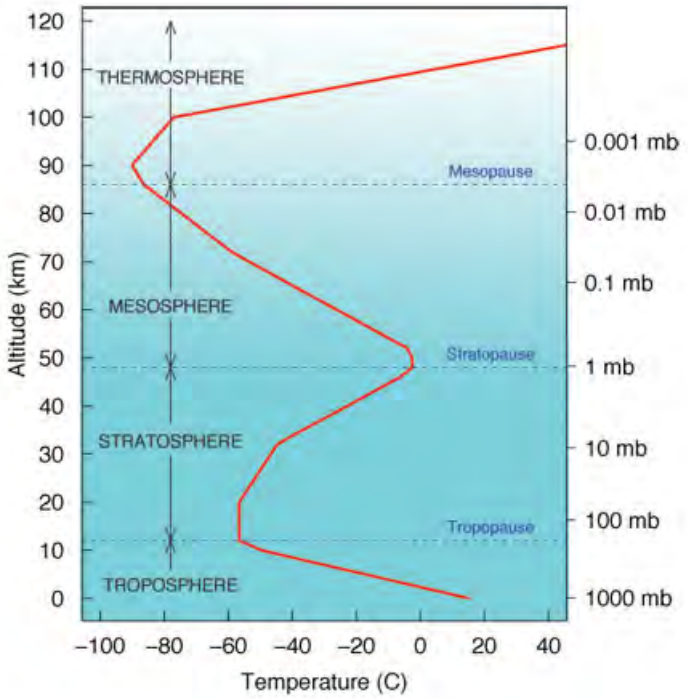

Figure 2.1 – Schematic representation of the atmospheric structure and temperature (°C) profil (red) as a function of altitude (km) and pressure (mb).
Source: © 2006. Steven C. Wofsy, Abbott Lawrence Rotch Professor of Atmospheric and Environmental Science, lecture notes.

minimum of temperature (Figure 2.1). In the troposphere, an air parcel rises adiabatically, cools down and expands with altitude up to high altitudes with cold temperatures such as in the troposphere top. In the stratosphere, because of the large O_3 content, which absorbs the solar ultra violet (UV) radiation and converts it to heat, temperature is back to increase with altitude. However, the level of the tropopause is used to be defined, in the extratropics, by the concept of dynamical tropopause through potential vorticity surfaces. More precisely, as the tropopause can be considered as a boundary, separating troposphere and stratosphere dynamical processes, numerical models have defined the tropopause as the break of the variability of the potential vorticity (PV). The PV describes the value of an air masses vorticity between two isentropic and adjacent surfaces. Thus, the

tropopause is defined as the altitude where the PV is about 2.10^{-6} K m^2 $kg^{-1}.s^{-1}$ (or 2.0 PV Unit (PVU)). In the tropics, the PV cannot be measured because of the PV surface goes to zero near the equator (Hoinka, 1998). Thus, within the tropics, the thermal definition is the only applicable criterion. Hoinka (1998) used both definition of the tropopause (thermal and PV definitions) to get a global tropopause profile, as shown in Figure 2.2. Figure 2.2 illustrates the annual mean meridional profile of the zonally-averaged tropopauses (1979-93; 1200UTC): thermal tropopause (THE); dynamical tropopause with PV = 1.6 (PV1), PV = 2.5 (PV2), and PV = 3.5 (PV3) PVU, from Hoinka (1998).

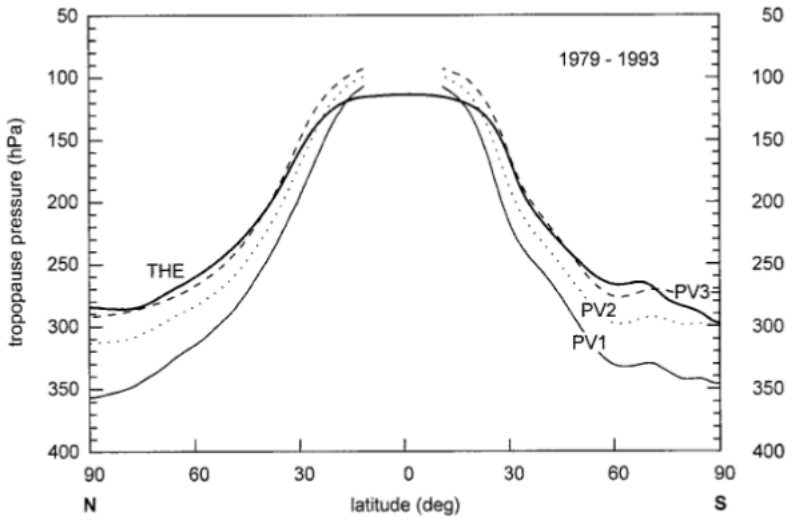

Figure 2.2 – Annual mean meridional profile of the zonally-averaged tropopauses (1979-93; 1200UTC): thermal tropopause (THE); dynamical tropopause with 1.6 (PV1), 2.5 (PV2), and 3.5 (PV3) PVU. (Hoinka, 1998)

Following the World Meteorological Organization (WMO), the tropopause level is also defined as the lowest level at which the lapse rate decreases to 2 K km^{-1} or less, that is, the average lapse rate between this specific level and all higher levels within 2 km does not exceed 2 K km^{-1}.

The level of the tropopause can also be defined by the maximum of wind: the jet

	Tropical	**Extra-tropical**
Temperature	Colder (-80°C)	Warmer (-60°C)
Latitudinal extension	Between the two subtropical jet streams	Between subtropical and polar jet streams
Height	18 km (80-100 hPa)	12 km (200-300 hPa)
Annual cycle altitude	Low amplitude of the annual cycle (lower in summer and higher in winter from 0° to 10° N, and the opposite signal from 0° to 10°S)	Higher in summer and lower in winter
Radiation	Radiative convective balance	Baroclinic wave dynamics
Vertical transport	Upward circulation	Downward circulation

Table 2.1 – Characteristics of tropical and extratropical tropopauses

streams. The change in horizontal temperature in a frontal zone creates a pressure variation at a given altitude. This tropospheric pressure variation helps the increase of winds with altitude up to the tropopause level. The jets tends to be where the tropopause is more vertical than horizontal (see in Figure 2.3). In the stratosphere, however, the variation is opposite and the wind decreases. Thus, four jet streams characterizing the tropopause have been identified: the Arctic, the polar, the subtropical, and the equatorial jet streams (see in Figure 2.3). Furthermore, if above the tropopause, the temperature gradient reaches -3°C km^{-1}, then it is possible to define a second tropopause (as illustrated in Fig. 2.3). Thus, the troposphere can be separated to the stratosphere by multiples tropopauses as defined using the lapse rate definition (Randel et al., 2007). This phenomenon is observed is all season, all longitudes and mainly in the mid-latitude (Wang and Polvani, 2011).

Table 2.1 synthesizes specific differences between the tropical and the extratropical tropopauses. As shown in Table 2.1, the altitude and the temperature of

the tropopause change as a function of the latitude and longitude (Randel et al., 2006b; Fueglistaler et al., 2009a; Suneeth et al., 2017), but it can be averaged around 4-6 km (≈ 300 hPa) and -65 °C in polar regions, 8-12 km (≈ 200 hPa) and near -55 °C in both hemispheres and around 15-18 km (≈ 100 hPa) and -85 °C in the tropics (Rieckh et al., 2014; Graversen et al., 2014)). The latitudinal variation of the tropopause from the poles to the equator is schematically illustrated in Figure 2.3 (Shapiro et al., 1987). In summer, because of the troposphere heating, the altitude of the extratropical tropopause is higher than in winter. However, while the tropopause temperature is stable, the tropopause height shows large variations with seasons, and day-to-day. Furthermore, in the tropics, the isentropic surface at 380 K is usually used as the tropopause level because this surface is located slightly above the surface representing the average level of zero radiative heating in clear sky (concept explained in detail in section 2.2.2.3).

2.1.3 Tropical Tropopause, a transition layer: the TTL

Many studies have tried to understand and define exactly what the tropopause is, and which method is the best for each region in the globe (Reed and Danielsen, 1958; Danielsen, 1959; Shapiro, 1980; Danielsen et al., 1987; Hoerling et al., 1991; Hoinka, 1998; Gettelman and Fothers, 2002; Fueglistaler et al., 2009a). Some authors define the tropopause, no longer as a level, but as a transition layer between the troposphere and the stratosphere, where an abrupt change in temperature lapse rate (K km^{-1}) usually occurs. Define the tropopause as a level has been shown to be difficult because its thickness will vary as a function of different physical processes. For instance, Atticks and Robinson (1983) have proposed the large range of altitudes of the tropopause between 130 and 60 hPa from the study of tropical radiosonde profiles. Randel and Wu (2007) also describe the tropopause by considering that the sharp gradient in radiative cooling affecting

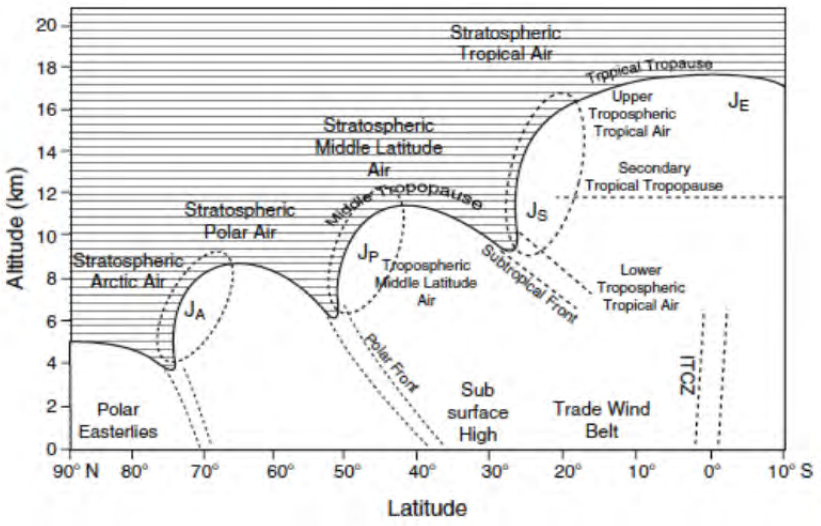

Figure 2.3 – Latitudinal variation of the potential vorticity discontinuity tropopause altitude. The 40 m s^{-1} isotach (thin dashed line) encircles the cores of the three jetstreams: the Artic, J_A; the polar, J_P; the subtropical, J_S; and the equatorial, J_E. The secondary tropical tropopause shows the level of the thermal tropopause. Fronts and the Inter-Tropical Convergence Zone (ITCZ) are marked by fine dashed lines. (Shapiro et al. (1987), Courtesy: American Meteorological Society)

the water vapour and ozone sharp gradient to the tropopause would be the main important mechanisms to sharp the tropopause.

In the tropics, because of strong convective activities (see section 2.2), the tropical tropopause layer presents a zone of mixing between the troposphere and the stratopshere. For that reason, and because the tropopause cannot be defined by the PV, special definitions have been given to the tropical tropopause layer (TTL). The most common definition of the TTL is from Fueglistaler et al. (2009a): delimited by the subtropical jets located around 30 °N and 30 °S, the layer is defined between the surface of 150 hPa (about 350 K and 14 km) and the surface of 70 hPa (about 425 K and 18.5 km) knowing that the surface at 350 K is the level where the jets limit the horizontal transport between the tropics and the extratropics (Haynes and Shuckburgh, 2000).

Others studies defined also the TTL by the layer between the level of maximum convective outflow (10-12 km, 200 hPa) that closely corresponds to a minimum in ozone and the CPT temperature (16-17 km, 100 hPa) (Gettelman and Fothers, 2002; Mehta et al., 2008; Birner and Charlesworth, 2017). An easy way to simulate the TTL in a dry mechanistic model has been to define the TTL as the structure represented by a relaxation to a baroclinically unstable radiative equilibrium (Birner et al., 2002; Birner, 2006; Son and Polvani, 2007). However, considerable discussion are still focused on the sharpness of the TTL and the processes implied. Birner (2010) suggests that the Brewer-Dobson circulation (defined in detail in section 2.3.3), would be an important process impacting the sharp gradient definition of the global tropopause layer. Whatever the definition of the TTL used, transport from the troposphere to the stratosphere (TST) in the tropics occurs through a combination of firstly, deep convective systems and secondly, large-scale three-dimensional circulation (Fueglistaler et al., 2009a; Randel and Jensen, 2013). The relative importance of theses two processes continues to be debated (Alcala and Dessler, 2002; Liu and Zipser, 2005; Carminati et al., 2014). The tropical tropospheric and stratospheric dynamics and transport processes are presented in the section 2.3.

2.2 Tropical convective structures and mechanisms

In the tropics, two types of clouds predominate: cirrus clouds at high altitudes and cumulus clouds at low altitudes (Lin, 2007). Cumulus clouds can be classified in three types as a function of their sizes: the smallest is the cumulus humilis, then the cumulus congestus and the highest is the cumulonimbus (Johnson et al., 1999). To develop a cumulonimbus, the convection has to be very strong, which is called "deep convection". High and thick cirrus clouds, but also slightly thinner, are

often close to the same altitude as the top of the deep convective clouds (mainly in the upper troposphere (UT) and TTL). In fact, cirrus clouds are formed at high altitudes mainly from deep convection. Near the TTL, cirrus clouds can have an impact on the transport of air parcels from convective clouds (Tissier, 2016). This section presents an overview of the convective developments until the convective dissipation, the convective structure and the associated diabatic processes, and its geographical and seasonal variations over the tropics.

2.2.1 Deep convective structures, diurnal variability and mechanisms

Deep convective systems are defined by cumulonimbus clouds extending from lower troposphere to upper troposphere, and formed inside a warm and humid air mass. Three stages are identified for the deep convective formation: the cumulus stage, the mature stage and the dissipating stage (illustrated in Figure 2.4). They are usually caused by daytime heating, are rather isolated and are not attached to a front. Over land, they reach their maximum strength in the late afternoon, and generally dissipate after sunset.

The cumulus stage is generated by an instability of the atmosphere: during daytime, the Sun's radiation heat the Earth's surface which, then, heat the atmosphere surrounding by infra-red radiation and by transfer from the surface. The amount of heat exchanged without taking account of water phase changes is calculated by the **sensible heat flux** while the thermal energy gradient, taking account of the surface water evaporation or water condensation, is calculated by the **latent heat flux** (see more in section 2.2.2.4). During this stage, the cumulus is developed in convective cells: air masses relax and cool down as the atmospheric pressure decreases with altitude (what is called the adiabatic cooling). The ascent is maintained as long as the air masses rising up are less dense than the surround-

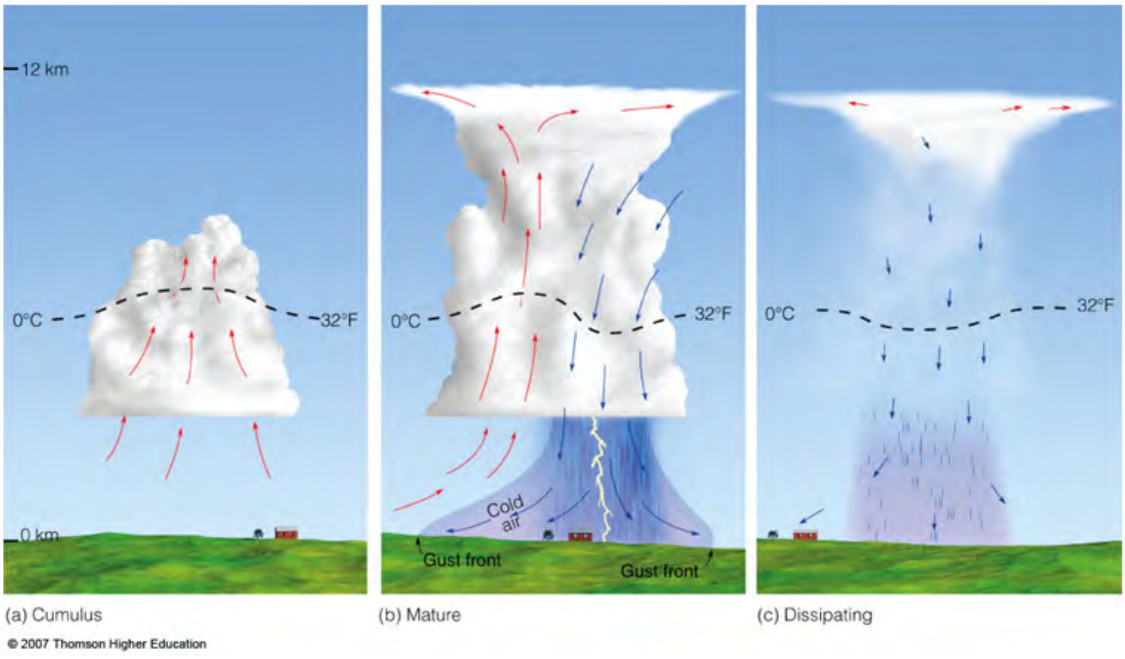

Figure 2.4 – Three different stages of deep convective development. (Image courtesy of Thomson Higher Education.)

ing environment. This difference of density is called the **buoyancy**. The **potential temperature**, θ, is used to evaluate the air masses ascent: it compares air mass temperatures at different pressure levels. In fact, in the tropopshere, θ decreases with altitude (and with the temperature) by reversible and adiabatic (without any exchange of energy or mass with the environment) expansion as follow:

$$\theta = T \left(\frac{p}{p_0} \right)^{\frac{R}{C_p}} \tag{2.1}$$

where T is the temperature, p the pressure, p_0 = 1000 hPa is the reference pressure, $R \approx 287$ J kg^{-1} K^{-1} is the air constant and $c_p \approx 1006$ J kg^{-1} K^{-1} is the thermal mass capacity of the air. The vertical motions are limited by cooler and drier environment and water vapour contained in the air parcels begins to condense: this is the **condensation level**. This level is the bottom of the cumulus cloud. The convection can also be defined as **shallow convection** if the convection is below 500 hPa.

Because of the condensation, droplets release latent heat of condensation, which increases the buoyancy of air masses allowing the air masses to rise even higher. If all the water vapour condenses to liquid phase, the balance between the cooling by expansion and the heating by latent heat can be calculated by the **equivalent potential temperature** θ_e. According to (Holton, 2004), θ_e depends to the mixing ratio of water vapour r_v, the specific heat of dry air at constant pressure c_p (1004J/(kg.K), the temperature T, the potential temperature θ and the latent heat L_v as follow:

$$\theta_e = \theta exp\left[\frac{L_v r_v}{c_p T}\right] \tag{2.2}$$

Because of precipitations which maintains convective systems by constraining the hot and humid air on the surface to rise up, the atmosphere continues to be unstable and larger convective cells can be formed (Khairoutdinov and Randall, 2006). This phenomenon can be amplified by the transport of water droplets that evaporate and cool the surrounding air.

Thus air parcels can firstly even reach the **level of free convection** (corresponding to positive buoyancy) and then quickly rise and reach their equilibrium levels: the top of the deep convective cloud. This is the mature stage of convective development. This stage is well-organized by updrafts and downdrafts. Updrafts can reach the TTL and spread out to form **anvil clouds**. This rapid ascent allows air parcels to be transported quickly from the planetary boundary layer to the UT. In some cases, if the convection is deep, updrafts can reach the TTL and even cross the TTL to penetrate the Lower Stratosphere (LS) by what it is called an "**overshoot**", and has an impact on the chemical composition of this layers. Section 2.2.2.2 details more precisely the ascending processes. Finally, when the cloud environment becomes cool and dry enough because of the mature stage, latent heat is released and the convection is inhibited. Downdrafts, led by en-

trainment of cool and dry air and by falling precipitation, can be then become compared to updrafts: this is the dissipating stage of the deep convection. Once the convective activity is completed, the cumulonimbus anvil often persists in the form of thick cirrus clouds. Section 2.2.2.7 gives more details on the convective descent processes. The time life of a convective cell can be around 30-60 minutes if the convective cell is isolated, and between 10 hours and even 2-3 days for tropical deep convective multi-cells systems (also called Mesoscale Convective Systems, MCS) (Beucher, 2010).

2.2.2 Diabatic processes

In this section, the main convective diabatic processes (processes involving a heat exchange) controlling the entire convective cycle is detailed and illustrated in Figure 2.5.

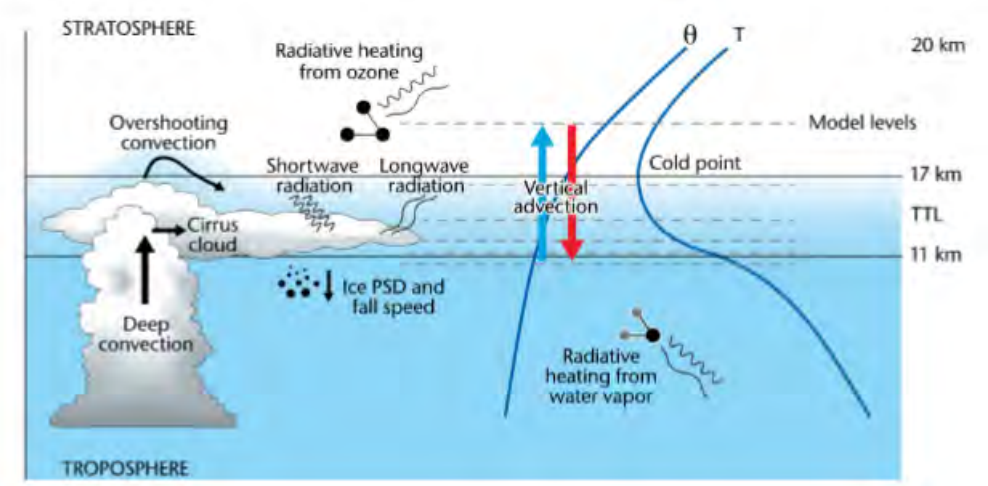

Figure 2.5 – Schematic illustration of the different processes in the TTL affecting the CPT and stratospheric water vapor concentrations. Blue shading represents water vapor concentration, decreasing throughout the TTL (Hardiman et al., 2015).

2.2.2.1 Theoretical model of the air parcel

The convective process of an air parcel can be evaluated by a theoretical model of the parcel (Morton, 1957; Turner, 1973) presented in an tephigram (Figure 2.6). The parcel is characterized by its temperature and its **dew point temperature** (i.e. the temperature when water vapour starts to condense). So the dew point temperature is a function of the amount of water vapour. The model estimates that the air parcel rises following firstly a **dry adiabatic** (T decreases whilst θ is constant) up to the point where its temperature equal its dew point temperature : the lifting condensation level (LCL), (i.e. the base of the cloud). The air parcel follows a **humid adiabatic** (T decreases and θ_e is constant). When the temperature of the air parcel reaches the environment temperature, the level of the **free convection (LFC)** is reached. The air parcel continues to rise up to the level where its temperature is less than the ambient temperature: this is the **level of neutral buoyancy (LNB)**. From the theoretical model of the air parcel, the **convective available potential energy (CAPE)** is used to evaluate the intensity of the convection. The CAPE is calculated by the integration of the area between the parcel trajectory and the environment profile. The **convective inhibition (CIN)** quantifies the energy that an air parcel has to reach the LFC in order to start the deep convection. Thus, in figure 2.6, the temperature of an ascending parcel is compared to the dew temperature (Td) profile of this parcel and to the speudo-adiabatic potential temperature (Tw) profile of this parcel.

2.2.2.2 Convective initiators and ascending processes

For deep convection to rise to its LFC, high energy combined with high mechanical action is required. Air mass **convergences**, for example promoted by breeze from surface heterogeneities (Land-Sea or Mountain-valley), generate the lifting of air masses (Wakimoto and Atkins, 1994). The formation of anabatic winds on

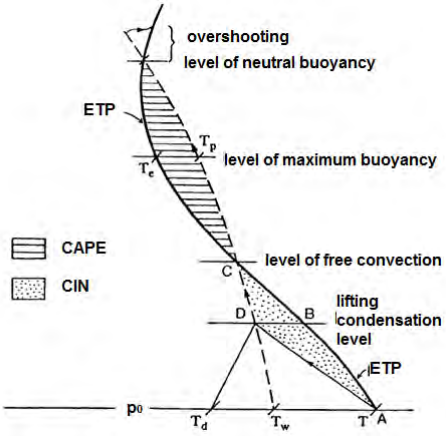

Figure 2.6 – Illustration of theoretical model of an air parcel ascent during a deep convection event. The thick solid line represents the environment temperature profile (T), the thin solid line represent the temperature of an ascending parcel initially at point A, the dew temparature profile is called Td and the dashed line represents the speudo-adiabatic potential temperature (Tw). Dotted area represent CIN, shaded area represent CAPE. Dotted area represents CIN and shaded area represents CAPE. Image from Cairo (2011) – open access peer-reviewed chapter: https://www.intechopen.com/books/thermodynamics-interaction-studies-solids-liquids-and-gases/atmospheric-thermodynamics

warming landforms, or the collision of a breeze front with a gust front (Kingsmill, 1995), also promotes convergences along with the rise of air masses. Furthermore, large-scale convergences such as in the Inter-Tropical Convergence Zone (ITCZ, see more in section 2.3.2), have also a strong role on the air rising into deep convection. The convergence flux of humidity at the surface determines the location of the convective cell. The **vertical wind shear** in the lowest layer of deep convective clouds also has a strong impact on the deep convective structure in shifting the precipitation and the downdrafts out of the center of the convective systems, where humid and hot updrafts provide the convection. This process makes the convective systems become larger because of its propagation, which form multi-cells and increasing considerably the time life of the deep convection.

Once the convection is generated, convective ascents transport air masses up

in altitude by **updrafts**. In general, convective updrafts are less than 500 m in size (Yang et al., 2016). However, in the tropics, deep convective updrafts can reach about 4-7 km in size (Yang et al., 2016) and more than 17 km in altitude (Fueglistaler et al., 2009a). The updraft speed can reach 11 m s^{-1} in median value (Varble et al., 2014), while shallow convections reach vertical speed of about twice less (Schumacher et al., 2015). In comparison, stratiform clouds (composing the convective anvil), has updraft speeds only about 1 m s^{-1}. Some studies have shown that, in deep convection, the updraft is composed by a succession of bubbles rising one above the others up to the top (Ludlam and Scorer, 1953; Zhao and Austin, 2005; Heus et al., 2009; Sherwood et al., 2013). Some study also suggests that the air masses transported in deep convective updraft come from a layer very close to the surface, within the planetary boundary layer (McGee and van den Heever, 2014).

2.2.2.3 Radiative processes

Solar radiation has an impact on the convective processes and on the stratospheric-tropospheric interaction processes (Hartmann et al., 2001; Fueglistaler et al., 2009a; Tzella and Legras, 2011). Solar radiation impacts heating of the air masses. Clouds in the UT and TTL have got a strong impact on radiation. Solar radiation penetrating into the stratosphere and the troposphere depends on the absorption of each constituent present in these layers (Mohanakumar, 2008). Greenhouse gases have a warm effect on the atmospheric temperature by the atmospheric emission of infra-red radiation such as water vapour in the troposphere, controlling the overall radiative balance of the troposphere.

In region of the atmosphere where clear sky condition occur, horizontal transport can facilitate air masses to cross the TTL. To reach the stratosphere, an air parcel of air must go through the level of Zero Radiative Heat (LZRH, about 360 K or

125 hPa (Gettelman et al., 2004a; Fueglistaler et al., 2009a)), which can be a barrier to the transport of air parcels of air to the stratosphere (Folkins et al., 1999). Below this level, as radiative heating is negative, air parcels tend to descend to the troposphere. Above this level, radiative heating is positive and air parcels tend to rise towards the stratosphere. Thus, the lower the LZRH will be, the easier the air parcel will ascend up to the TTL or even the LS (Corti et al., 2005). Figure 2.7 presents the vertical profile of the different fluxes into the tropical troposphere during convective activity.

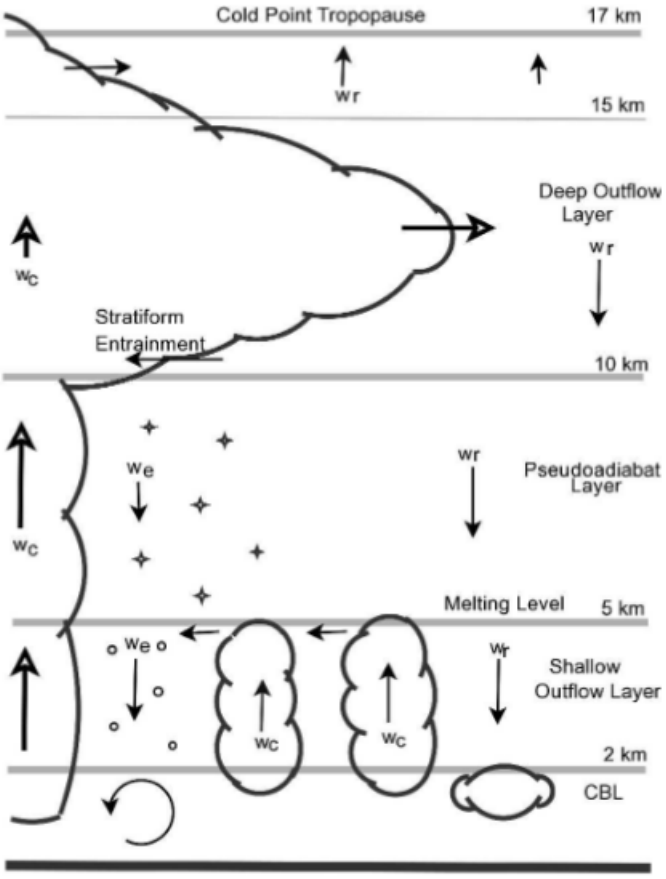

Figure 2.7 – Vertical profile of the mass flux associated with in-cloud heating (w_c), clear sky evaporative cooling (w_e), and clear-sky radiative cooling (w_r), (Folkins and Martin, 2005)

2.2.2.4 Microphysical processes

The water convective microphysical processes are characterized by the water phase changes and the absorption or the release of latent heat flux in an air mass. Condensation or freezing release latent heat while evaporation or melting absorbs latent heat. Furthermore, condensation and evaporation release and absorbs respectively, the vapour latent heats (whilch varies strongly with the temperature). However, freezing and melting, release and absorbe respectively, the fusion latent heats (which varies little with the temperature). Water vapour can also be deposited on ice crystals, which also releases heat into the environment. Conversely, the ice sublimation into water vapour absorbs latent heat. In this case, the sublimation latent heat varies little with the temperature. According to Seigel et al. (2013), the release and the absorption of the latent heat can appear alternatively by cycles, following the ice crystal formation, fall, melting and then, training for a new ascent, which can freeze again. Figure 2.8 illustrates the water microphysical processes.

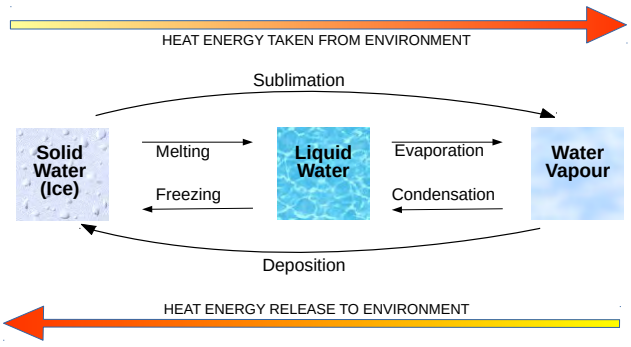

Figure 2.8 – Water Vapour phase changes and associated energy transfers

2.2.2.5 Turbulent processes

Convective wind shears promote the convective turbulence by formation of eddies in the convective cell. An energy cascade is built among the various vortices composing the convective system, helping the air masses to exchange with the surrounding environment. Unsaturated air transported by non-turbulent flow from the environment (dry wind) can be captured by the convective turbulent flow and transported into the convective system. This phenomenon is called the **entrainment phenomenon** and happens on the sides of the convective system and not on its top (Heus and Jonker, 2008). Usually, the entrainment occurs in the lower part of the cloud and can be transported by updrafts. However, the higher in altitude the entrainment occurs, the drier are air masses transported by updraft up to the cloud top. In contrast, the turbulent phenomenon ejecting air masses from the convective system to the environment is called the **detrainment phenomenon**. The detrainment occurs usually at the top of the deep convection and participates in the formation of the anvil. These two phenomena induce mixing of air in the convective system, decreasing the buoyancy and promoting a decrease of water vapour in the convective system because the air transported from the environment is drier than the air inside the cloud.

2.2.2.6 Overshoots

Deep convective overshoots are the part of the cloud overtaking the flat top of the cumulonimbus clouds (see illustration in Figure 2.5). Overshoots can measure several kilometres of height over the top of the cumulonimbus, even crossing the TTL and reaching the lower stratosphere. The overshoot time life is short (30-60 minutes according Chaboureau et al. (2007) and Frey et al. (2015)) and can cover large horizontal surfaces (tens to hundreds of kilometers depending on the altitude, Hassin and Lane, 2010). Overshoots are an important way for the tropo-

sphere to stratosphere transport of air masses and water. However, the frequency of overshoots is low (Liu and Zipser, 2005; Fu et al., 2007)). Dauhut et al. (2015) have estimated to 18% the amount of overshoot compared to the total deep convective events. According to a study from Luo et al. (2008), using datasets from the space-borne CloudSat, only 1.3% of convective clouds reach surfaces higher than the CPT. Fu et al. (2007) have determined from datasets from the CALIOP lidar that, over all the tropics, 0.5% of clouds reach 18.5 km whereas 5% reach 17 km. But only overshoots would not be enough to explain the amount of air crossing the tropopause and maintaining the global circulation controlled by the Brewer-Dobson circulation (circulation detailed in section 2.3.3). Many other studies have tried to quantify the impact of deep convective overshoots on the transport of air masses up to the LS at global and local scales (Zhang, 1993; Gettelman and Fothers, 2002; Liu and Zipser, 2005; Rossow and Pearl, 2007; Dauhut, 2016). Although the convective overshoots are still difficult to represent in models, measurements from high altitude aircraft, groundbased radar or space-borne observations of brightness temperatures (highlighting overshoots because of their very cold temperature) are currently being used to better understand the impact of overshoots on the troposphere to stratosphere transport (Schmetz et al., 1997; Romps and Kuang, 2009; Bedka et al., 2010).

2.2.2.7 Subsidence, precipitation and cold pockets

Precipitation is classified into three main types: stratiform rainfall, shallow convective rainfall and deep convective rainfalls, as presented in Figure 2.9. Stratiform and convective precipitations are the two main forms of precipitation with the strongest amount of precipitation.

Stratiform precipitation (or stable precipitation) results from slow and large-scale lifting of a moist air mass that condenses uniformly. Associated clouds are strat-

iform clouds (grey and uniform slick appearance: nimbostratus, stratocumulus, stratus). Stratiform precipitations have low or moderate intensity (less than 10 mm^{-1}) and long duration due to the slow displacement or orographic blockages. These precipitations are well simulated in models. Convective precipitations (or unstable precipitations) result from the quick rise of moisture-laden air masses by Archimedes' principle. This type of precipitation comes from cumuliform clouds able to reach 10 to 18 km of altitude. Convective precipitations are characterised by very strong intensity and short duration (between 30 minutes and few hours). This precipitation can be accompanied by thunderstorms, ice pellets or hail and gusts of wind. Stratiform and convective precipitations can be observed together, resulting into unstablilities into stratiform rain or snow masses and on heavier showers. Conversely, mature or aged storm systems often have a more or less extensive stratiform zone in which precipitation is regular and less intense.

Convective subsidences are controlled by downdrafts, which are formed as a result of the evaporation of some of the hydrometeors. In fact, because of the cooling effect of evaporation, the air masses buoyancy is decreasing, and the air masses heading towards the surface. Usually, downdrafts form a sort of shell surrounding the updrafts. When the downdrafts reach the surface, **cold pockets** of dense and cold air masses are formed and spread at the surface. The cold pockets are responsible for cold front causing surface gust winds. Sometimes, gust winds can carry again hot and humid air masses a little further away, towards a new deep convection cell. Thus, while the convection is still active, some new deep convective cells can appear near the cold pockets of the convection, and make the convection become deeper.

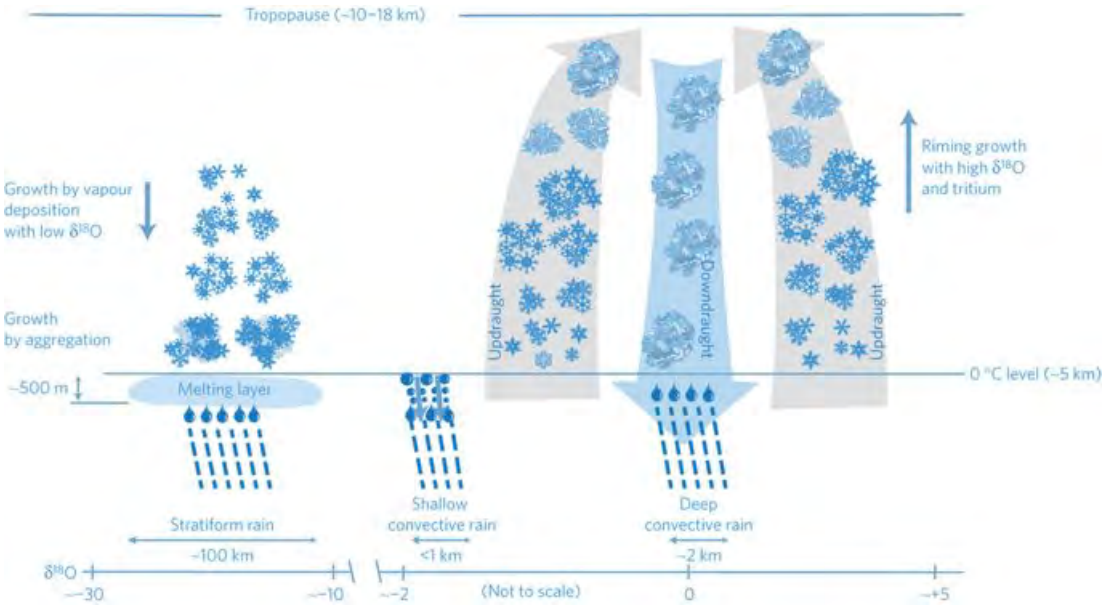

Figure 2.9 – Figure 2 from Aggarwal et al. (2016): Schematic representation of differences in dynamical and microphysical processes in convective and stratiform precipitation resulting in isotope variations.

2.2.3 Geographical and seasonal variability of deep convection

In general, deep convection is observed in the tropics, in the Walker cell ascent areas, over continents (see definition of the Walker cells in section 2.3.1). In fact, above land, as the atmosphere is more unstable, the dilution of convective cells by the surrounding air is slightly lower (Zipser, 2003), and the convection is stronger than over ocean. However, deep convection is also observed over ocean but at lower frequencies (Liu and Zipser (2005)). Cumulonimbus clouds formed over ocean decrease in intensity when they are transported over the continent at night and increase during the day. Cumulonimbus clouds intensity is also stronger in summer and weaker in winter. More precisely, in Africa, deep convection is observed from the equator to about 15°N between March and November, and from the equator down to 15°S between December and January. The Congo Basin is an area where the deep convection can be active all over the year, as well as over

the Asian region such as over the Indonesian archipelagos (also called and defined later the Maritime Continent region). In South America, deep convection is observed from the equator down to 40°S from September to March. June, July and August are the three months when deep convection is mainly active in the Northern hemisphere, especially in Central America. In contract, the austral convective season is mainly found during December, January and February (Fueglistaler et al., 2009a).

2.3 Tropical tropospheric and stratospheric dynamic processes

Processes controlling the troposphere to stratosphere transport (TST) are dynamical, microphysical and radiative processes. In the tropics, three main atmospheric circulations have been identified to influence exchanges between the tropical troposphere to the stratosphere and to control the global air masses distribution: the Hadley circulation, the Walker cells, and the Brewer - Dobson circulation. More precisely, Walker cells and Hadley cell do not play a direct role in TST, but they influence it in affecting spatial distribution. These circulations help to transport the excess of energy received in the tropics towards mid-latitudes (Berson, 1961; Krueger and Winston, 1974; Bony et al., 2015) (see below sections 2.11 and 2.10). This section presents the main tropical tropospheric and stratospheric characteristics and links.

2.3.1 Tropospheric zonal transport of energy: the Walker cells

The Walker cells are aligned in the an east-west direction and result from the zonal gradient in surface temperature linked to the differences between the ocean

and land surface temperatures. Over the warm South America, Africa and the area called Maritime Continent (between the Indian Ocean and the Pacific Ocean) the air masses rise up to the tropopause by deep convection in summer when the solar radiation is maximum. The calorific capacity of the ocean is stronger than the calorific capacity of the continent. Thus, ocean stores thermal energy more easily than continent. In addition, this energy is redistributed more easily by the ocean, via subtropical gyres and thermohaline circulation, whereas continental surfaces have low thermal conductivity. Thus, the excess of energy accumulated over tropical continents requires a faster vertical redistribution, which leads to strong atmospheric vertical movements observed in the Walker circulation (Figure 2.10).

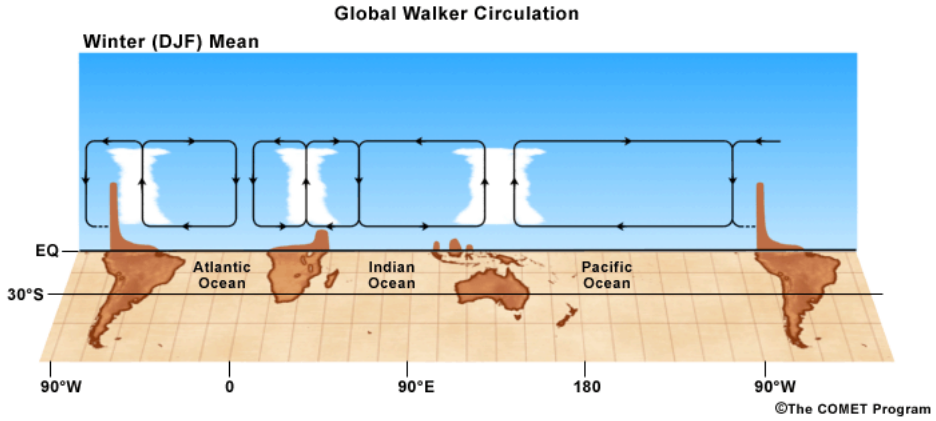

Figure 2.10 – Walker circulation: Schematics of the (upper) Pacific Walker Circulation and (lower) global Walker Circulation for Winter (DJF) based on computations of upper and lower tropospheric divergent winds.

2.3.2 Tropospheric meridional transport of energy : the Hadley circulation

The meridional thermal surface gradient has a strong impact on the atmospheric circulation. In the tropics, the Hadley cells are the largest tropospheric cells

among the three wind cells (with Ferrel and Polar cells, located in the mid-latitude and polar regions, respectively). More precisely, theses wind cells are circulations in the height-latitude plane. The energy received in the equator surface is transported by air masses during convective activity up to the tropopause. Because of the very low temperature of the tropopause, air masses cool down and dry and water vapour condensates during the air masses ascent. Then, the air flows poleward to 30°-40°latitudes in both hemispheres where the air masses sink (Figure 2.11). Coriolis strong winds transport a part of the air toward the equator, which becomes warmer and start to rise again in a new cycle. This produces winds called the trade winds and the tropical easterlies. The area between the northern and southern Hadley cell is called the Inter Tropical Convergence Zone (ITCZ) and is defined by the low pressure where the bottom of the cells converge. The ITCZ moves around the equator in shifting north or south as a function of the season.

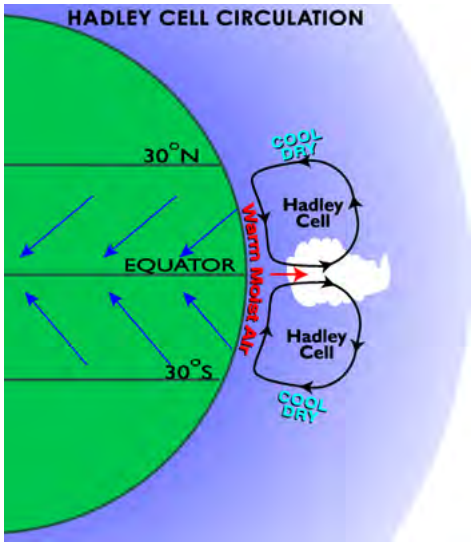

Figure 2.11 – Hadley Cell illustration (Image courtesy of Tinka Sloss – `https://www.windows2universe.org/earth/Atmosphere/hadleyCell.html`)

2.3.3 Tropical stratospheric dynamics: the Brewer and Dobson cirulation

Air masses following the Hadley cell, reach the TTL by deep convection and can enter into the tropical stratosphere where they join the rising branch of the global circulation called the Brewer-Dobson Circulation (BDC), transported upward and poleward. After cooling during the transport toward middle and high latitudes, air masses descend back into the troposphere (Dobson et al., 1929; Brewer, 1949; Holton et al., 1995; Butchart, 2014). This circulation has a strong impact on the global air masses distribution (and affects the distribution of important chemical species). One evidence of the BDC is the transport of the stratospheric water vapour in the winter hemisphere from the tropics upward and towards extra-tropics (Brewer, 1949; Potter and Holton, 1995; Randel et al., 2006a). Combined with seasonal variation, the transport of water vapour from tropics to extra-tropics is called the Tape Recorder effect (Mote et al., 1996). Figure 2.12 illustrates the stratospheric transport of air from the tropics to higher latitudes (Randel and Jensen, 2013). Although the altitude of the TTL upper boundary is nearly uniform throughout the tropics, water vapour in the LS has a pronounced annual cycle. The South Pacific Convergence Zone (SPCZ), the band extending from the East of the Maritime Continent to the French Polynesia (160W, 20S), and a portion of the Intertropical Convergence Zone (ITCZ), is also a consequence of the tropical convergence affecting strongly the precipitation annual and interannual variabilities and the TTL temperature and altitude. Furthermore, the interannual variations of the TTL result from changes in the large-scale organization of convective activity, such as the annual cycle of the strength of the upwelling in the BDC, the descending zonal wind regimes in the quasi-biennial oscillation (QBO), and the interannual El-Nino-southern Oscillation (ENSO) (Gettelman and Fothers, 2002).

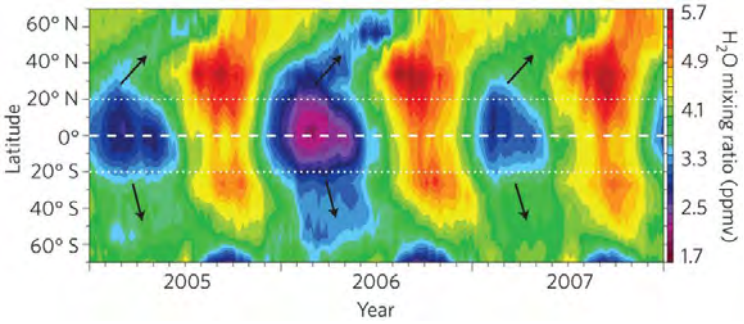

Figure 2.12 – Satellite Observation of water vapor in the lower stratosphere demonstrates the transport of air from the equator to higher latitudes (Randel and Jensen, 2013).

2.3.4 Equatorial Waves

A wave is a form of disturbance which can propagate in space and through this propagation transmit energy. The wave speed can be controlled by the temperature (acoustic waves), the stability (gravity waves), the Coriolis parameter (Kelvin waves) or the latitudinal variations in the Coriolis parameter (Rossby waves). There are a lot of waves that are trapped near the equator, i.e. their amplitude is largest near the equator and decrease with latitude. Kelvin and mixed Rossby gravity waves play a role on the Walker circulation in the troposphere, but also the Madden-Julian Oscillation (MJO, presented in chapter 4), and the ENSO mainly because of the Kelvin waves which are always propagating eastward at the equator (Asnani, 2005). Furthermore, some studies have shown that tropospheric and lower stratospheric spatial distribution of the gravity waves energy would have a little correlation (Wang and Geller, 2003). Thus, equatorial waves have a significant role on the troposphere-stratosphere interactions (Mohanakumar, 2005).

2.3.5 Times scales in the tropics: annual and diurnal cycles

Annual and diurnal cycles are the two time components known as the main tropical atmospheric time variations and corresponding to the time period of the Earth

rotation and Sun revolution, respectively (Seidel et al., 2001; Jain et al., 2006). In the tropical band, the annual cycle time can be divided in two convective seasons: the austral convective season (December, January, February, or DJF) and the boreal convective seasons (June, July, August or JJA). The pronounced annual cycle of water vapour in the LS is shown figure 2.12. Furthermore, the easterlies tendency of the lower stratospheric winds in the summer hemisphere and the westerlies tendency in the winter hemisphere is called the Annual Oscillation (AO) (Reddy and Vijayan, 1993; Guharay et al., 2009). The annual cycle can also be interspersed by intra-seasonal oscillations, sush as the Madden Julian Oscillation (MJO) or the ENSO. These two intra-seasonal oscillations will also have a strong impact on the global climate and weather. Chapter 4 will focus on the importance of these two intra-seasonal oscillations on the water budget in the TTL. However, the amplitude of the convective activity diurnal cycles in tropics is ten times stronger than the amplitude of the convective activity annual cycles (Beucher, 2010) and it is one of the main characteristics of tropical deep convection. In fact, diurnal cycle time scales influence many diurnal processes such as land and sea breezes or mountain and valley winds or thermal tides, characterized by thermal differences following the diurnal Sun heating at local and global scales. Many studies have studied to the diurnal cycle of precipitation in the tropics. For instance, based on the measurements from the Tropical Rainfall Measuring Mission (TRMM) instrument, the tropical diurnal cycle of deep convection has been studied by Liu and Zipser (2005). Figure 2.13 illustrates the diurnal cycle of precipitation over the tropical land and ocean. This figure shows that Mesoscale Convective Systems (MCSs) impact strongly the amplitude of the diurnal cycle of the Rainfall volume over oceans. Over land, the amplitude of the diurnal cycle of the rainfall volume is mostly characterized by features with significant ice scattering. Thus, this figure highlights the processes differences between lands and

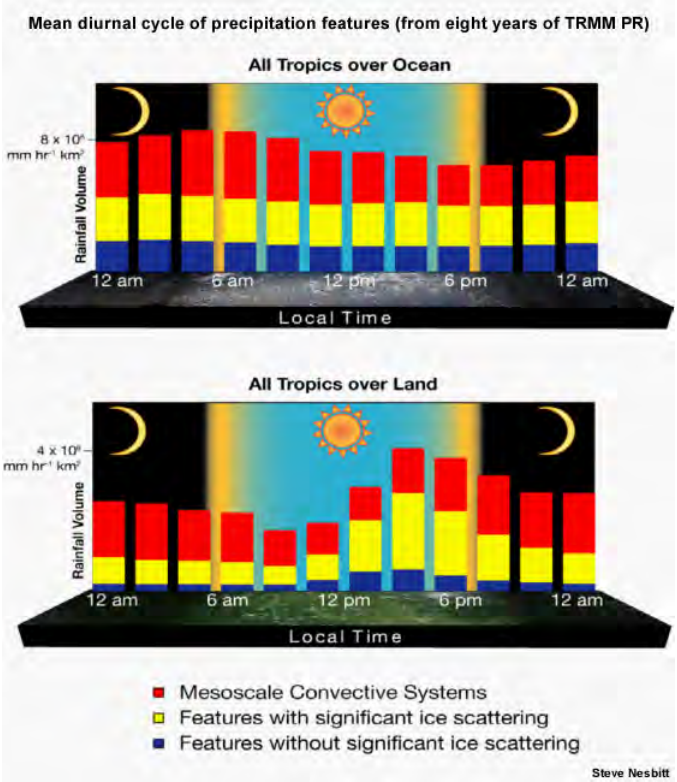

Figure 2.13 – The mean diurnal cycle of precipitation features identified from eight years of TRMM PR data over the tropical oceans (upper) and land (lower). (Image courtesy of Dr. Steve Nesbitt COMET® ©1997-2017, University Corporation for Atmospheric Research. All Rights Reserved.)

ocean impacting on the diurnal cycle of the rainfall volumes.

Over ocean, many hypotheses have been proposed to explain the diurnal maximum in the morning and minimum in the afternoon. One of the explanations can be that, during the afternoon, the top of the deep convection stops the sunlight reaching the surface by absorbing it, increasing the static stability of the clouds and reducing the active convection and precipitation (Cox and Griffith, 1979; Webster and Stephens, 1980; Randall and Dazlich, 1991). However, during the night, oceanic clouds would lose heat quickly, increasing the instability and the strong precipitations during the early morning. The diurnal cycle could be also modulated by the heating gradient between convection and the surrounding air im-

pacting the winds which control the convection (Gray and Jacobson J., 1977). An other factor could be the loss of long-wave radiation at night, cooling the cloud, and increasing the relative humidity, which helps the cloud development (Dudhia, 1989; Tao et al., 1996; Dai, 2001). The diurnal cycle of temperature up to the TTL has been studied by Khaykin et al. (2013): over land and during the convective seasons, diurnal maxima of temperature are found at the end of the morning, while diurnal minima are found at the end of the afternoon.

The diurnal cycle of convective and stratiform precipitations has been studied by Churchill and Houze (1984) for a MCS near Borneo (Figure 2.14). Diurnal cycle of convective precipitation starts to increase around 12:00 greenwich mean time (GMT) while diurnal cycle of stratiform precipitation start to increase 2 hours later around 14:00 GMT. Diurnal maximum of convective precipitation is reached around 23:00 GMT while diurnal maximum of stratiform precipitation is reached 1.5 hour later, around 00:30 GMT. After the diurnal maximum, convective precipitation rate decrease quickly by about 3 area-integrated precipitation rate in 2 hours, while stratiform precipitation decrease slowly by about 1 area-integrated precipitation rate in 4 hours.

2.3.6 Madden Julian Oscillation

The Madden Julian Oscillation (MJO) is defined as a intraseasonal oscillation occuring mostly between September and April and lasts 40 to 80 days in tropics. The MJO is a large signal in atmospheric circulation, deep convection, and others variables. The MJO effects impact mostly the Indian Ocean, Maritime Continent and the Western Pacific regions, by developping intense precipitations evens propagatating eastward from Indian Ocean to the Pacific Ocean. More precisely, the MJO is divided in to 8 phases (Figures 2.16 and 2.17). Each phase can be defined by its geographical location from the West to the East of the MariCont

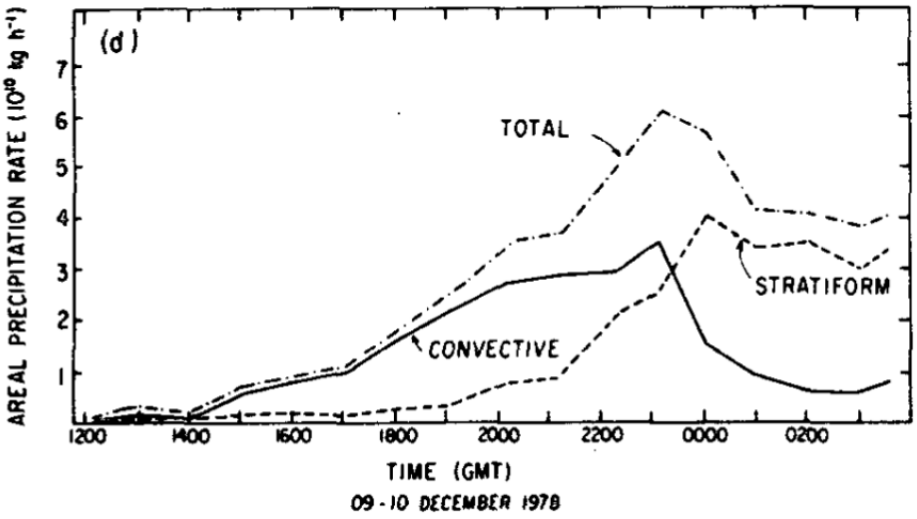

Figure 2.14 – Area-integrated Precipitation Rate (at 3km) for a Mesoscale Convective System near Borneo. Comparision between convective and stratiform precipitation, from Churchill and Houze (1984) (Figure 19 d).

region. Figure 2.16 presents the geographical moving of precipitation anomaly during MJO events (averaged from 1979 to 2012, Gottschalck et al. (2013)). Each phases are modulate by the underlying surface properties and the solar diurnal cycle. Furthermore, it is known that the MariCont presence can also modulate the phase speed of the MJO (Neale and Slingo, 2003). For each of the 8 phases, the MJO is composed into two parts: the enhanced rainfall (composed by deep convection) part surrounding by two suppressed rainfall parts, as presented in Figure 2.15. This two phases works as a dipoles with two main opposite center of action propagating eastward. During the convective phase of the MJO, convergence of winds at the surface imply upward motion. The rising air masses make condensate water vapour and make increase the rainfall. Near the tropopause, winds diverge. Active convective phase results on extreme rains. Suppressed convective phase is characterized by divergence of winds at the surface and convergence of winds in the top of the troposphere, forcing air to sink down to the surface.

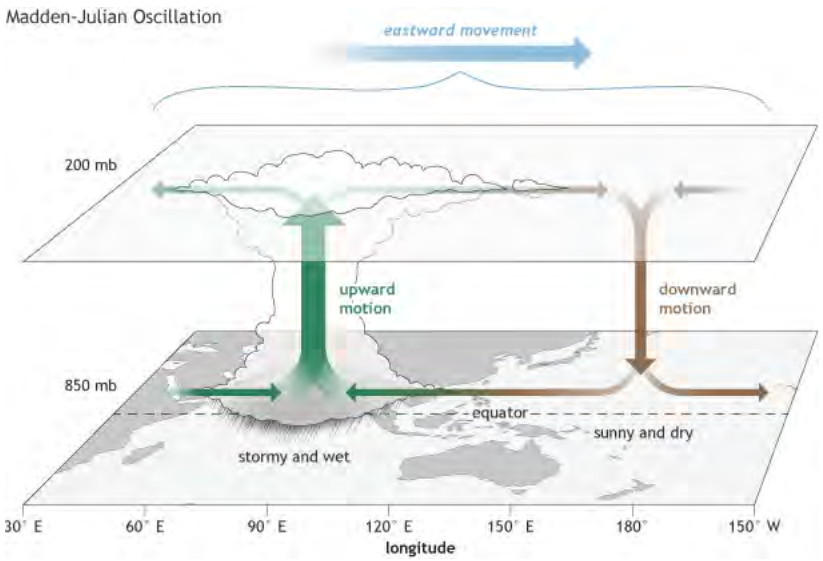

Figure 2.15 – Illustration of processes during the active (green) and suppressed (brown) phases of the MJO. Horizontal arrows represents the local wind directions, while the entire system shifts eastward over time (circling the globe to return to its point of origin). Climate.gov drawing by Fiona Martin.

The phase and the intensity of the MJO can be defined by the Real-time Multivariate MJO (RMM) index. Figure 2.17 presents the MJO diagram, illustrating the progression of the MJO through the 8 phases. The diagram is used in a real-time to produce the signal describing the MJO, through the geographical location of the active phase of the MJO. RMM1 and RMM2 are mathematical methods using several parameters such as the clouds amount, the winds at the surface and in the upper troposphere, providing the intensity and the location of the active phase of the MJO as a function of time. Higher than 1 RMM1 and 1 RMM2 the MJO can be defined as in active phase.

The MJO typically recurs every 30 to 60 days. The MJO is generally observed from outgoing longwave radiation (OLR) because of the important amount of thunderstorms during the MJO (having very cold tops which emits low levels of longwave radiation).

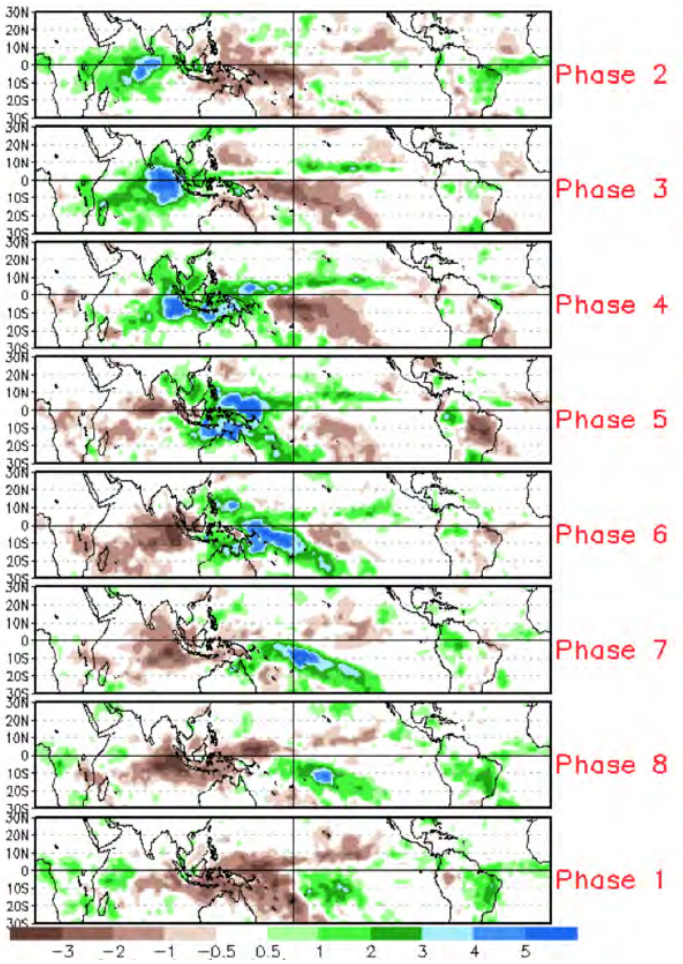

Figure 2.16 – Anomaly of precipitation (during MJO from 1979 to 2012 for November-March) defining the 8 phases. Green shading areas denotes the enhanced convective phase of the MJO while the brown shading areas correspond to the suppressed convective phase of the MJO.

2.3.7 El Nino Southern Oscillation

The El Nino Southern Oscillation (ENSO), is an inter-annual climate and oceanic variability around the world but having also a strong impact on climate over the MariCont. It is called El Niño, episodes of warm oceanic current near the coast of Peru and Ecuador associated with an unusually large warming occurring few years and changing the local and regional ecology (Trenberth, 1997). El Niño episodes

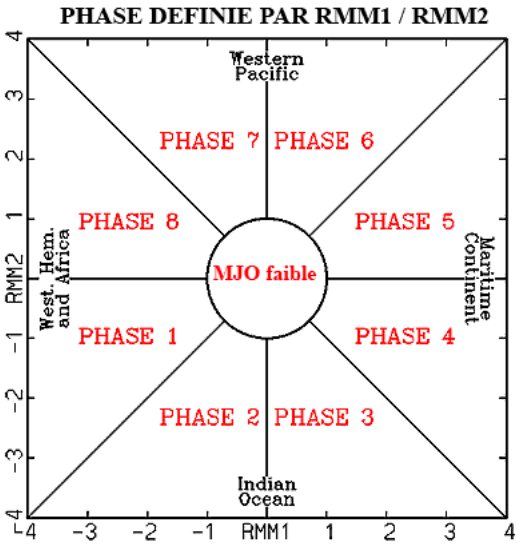

Figure 2.17 – 8 phases of MJO defined from RRM 1 and RMM2. Localisation of the MJO RRM1 and RMM2 parameters, defines the MJO intensity and phase.

also impact the global atmospheric conditions. During El Niño, convective activity increase over Pacific ocean and Africa while dry sinking air, representative of inhibited convection occurs over the region called Maritime Continent and South America (see (Fig. 2.18). The opposite signal is called La Niña and is marked by cold oceanic current and inhibited convection over the Pacific Ocean while strong convection is observed over the Maritime Continent region. During La Niña, atmospheric circulation is also impacted with strong convective activity over the Maritime Continent (see Fig. 2.18). Finally, it is called Neutral condition, periods without La Nina nor El Nino episodes. El Niño, La Niña and Neutral conditions of ENSO vary erratically as a function of time, as presented in Figure 2.19.

2.3.8 Transport across the tropopause

The tropopause is considered as a boundary where air masses have difficulties to cross the CPT, limiting the formation and extension of convective clouds. To cross

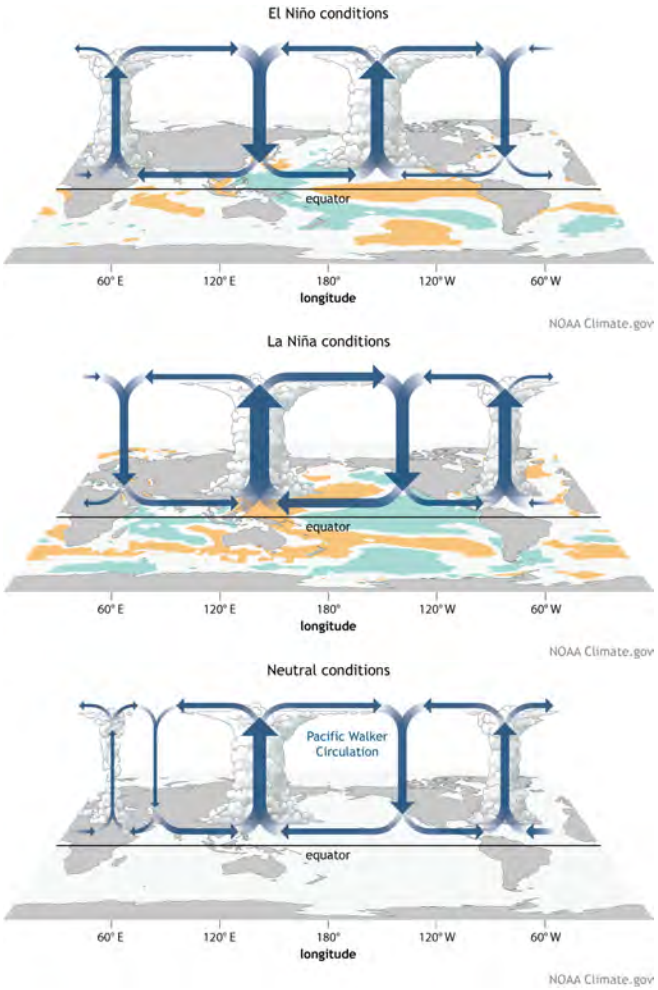

Figure 2.18 – Atmospheric circulations during El Niño (top), La Niña (middle) and Neutral (down) periods over tropics – NOAA.Climate.gov

the tropopause, in either direction, a parcel of air must go through isentropes under the effect of heating, radiative cooling, diffusion, or phase change (condensation or evaporation). However, the latter case is negligible since the water vapour concentration is too low for this effect to be significant, except in deep convection with overshoots. Thus, for instance, an air parcel during storm events will enter more easily and quickly into the stratosphere (few hours) than an air parcel during clear-sky conditions (few months) (Corti et al., 2006). It is hard for an air parcel

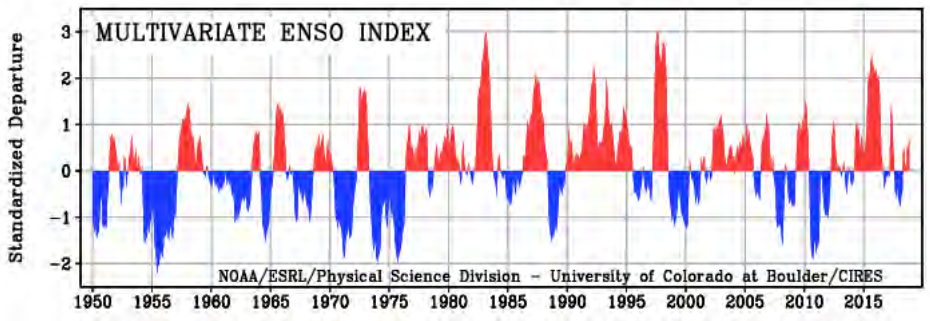

Figure 2.19 – Temporal variability of ENSO Index from 1950 to 2015 – NOAA/ESRL/ Physical Science Division

to directly reach the stratosphere. One hypothesis is that the air parcel would be transported firstly horizontally by the wind until crossing a low in altitude LZRH, allowing the ascent of the air parcel (Tzella and Legras, 2011). With this hypothesis, in the absence of clouds, the ascent is slow (Holton and Gettelman, 2001; Gettelman et al., 2004b). Tropical cirrus would through its radiative effect down the LZRH and favour the vertical advection for a quicker ascent (Dinh et al., 2012; Corti et al., 2006). Thus, the TST depends on the association of convection, radiative heating, and large-scale transport (Gettelman et al., 2004a; Gettelman and Fothers, 2002; Devasthale and Fueglistaler, 2010; Corti et al., 2006; Tzella and Legras, 2011). Many authors have shown that the air enters the stratosphere from the troposphere preferentially above deep convective clouds during convective periods and over convective areas where the tropical tropopause temperature is the lowest. This phenomenon mainly occurs over the specific region between the Indian Ocean and the Pacific Ocean and have been called the "Stratospheric Fountain" (Newell and Gould-Stewart, 1981). However, this phenomenon has been contradicted because of low temperature of this region, making the subsidence predominant (Sherwood and Dessler, 2000; Gettelman et al., 2000). Furthermore, the injection of water vapour into the stratosphere would be increased by a warmer forenoon tropopause (Suneeth et al., 2017).

2.4 Water Budget in the tropics: Troposphere to Stratosphere

Water is one of the rare chemical compounds to be present in 3 phases (solid, liquid and gas) in the atmosphere. However, near the TTL, because of the very low temperature, water is only found as vapour and ice. Many studies have worked on the amount and impact of water budget in the troposphere and stratosphere on climate and weather (e.g. (Folkins and Martin, 2005; Carminati et al., 2014; Tian et al., 2018)). The state-of-the-art of the main characteristics and roles of the water budget, is detailed as follow: in the troposphere (section 2.4.3), the TTL (section 2.4.4) and in the stratosphere (section 2.4.5).

2.4.1 Water Vapour and Ice

Water Vapour (WV) is one of the main greenhouse gases (with ozone and carbon dioxide), and controls the radiation balance of the Earth's atmosphere system. The main atmospheric source of WV in the troposphere is the evaporation from the surface (and evapotranspiration from the vegetation) and the main sink of WV in the troposphere is its condensation resulting into clouds and precipitation. Thus, the troposphere contains about 99% of the total atmospheric WV. The WV lifetime in the atmosphere is on average about 10 days (Mohanakumar, 2005). Furthermore, WV is the unique constituent able to reach saturation conditions in the atmosphere (see section 2.4.2 and 2.4.3). WV is used to be measured in **mixing ratio**, i.e. the mass of water vapour divided by the mass of dry air, in g kg^{-1} or ppmv (concentration of WV divided by the density of air and multiplied by 10^6). Because WV is less dense than dry air, the density of an air mass ρ depends on its temperature and its humidity. In the atmosphere, above the 0°level, rising air masses into deep convection, are mostly composed of ice crystals (2.9). In fact, ice in

the UT mainly comes from liquid water transported into the UT by convection, which freeze with the decrease of the temperature in altitude. Thus, ice is formed by condensation of WV onto insoluble nucleating particles (mean radius < 2 μm) (Mossop, 1963). The most active nuclei spread worldwide are soil dust as well as particles of extraterrestrial origin (Mossop, 1963; Cantrell and Heymsfield, 2005). However, some debates still exist on the mechanisms and differences of ice homogeneous and heterogeneous nucleation. According to Cantrell and Heymsfield (2005), cumulus and stratus clouds would be dominated by heterogeneous nucleation of ice. This first ice production would be follow by a second ice production by using the previously produced ice as new element of nucleation. Thus, this process multiply the ice nucleation and control the amount of ice concentration (Cantrell and Heymsfield, 2005). The nucleation rate (estimated in cm^{-3} s^{-1}) has been shown increasing linearly with temperature decrease (Cantrell and Heymsfield, 2005). However, the ice nucleating particles are difficult to estimate because of their low numbers (Lacher et al., 2017). The crystal number distribution peaks diameters have been estimated below 10 μm (Gayet et al., 2004). However, Ström et al. (1997) have shown that the size distribution of the ice crystal is impacted by small aerosol particles (diameters <0.5 μm) participating in the nucleation of cirrus crystals at low temperatures. Furthermore, some chemical reactions can occur on the ice formed in the upper troposphere. For instance, a liquid layer surrounding the ice surface can be formed in ice exposed to HCl vapour at certain pressure conditions (Abbatt and Molina, 1992). This liquid layer will have consequence on the amount of ice concentration. Ice concentration is usually calculated by the **ice water content** (IWC, in mg m^{-3}). In the tropical tropopause, the IWC decreases from 40 mg m^{-3} in the middle troposphere to 10^{-2} g m^{-3} near the tropopause (Reus et al., 2009). Tropospheric and lower stratospheric ice affects many processes in the tropics, such as the albedo, the formation of precipitation and the cloud

lifetime. For instance, the ice nucleation is an important factor of dehydration in the tropical tropopause layer (Jensen et al., 2012, 2013). Furthermore, ice cirrus clouds can act like a greehouse gas by warming the atmosphere but can also cool the atmosphere by reflection of the solar radiation back to space. Thus, warming or cooling from cirrus clouds depends of the thickness of the ice cloud (Stephens and Webster, 1981). However, the entire ice formation mechanisms in these two layers, and its impact on the atmospheric processes and sink, are still not well understood (Lacher et al., 2018). This thesis aims to bring new elements to the understanding of the processes related to the formation and destruction of ice in the UT and the TTL.

2.4.2 Water Saturation and Relative Humidity

Equilibrium is the condition of the atmosphere when the condensation rate is equal to the evaporation rate. The air mass is called saturated when the amount of WV in the air mass is the maximum that the air mass can contain at a particular temperature and pressure. Thus, the **saturated vapour pressure of water** is the pressure at which WV is in thermodynamical equilibrium with its condensed state. When the **partial pressure** of WV increases, WV condenses. The partial pressure is determined by the Clapeyron formula. The amount of water vapour contained in an air mass compared with the amount of water vapour required for saturation (at a particular temperature and pressure), is called the relative humidity. As a function of the saturation of an environment, the **relative humidity with respect to ice (RHI)** indicates whether the air moisture freezes into ice crystals, and makes ice clouds. The RHI is calculated by the ratio between the water pressure and the saturation vapour pressure with respect to ice. When the air is under-saturated (RHI < 100 %), ice can sublimate into WV. When the air is saturated (RHI close to 100 %) or supersaturated (RHI > 100 %), ice cannot sublimate because there

is no space any-more in the air mass for WV. However, in that last case, ice can grow and fall.

2.4.3 Tropospheric Water Budget in the tropics

In the tropical troposphere, between 0 and 12 km, the main source of WV is the evaporative moistening. However, between 12 and 15 km (in the upper troposphere), the balance between detrainment moistening and subsidence drying controls the tropospheric water budget and determines the relative humidity profile (see Figure 2.20 from Folkins and Martin (2005). More precisely, Figure 2.4 synthestizes of the tropospheric water cycle: water is firstly elevated by convection, secondly cooled and condensed in the upper troposphere and thirdly descended through precipitation. Deep convective diurnal cycle over the tropics has been studied by Liu and Zipser (2005), differentiating two diurnal cycles: over land with the diurnal maxima of deep convection found in the early afternoon and over ocean with the diurnal maxima of deep convection found in the early morning.

The amount of WV, ice, or liquid water during the tropospheric water cycle depends on the temperature and the pressure of the clouds. For instance, mixed-phase clouds have ice crystals and super-cooled droplets whereas, below - 40°C, near the CPT, clouds consist entirely of ice. Martins et al. (2011) have shown that the presence of cirrus in the upper troposphere has shown an anomaly of water vapour varying between 5 and 20 ppmv (and a change of about -1 °C in temperature) according to the type of cirrus. Furthermore, the amount of WV in the troposphere can also be impacted by interannual variation such as the ENSO. For instance, Tian et al. (2018) have shown that, during the warm ENSO phases, the interannual tropical WV anomalies in the UT are positive while, during the cold ENSO phases, the WV anomalies in the UT are negative.

In the UT, the environment is generally not saturated (RHI < 100 %). Thus,

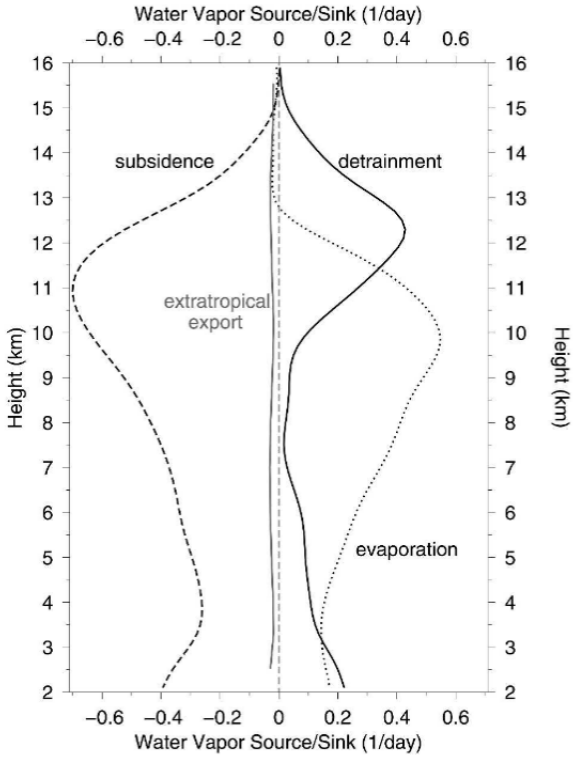

Figure 2.20 – Vertical profiles of the water vapour source/sink per day averaged over tropics (20°S–20°N). Subsidence, evaporative , detrainment, and extratropical terms are defined as a function of the tropical mean water vapor mass mixing ratio at that height. The inverse of each term gives the time scale at which that process removes or produces water vapor at that altitude. Figure from Folkins and Martin (2005)

ice can sublimate into WV. However, the main tropospheric WV is transported to the UT by convection. Because of the under-saturated environment in the UT, the condensation of WV forms ice crystals.

2.4.4 TTL Water Budget

The two main processes impacting the water budget in the TTL are the vertical advection and the ice optical and microphysical properties (Hardiman et al., 2015). Once into the TTL, the amount of the relative humidity of the layer impacts the

ice nucleation, growth and sedimentation (Peter et al., 2006). In the TTL, the amount of ice can be higher than the amount of water as a function of the daily or nightly hour (Carminati et al. (2014); and studies in the chapter 4). However, the amount of water injected into the TTL and their processes associated are still not well quantified and understood.

Ueyama et al. (2015) have shown that tropical waves dehydrate the TTL by 0.5 ppmv while the cloud microphysical processes and convection moisten the TTL by 0.7 and 0.3 ppmv, respectively. These results are consistent with Sherwood and Dessler (2000) presenting the hypothesis that the stratospheric hydration and dehydration would come from two different processes which occur on different time scales and involving vertical and horizontal air mixing into the TTL. Regarding the hydration of the TTL, some studies have shown that fast overshoots from tropical deep convection transport very rapidly water upward (from few minutes to one hour) across the TTL into the stratosphere (Pommereau, 2010; Dauhut et al., 2015). Dauhut et al. (2015) have estimated with the study case of the Hector cumulonimbus in north of Australia, that 18% of the water mass flux across the 380 K potential temperature level is due to overshooting deep convection. Liu and Zipser (2005) have found that 1.3% of tropical convection systems reach 14 km and 0.1% of them may even penetrate the 380 K potential temperature level which corresponds to the CPT. Tropical cyclones play also a role on the water vapour injection across the TTL and up to the stratosphere due to the convective overshoots (Allison et al., 2018). The other path for water to enter into the TTL and the LS is the slow vertical advection (300 m month^{-1}) governed by radiative heating (Holton and Gettelman, 2001; Gettelman and Fothers, 2002; Corti et al., 2006; Fueglistaler et al., 2009a). The impact of tropical land convection on the water vapour budget in the TTL has been studied by Carminati et al. (2014). The diurnal cycle of WV in the TTL has been shown to be delayed by few hours com-

pared to the diurnal cycle of deep convection calculated by Liu and Zipser (2005). In the TTL, as temperature decreases up to the tropopause and as air rises with the LZRH upward, air becomes close to saturation (Fueglistaler et al., 2009a). Thus, as high RHI is consistent with low temperature, saturation is more frequent in the TTL than in the UT. In in TTL, air masses encounter maximum values of RHI (with frequent supersaturation) and ice is less likely to sublimate into WV (Hartmann et al., 2001; Fueglistaler et al., 2009a; Khaykin et al., 2013). Thus, ice sublimation in the TTL occurs in specific conditions as a function of pressure, temperature and RHI. A study from Inai et al. (2012) has shown that cirrus with thin layers of high supersaturation in RHI are often observed at altitudes of $\sim$15 – 18 km, while cirrus with undersaturation in RHI are limited to altitudes below 16 km. Thus, there will be more likely ice sublimation into WV in cirrus above 16 km. Furthermore, the study shows that large-scale disturbances such as the Madden-Julian Oscillation (oscillation detailed in chapter 4) can strongly play a role on the formation of cirrus and on the variability of the RHI measured in the cirrus clouds.

2.4.5 Stratospheric water budget in the tropics

A first large source of the stratospheric WV is the methane oxidation in the upper stratosphere. Another source of stratospheric WV could come from the quick convective overshoots during deep convective activity (Adler and Mack, 1986; Danielsen, 1993; Oltmans et al., 2000; Dessler, 2002; Chaboureau et al., 2007; Grosvenor et al., 2007; Corti et al., 2008; Fueglistaler et al., 2009a; Liu et al., 2010). The, Hadley and Walker circulation strongly influence WV up to the LS, by air masses rising during deep convection and overshoots. Avery et al. (2014) have suggested that tropical convective ice cloud in the TTL and associated cirrus sublimating at unusually high altitudes might also have a role in stratospheric

hydration. However, only a small part of the air from overshoots is irreversibly transported into the stratosphere, while the remaining part is transported back into the troposphere. Furthermore, air masses impacted by the TTL very low temperature during long enough time become dehydrated due to saturation effect of the WV condensation and then by the sedimentation of ice crystals (Sherwood and Dessler, 2001; Holton and Gettelman, 2001; Corti et al., 2008). Thus, extremely cold and dry air masses transported up to the LS can also be considered as a sink of WV in the stratosphere. WV in the stratosphere has a direct radiative impact on surface temperatures (e.g., Forster and Shine, 1999) and participates in the warming of the troposphere and the cooling of the stratosphere (Solomon et al., 2010). It also has a strong impact on stratospheric chemistry, especially on the ozone equilibrium (Stenke and Grewe, 2005). In fact, WV contributes to the ozone destruction in the polar regions via the formation of HOx and in the activation of chlorine on polar stratospheric clouds (PSCs) (Solomon et al., 1986; Vogel et al., 2011). According to observations, stratospheric WV concentrations increased by $\sim 30-40$ % between 1980 and 2000 (Scherer et al., 2008; Hurst et al., 2011; Gettelman et al., 2010) and would increase by up to a factor of 2 over the twenty-first century (Maycock et al., 2013). After 2000, some studies have related the stratospheric WV drop in the tropics with the decrease of the Cold Point Tropopause (CPT) temperature (Randel et al., 2006a). The stratospheric WV variabilities are important to understand because they control the climate changes by the greenhouse effect and influence the ozone layer thickness. However, models still have difficulties to reproduce the stratospheric WV variabilities (Garcia et al., 2007).
In the stratosphere, ice crystals can reach a high dimension of 400 μm mean radius, IWC ranging between 7.7×10^{-2} and 8.5×10^{-1} mg m^{-3}, and relative humidity with respect to ice (RHI, see section 2.4.2) between 75 and 157% (Reus et al., 2009). It has been shown that the size distribution of the stratospheric ice clouds is

similar to the one observed in the upper troposphere (Reus et al., 2009). Reus et al. (2009) have also shown that the ice crystals entering into the LS can humidify the stratosphere locally by sublimation. Furthermore, Hassim and Lane (2010) have shown that the effects of the overshoots on the stratospheric water budget vary according to the WV saturation level of the area considered. The zonal tropical stratospheric WV distributions are nearly constant because of the quick zonal mixing of WV in the whole stratosphere. However, the main stratospheric WV variation is lead by the stratospheric meridional circulation: the increase of WV is observed upward and poleward because of the methane oxidation. Furthermore, it has been show that, once in the stratosphere, WV can be controlled by long and short time scale fluctuations, such as the quasi-biennial oscillation in the stratosphere (QBO) or the ENSO as a function of the location and altitude in the stratosphere (Tian et al., 2018). For instance, the QBO modulates the tropopause temperature and resulting water vapour anomaly is transported upwards. However, while the impact of the ENSO on the WV anomalies would be less than 3-months lag in the LS (Tian et al., 2018), the QBO would have an impact on about 7 to 24-month lag on the interannual tropical WV anomalies in the stratosphere.

2.5 Atmospheric characteristics over the Maritime Continent

In the tropics, the exchange between the troposphere and the stratosphere is larger over the region called Maritime Continent (MariCont), the region between the Indian Ocean and the West Pacific, than elsewhere on Earth (Newell and Gould-Stewart, 1981). Africa and South America are also two important continental centers of convection in the tropics, with the MariCont. Oceanic and continental convective activities show different behaviours in the tropics. As two huge land

surfaces, Africa and South America favour the Hadley cells, the Walker circulation and deep convection to evacuate the excess of energy received in the tropics, with rising motion of air towards mid-latitudes. Conversely, tropical oceans can more easily balance and transfer the excess of energy received in the tropics toward mid-latitudes by marine streams. Thus, the deep convection frequencies are more important over lands than over oceans (Liu and Zipser, 2005). However the MariCont is a mixing of land and ocean characteristics, with large and small islands and seas. More precisely, the MariCont region is a region where the sea circulations transfer hardly no energy toward lower latitudes by marine streams (because of obstacles formed by numerous islands). As a consequence, there will be more convection over the seas in this region than over other tropical oceans. Regarding the convection over the MariCont islands, the huge land-sea contrast as well as the orography that can quickly reach 2000 to 4000 m of altitude on some islands strongly influence the deep convection of this region.

2.5.1 Precipitations over the MariCont

Many studies focussed on the diurnal cycle of precipitations over the MariCont region. Annual maxima of precipitations over the MariCont have been calculated at 8 mm day^{-1} during the DJF seasons, compared to 5 mm day^{-1} in August and September (Zhang et al., 2016). Recent studies used the TRMM instrument to evaluate the diurnal cycle of precipitation over this region (Qian et al., 2010; Love et al., 2011).

Nesbitt and Zipser (2003) have highlighted this region to show a very clear separation between the diurnal cycle of precipitations over islands and seas. According to this study, the diurnal cycle of precipitation is less intense over ocean (30% of variability) than over continent (125% of variability). Diurnal variability in the tropics is well influenced by orography, coasts and island size (Beucher,

2010). Over islands, the diurnal convection can be formed by the heating differences between sea and land. Large islands with high orography can create vapour trail, whereas large islands without orography can create mesoscale convection led by coastal breeze sea convergence. Small islands can produce convective clouds even if they usually do not have sea breeze phenomena. In each case, the diurnal cycle of precipitation shows an opposite signal between the day and the night, with air masses transported by the wind towards the island and up to the mountains during the day and an opposite movement to the sea and down to the coast during the night. The Island Thunderstorm Experiment (ITEX, Keenan et al. (1994)) experiment focussed on the understanding of the convective activity over the MC region (and more precisely over the Tiwi islands (11°S, 130°E)). During the campaign, 3 phases of the convection were characterized in this island: i) the cells initialization, ii) the cell fusion and the quick growing phase (covering the maximum of precipitation), and iii) the mature line grain phase.

2.5.2 Troposphere and stratosphere air masses exchanges over the MariCont and "Stratospheric fountain"

Originally, it has been called “stratospheric fountain” the concept of slow phenomenon occurring over the MariCont region during the austral convective season (from November to March), and transporting air only from troposphere to stratosphere at certain locations and times of year (Newell and Gould-Stewart, 1981). As presented in section 2.4, it is now know that its simple picture does not apply. Quick phenomenon, as strong convective overshoots, also favours air masses and WV to exchanges between troposphere and stratosphere over the MariCont. Nevertheless, below the stratosphere, the TTL over the MariCont region is known to be the driest and coldest in tropics and the WV budget into this TTL is still not well understood. For that reason, this thesis examines the question of water

budget in the TTL over both, the whole tropics and the MariCont region.

2.6 Chapter summary and Thesis objectives

This Chapter 2 has recalled the main definitions and processes related to the convection in the tropics. Based on this context, the main objective of this thesis is to understand the impact of the **deep convection** on the **water budget** into the **TTL**, with an emphasis on the solid phase of water.

For that this thesis proposes to estimate the amount of **ice injected** up to the TTL from deep convection over convective regions and during convective periods. Chapter 3 will present the main tools that have been used to study the impact of the deep convection on the water budget into the TTL. Next Chapters will present the study of the relationship between deep convection and water budget – focused mainly on the solid phase of water – into the TTL. Different spatial scales are explored, from the scale of the whole tropical band (Chapter 4) to the scale of individual islands and seas over the Maritime Continent region (Chapter 5). The impact of the intra-seasonal and inter-annual large-scale oscillations of the MJO and the La Nina on the ice injected in the TTL will be studied in Chapter 6. Further work will be focused on the Asian areas during the monsoon period in Chapter 7.

Chapter 3

Instruments and models used

In order to study the climatology of the water budget into the tropical tropopause layer and its link with the convective processes, we have used satellite observations providing long time series of measurements, combined with models outputs from mesoscale and meteorological reanalysis. This chapter is composed of three sections. Firstly, we will recall remote sensing characteristics and related key definitions. Secondly, we will present and justify the list the instruments used in our analyses. The third part will be focused on the presentation of the mesoscale model and the meteorological reanalysis used. The question of the diurnal cycle of each dataset used will be addressed within each section.

3.1 Satellite remote sensing observations: definitions and motivations

3.1.1 Orbital and viewing modes

Instruments on board satellite platforms are sent each year to space for climate science researches. The space observational modes are firstly defined by the orbit

paths followed by the space-borne platform. The main orbital paths followed by a platform are called Geostationary orbit (from 384 000 km to the Earth), Medium Earth Orbit (MEO) and Low Earth Orbit (LEO) (less than 2000 km form Earth and including polar orbit satellites, the International Space Station, and any lower-inclination orbit precesses), illustrated in Figure 3.2. Geostationary orbits follow an equatorial plane orbiter with a distance of about 36.000 km from the surface. The satellite has fixed position relative to the Earth because the velocity of the platform's rotation around the Earth is the same as the one of the Earth. This orbital mode provide parallel measurements in a limited area from low to middle latitudes. This type of orbiter allowed to monitor the daily evolution of meteorological phenomena dynamics, as well as dust clouds, volcanic eruptions, smoke plumes or regional pollution events (Verma et al., 2019). Near-polar orbits follow a plane orbit around the Earth, crossing the two poles with an inclination of about 90° from Equator. The platform is at an altitude lower than 1500 km from the Earth's surface and can do a full rotation in 90 minutes. Because of the low orbit, the sensor is able to have higher spatial resolution and geo-location accuracy than geostationary satellites. A category of near-polar orbit is the sun-synchronous mode: the sensor is always crossing the Equator at the same local time of the day. However, the limit of the sun-synchronous polar orbit is that it is able to measure only two times per day (night and day time) at a given location on Earth's surface. Thus, some satellites on platform following sun-synchronous polar orbits, such as MLS (see more in section 3.2.1) or CALIPSO for instance and all other instruments onboard platforms of the A-Train, are able to provide observations only during the ascending orbit at 13:30 local solar time (LST) and during the descending orbit at 01:30 LST when crossing the Equator. When the near-polar orbit is not sun-synchronous, the orbit can be precesses, allowing to cross the Equator at any time of the day. Thus, after several orbits, measurements from the

sensor on board the satellite platform, can be averaged to the one hour temporal resolution. This is the case of measurements provided by the TRMM sensor and the SMILES sensors, on board to platforms following near-polar precess orbits (see more in section 3.2.2 and 3.2.3).

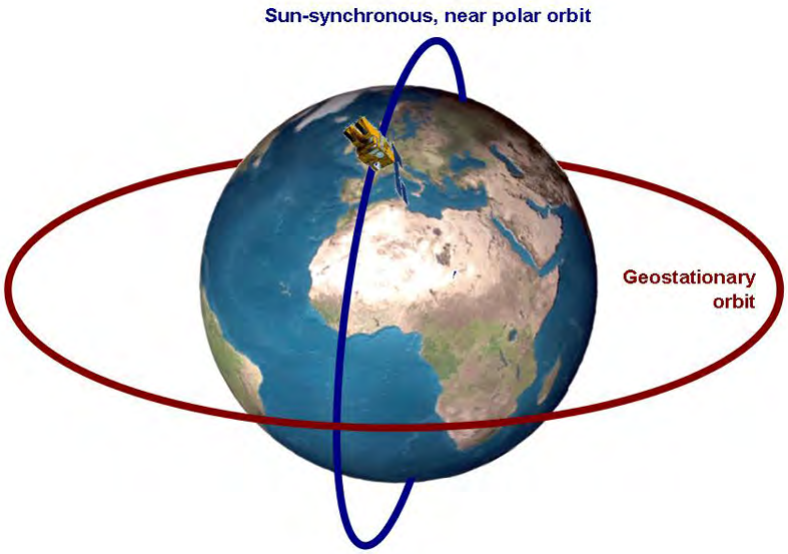

Figure 3.1 – Two mains orbiters: geostationary and sun-synchronus near-polar orbits, from: `http://seos-project.eu/remotesensing/remotesensing-c02-ws01-t.html,lastaccess:June2019`

The three main viewing geometry modes are at **nadir**, at **limb** and by **occultation** (illustrated in Figure 3.2). At nadir, the satellite instrument measures vertically the radiation coming from the Earth's surface. This observation mode provides good spatial coverage and high horizontal resolution observation but low vertical resolution with few point on the vertical or a column integrated products. At the limb or occultation viewing geometry, the atmosphere is observed at various depths at an certain altitude and geo-location of the tangent point. Satellite instrument in occultation geometry measures directly the sun radiation through the atmosphere, with high vertical resolution but low spatial resolution and low

spatial coverage. Satellite instrument at limb viewing geometry records the signal emitted along a horizontal path through the atmosphere. The instruments scattered light at the limb from the UV to the Vis. Limb provides high spatial coverage and hight vertical resolution but low spatial resolution. In general, horizontal resolution in limb is about 300 km and the vertical resolution can be lower than 10 km.

Derivation from the atmospheric information from the radiation characteristics measured by the instruments are named retrieval. As a function of the wavelength ranges used in remote sensing, the instrument can provide different informations. The infra-red (IR) are used to provides informations on temperatures, clouds, water and ice distribution and distinctions, while with nadir micro-waves (MW) sounders, clouds are transparent allowing to observed ice and water at the Earth's surface.

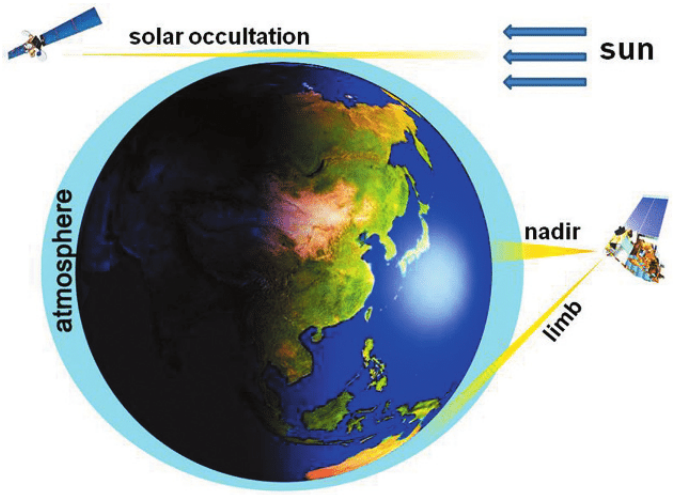

Figure 3.2 – Observation modes of satellites: limb, solar occultation, and nadir (https://www.researchgate.net/figure/ertical-nadir-and-horizontal-limb-and-solar-occultation-satellite-fig1_233779970)

3.1.2 Overview of the satellites measuring Water vapour in the UTLS

Many instruments are able to measure the atmospheric water vapour. The Stratosphere-troposphere Processes And their Role in Climate (SPARC) project has proposed a Water Vapour Assessment (WAVAS), reporting analysing long-term changes of UTLS water vapour, since 2000 (`https://www.sparc-climate.org/activities/water-vapour/`, last access: May 2015). One of the main question treated in WAVAS is about the implications of changing UTLS water vapour for radiation, dynamics, chemistry, clouds, and climate (WAVAS II). In the WAVAS II report, authors have presented the overview of all the sensors able to measure water vapour and others chemical constituents, temperature, pressure and aerosols from the troposphere to the stratosphere. Figure 3.3 presents the list of these instruments: ACE-FTS, COMOS, HALOE, HIRDLS, ILAS-II, MAESTRO, MIPAS, MLS, POAM III, SAGE II, SAGE III, SCIAMACHY, SMILES, SMR and SOFIE. Thus, all of these instruments can measure WV into the troposphere, stratosphere or both. In addition to the list drawn in Fig. 3.3, the Interféromètre Atmosphérique de Sondage Infrarouge (IASI), following a sun-synchronous mid-morning orbit since October 2006, is also able to provide WV measurement in the troposphere with high temporal resolution. However, because the IASI instrument observes at nadir, WV measured in the UTLS have got a too low signal-to-noise ratio. Furthermore, Payra et al. (2016) have shown a dry bias in the UTLS by comparing assimilate MLS H_2O with IASI H_2O observations. In this thesis, among all the instruments available and able to measure WV in the UT and LS during a long time period, greater than 10 years, we decided to use the Microwave Limb Sounder (MLS) instruments for two main reasons: i) firstly, because MLS is the only instrument providing ice and water vapour in the TTL during a long time serie, and ii) secondly, to be consis-

tent with the previous study of Carminati et al., (2014) stuying the diurnal cycle of water vapour in the TTL from MLS datasets. In fact, MLS has the particularity to follow a sun-synchronous near-polar orbit, providing long time series (2004-2019) of WV measurements in the UT and LS (200, 177, 146, 100 and 82 hPa) at global scale. This instrument have the advantage to be able to measure other parameters than ice or WV, such as the relative humidity and temperature, providing information and interpretation on the evolution of water budget into the UTLS. More details on the MLS instrument are given in the section 3.2 and in Table 3.1.

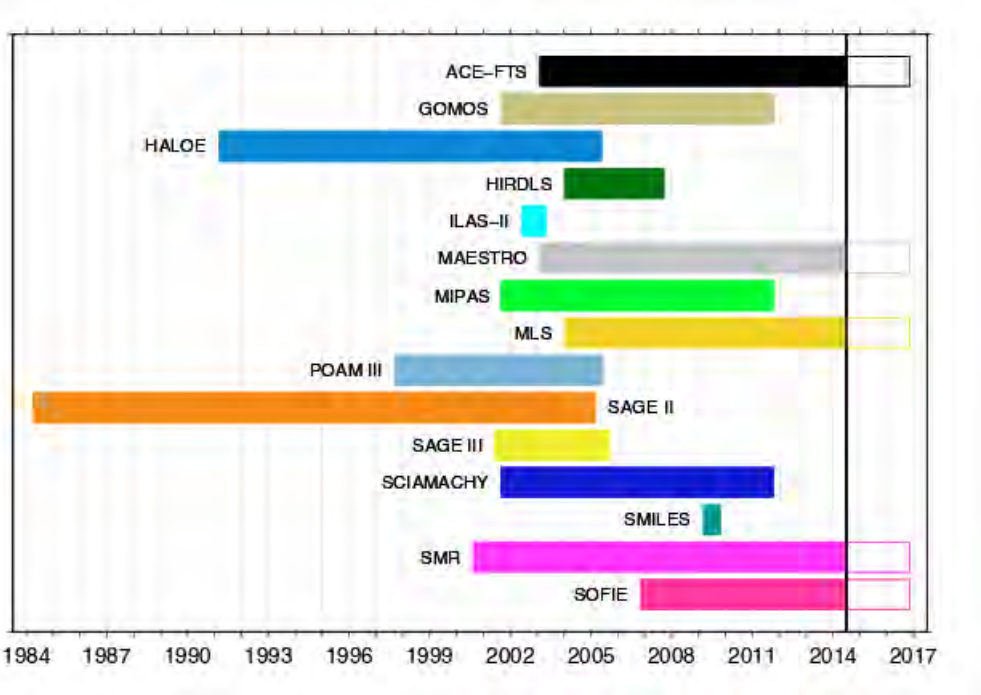

Figure 3.3 – Satellite measurements of water vapour considered in the stratospheric comparisons of the WAVAS-II activity. Tropospheric comparisons will include additional satellite measurements from TOVS, AIRS, IASI, and TES. Figure from: www.sparc-climate.org, last access: June 2019

3.1.3 Overview of satellites measuring the Ice Water Content in the UTLS

While WV measurements in the UTLS have been measured from many space-borne instruments, measurements of ice at these altitudes are rare. Optical thickness of ice cloud is available from the Chinese and Japanese development of the polar orbiting GCOM-C/SGLI satellite launched on December 2017 by JAXA, but does not provide ice water content. The ice cloud product from GCOM-C/SGLI is only available from March 2019 (`https://gportal.jaxa.jp/gpr/index/index`, last access : May 2019). The Superconducting Submillimeter-Wave Limb-Emission Sounder (SMILES, presented in section 3.2.2) on board the International Space Station (ISS) is able to measure ice cloud water content (IWC) (in addition to WV) in the troposphere and the tropopause. SMILES orbit is near-polar and precess, allowing to the instrument to provide high temporal resolution of IWC and to build the full 24-hour diurnal cycle of IWC. However, SMILES has been operational only one year from 2009 to 2010 (Fig. 3.3). The Microwave Limb Sounder (MLS, presented in section 3.2.1) is able to measure IWC but also WV in the TTL for a long time period (2004 - 2019). However, MLS is able to measure IWC only twice a day and at fixed time over tropics (see details in section 3.2.1).

As stated in section 3.1.2, our study will mainly use the MLS instrument to analyse water budget in the TTL. IWC and WV from MLS will be studied and compared to the less than one year SMILES IWC observations. Thus MLS and SMILES instruments are presented below in section 3.2, explaining in detail the choice and characteristics of the two instruments used.

3.2 Instruments used

This section presents the instruments used in our study: MLS, SMILES, TRMM-3B42 and TRMM-LIS. The question relative to the diurnal cycle representation from each instrument is also discussed.

3.2.1 MLS

3.2.1.1 MLS instrument on the Aura platform

The version 4.2 of the Microwave Limb Sounder (MLS) instrument is the main datasets used in our works for studying the water budget (WV and IWC) into the TTL. Launched in 2004, MLS instrument is on board the NASA's Earth Observing System (EOS) Aura platform (Waters et al., 2006; Livesey et al., 2018b). Aura is part of NASA's A-train group of Earth observing satellites flying in formation with the different satellites (illustrated in figure 3.4).

The Aura orbit is in a **near-polar** 705 km altitude, staying fixed relative to the sun (sun-synchronous), and providing daily global coverage with about 15 orbits per day. The Earth's limb is observed by MLS thermal microwave emission, scanning the atmosphere from the ground to $\sim$ 90 km every $\sim$ 25 seconds. MLS instrument consists of seven radiadiometers observing emission in the 118 GHz, 190 GHz, 240 GHz, 640 GHz and 2.5 THz regions. MLS instrument completes almost all the tropical band with 233 revolution cycles every 16 days. Figure 3.5 illustrate the MLS measurement at limb to produce a vertical profile of any component measured by MLS. Furthermore, in the tropics, the MLS observations, such as all other instruments onboard platforms of the A-Train, samples the atmosphere at 01:30 LT and 13:30 LT, providing one single night and one single day observation. Figure 3.6 presents an example of 24 hours of WV measurements from MLS compared to the average of 13 years of WV data, and shows the

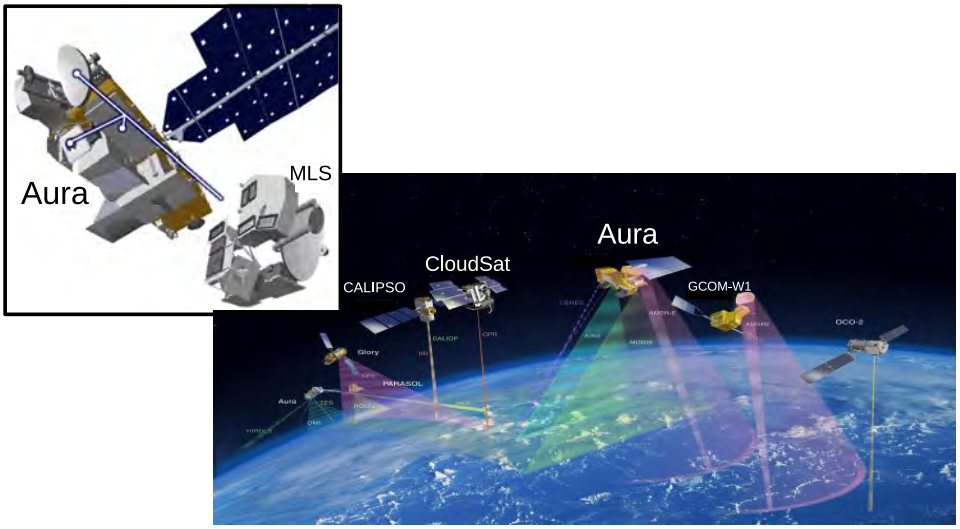

Figure 3.4 – (right) The Earth Observing System (EOS) MLS instrument on Aura and (left) Aura on the A-Train (images from `https://mls.jpl.nasa.gov/index-eos-mls.php`)

importance to gather long enough time series of MLS datasets to study the full tropical band climatology of MLS components.

The three main scientific objectives of the MLS NASA team are i) the study of the stratospheric ozone layer stability, ii) the study of climate change variability and iii) improve understanding of global air quality. The present thesis takes place in the improvement predictions of climate change variabilities by studying 13 years (2004-2017) climatology of water budget (WV and IWC) from MLS into the TTL.

3.2.1.2 MLS components characteristics

MLS provides 21 products of atmospheric composition. For studying the water budget into the TTL, this thesis use several products from MLS: the cloud ice water content measurements (IWC, mg m^{-3}), is compared to WV (ppmv), temper-

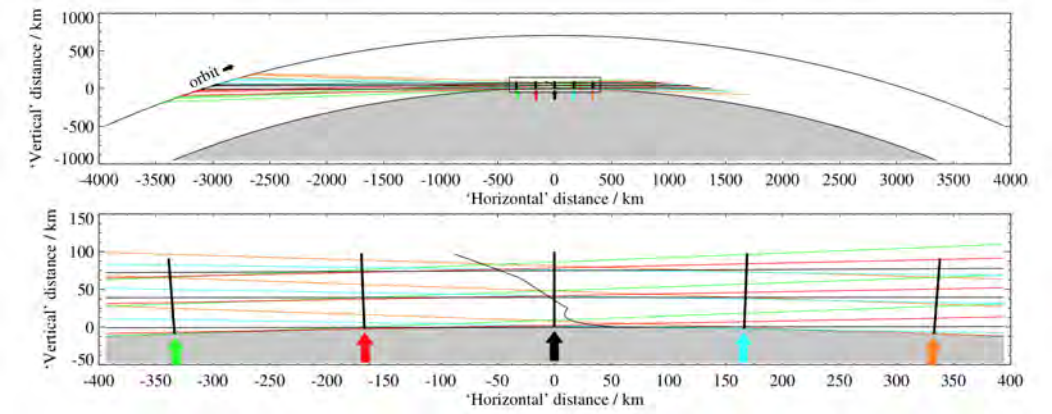

Figure 3.5 – The top diagram shows a section of one orbit. Three of the 120 limb ray paths per scan are indicated by the "horizontal" lines. The lower diagram shows an expansion of the boxed region above. The straight radial lines denote the location of the retrieved atmospheric profiles. The limb ray scan closed to each profile is that whose color is the same that of the arrow underneath. The limb black line under the central profile indicates the locus of limb tangent point for this scan, including the effects of refraction. Figure 2.2.1 from Livesey et al. (2018a).

ature (K), and relative humidity (%) measurements from MLS at 146 hPa and at 100 hPa (studied in chapter 4). The version v4.2x processing is presented in the report from Livesey et al. (2018a). Major and minor differences with the previous MLS version are detailed. Main characteristics of MLS products from the version 4.2x Level 2 used in our study are presented in Table 3.1. The MLS measurement error (estimate of precision) of IWC at 146 hPa is between 0.25 – 0.35 mg m^{-3} (Livesey et al., 2018a). Thus, the error, averaged over the study zones and over the 13 years of study, become negligible.

IWC measurements have horizontal resolution of $\sim$ 300 and 7 km along and across the track, respectively and the vertical resolution is $\sim$ 4 km. Thus, IWC is valid between 215 and 82 hPa. Although optimal estimation is used to retrieve almost all other MLS products, the cloud-induced radiance technique is used to estimate the MLS IWC (Wu et al., 2008; Wu et al., 2009). Thus, the standard

Instruments	Products	Levels used (hPa)	Resolution used	Satellites orbit and observation geometry	Temporal resolution used	Further information
MLS	Ice Water Content (IWC) (g m^{-3})	146 100	2°×2° (~ 200 km × 200 km)	Sun-synchronous near-polar orbit measuring at limb viewving geometry.	From December 2004 to December 2017 : 01:30 LT and 13:30 LT	http://mls.jpl.nasa.gov/data/v4-2_data_quality_document.pdf
	H_2O (WV) (ppmv)					
	Relative humidity with respect to Ice (RHI) (%)					
	Temperature (TEMP) (K)					
SMILES	Ice Water Content (IWC) (g m^{-3})	Avergaed between 120 and 80 hPa.	2°×2° (~ 200 km × 200 km)	Near-polar precess orbit measuring at limb viewvinf geometry.	From December 2009 to February 2010 : One-hour temporal resolution	http://mls.jpl.nasa.gov/data/smiles/
	Partial Ice Water Path (pIWP) (g m^{-2})	Integrated between 1000 and 180 hPa.				
TRMM-3B42	Precipitation (Prec) (mm h^{-1})	Vertically integrated	2°×2° (~ 200 km × 200 km) and 0.25°×0.25° (~ 30 km × 30 km)	Near-polar precess orbit measuring at limb viewvinf geometry.	From December 2004 to december 2017 : One-hour temporal resolution	http://pmm.nasa.gov/data-access/downloads/trmm
TRMM-LIS	Number of flashes (Flash)		2°×2° (~ 200 km × 200 km) and 0.25°×0.25° (~ 30 km × 30 km)		From 2005 to 2015 One-hour temporal resolution	http://ghrc.nsstc.nasa.gov/lightning/data/data_lis_trmm.html
ERA5	Cloud Ice Water Content (IWC) (kg kg^{-1})	150 100	0.25°×0.25° (~ 30 km × 30 km)		One temporal resolution	https://cds.climate.copernicus.eu/cdsapp#!/dataset/reanalysis-era5-pressure-levels-monthly-means?tab=form
MESO-NH	Mixing ratio ice (MRI) : non-precipitating ice (kg kg^{-1})	146 100	0.035°×0.035° (~ 4km × 4km)		One temporal resolution	http://mesonh.aero.obs-mip.fr/mesonh54
NCEP/NCAR NOAA	Tropopause pressure (hPa)	From 120 to 105	2.5°×2.5° (~ 300 km × 300 km)		Monthly values from 1948 to present	https://www.esrl.noaa.gov/psd/data/gridded/data.ncep.reanalysis.html
	U and V wind direction and speed (m s^{-1})	146 100	2.5°×2.5° (~ 300 km × 300 km)		One data per day	https://www.esrl.noaa.gov/psd/thredds/catalog/Datasets/ncep/catalog.html

Table 3.1 – Main characteristics of instruments and datasets used in the thesis.

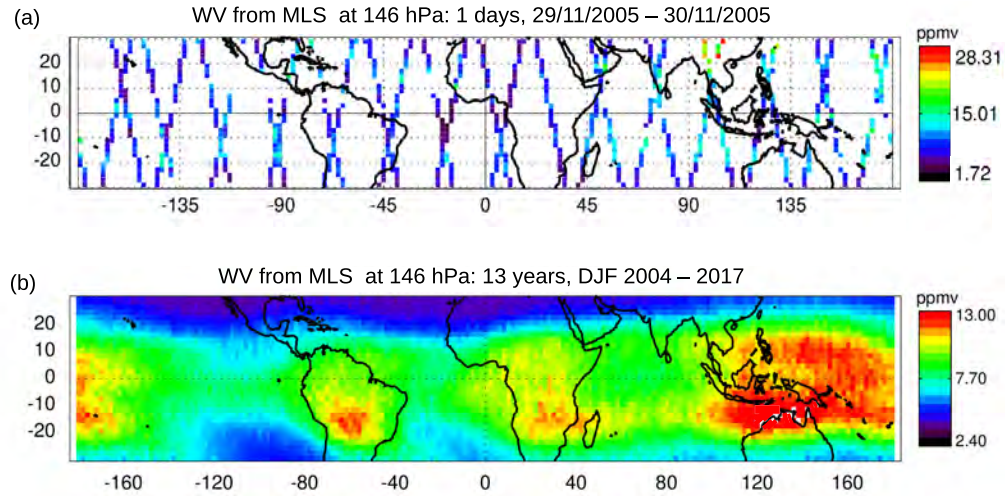

Figure 3.6 – Illustration of one day (29/11/2005 to 30/11/2005) (a) and 13 years (DJF, 2004-2017) (b) of the WV (ppmv) at 146 hPa from MLS measurements, at $2^\circ \times 2^\circ$ horizontal resolution, over Tropics. (White pixels in (b) results of the oversaturated color scale).

product for IWC is retrieved from the 240 GHz cloud-induced radiances between 215 and 68 hPa. In our study, we will use IWC at 146 and 100 hPa. However, at 82 hPa, IWC data provides a too low signal-to-noise ratio to be used. The MLS IWC vadid range are 0.1-50 mg m^{-3} in the UT and 0.02-50 mg m^{-3} in the TL (Livesey et al., 2018b). The WV precision is 0.10 mg m^{-3} at 146 hPa and 0.25-0.35 mg m^{-3} at 100 hPa. The WV acuracy values are 100% <10 mg m^{-3} at both levels. As presented in Table 3.1, IWC from MLS is processed by following the $2\sigma - 3\sigma$ screening method consisting to filter clear-sky residual noise in the cloud detection. More precisely, this method consists to average IWC data at 10° latitude bins and outliers rejected iteratively by excluding measurements greater than 2σ standard deviation about the mean (μ) of the bin. σ and μ are repeated after every new set rejection. After about 5 - 10 iterations, σ converges to one

value which is considered as the precision value for IWC measurements. Finally, the precision is interpolated to each measurement and a 3σ threshold is applied to IWC to determine whether IWC is statically significant (where IWC must be higher than $\mu+3\sigma$ to be considered as significant cloud hit) (Livesey et al., 2018a). According to Wu et al. (2008), IWC from MLS estimation derived from MLS represents spatially averaged of IWC MLS whose volume can be approximated by a box of $\sim 300 \times 7 \times 4$ km^3 near the pointing tangeant height. In our study, IWC MLS is then averaged over boxes of $2^\circ \times 2^\circ$($\sim$ 200km$\times$200km).

WV measurements (H_2O) are retrieved from the 190-GHz and valid between 316 and 0.002 hPa with a vertical resolution of 2.5 $\pm$ 1.2 km. The WV along track horizontal resolution is between 170 and 350 km. MLS WV main characteristics are presented in Table 3.1.

Temperature is retrieved fom band 118 GHz and 239 GHz. The vertical resolution of MLS temperature measurements is $\sim$ 4.5 km from 261 to 100 hPa. The pressure range is from 261 to 0.001 hPa. The temperature is given with a precision at $\pm$ 0.7 K and an accuracy at + 1.8 $\pm$ 1.2 K for the two levels 146 and 100 hPa. **Relative humidity with respect to ice (RHI)** is provided from 316 to 0.002 hPa. The vertical and horizontal resolutions of RHI are provided from a convolution of the temperature and H_2O resolutions.

3.2.1.3 WV and IWC diurnal cycles from MLS in tropics: the Day-Night method

Liu and Zipser (2009) have used MLS datasets to study the diurnal cycle of carbon monoxide and WV in the tropics from 2005 to 2008. As MLS provides only two data per day and at fixed time, their method has been to study the difference between the day (13:30 LT) minus the night (01:30 LT) measurement: called "Day-Night". The Day-Night differences has been studied at 146 and 100 hPa

over $10^\circ \times 10^\circ$ horizontal resolution. At 146 hPa, WV Day-Night observations have shown strongly negative signals over land (WV Day < WV Night) and positive signals over ocean (WV Day > WV Night)(see Fig.3.7a). The remarkable result is that, at 100 hPa, the WV Day-Night over land is in opposite signal (WV Day > WV Night) than at 146 hPa. These results highlight the strong differences in the vertical distribution of the WV diurnal cycle by approaching the CPT.

Carminati et al. (2014) have used a longer time series of MLS measurements (2005-2014) than Liu and Zipser (2009), in order to study the WV and IWC Day-Night signals at 177 and 100 hPa with a $10^\circ \times 10^\circ$ horizontal resolution. For WV, results from Carminati et al. (2014) are consistent with the ones from Liu and Zipser (2009) (see at 177 hPa in Fig. 3.7). However, the IWC Day-Night signal have been shown to be positive over land at 177 and 100 hPa and negative over ocean. Thus, it is expected that, along the vertical, the diurnal cycle of IWC present less changes than the diurnal cycle of WV. Furthermore, because IWC and WV show opposite Day-Night signals over land at 177 hPa, it is expected that the diurnal cycles of WV and IWC are not coinciding.

In the present thesis, studies use time series (2004-2017) of WV and IWC measurements from MLS longer than in Liu and Zipser (2009) and Carminati et al. (2014) allowing to calculate for the first time the Day-Night of WV and IWC with $2^\circ \times 2^\circ$ horizontal resolution. Figure 3.7 illustrates the evolution in the Day-Night study of the WV measurements from MLS in the UT (146 and 177 hPa) and with the version v3 (Carminati et al., 2014) vs v4.2 (our study) from MLS. However the Day-Night method is still limited to study the full 24-h WV and IWC diurnal cycles. For that reason, our study proposes a method, presented in Chapters 4 and 5, to estimate the full diurnal cycle of IWC, by combining MLS observations at 01:30 LT and 13:30 LT with higher 1-hour temporal resolution observation of convective activity from TRMM observation of precipitation and/or lightning

(presented in section 3.2.3).

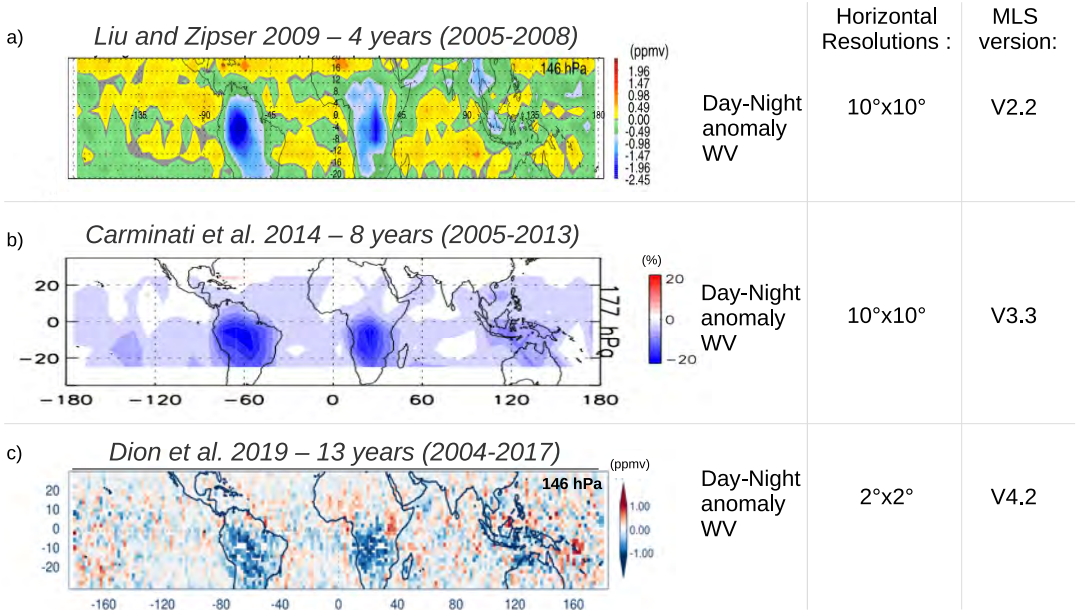

Figure 3.7 – Day-Night of WV measured from MLS. Results from Liu and Zipser (2009) (a), Carminati et al. (2014) (b) and Dion et al. (2019) (c) studies at 146, 177 and 146 hPa, respectively. Horizontal resolutions and MLS version used are mentioned.

3.2.2 SMILES

The Japanese Superconducting Submillimeter-Wave Limb-Emission Sounder (SMILES) has been on board the International Space Station (ISS) during less than one year from September 2009 to April 2010. SMILES on the ISS follows about 15 orbits a day and measures to the Earth's limb between 10 and 60 km and about 1600 times per day over the whole tropical band from 38° S to 65° N (the entire band can be provides in about two months). The instrument measured at three frequency bands: 624.32–625.52 GHz (band A), 625.12–626.32 GHz (band B), and 649.12–650.32 GHz (band C) in which IWC and pIWP are

measured. Thus, SMILES derives cloud ice water content (IWC) and partial Ice Water Path (pIWP) from the difference between the measured radiance and the expected clear-sky radiance. IWC is measured between 100 and 70 hPa while pIWP is integrated between 1000 and 180 hPa. Because ISS orbit drifts about 20 min earlier each day, the diurnal cycle of IWC and pIWP can be sample over the course of couple of months. Thus the full diurnal cycle of IWC and pIWP from SMILES can be drawn over the tropics where integrating over a long period (> 1 month). SMILES is also able to provide WV and relative humidity with respect to ice (RHi) retrieved directly from the WV continuum. SMILES dataset is available at: `https://mls.jpl.nasa.gov/data/smiles/` (last access: July 2019).

Millán et al. (2013) and Jiang et al. (2015a) have used SMILES to calculated the diurnal cycle of IWC and pIWP in the troposphere over convective areas in the tropics. Figure 3.8 presents results from Millán et al. (2013) showing stronger amplitude in the diurnal cycle of IWC in the UT over Africa and South America than over Pacific and Indian oceans and the MariCont region. Figure 3.9 presents results from Jiang et al. (2015a) showing diurnal cycle of pIWP from SMILES over tropical, northern mid-latitude and southern mid-latitude lands. The analyses from Jiang et al. (2015a) are consistent with the two daily MLS measurements of IWC, particularly in the tropics. In a validation phase, SMILES datasets will be used in chapter 4 as reference of few months full diurnal cycle of IWC and pIWP near the tropopause.

3.2.3 TRMM

The Tropical Rainfall Measuring Mission (TRMM) is a joint mission between NASA and the Japan Aerospace Exploration Agency (JAXA) with objectives to study rainfall for weather and climate research. TRMM satellite delivered a

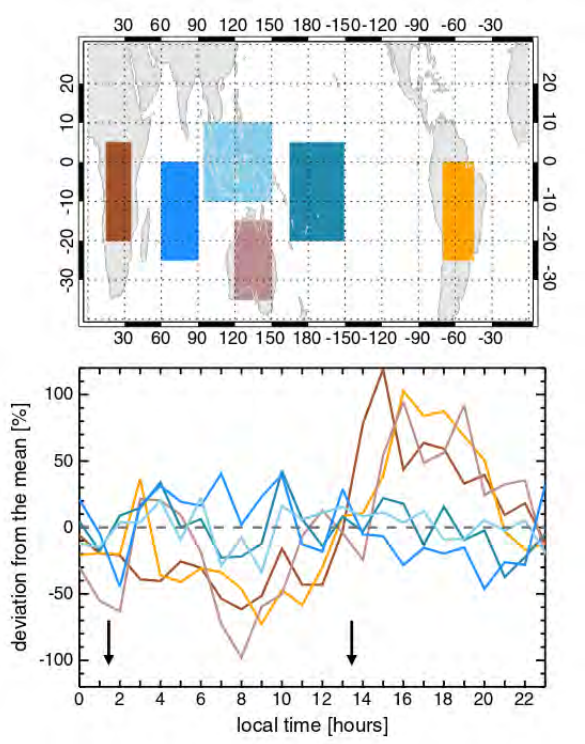

Figure 3.8 – (top) Study zones selected in the Millán et al. (2013) study. (bottom) Deviation from the mean of the pIWP diurnal cycle calculated from the average of the three frequency bands measurements of SMILES at about 12.5 km over the land and ocean study zones. (Figure 11. from Millán et al. (2013))

unique 17-year dataset (launched in late November 1997 and ended collecting data on April 15, 2015). TRMM was composed of 5 instruments: 3-sensor rainfall suite (precipitation radar (PR), TRMM microwave imager (TMI) and visible and infrared scanner (VIRS)), a lightning imaging sensor (LIS) and a cloud and energy balance sensor (CERES). The purpose of TRMM is to provide an extensive database on rainfall distribution and latent heat exchange over a domain between latitudes 50° N and 50° S. Furthermore, the advantage of the datasets provided by TRMM is that the TRMM platform follows an orbit precession, shifting few minutes per day, providing a 24-hour diurnal cycle for any of the TRMM components measurements with one-hour temporal resolution in tropics, where averaged over

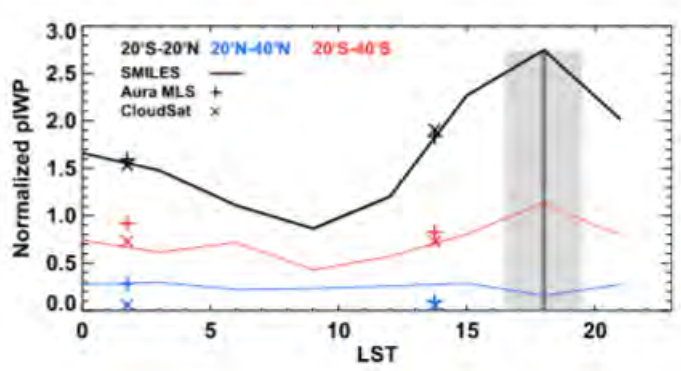

Figure 3.9 – Diurnal cyle of normalized pIWP over land in tropic (black), northern mid-latitude (blue), southern mid-latitude (red). pIWP from Aura MLS (+) and CloudSat (x) are added to the figure. pIWP is vertically intergated IWC above the 200-hPa pressure level and the all values are averaged over the period (October 2009 to April 2010) and the normalize by the 40° S-40° N-mean pIWP. (Fig. A3 from Jiang et al. (2015a))

a long period as it is the case in our analysis.

3.2.3.1 Deep convection estimation from TRMM

The deep convective activity is not directly measured from satellite observations. However, some studies such in Liu and Zipser (2005), have used a sophisticated method from TRMM precipitation radar (PR) and TRMM precipitation features measurements at five levels characterizing the level of the top of deep convective clouds, to estimate the diurnal cycle of the overshoot precipitation features (OPFs, representative of the deep convective activity) over tropical land and ocean. Figure 3.10 presents the diurnal cycle of the OPFs calculated by Liu and Zipser (2005) over tropical land and ocean during the short period from 1998 to 2000 and from 2001 to 2003. Two well-distinguished diurnal cycles of OPFs over tropical land and ocean are depicted, with larger amplitudes over land than ocean.

This thesis, based on the Liu and Zipser (2005) study, will combine rainfall and lightning informations from TRMM (presented in sections 3.2.3.2 and 3.2.3.3), to

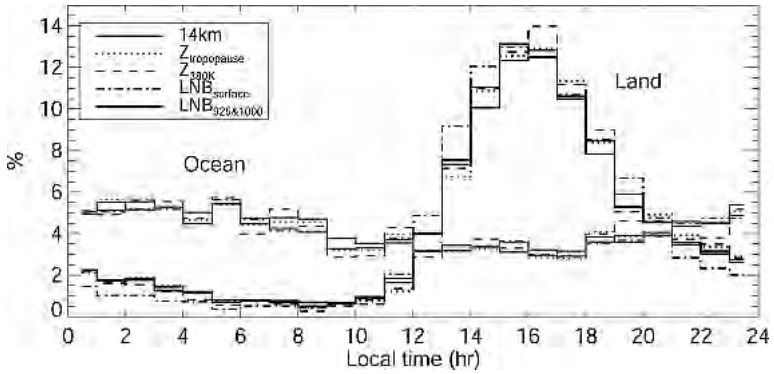

Figure 3.10 – Diurnal variation of population of 20° N-20° S overshoot precipitation features (OPFs) identified with five reference heights over land (solid) and ocean (shaded) during the periods of 1998-2000 and 2001-2003 (from Figure 3 in Liu and Zipser (2005))

provide information on the tropical deep convective activity (studies in chapters 4, 5 and 6). Thus, the question of the representation of the tropical deep convection will be drawn all along the thesis and discussed progressively over the manuscript.

3.2.3.2 TRMM - 3B42

Precipitation observation, measured by TRMM from 1997 to 2015, have been merged to vertically integrated precipitation datasets produced by the algorithm 3B42. TRMM transition to the Global Precipitation Measurement (GPM) mission products (the TRMM-3B42) has started in 2014 and continues since then. The new multi-satellite products is called TRMM Multi-satellite Precipitation Analysis (TMPA) and is an intercalibration of the passive microwave precipitation from TRMM production, providing precipitation datasets by following the 3B42 algorithm (Huffman, 2016). TRMM-3B42 data are provided over the region 60° N-S at 0.25° $\times$0.25° horizontal resolution one-hour temporal resolution. TRMM-3B42 product have been used in numerous studies to improve the understanding of tropical convective system properties, cyclone structure and evolution, climate and weather modelling, and human impacts on rainfall (Kikuchi and Wang, 2008;

Jiang et al., 2011; Tan et al., 2015).

Figure 3.11 shows annual mean of precipitation measured from TRMM-3B42, averaged over the period 2004-2017 over the tropical band available from TRMM at 0.25° ×0.25°.

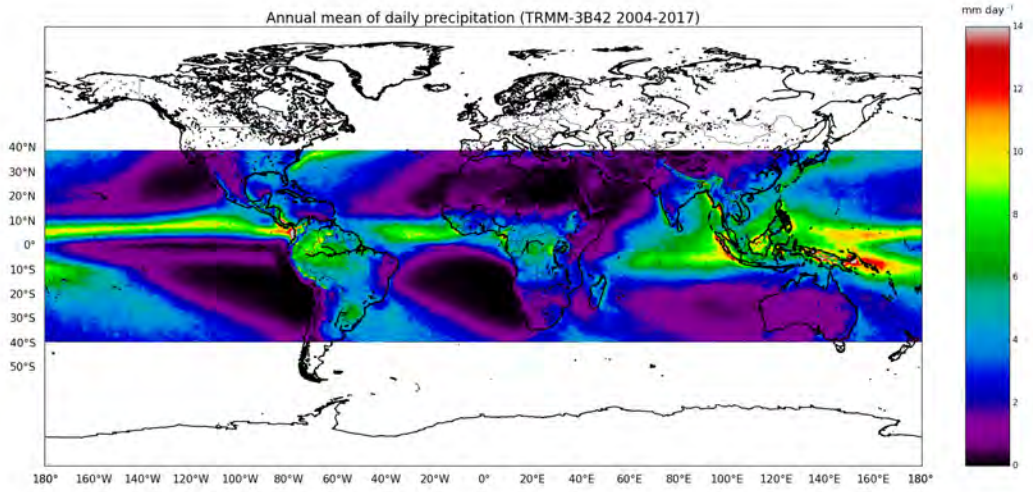

Figure 3.11 – Annual mean of daily precipitation (mm day^{-1}) (from 2004-2017) over the latitudinal band provided by TRMM-3B42

3.2.3.3 TRMM - LIS

The Lightning Imaging Sensor (LIS) aboard of the TRMM platform has detected the distribution and variability of total lightning (cloud-to-cloud, intracloud, and cloud-to-ground lightning) from 1998 to 2015 over the tropics (38° N – 38° S). The centroid projection of LIS allows to cover the tropics within 3 km at nadir and 6 km off-nadir with 1 file per orbit temporal resolution. Thus LIS provides datasets with hight 0.25° × 0.10° horizontal resolution. The instrument was able to locate and detect lightning at millisecond timing with storm-scale resolution

over the Earth's surface. LIS was composed by a grid of 128 $\times$ 128 detectors observing each 90 seconds with a temporal resolution of 2 milliseconds. The most fundamental detection of the sensor is the lightning event defined as a light anomaly on a pixel. More precisely, the Real-Time Event Processor (RTEP) used by LIS discriminated lightning event from Earth albedo light and is used to determine when a lightning flash occurs. Thus, the sensor was able to determine both the number of events and the number of flashes. Figure 3.12 illustrates the annual mean of the number of flashes per day over the tropical band provided by LIS. Maxima of flashes per day are mainly observed over lands and, over some oceans in tropics.

In our study, we have averaged LIS data to within 0.25° $\times$0.25° bins to be compared with precipitation from TRMM-3B42 data at the same horizontal resolution.

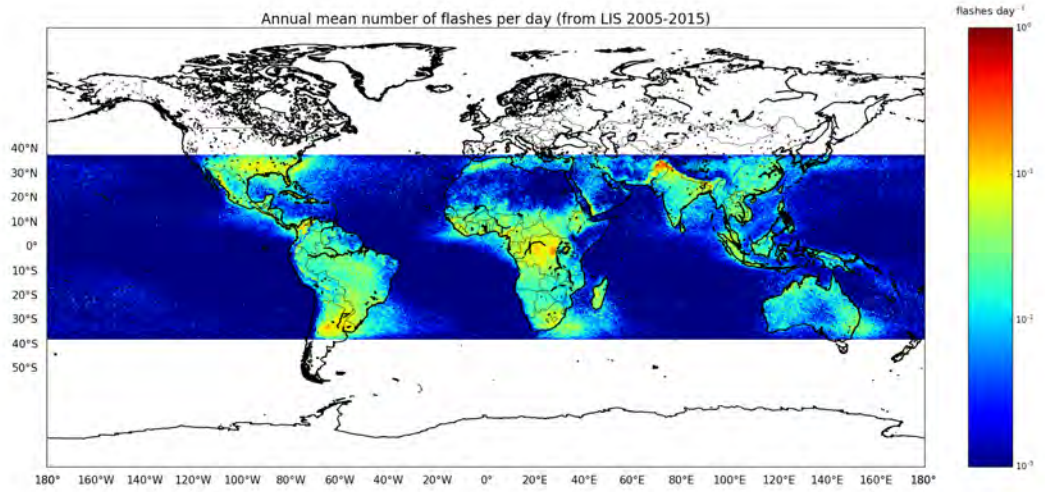

Figure 3.12 – Annual mean of the number of flashes from lightning per day (from 2004-2015) over the latitudinal band provided by TRMM-LIS

3.3 Meso-scale models and meteorological reanalysis used

Complementary to the observations, atmospheric numerical models and reanalyses provide information over areas and at times where and when observations could not be done. The comparison between models and observations allows to quantify the uncertainties of the model, to evaluate the capacity of the model to reproduce the atmospheric state and to interpret the variability of the meteorological variables under consideration via the representation of different processes.

Solar diurnal cycle related to the surface heating diurnal cycle is the main parameter controling the diurnal cycle of atmospheric temperature in the tropics (Yang and Slingo, 2001). Thus, the diurnal variations are known to affect atmospherics circulation from mesoscale convective systems (Yang and Slingo, 2001) to intraseasonal oscillation (Tian et al., 2018). In model, diurnal cycles simulations are a key metric of climate model performance (Jiang et al., 2015b). For that reason, Jiang et al. (2015b) have tried to improve the accuracy of the diurnal cycle simulation. The authors have evaluate of the ice cloud diurnal variability in the upper troposphere considering 10 models and MERRA reanalysis. Model results are all in agreement with IWC observations from SMILES showing higher diurnal cycle amplitude over land than over ocean. However, the phase of the diurnal cycles are distributed over the 24-h period, showing the difficulties for models to estimate the diurnal cycle of ice clouds. In the presents thesis, the diurnal cycles of ice in the UT and the TTL are studied firstly from ERA5 reanalyses and from Meso-NH outputs with one-hour temporal resolution. The two models are presented below.

3.3.1 ERA5

The European Centre for Medium-range Weather Forecasts (ECMWF) Reanalysis 5, known as ERA5 is the new and fifth version of the European Centre for Medium-Range Weather Forecasts (ECMWF), replacing ERA-Interim reanalysis. The ERA5 reanalysis combines observations and physics laws by the 4D-Var method of data assimilation. A large number of atmospheric, ocean and land species are provided hourly at global scale from 1979 to date. Information on global climate and weather is thus provided by ERA5. The Earth is covered on a 30 km grid with 137 levels from the surface up to a height of 80 km. ERA5 has the advantage to be able to differentiates precipitating and non-precipitating ice, classifying as snow water and cloud ice water, respectively. Among all the species proposed by ERA5, cloud ice water content (IWC, kg kg^{-1}) and temperature (K) are provided at $0.25° \times 0.25°$ horizontal resolution. Note that although ERA5 does not output convective ice (Geer et al., 2018), which is parameterized in the model as a convective flux, we use the ice water content provided by ERA5 at altitudes near the tropopause in our studies. Levels available in the UTLS are at 200, 175, 150, 100, 70 and 50 hPa. Ice, the water vapour and the liquid water are provided by ERA5 into the UTLS, allowing to study the water budget into these layers. Our study will focus on ice water content at the levels 150 hPa (UT) and 100 hPa (near the CPT). ERA5 reanalysis provides outputs with one-hour time resolution, allowing to study the 24-hour diurnal cycle of the selected species.

3.3.2 Meso-NH

The atmospheric non-hydrostatic regional model Meso-NH (Lafore et al., 1997; Lac et al., 2018) has been developed by the Laboratoire d'Aérologie (LA) and Centre National de Recherches Météorologiques (CNRM) since 1993

(model–related documents can be found on the Web site: `http://mesonh.aero.obs-mip.fr/`, last access: July 2019). The Meso-NH model performs simulations from large synoptic scales to convective and turbulent scales (order of 100 m). The anelastic approach used in Meso-NH allows to eliminate the acoustic waves from the considered set of equations. This approach uses the assumption that the atmosphere will stay close to a chosen "reference state".

The diurnal cycle of hydrometeor content and precipitation from Meso-NH simulation (Dauhut et al., 2015) has been studied by Dauhut et al. (2016) over the Tiwi Islands, in North of Australia and during 10 hours with initial condition coming from meteorological sounding on the 30 November 2005. The authors have compared the vertical distribution of the diurnal cycle of hydrometeror to the integrated precipitation features (Figure 3.13). These results have mainly shown that maxima of hydrometeor content in the troposphere is found at the same hour than maxima of precipitations, near 14:15 LT and between 6 and 14 km in altitude.

In this thesis we will use the simulations from Meso-NH, version 5-1-3, focused over the region of 26.7° S – 26.7° N, 44.6° E– 155.4° E. This domain has been selected to study large-scale variability induced by the MJO transits over the Indian Ocean and the Maritime Continent (Kuznetsova et al., 2019). Eight days of MJO active phases have been simulated from 23 to 30 November 2011 (starting at 00:00 UTC on 23 November 2011). The domain represents $1538 \times 3074 \times 72$ (about 340 million) grid points with a 4-km horizontal grid and 72 vertical levels following the surface elevation with grid spacing of 60 m near the surface and 600 m at the top of the model. The initial conditions are provided by 6-hourly operational analyses of the European Centre for Medium-Range Weather Forecasts (ECMWF), as well as the sea surface temperature. Precipitation from TRMM 3B42 are used to assess the simulated rain every 3-hours (Huffman et al., 2007). Thus, 8 files per days provided one data per 3-hours. Ice in the model can be found

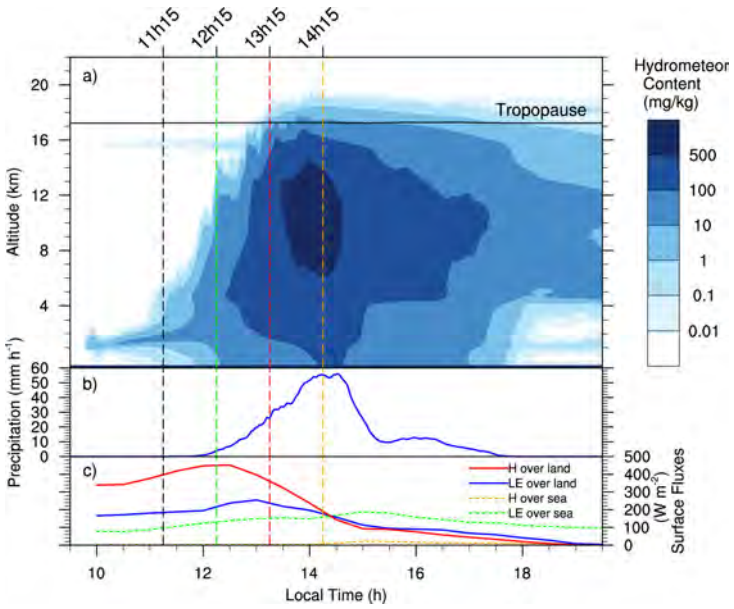

Figure 3.13 – Figure 5 from Dauhut et al. (2016): Temporal evolution of (a) hydrometeor content, (b) precipitation rate at the surface, and (c) surface fluxes. In (c), sensible and latent heat fluxes are in red and blue solid lines over the islands and in orange and green dashed lines over the ocean, respectively. The key moments representative of the congestus, deep, very deep, and mature convection phases are highlighted with the black, green, red, and orange vertical dashed lines, respectively.

into three stages: the mixing ratio of ice (MRI, non-precipitating ice), mixing ratio of snow (MRS) and ice pellets (MRG). Because we are interested by only the ice phase of water available in the TTL, our study focus on the MRI variables near the tropopause in chapter 6. The levels have been selected at 12.9 km ($\sim$ 146 hPa) and 15.9 km ($\sim$ 100 hPa).

3.3.3 NCEP/NCAR Reanalysis

The NCEP/NCAR Reanalysis Project at the NOAA/ESRL Physical Sciences Division is a joint project between the National Centers for Environmental Prediction (NCEP, formerly "NMC") and the National Center for Atmospheric Re-

search (NCAR). The goal is to produce new atmospheric analyses using historical data (1948 onwards). Analyses of the current atmospheric state (Climate Data Assimilation System, CDAS) are also produced. These analyses are useful for climate monitoring studies. The quality and utility of the reanalyses are superior to NCEP's original analyses because a state-of-the-art data assimilation using more observations. These analyses provide 6-hourly, daily and monthly data available on-line (`https://www.esrl.noaa.gov/psd/data/reanalysis/reanalysis.shtml`).

In this thesis, we will use NOAA reanalysis to study firstly the tropopause pressure (Chapter 4). The pressure of the tropopause from NOAA is provided in Pascal.

3.4 Chapter summary

This chapter firstly dealt with the theory of remote sensing observations and introduced the main space-borne instruments able to measure ice and water vapour in the UTLS. Secondly, we have presented the four space-borne instruments – MLS, SMILES, TRMM-3B42 and TRMM-LIS – used in our studies together with the associated variables. WV, IWC, precipitation, temperature, relative humidity with respect to ice and number of flashes from thunderstorms. The 11 – 13 years of datasets provided from each instrument will be used in this thesis to build a climatology of the water budget up to the TTL at diurnal scales. Thirdly, a section has presented the Meso-NH model and ERA5 reanalyses, providing ice in the UT at 150 hPa and in the TTL at 100 hPa, with NOAA analyses providing tropopause pressure.

In order to study the impact of the deep convective activity on the amount of ice injected up to the TTL, the question of the representation of the tropical deep convection is addressed and discussed all along in the document. The amount of

ice injected by deep convection up to the TTL is studied over the tropics with observations from MLS, TRMM-3B42, SMILES and NOAA analyses in Chapter 4; over the MariCont region from MLS, TRMM-3B42, TRMM-LIS, and ERA5 reanalyses in Chapter 5; and during ENSO and MJO periods, over the MariCont region, from MLS, TRMM-3B42 and Meso-NH in Chapter 6. From results presented in this thesis, a further study using MLS, TRMM-3B42, TRMM-LIS data and ERA5 reanalysis has been focus on the ice injection by deep convection over the Asian region and during the Asian monsoon periods, as part of Cyrille Dallet's Master 2 internship in collaboration with P. Ricaud and myself, and will be reported in Chapter 7.

Chapter 4

Ice injected into the TTL in the austral tropics

This Chapter presents the first study of this thesis. The roles and mechanisms of the convective activity in the tropics have been recalled in Chapter 2, showing the impact of the tropical deep convection on the global atmospheric circulation, radiative budget and climate changes. Furthermore, the TTL, playing the role of a boundary layer between the troposphere and the stratosphere, is known to be the key layer regulating radiative, chemical and dynamical atmospheric processes.

The goal of the study presented in this chapter is to improve the knowledge on the water budget into the TTL impacted by deep convection. This chapter focuses on the tropical band area during the austral convective season and presents the study published in Atmospheric Chemistry and Physics (ACP): Dion, I. A., Ricaud, P., Haynes, P., Carminati, F., and Dauhut, T. (2019) Ice injected into the tropopause by deep convection–Part 1: In the austral convective tropics. Atmospheric Chemistry and Physics, 19(9), 6459-6479., (`https://www.atmos-chem-phys.net/19/6459/2019/acp-19-6459-2019.pdf`). The MLS instrument is used in this study be-

cause in the only instrument able to provid IWC and WV during a long time serie. TRMM-3B42, and SMILES instruments and NOAA reanalysis, presented in Chapter 3 are also used in this study. In order to simplify the reading, TRMM-3B42 is abbreviated into TRMM in Dion et al. (2019) presented below.

4.1 Article-1: Ice injected into the tropopause by deep convection – Part 1: In the austral convection tropics

Atmos. Chem. Phys., 19, 6459–6479, 2019
https://doi.org/10.5194/acp-19-6459-2019

Atmospheric Chemistry and Physics
Open Access
EGU

Ice injected into the tropopause by deep convection – Part 1: In the austral convective tropics

Iris-Amata Dion[1], Philippe Ricaud[1], Peter Haynes[2], Fabien Carminati[3], and Thibaut Dauhut[4]

[1]CRNM, Meteo-France – CNRS, Toulouse, 31057, France
[2]DAMTP, University of Cambridge, Cambridge, CB3 0WA, UK
[3]Met Office, Exeter, Devon, EX1 3PB, UK
[4]Laboratoire d'Aerologie, Université de Toulouse, CNRS, UPS, Toulouse, 31400, France

Correspondence: Iris-Amata Dion (iris.dion@meteo.fr)

Received: 21 September 2018 – Discussion started: 30 October 2018
Revised: 21 March 2019 – Accepted: 17 April 2019 – Published: 16 May 2019

Abstract. The contribution of deep convection to the amount of water vapour and ice in the tropical tropopause layer (TTL) from the tropical upper troposphere (UT; around 146 hPa) to the tropopause level (TL; around 100 hPa) is investigated. Ice water content (IWC) and water vapour (WV) measured in the UT and the TL by the Microwave Limb Sounder (MLS; Version 4.2) are compared to the precipitation (Prec) measured by the Tropical Rainfall Measurement Mission (TRMM; Version 007). The two datasets, gridded within $2° \times 2°$ horizontal bins, have been analysed during the austral convective season, December, January, and February (DJF), from 2004 to 2017. MLS observations are performed at 01:30 and 13:30 local solar time, whilst the Prec dataset is constructed with a time resolution of 1 h. The new contribution of this study is to provide a much more detailed picture of the diurnal variation of ice than is provided by the very limited (two per day) MLS observations. Firstly, we show that IWC represents 70 % and 50 % of the total water in the tropical UT and TL, respectively, and that Prec is spatially highly correlated with IWC in the UT (Pearson's linear coefficient $R = 0.7$). We propose a method that uses Prec as a proxy for deep convection bringing ice up to the UT and TL during the growing stage of convection, in order to estimate the amount of ice injected into the UT and the TL, respectively. We validate the method using ice measurements from the Superconducting Submillimeter-Wave Limb-Emission Sounder (SMILES) during the period DJF 2009–2010. Next, the diurnal cycle of injection of IWC into the UT and the TL by deep convection is calculated by the difference between the maximum and the minimum in the estimated diurnal cycle of IWC in these layers and over selected convective zones. Six tropical highly convective zones have been chosen: South America, South Africa, Pacific Ocean, Indian Ocean, and the Maritime Continent region, split into land (MariCont-L) and ocean (MariCont-O). IWC injection is found to be 2.73 and 0.41 mg m^{-3} over tropical land in the UT and TL, respectively, and 0.60 and 0.13 mg m^{-3} over tropical ocean in the UT and TL, respectively. The MariCont-L region has the greatest ice injection in both the UT and TL (3.34 and 0.42–0.56 mg m^{-3}, respectively). The MariCont-O region has less ice injection than MariCont-L (0.91 mg m^{-3} in the UT and 0.16–0.34 mg m^{-3} in TL) but has the highest diurnal minimum value of IWC in the TL (0.34–0.37 mg m^{-3}) among all oceanic zones.

1 Introduction

Water vapour (WV) is one of the main greenhouse gases and has an important impact on the climate, particularly in the tropics. WV concentrations are limited by temperature, which regulates the saturation mixing ratio in air masses (Hartmann et al., 2001; Fueglistaler et al., 2009; Khaykin et al., 2013). In consequence, WV is much smaller in the upper troposphere (UT) and stratosphere than in the lower troposphere. However, despite the small concentrations, the WV distribution in the tropical upper troposphere (e.g. Soden et al., 2008) and stratosphere (e.g. Solomon et al., 2010) plays an important role in climate, including the determination of the overall radiative balance of the troposphere.

The WV distribution in this region of the atmosphere is strongly coupled to the distribution of cirrus clouds which, despite being thin, can have a significant effect on the overall thermal balance of the troposphere (e.g. Zhou et al., 2014). The tropical upper stratosphere and lower stratosphere recognised as a distinct region of the atmosphere – the tropical tropopause layer (TTL) – is defined by the layer between the level of maximum convective outflow (10–12 km, $\sim$ 200 hPa) that closely corresponds to a minimum in ozone and the cold point tropopause (CPT) (16–17 km, $\sim$ 100 hPa) (Gettelman and Forster, 2002; Mehta et al., 2008; Birner and Charlesworth, 2017). Within the TTL, a complex set of physical processes interact to determine the distribution of temperature, WV and clouds, and other radiatively active chemical species (e.g. Fueglistaler et al., 2009; Randel and Jensen, 2013). The TTL is important in determining several aspects of troposphere–stratosphere exchange and therefore determining the chemical composition of the stratosphere. Much attention has therefore been focused on the role of TTL processes in setting the value of WV concentrations that enter the stratosphere. In particular, there has been an ongoing debate of the relative importance of large-scale processes in which air masses move slowly from the troposphere to the stratosphere within the large-scale three-dimensional circulation and dehydrate as they encounter very cold temperatures and small-scale processes, in which convection injects WV (and ice) directly into the TTL, and the stratosphere, with potentially hydrating impact. The relative importance of the three-dimensional circulation processes and convective processes continues to be debated (e.g. Alcala and Dessler, 2002; Liu and Zipser, 2005; Carminati et al., 2014).

For instance, Ueyama et al. (2015) have shown that tropical waves dehydrate the TTL by 0.5 ppmv, while the cloud microphysical processes and convection moisten the TTL by 0.7 and 0.3 ppmv, respectively. Some authors have shown that fast overshoots from deep convection transport water upward very rapidly (from a few minutes to 1 h) into the stratosphere (Pommereau, 2010; Dauhut et al., 2015). Liu and Zipser (2005) have found that 1.3 % of tropical convection systems reach 14 km, and 0.1 % of them may even penetrate the 380 K potential temperature level, which corresponds to the CPT. Avery et al. (2017) have also suggested that tropical convective ice cloud and associated cirrus sublimating at unusually high altitudes might also have a role in stratospheric hydration. The other path for water entering the lower stratosphere (LS) is the slow vertical advection (300 m per month) governed by radiative heating (Holton and Gettelman, 2001; Gettelman and Forster, 2002; Corti et al., 2006; Fueglistaler et al., 2009). Once in the UT or the TTL, the amount of the relative humidity of the layer impacts the ice nucleation, growth, and sedimentation (Peter et al., 2006).

Whilst there is observational evidence for convective hydration events (Liu and Zipser, 2005; Pommereau, 2010; Avery et al., 2017), and convective hydration of the stratosphere has been clearly corroborated by state-of-the-art numerical simulations (e.g. Dauhut et al., 2015), the quantitative role of convective hydration in determining water vapour concentrations in the main body of the stratosphere remains uncertain. One approach has been to combine observational estimates of overshooting convection frequency with information from short-localised-duration numerical simulations. Using this approach, Dauhut et al. (2015) have estimated that 18 % of the water mass flux across the 380 K potential temperature level is due to overshooting deep convection. Another has been to include estimates of convective penetration, e.g. from satellite observations, in large-scale trajectory calculations. The conclusions are sensitive to the assumptions made, but, for example, Wright et al. (2011) and Schoeberl et al. (2018) both conclude that the effect of convective penetration on WV concentrations in the stratosphere is very weak, essentially because most air masses that are moistened by convective injection are subsequently dehydrated when they encounter cold temperatures on a large scale before they reach the main body of the stratosphere.

Whether or not convective processes play a direct role in determining stratospheric WV concentrations, it is clear that, moving from the lower TTL to the upper TTL, convective-scale processes play an increasingly important role in determining the distributions of WV and of cirrus. Representing convective-scale processes in global models used for weather climate prediction is challenging, and it is important where possible to evaluate model representations by finding observed characteristics of WV and cirrus in the TTL that can be usefully compared to model simulations. One opportunity is provided by diurnal variations. The timescale is of course very different to the decadal and longer timescales of interest in climate prediction, but the short timescale has the advantage of providing time series with many cycles which is therefore well characterised statistically. The diurnal cycle is one of the most fundamental modes of variability of the global climate system and is associated with large and well-defined variations in the solar forcing (Yang and Slingo, 2001). The amplitude of the surface thermal diurnal cycles in the tropics is 10 times stronger than the amplitude of the surface thermal annual cycle (Beucher, 2010), and the diurnal cycle of deep convection is mainly governed by the surface thermal diurnal cycle. Understanding the diurnal cycle of the total water in the tropical UT, TTL, and LS contributes to the characterisation of the total water exchange between the UT and the LS in the tropics. Many studies (e.g. Jiang et al., 2015) have shown that the diurnal cycle of ice in the UT is linked to the diurnal cycle of the convection. The maximum of deep convection in the UT has been shown to peak in the local afternoon over land and in the local early morning over ocean (Liu and Zipser, 2005). Based on these studies and data from the space-borne Microwave Limb Sounder (MLS) instrument, Carminati et al. (2014) studied the diurnal cycle of WV and ice in the TTL over Africa and South America and have shown the presence of a strong diurnal signal over the two continents. Suneeth et al. (2017) have shown the differ-

ences in the diurnal cycles of CPT altitudes and CPT temperatures over tropical land and ocean. The diurnal cycle of temperature has also been studied in the TTL (Khaykin et al., 2013), showing that the amplitude of temperature anomalies increases with the intensity of the convection.

In summary, the processes driving the total water diurnal cycle are different in the UT and at the tropopause layer; e.g. only the deepest convection directly impacts water content in the tropopause layer, and saturation is more frequent in the tropopause layer than in the UT. Since the total water diurnal cycle in the tropopause layer is still not well described in global models (Jiang et al., 2015), space-borne observations may improve our understanding of the processes occurring in this layer. This provides motivation for the study presented in this paper, in which we consider the diurnal cycle of ice in the TTL, for which limited, but nonetheless valuable, data are provided by the MLS instrument.

The aim of the present study is to quantify the role of deep convection in the hydration and dehydration of the TTL. For this, we focus on the diurnal injection of ice into the tropical UT and the tropopause layer from the deep convective activity and address the question relative to the diurnal cycle of total water over tropical deep convective areas.

Africa and South America are two land regions of intense deep convective activity in the tropics, together with the Maritime Continent region (MariCont, the region made up of lands and oceans, between the Indian Ocean and the western Pacific, presented by the red box in Fig. 1). However, the deep convective systems occur more frequently and strongly over the MariCont region (Liu and Zipser, 2015) than over the other continental zones. It is known that excess of energy received by tropical surfaces is mainly balanced and transferred over land by convection toward mid-latitudes and over ocean by both convection and oceanic circulation. However, over the MariCont region, sea and ocean currents transferring energy toward mid-latitudes are slowed down and blocked by thousands of islands. Consequently, the excess of energy in the oceanic surface over the MariCont region is mainly balanced by transfer from convection. The diurnal cycle of WV and ice has already been studied over Africa and South America and over the whole tropical band (see, for example, Liu et al., 2007; Millán et al., 2013; Carminati et al., 2014). The MariCont region is the driest and coldest area at the CPT, and the water budget in the TTL over the MariCont region separating MariCont land and MariCont ocean is still unknown. Furthermore what the physical mechanism is governing the diurnal cycle of convection and surface precipitation over ocean is still an open question.

In order to understand the total water diurnal cycle up to the TTL, we first use 13 years of the ice water content (IWC) and WV measurements from the MLS (Version 4.2x) and surface precipitations (Prec) from the TRMM instrument. Then, we use WV, IWC, total water ($\sum W = \mathrm{WV} + \mathrm{IWC}$), relative humidity with respect to ice (RHI), and temperature (TEMP) from the MLS and Prec from the TRMM over the period 2004 to 2017 in order to better understand the water fraction ($\mathrm{IWC}/\sum W$) in the UT (~ 146 hPa) and the tropopause level (TL; ~ 100 hPa, around the CPT). The relationships between surface precipitation and the processes in the UT and the TL are investigated. Our study intends to evaluate the mechanisms affecting the diurnal cycle of total water in the TL above land and ocean with a particular emphasis over the MariCont region due to its topographical complexity. Thus, the diurnal cycle of ice (provided by the MLS but with very poor time resolution) is improved and better understood thanks to the relation with the diurnal cycle of precipitation (provided by the TRMM with a much better time resolution).

The main instruments used are presented in Sect. 2. The methodology developed to establish the link between the diurnal cycle of surface processes and the diurnal cycle of water in the UT and TL is presented in Sect. 3. The estimated diurnal injection of IWC in the UT and TL from deep convective activity is presented in Sect. 4. Finally, the influence of the convective dissipating stage on the decreasing phase of the IWC diurnal cycle in the UT and the TL is discussed in Sect. 5, and conclusions will be drawn in Sect. 6. This paper contains many abbreviations and acronyms. To facilitate reading, we compile them in the Appendix.

2 Instruments

2.1 MLS

The MLS is a microwave instrument aboard the NASA's Earth Observing System (EOS) Aura platform (Livesey et al., 2017), measuring in a limb viewing geometry to maximise signal intensities and vertical resolution. The MLS instrument is aboard a sun-synchronous near-polar orbiter completing 233 revolution cycles every 16 d, giving a daily global coverage with about 14 orbits. Aura crosses the Equator at 01:30 local time (LT) and 13:30 LT. Among all the atmospheric parameters measured by the MLS, we focus on IWC, WV, TEMP, and RHI. Although IWC ($\mathrm{mg\,m^{-3}}$) is valid between 215 and 82 hPa, the number of scientifically exploitable measurements at 82 hPa within a $2^\circ \times 2^\circ$ pixel is not significant. In our study, we will only use two levels to analyse IWC, at 180 and 100 hPa. WV (ppmv) is valid between 316 and 0.002 hPa, TEMP (K) between 261 and 0.001 hPa, and RHI (%) between 1000 and 1.0 hPa. The MLS IWC sensitivity thresholds are $0.1\,\mathrm{mg\,m^{-3}}$ in the UT and $0.02\,\mathrm{mg\,m^{-3}}$ in the TL (Livesey et al., 2017) and will imply an underestimation of the IWC measured values.

The MLS v4.2x data processing validated by Livesey et al. (2017) presents significant and minor differences with the previous MLS version. The total random noise in v4.2x IWC is larger than in v2.2. Compared with v3.3 of the MLS (used for instance in Carminati et al., 2014), v4.2 improves IWC composition profiles in cloudy regions, especially in the up-

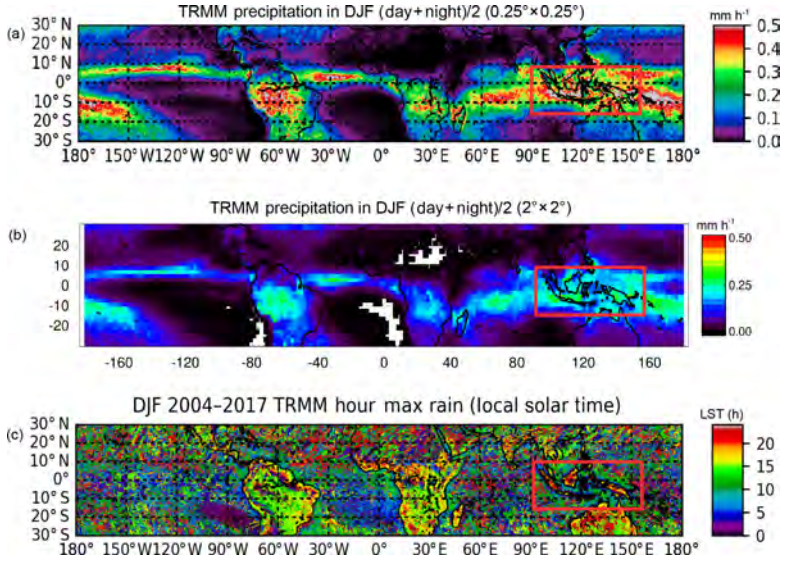

Figure 1. (a) Daily averaged ((day+night)/2) precipitation measured by the TRMM at 0.25° × 0.25° resolution (mm h^{-1}), **(b)** daily averaged ((day + night)/2) precipitation at 2° × 2° resolution (mm h^{-1}), and **(c)** hour of diurnal maximum precipitation at 0.25° × 0.25° resolution (h in local solar time, LST) in DJF over the period 2004–2017. The red box surrounds the MariCont region.

per troposphere over the tropics, and improves the WV at global scale (Livesey et al., 2017).

Level 2 data quality tests (filter and data screening) from the v4.2x have been applied to WV, IWC, RHI, and TEMP as suggested by Livesey et al. (2017). The MLS measurements estimated from the averaging kernels (Livesey et al., 2017) are used to characterise the distribution of the four parameters on two layers: one at 146 hPa (UT) and one at 100 hPa (TL). The vertical resolution of the IWC measurements is ∼ 3 km; the horizontal resolution is ∼ 300 and 7 km along and across the track, respectively. The WV vertical resolution is 2.5 ± 1.2 km, and the WV along-track horizontal resolution is between 170 and 350 km. The TEMP vertical resolution is 4.5 km.

In the study of Carminati et al. (2014), a 10° × 10° resolution was chosen with 7 years of MLS data processed with Version 3.3 (v.3.3). In our study, MLS data have been averaged over a much longer period (2004 to 2017) at a much higher horizontal resolution of 2° × 2° (∼ 200 × 200 km). In each 2° × 2° bin, and for the 13-year average, any bin with fewer than 60 measurements in the daytime (day at 13:30 LT) or the nighttime (night at 01:30 LT) is excluded in order to obtain significant statistics. Thus, the maximum measurements per bin during the 13-year period is ∼ 470, and the minimum is fixed to be 60. The number of measurements over the MariCont region is on average the lowest over the tropics. Consistent with Carminati et al. (2014) and Liu and Zipser (2005), we use the difference between the MLS measurements performed during the day and the night to study the "day minus night" (day − night) signal.

2.2 TRMM

The TRMM satellite was launched in November 1997 (https://trmm.gsfc.nasa.gov/publications_dir/publications.html, last access: April 2019). The TRMM carried five instruments: a 3-sensor rainfall suite, the precipitation radar, the TRMM Microwave Imager, the Visible and Infrared Scanner, and two related instruments, the Lightning Imaging Sensor and the Clouds and the Earth's Radiant Energy System. In our study, we use Algorithm 3B42 which produces high-quality infrared precipitation and root-mean-square precipitation-error estimation from the TRMM Version 007. The rainfall level 3 measurements (mm h^{-1}) are vertically integrated precipitation (Prec). TRMM Prec data are provided in the tropics within a 0.25° × 0.25° horizontal resolution extending from 50° S to 50° N. TRMM datasets used in our study are in coincidence with the MLS period of measurements from 2004 to 2017. In order to compare to the MLS measurements, we degraded the TRMM resolution to 2° × 2° in averaging the TRMM measurements in each 2° × 2° box of the MLS. Furthermore, as the TRMM follows an orbit precession, shifting a few minutes per day, the 24 h diurnal cycle can be averaged over the period of study, with 1 h resolution over the 24 h diurnal cycle.

2.3 SMILES

The Superconducting Submillimeter-Wave Limb-Emission Sounder (SMILES) was a Japanese atmospheric limb sounding instrument on board the International Space Station (ISS) platform. SMILES measurements of ice are used in this study. The instrument measured IWC between 120 and 80 hPa and the measurement of tropospheric ice, the partial ice water path (pIWP), integrated between 1000 and 180 hPa, during the short period of October 2009 to April 2010. As the ISS follows a low Earth orbit, with about 15 orbits a day, the ice measurements in the troposphere and tropopause layer over the entire 40° N–40° S band can be provided in about 2 months. Thus, the austral convective season of DJF is enough to cover the entire tropical band. Furthermore, as each orbit drifts about 20 min earlier each day, the entire diurnal cycle of ice can be provided during this period. In the present study, SMILES measurements will be used as a reference of the diurnal cycle of ice and will be compared to the climatology of the diurnal cycle of ice estimated in the UT and the TL.

3 Relationship between Prec and water budget in the austral convective UT and TL

In this section, we analyse the relationships between Prec and the water budget in the UT and the TL during the DJF season, a highly convective season of the Southern Hemisphere. Deep convection can affect water vapour and ice in the UT and the TL, whereas Prec measurements include the contribution of both shallow convection (that does not reach the UT) and deep convection (reaching the UT and the TL).

3.1 Tropical distribution of Prec and water budget in the UT and TL

The daily averaged ((day + night)/2) Prec measured by the TRMM at the resolution of $0.25° \times 0.25°$ and $2° \times 2°$ (the same horizontal resolution as the MLS) is shown in Fig. 1a and b, respectively. The fine structure of the horizontal distribution of Prec at the high resolution ($0.25° \times 0.25°$) over South Africa, South America, the western Pacific Ocean, and the Maritime Continent is degraded when considering Prec at low resolution ($2° \times 2°$). Figure 1c presents the local solar time (evaluated for each bin of $0.25° \times 0.25°$) at which the diurnal cycle of Prec reaches its maximum in TRMM observations, showing the large variability and complexity of the diurnal maximum of Prec over the tropics. The daily averages of IWC, WV, the IWC fraction ($\mathrm{IWC}/\sum W$), TEMP, and RHI from the MLS in the tropics are shown in Fig. 2 for the UT (at 146 hPa) and Fig. 3 for the TL (100 hPa).

In DJF, local maxima of Prec (Fig. 1), IWC, WV, the IWC fraction, and RHI in the UT (Fig. 2) are found over the main convective areas: South America, South Africa, MariCont, northern Australia, and along the intertropical convergence zone (ITCZ) and the South Pacific convergence zone (SPCZ). Maximum values of Prec, IWC, WV, and RHI over the whole tropics are located over the MariCont (and northern Australia) (Figs. 1a and b and 2a, b, c and e). Minima of Prec, IWC, WV, the IWC fraction, and RHI are found over the eastern Pacific Ocean and South Atlantic Ocean. Over the MariCont region, we observe the maximum of tropical IWC and the minimum of temperature (Fig. 2a and d). The IWC fraction shows that, over the region of high Prec ($> 0.20\,\mathrm{mm\,h^{-1}}$), up to 70 % of the $\sum W$ is composed of ice. The RHI is higher over land than over ocean but never exceeds 100 % at 146 hPa, on average at $2° \times 2°$ resolution (consistent with the RHI tropical vertical profile shown by Fueglistaler et al., 2009). The MariCont region exhibits the highest RHI, with values close to 100 %. In summary, there is a strong spatial link between Prec and water (IWC and WV) in the UT.

In the TL (Fig. 3), IWC is lower than in the UT ($\sim 3\,\mathrm{mg\,m^{-3}}$ at 146 hPa vs. $< 1\,\mathrm{mg\,m^{-3}}$ at 100 hPa), but the horizontal distribution of IWC is correlated with the horizontal distribution of Prec and shows maxima over South America, South Africa, the MariCont region, and the western Pacific Ocean. The main difference between the UT and the TL is the minimum of WV observed over the MariCont region (> 8 ppmv at 146 hPa and < 3 ppmv at 100 hPa). With the decrease of temperature from the UT to the TL (Figs. 2 and 3) and the associated decrease of WV at saturation, the observed WV decreases by more than 11 ppmv over the MariCont region and by around 5 ppmv in other regions. In the TL, the IWC and the fraction of water in the ice form is larger over MariCont (beyond $1\,\mathrm{mg\,m^{-3}}$ and near 78 %, respectively) than elsewhere in the tropics. RHI in the TL reaches high values (RHI $\sim$ 100 %), highlighting a saturated environment over central South America, Africa, the east of MariCont, and the western Pacific Ocean. In comparison to other tropical regions, the larger IWC over the MariCont can be explained by (i) the larger condensation of water vapour associated with the larger temperature drop from the UT to the TL and (ii) a larger transport of ice into the TL by deep convection.

To investigate the vertical distribution and the diurnal cycles of water species in the TL, we have defined, from results presented in Figs. 1–3, seven tropical convective zones, shown in Fig. 4: South America (SouthAm; 0° N–30° S), South Africa (SouthAfr; 0° N–30° S), Pacific Ocean (PacOc; 0° N–30° S; 180° W–150° W), Indian Ocean (IndOc; 0° N–30° S; 60° E–90° E), MariCont (10° N–15° S; 90° E–160° E), MariCont land (MariCont-L), and MariCont ocean (MariCont-O). Land and ocean over the study zones have been separated using the Solar Radiation Data (SoDa; http://www.soda-pro.com/web-services/altitude/srtm-in-a-tile, last access: April 2019), providing a TIFF image with values from the Shuttle Radar Topography Mission (SRTM) digital elevation model. Each zone is defined at a horizontal resolution of $2° \times 2°$.

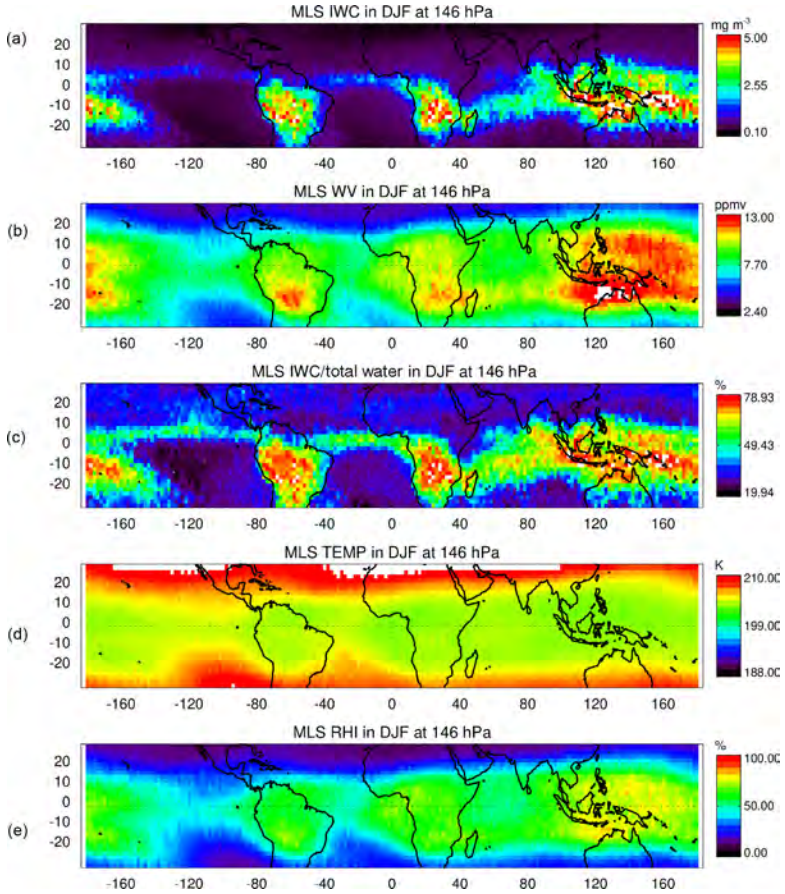

Figure 2. (a) Daily averaged ((day + night)/2) ice water content (IWC), **(b)** water vapour (WV), **(c)** IWC fraction (IWC/$\sum W$), **(d)** temperature, and **(e)** relative humidity with respect to ice (RHI) in the upper troposphere (146 hPa) measured by the MLS over the tropics in DJF over the period 2004–2017.

3.2 Water budget in the UT and the TL

To investigate the processes in the UT and TL which drive the water budget, the vertical profiles of TEMP, WV, IWC, and RHI are shown for the different study zones in Fig. 5. To complete the comparison between the study zones, the DJF average of the tropopause pressure level is represented over all the tropics in Fig. 6 from the National Centers For Environmental Prediction (NCEP).

In Fig. 5a, the tropical CPT is found between 100 and 80 hPa, consistent with previous results presented in, for example, Fueglistaler et al. (2009) and Kim and Son (2012). The tropical tropopause defined by NCEP (Fig. 6) is close to the level given by the MLS at 100 hPa, which we named the TL in this study (∼ 100–115 hPa). Furthermore, the tropopause pressure shown in Fig. 6 is lower (higher altitude) over ocean than over land, while the pressure at the tropopause over the western Pacific, the southern region of the Arabian Peninsula, and Caribbean Sea is the lowest (∼ 105 hPa). Furthermore, the tropopause is the coldest (Fig. 5a) and has the highest pressure (lower altitude) (Fig. 6) over the MariCont. Regarding WV, the tropical UT is more humid than the TL: the decrease from the UT at 146 hPa to the TL at 100 hPa is about 7 ppmv for WV and 1 mg m^{-3} for IWC (the two dashed lines in Fig. 5b and c, respectively). These results are consistent with previous studies, all presented in Fueglistaler et al. (2009).

RHI is lower in the UT than the TL by ∼ 10 % (Fueglistaler et al., 2009) (Figs. 2d and 3d, respectively). Since the UT is on average sub-saturated, convective-lifted ice can sublimate and can be seen as a source of WV. In the TL, as the atmosphere is on average close to saturation

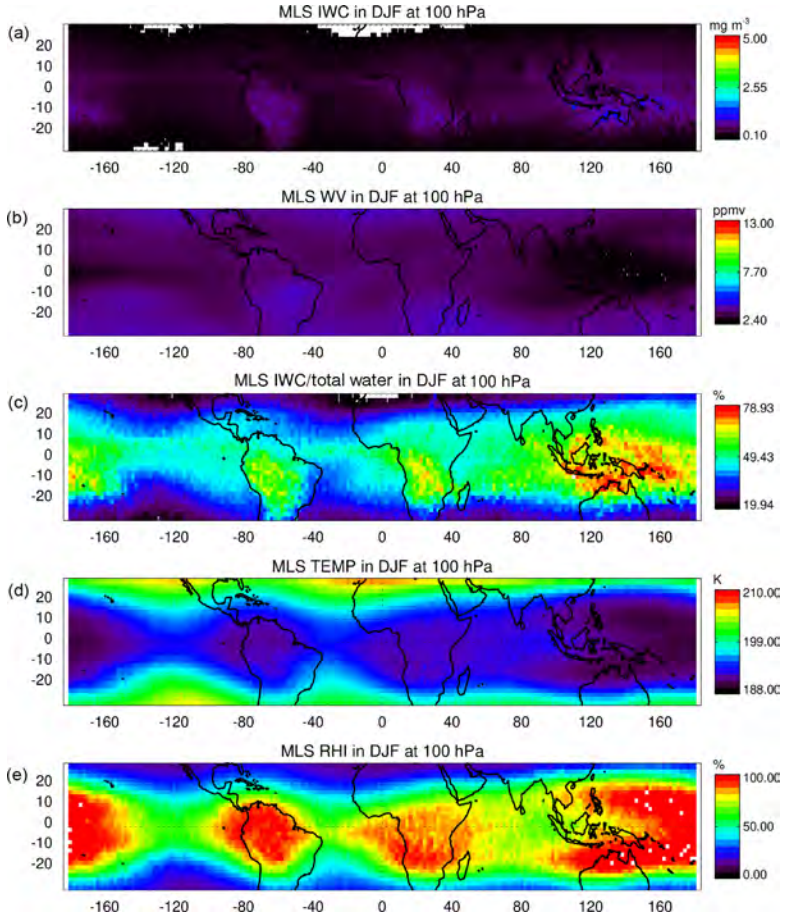

Figure 3. **(a)** Daily averaged ((day + night)/2) ice water content (IWC), **(b)** water vapour (WV), **(c)** IWC fraction (IWC/$\sum W$), **(d)** temperature, and **(e)** relative humidity with respect to ice (RHI) in the tropopause layer (100 hPa) measured by the MLS over the tropics in DJF over the period 2004–2017.

(RHI $\sim$ 100 %) over SouthAm, SouthAfr, MariCont, and the western Pacific Ocean (Fig. 3), the convective-lifted ice is statistically more often transported into a saturated or supersaturated region. In such a context, the associated ice hydrometeors grow and sediment and can also be transported down by convective downdrafts. These processes contribute to the loss of ice in this layer. Furthermore, the TL is the level of greatest dehydration because of supersaturation with respect to ice (Jensen et al., 1996, 2005). In supersaturation conditions, the excess of water vapour can condensate on existing ice crystals (or form new ones in the presence of a condensation nucleus), allowing ice crystals to grow and sediment, which dehydrates the layer. Conversely, hydration may occur in the LS (if reached by convection) because this layer is subsaturated with respect to ice (Khaykin et al., 2009; Allison et al., 2018; Dauhut et al., 2017).

3.3 Spatial correlation between Prec and water in the UT

This section presents the relationship between deep convection and the water vapour and ice injected into the UT. We have calculated the Pearson linear correlation coefficient R between the horizontal distribution of Prec and both IWC and WV at 146 hPa during the day, the night, and the day − night over the study zones (see Table 1). We denote Prec, IWC, and WV at 146 hPa during the day, night, and day − night, by Prec_x, IWC_x^{146}, and WV_x^{146}, respectively (where x = day, night, or day − night). The spatial correlation between IWC

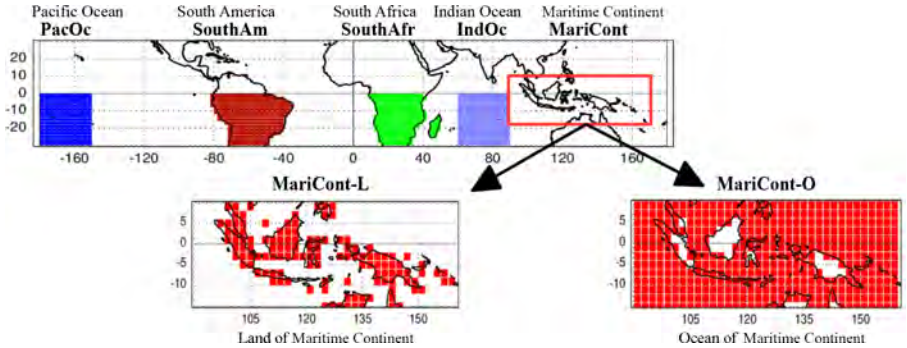

Figure 4. Representation of the study zones: PacOc, Pacific Ocean; SouthAm, South America; SouthAfr, South Africa; IndOc, Indian Ocean; MariCont-L, land of the Maritime Continent; and MariCont-O, ocean of the Maritime Continent. Each zone is defined at a horizontal resolution of $2° \times 2°$.

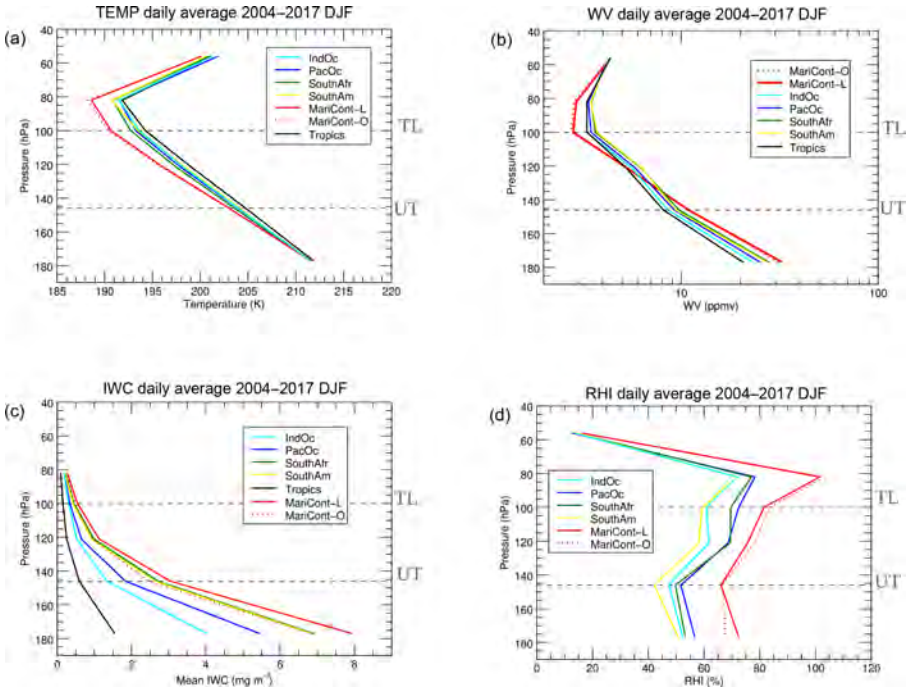

Figure 5. Vertical profiles of **(a)** temperature, **(b)** water vapour (WV), **(c)** ice water content (IWC), and **(d)** relative humidity with respect to ice (RHI) from MLS data averaged from 2004 to 2017 in DJF over the six study zones: IndOc (light blue), PacOc (dark blue), SouthAfr (green), SouthAm (yellow), tropics (black), MariCont-L (red solid line), and MariCont-O (red dashed line).

and Prec is defined by the following equation:

$$\mathrm{IWC}_x^{146} = \alpha_x \times \mathrm{Prec}_x + \beta_x, \quad (1)$$

where α_x is the regression coefficient, and β_x is the offset.

The spatial correlation for the six zones is shown in Table 1. The spatial correlation of $\mathrm{IWC}_{\mathrm{day}}^{146}$ and $\mathrm{IWC}_{\mathrm{night}}^{146}$ with Prec is high ($R \sim 0.7$–0.9) over SouthAm, SouthAfr, PacOc, and IndOc and smaller ($R \sim 0.5$–0.6) over the MariCont region (MariCont-L, MariCont-O, and MariCont). The spatial inhomogeneity of the MariCont surface with thousands of islands, seas, and coastal areas may probably explain the lower space correlation between Prec and IWC^{146}.

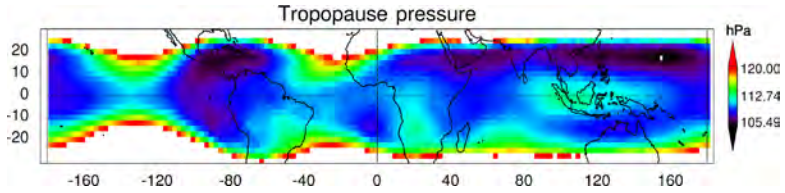

Figure 6. Pressure of the tropopause (hPa) over the tropics during DJF from 2004 to 2017, defined from the NCEP datasets.

Table 1. Pearson's linear correlation coefficient R, regression coefficient α ($\mathrm{mg\,m^{-3}\,mm^{-1}\,h}$), and the offset β ($\mathrm{mg\,m^{-3}}$) from the correlation between precipitation and ice water content (IWC), and water vapour (WV) in the upper troposphere (UT, at 146 hPa), at day, night, and day − night over the seven tropical zones and the average over the six zones ($\mu_{6\mathrm{zones}}$).

		Land			Ocean				
		SouthAm	SouthAfr	MariCont-L	IndOc	PacOc	MariCont-O	MariCont	$\mu_{6\mathrm{zones}}$
IWC	R ($\mathrm{IWC}^{\mathrm{UT}}_{\mathrm{day}}$, P_{day})	0.7	0.8	0.5	0.8	0.8	0.6	0.5	0.7
	α ($\mathrm{IWC}^{\mathrm{UT}}_{\mathrm{day}}$, P_{day})	8.1	15	9.3	4.8	5.9	7.5	8.9	8.4
	β ($\mathrm{IWC}^{\mathrm{UT}}_{\mathrm{day}}$, P_{day})	0.9	0.0	1.1	0.3	0.4	0.7	1.0	0.6
	R ($\mathrm{IWC}^{\mathrm{UT}}_{\mathrm{night}}$, P_{night})	0.7	0.7	0.6	0.9	0.7	0.6	0.6	0.7
	α ($\mathrm{IWC}^{\mathrm{UT}}_{\mathrm{night}}$, P_{night})	4.8	6.1	5.6	4.7	6.8	7.7	5.4	5.9
	β ($\mathrm{IWC}^{\mathrm{UT}}_{\mathrm{night}}$, P_{night})	0.6	0.6	1.4	0.3	0.2	0.6	1.6	0.6
	R ($\mathrm{IWC}^{\mathrm{UT}}_{\mathrm{day-night}}$, $P_{\mathrm{day-night}}$)	0.6	0.7	0.7	0.1	0.2	0.5	0.5	0.5
WV	R ($\mathrm{WV}^{\mathrm{UT}}_{\mathrm{day}}$, P_{day})	0.4	0.3	0.2	0.0	0.3	0.1	0.2	0.2
	α ($\mathrm{WV}^{\mathrm{UT}}_{\mathrm{day}}$, P_{day})	0.0	0.0	0.0	0.0	0.0	0.0	0.0	0.0
	R ($\mathrm{WV}^{\mathrm{UT}}_{\mathrm{night}}$, P_{night})	0.5	0.5	0.1	0.0	0.5	0.0	0.0	0.3
	α ($\mathrm{WV}^{\mathrm{UT}}_{\mathrm{night}}$, P_{night})	0.0	0.0	0.0	0.0	0.0	0.0	0.0	0.0
	R ($\mathrm{WV}^{\mathrm{UT}}_{\mathrm{day-night}}$, $P_{\mathrm{day-night}}$)	−0.0	−0.1	0.2	0.2	0.0	0.1	0.2	0.1

The regression coefficient between Prec_x and IWC_x (Table 1), α_x, can be interpreted as the efficiency of the convective system to inject ice in the UT. Comparing α_x in day and night conditions, SouthAfr, SouthAm, MariCont-L, MariCont-O, and MariCont stand out with larger day values ($\alpha_{\mathrm{D}} = 7.5$–$15.0\,\mathrm{mg\,m^{-3}\,mm^{-1}\,h}$) than IndOc and PacOc or than night values ($\alpha_x = 4.7$–$7.7\,\mathrm{mg\,m^{-3}\,mm^{-1}\,h}$). Over land, all regions under consideration show a better efficiency of injecting ice into the UT during the day than during the night. β_x is considered as the IWC background. Over land and ocean regions, β_x is close to zero. β_{day} is the highest over the MariCont-L ($1.1\,\mathrm{mg\,m^{-3}}$) and null over SouthAm ($0.0\,\mathrm{mg\,m^{-3}}$). Over the oceans, there is no significant differences between β_{day} and β_{night} for the injected ice in the UT, except over PacOc.

Following Liu and Zipser (2009) and Carminati et al. (2014), we also study the difference between day and night, to obtain information on the IWC^{146} diurnal cycle. Figure 7 shows the $\mathrm{Prec}_{\mathrm{day-night}}$, $\mathrm{IWC}^{146}_{\mathrm{day-night}}$, and $\mathrm{WV}^{146}_{\mathrm{day-night}}$, respectively. Convective regions such as SouthAm and SouthAfr, even along the ITCZ, are characterised by a positive day − night signal in $\mathrm{Prec}_{\mathrm{day-night}}$ and IWC^{146}_x with values greater than $0.10\,\mathrm{mm\,h^{-1}}$ and $0.20\,\mathrm{mg\,m^{-3}}$, respectively (Fig. 7a and b). The spatial correlation R between $\mathrm{Prec}_{\mathrm{day-night}}$ and $\mathrm{IWC}^{146}_{\mathrm{day-night}}$ is greater over the three land zones ($R \geq 0.6$–0.7) than over the three ocean zones ($R \leq 0.1$–0.5). The MariCont-O region shows the highest oceanic correlation ($R \sim 0.5$) compared to the PacOc and IndOc regions ($R = 0.2$ and 0.1, respectively). The low R values over IndOc and PacOc could be explained by (i) the low $\mathrm{IWC}_{\mathrm{day-night}}$ variability compared to the high $\mathrm{Prec}_{\mathrm{day-night}}$ variability observed over ocean and (ii) the low amplitude of the deep convection diurnal cycle over ocean (Liu and Zipser, 2005). We could hypothesise that IWC^{146} over the MariCont-O is more influenced by local deep convection than over IndOc and PacOc. However, considering IWC^{146} and Prec during the day and night independently, we find good correlation over the ocean (~ 0.6–$0.8\,\mathrm{mg\,m^{-3}}$).

The spatial correlation R between Prec_x and WV^{146}_x remains low in all configurations, with values of 0.0–0.5 (Ta-

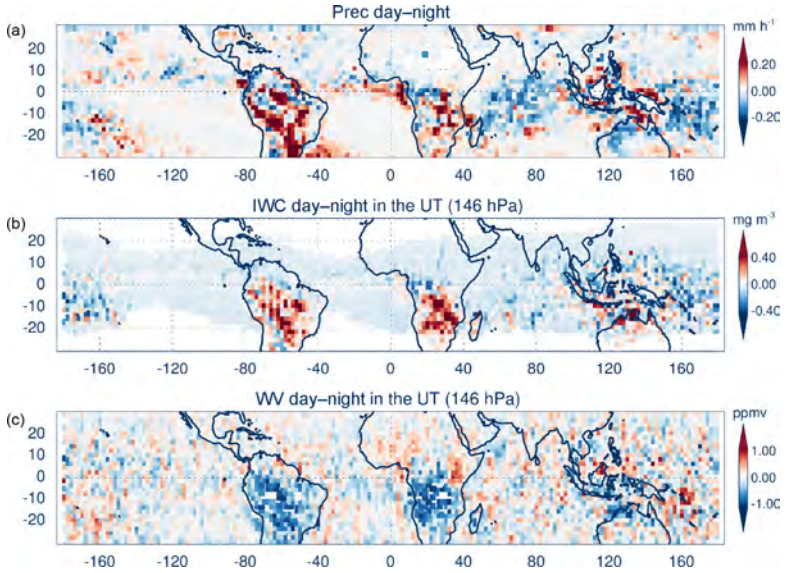

Figure 7. Day − night of **(a)** precipitation (Prec) from the TRMM, **(b)** ice water content (IWC) from the MLS at 146 hPa, and **(c)** water vapour (WV) from the MLS at 146 hPa over the tropics and the period 2004–2017 in DJF.

ble 1). The spatial correlation between the $WV^{146}_{day-night}$ and $Prec_{day-night}$ shows an average over the seven study zones of $\mu_{zones} \sim 0.07$ with small negative correlations over SouthAm and SouthAfr and with a regression coefficient α_x between WV^{146} and Prec calculated to be $\alpha_x = 0$ (Table 1). We conclude that WV is not spatially correlated with the diurnal cycle of deep convection. These results are consistent with results from Liu and Zipser (2009) and Carminati et al. (2014) showing that the day − night signal of WV measured by the MLS is very different with the day − night signal of IWC measured by the MLS in the UT over land.

Deep convection does not inject WV directly into the UT, but it injects ice, which then may sublimate into WV. Modelling studies with cloud resolving models illustrate the sequence of mechanisms (ice uplift, mixing, sublimation) that leads convection to hydrate initially subsaturated layers (Dauhut et al., 2015, 2018; Lee et al., 2018). In Dauhut et al. (2015), the onset of the WV increase is delayed by 1–3 h with respect to the onset of deep convection ($\sim$ 12:00 LT). Such a delay can explain why $WV^{146}_{day,\,night}$ and $Prec_{day,\,night}$ are not spatially correlated in observations ($R \sim 0.2$), while the space correlation R between $IWC^{146}_{day,\,night}$ and $Prec_{day,\,night}$ is stronger ($R \sim 0.7$). For this reason, we now focus on the diurnal cycle of ice and on the amount of ice injected into the UT and the TL by deep convective systems traced by Prec.

3.4 Diurnal cycle of Prec

This section presents the diurnal cycle of Prec over the six study zones during the Southern Hemisphere convective season (DJF) from 2004 to 2017 over land and ocean, respectively (Fig. 8a and b).

Over land, the amplitude (peak to peak) of the Prec diurnal cycle varies between 0.2 and 0.3 mm h^{-1}, with simultaneous minima between 08:00 and 09:00 LT within the regions. The MariCont-L area shows the driest minimum (0.09 mm h^{-1}) and the wettest and latest maximum (16:00–17:00 LT, 0.385 mm h^{-1}). SouthAm and SouthAfr maxima are found at 14:00–15:00 LT and 15:00–16:00 LT, respectively.

Over ocean, the amplitude of the Prec diurnal cycle varies between 0.08 and 0.1 mm h^{-1}, with simultaneous minima between 17:00 and 18:00 LT. However, the maxima are spread between 01:00 and 06:00 LT.

The main differences between Prec diurnal cycle over tropical ocean and land are that (i) there is a morning maximum over ocean compared to early afternoon over land, (ii) the peak-to-peak diurnal cycle of Prec is larger over land than over ocean, and (iii) minima can be twice lower over land (0.1 mm h^{-1}) than over ocean. The comparison of the Prec diurnal cycle over MariCont and MariCont-O or MariCont-L highlights the importance of analysing the diurnal cycle over land and over ocean in this region separately because MariCont-O and MariCont-L have two distinct be-

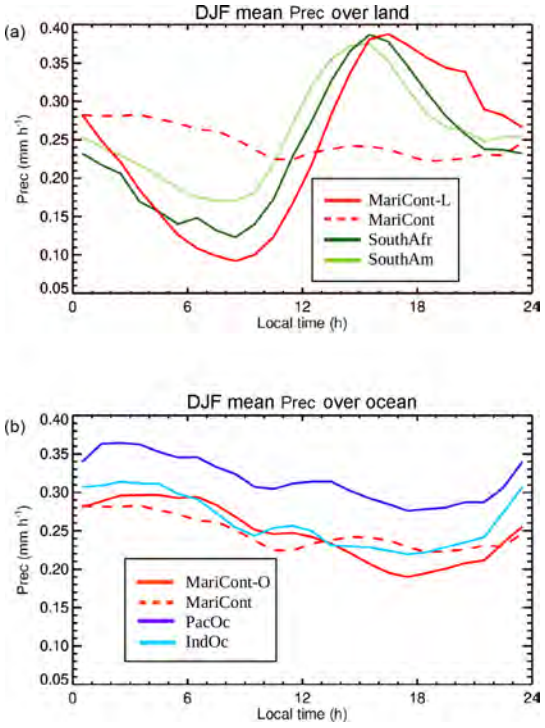

Figure 8. Diurnal cycle of precipitation (Prec) over **(a)** the land study zones and **(b)** the ocean study zones during the period DJF 2004–2017.

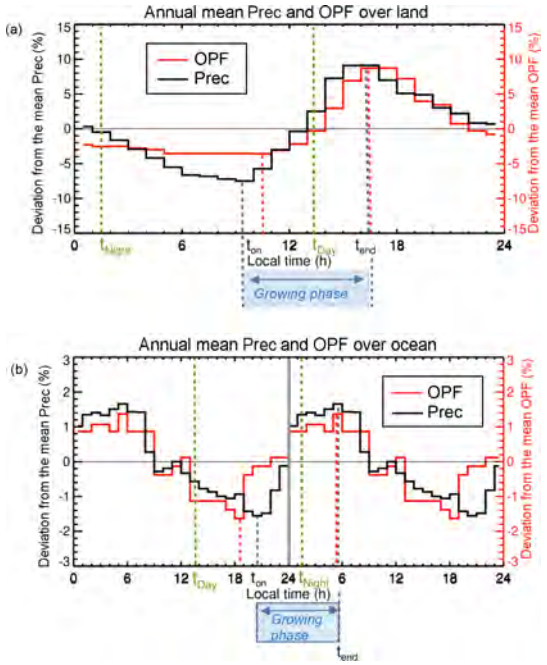

Figure 9. **(a)** Deviation from the mean of the annual mean diurnal cycle of TRMM precipitation (Prec; black solid line) over land, from 2004 to 2017 and diurnal cycle of overshooting precipitation features (OPFs) at the tropopause (red solid line) over land, from 1998 to 2000 and from 2001 to 2003, adapted from Liu and Zipser (2005) over the tropics (20° N–20° S). **(b)** Same as **(a)** but over the ocean. Minimum and maximum Prec and OPFs are shown by vertical dotted lines (in black and red, respectively). t_{on} is the time of the onset of the Prec, t_{end} is the time of the diurnal maximum of Prec, and t_{day} and t_{night} are the times of the two MLS measurements at day and night, respectively.

haviours which are hidden when the diurnal cycle is only considered over the MariCont global area.

3.5 Time correlation between Prec and IWC during the growing convective phase in the UT

In this section, we quantify the link between deep convection reaching the UT and Prec. The diurnal cycle of Prec is compared to the diurnal cycle of the frequency of overshooting precipitation feature (OPF) events (i.e. the proportion of all OPF events that occur in various ranges of time of day, adapted from Fig. 3 of Liu and Zipser (2005) from global satellite radar measurements) over land (Fig. 9a) and ocean (Fig. 9b) in the tropical band (20° S–20° N). The OPFs considered by Liu and Zipser, 2005, are tropical deep convective systems penetrating the tropical TL (called $Z_{\text{tropopause}}$ in Liu and Zipser, 2005). The OPFs are calculated from measurements from January 1998 to November 2000 and from December 2001 to December 2003 based on TRMM precipitation radar (PR) measured reflectivity into precipitation features (PFs) and using the method described by Nesbitt et al. (2000). The OPFs can be identified thanks to the high vertical resolution of the TRMM PR.

Over land, the diurnal cycle of Prec and OPFs shows a maximum at 16:00–17:00 LT and a minimum at 09:00–10:00 LT (Fig. 9a). The duration of the growing phase, defined as the period between the minimum and the maximum of Prec, is the same for OPFs and Prec and lasts $\Delta t = 7$ h. The major difference in the diurnal cycles of Prec and OPFs occurs after the growing phase: the fraction of OPFs decreases more rapidly than that of Prec and stops decreasing around 00:00 LT, whereas that of Prec continues to decrease. This difference can be explained by the contribution to Prec of (1) the convection that does not reach the stratosphere and (2) the mature phase of the OPFs that produces stratiform rain for some hours after the overshooting time. These results over land are consistent with Pereira et al. (2006), showing that shallow convection is associated with 10 % of precipitation over the Amazonian region. Although OPF and Prec diurnal cycles are not calculated over the same study period, we

can deduce from the present analysis that during the growing phase, the time evolution of Prec is a good proxy for the time evolution of deep convection reaching the TL (OPFs).

Over ocean, the sea surface temperature (SST) does not have a strong diurnal cycle (less than ~ 1 K), with a peak in the early afternoon (e.g. Chen and Houze, 1997; Stuart-Menteth et al., 2003). The convective clouds usually develop after the SST peak, during the afternoon, and during the night, with a maximum in the early local morning. The diurnal cycles of Prec and OPFs (Fig. 9b) over the ocean have a maximum over night (05:00–06:00 LT) and a minimum at the end of the afternoon (18:00–19:00 LT for the OPFs and 20:00–21:00 LT for the Prec). The diurnal cycles of OPFs and Prec over the ocean show similar amplitudes in deviation from the mean. This result is consistent with Peirera and Rutledge (2006), showing that the shallow convection is associated with only 3 % of precipitation over the eastern Pacific region.

In summary, although OPFs are representative of deep convection reaching the TL, OPFs developed and presented in Liu and Zipser (2005) are not available during our study period of 2004–2017. However, our results in this section have shown that during the growing stage of deep convection, Prec is a good proxy for convection reaching the TL over land and ocean. Thus, as Prec is available in time coincidence with the MLS IWC and WV over 2004–2017, we will use Prec to interpret the time evolution of IWC in the UT and the TL.

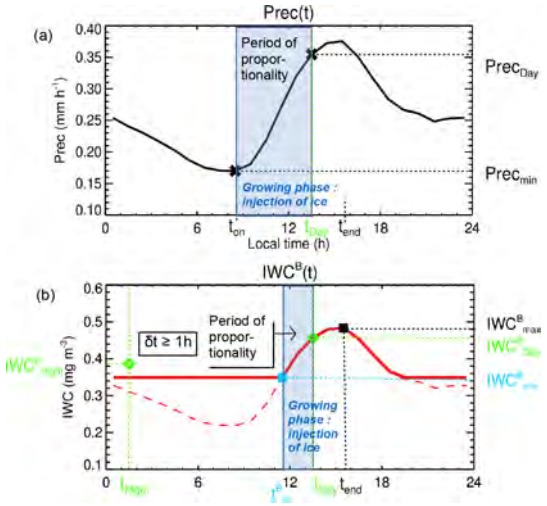

Figure 10. Methodology to estimate the diurnal cycle of ice water content (IWC) over land: **(a)** diurnal cycle of precipitation, with × representing the minimum of precipitation ($\mathrm{Prec_{min}}$) with its associated time (t_{on}) and Prec during the day ($\mathrm{Prec_{day}}$) at $t_{\mathrm{day}} = 13{:}30$ LT. **(b)** The diurnal cycle of $\mathrm{IWC}^B(t)$ is shown by the red solid line, estimated from the diurnal cycle of Prec and from the two MLS measurements of ice (green diamonds, IWC^B_x), with the timing of the onset of the ice injection at $t^B_{\mathrm{on}} = t_{\mathrm{on}} + \delta t^B$. The black square represents the IWC maximum ($\mathrm{IWC}^B_{\mathrm{max}}$) and the blue square the $\mathrm{IWC}^B_{\mathrm{min}}$ when $\delta t^B > 1$ h. Note that when $t_{\mathrm{on}} \approx t^B_{\mathrm{on}}$, the diurnal cycle of IWC is represented by the red dashed line.

4 Amount of ice injected into the UT and the TL by deep convection

In this section, we present the method we have developed to estimate the diurnal cycle of IWC in the UT ($\mathrm{IWC}^{\mathrm{UT}}(t)$) and in the TL ($\mathrm{IWC}^{\mathrm{TL}}(t)$) based on the diurnal cycle of Prec and on the two IWC measurements by the MLS per day. Like in the previous section for OPFs, we separate the diurnal cycle of IWC into a growing phase (period when deep convection develops to reach the UT and the TL) and a decreasing phase (period when deep convection dissipates). During the growing phase, Prec is a good indicator (proxy) of deep convection both over land and ocean (Sect. 3.5). This is not true during the decreasing phase, when shallow convection can have a significant impact on Prec. Since IWC is spatially highly correlated with Prec, and since the deep convection (OPFs) bringing ice into the TL increases with Prec during the growing phase, we expect ice to be injected up to the UT and the TL with a delay $\left(\delta t^{\mathrm{UT,TL}}\right)$ after the onset of the deep convection t_{on} during the growing phase.

The method developed focuses on the growing stage of deep convection. We quantify the amount of ice injected to the UT and the TL and determine the onset time of the ice injection and its duration. The amount of ice injected will be calculated from the estimation of the amplitude of the diurnal cycle of IWC in the UT and the TL.

4.1 IWC diurnal cycle in the UT and TL

The method to estimate $\mathrm{IWC}^B(t)$ (B = UT or TL) is presented in this section. Figure 10 illustrates the methodology to find the $\mathrm{IWC}^B(t)$ over land (the diagram over ocean would look different since maxima appear during local night). t_{on} is defined as the time when Prec starts to increase, and t^B_{on} is defined as the time when IWC^B starts to increase. Our two main hypotheses are to assume that (i) IWC^B starts to increase later than Prec (a delay δt^B is assumed) because convective systems precipitate before reaching UT and TL, as follows,

$$t^B_{\mathrm{on}} = t_{\mathrm{on}} + \delta t^B, \tag{2}$$

and (ii) the $\mathrm{IWC}^B(t)$ is proportional to the $\mathrm{Prec}(t)$ during the convective growing phase (see the period of proportionality in Fig. 10). This hypothesis considers deep convection represented by Prec as the main process bringing ice into the UT and the TL during the growing phase of the convection. Based on these two hypotheses, and knowing Prec_x and

IWC_x^B at t_x and t_{on}^B, we estimate $\mathrm{IWC}^B\left(t_{\mathrm{on}}^B\right)$ as follows:

$$\mathrm{IWC}^B\left(t_{\mathrm{on}}^B\right) = \frac{\mathrm{Prec}\left(t_{\mathrm{on}}^B\right)}{\mathrm{Prec}_x} \times \mathrm{IWC}_x^B, \tag{3}$$

where $x =$ day or N. We use $t_x = t_{\mathrm{day}}$ for land since only the day measurement occurs during the growing phase over land, and $t_x = t_{\mathrm{night}}$ over sea since only the night measurement occurs during the growing phase over ocean. Knowing $\mathrm{IWC}^B\left(t_{\mathrm{on}}^B\right)$ and t_{on}^B, the time evolution $\mathrm{IWC}^B(t)$ during the growing phase is then

$$\mathrm{IWC}^B(t) = \begin{cases} \dfrac{\mathrm{Prec}(t)}{\mathrm{Prec}\left(t_{\mathrm{on}}^B\right)} \times \mathrm{IWC}^B\left(t_{\mathrm{on}}^B\right) & \text{if } \mathrm{Prec}(t) > \mathrm{Prec}\left(t_{\mathrm{on}}^B\right) \\ \mathrm{IWC}^B\left(t_{\mathrm{on}}^B\right) & \text{else.} \end{cases} \tag{4}$$

Our method can then estimate the magnitude of the diurnal variation in the UT and the TL($\Delta\mathrm{IWC}^B$) over different regions of the tropics:

$$\Delta\mathrm{IWC}^B = \mathrm{IWC}^B(t_{\mathrm{end}}) - \mathrm{IWC}^B\left(t_{\mathrm{on}}^B\right) = \mathrm{IWC}_{\mathrm{max}}^B - \mathrm{IWC}_{\mathrm{min}}^B, \tag{5}$$

with t_{end} being the time of the diurnal maximum of Prec. t_{end} can be considered as the time of the end for ice injection or the time from which the downdraft processes are more important than the updraft processes. Thus, we define $\delta t_{\mathrm{end}}^{\mathrm{UT}}$ as the delay between t_{end} and $t_{\mathrm{end}}^{\mathrm{UT}}$. Following hypothesis (ii) that considers that deep convection is the main process bringing ice into the UT and the TL, calculated $\Delta\mathrm{IWC}^B$ represents the amount of ice injected by deep convection in these two layers. Thus, the duration of the injection of ice during the growing phase, Δt^B, is then

$$\Delta t^B = t_{\mathrm{end}} - t_{\mathrm{on}}^B. \tag{6}$$

In order to validate this method, we compare the estimation of the amount of ice injected ($\Delta\mathrm{IWC}^B$) into the UT and the TL with the amount of ice measured in the troposphere and in the TL by the SMILES instrument on board the ISS during the short convective period of December 2009 to February 2010.

4.2 Evaluation of the method with SMILES measurements

The SMILES instrument measured IWC between 120 and 80 hPa and the overall measurement of tropospheric ice, the partial ice water path (pIWP) integrated between 1000 and 180 hPa, from October 2009 to April 2010. This period is an El Niño–Southern Oscillation (ENSO) period, increasing the convective activity over South Africa and the western Pacific Ocean and decreasing the convective activity over the MariCont region and South America. The diurnal cycle of

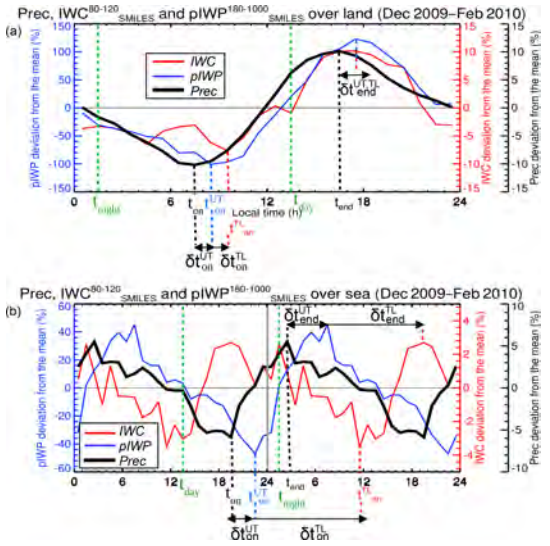

Figure 11. Deviation from the mean (%) of the diurnal cycle of partial ice water path (pIWP; integrated between 1000 and 180 hPa), ice water content (IWC; averaged between 80 and 120 hPa) measured by SMILES, and precipitation (Prec) over **(a)** the tropical land (0–30° S) and **(b)** tropical ocean (0° N–30° S) from December 2009 to February 2010. t_{on}, $t_{\mathrm{on}}^{\mathrm{UT}}$, and $t_{\mathrm{on}}^{\mathrm{TL}}$ are the onsets of the Prec, pIWP, and IWC increase, respectively. t_{end} is the end of the Prec increase. $\delta t_{\mathrm{on}}^{\mathrm{UT}}$ and $\delta t_{\mathrm{on}}^{\mathrm{TL}}$ are the delays between t_{on} and $t_{\mathrm{on}}^{\mathrm{UT}}$ and $t_{\mathrm{on}}^{\mathrm{TL}}$, respectively, and $\delta t_{\mathrm{end}}^{\mathrm{UT}}$ and $\delta t_{\mathrm{end}}^{\mathrm{UT}}$ are the delays between t_{end} and the end of the pIWP and IWC increase, respectively. Data have been smoothed out using a 6 h running average.

IWC and pIWP calculated from SMILES has shown the well-separated signal over tropical land and ocean (Millán et al., 2013; Jiang et al., 2015). The anomalies of the diurnal cycle of IWC measured by SMILES near the TL, the diurnal cycle of pIWP in the troposphere, and the diurnal cycle of Prec measured during the convective period of December 2009 to February 2010 are presented in Fig. 11a over the three land study zones and in Fig. 11b over the three ocean study zones, both with a running average of 6 h. t_{on}, $t_{\mathrm{on}}^{\mathrm{UT}}$, and $t_{\mathrm{on}}^{\mathrm{TL}}$ are the times of the minimum of Prec ($\mathrm{Prec}_{\mathrm{min}}$), pIWP ($\mathrm{pIWP}_{\mathrm{min}}$), and IWC ($\mathrm{IWC}_{\mathrm{min}}$), respectively.

Over land, during the growing phase, pIWP is proportional to Prec (Fig. 11a). Assuming that IWC^{146} evolves like pIWC, this implies that $t_{\mathrm{on}}^{\mathrm{UT}} \approx t_{\mathrm{on}}\left(\delta t_{\mathrm{on}}^{\mathrm{UT}} = 0\right)$ at $\sim$ 08:00–09:00 LT, and $t_{\mathrm{end}}^{\mathrm{UT}} \approx t_{\mathrm{end}} + \delta t_{\mathrm{end}}^{\mathrm{UT}}$ at $\sim$ 16:00–17:00 LT, with $\delta t_{\mathrm{on}}^{\mathrm{UT}} \leq 1$ h and $\delta t_{\mathrm{end}}^{\mathrm{UT}} \leq 1$ h. Then, the pIWP decreasing phase follows the same time evolution as Prec, reaching minima ($\mathrm{Prec}_{\mathrm{min}}$ and $\mathrm{pIWP}_{\mathrm{min}}$) around 07:00–09:00 LT. Thus, ice in the troposphere follows the same diurnal cycle as the Prec within a time resolution of 1 h. In the TL, IWC is still proportional to Prec, but IWC starts to increase later than ($\delta t_{\mathrm{on}}^{\mathrm{TL}} \sim 1$ h) the pIWP in the UT (Fig. 11a). After t_{end}, IWC decreases more

rapidly than Prec and varies between +2 % and −7 % compared to the mean between 23:00 and 09:00 LT. Thus, as soon as the deep convection reaches one of these two levels, ice is brought by the updraft during the growing and mature stage of the convective activity. Then, ice decreases with the downdraft of the convective dissipating stage. However, the very deep convective activity reaching the TL starts later than the deep convection reaching the UT ($\delta t \approx 1$ h) and decreases quickly before reaching a background IWC minimum between 23:00 LT and 09:00 LT.

Over ocean during the growing phase (Fig. 11b), pIWP also increases proportionally to Prec. Assuming that IWC[146] evolves like pIWC, this implies that $t_{on}^{UT} \approx t_{on} + \delta t_{on}^{UT}\left(\delta t_{on}^{UT} \geq 1\,\text{h}\right)$ at $\sim$ 21:00–22:00 LT, and $t_{end}^{UT} \approx t_{end} + \delta t_{end}^{UT}$ at $\sim$ 04:00–05:00 LT, with $\delta t_{end}^{UT} > 1$ h. Thus, as $\delta t_{on}^{UT} \approx \delta t_{end}^{UT}$, the diurnal cycle of pIWP over ocean is synchronised with the diurnal cycle of Prec but delayed. In the TL and during the growing phase, IWC starts to increase later than pIWP (where $\delta t_{on}^{TL} \approx 15$ h; Fig. 11b). This result is consistent with the diurnal cycle of OPFs presented in Fig. 9, where OPFs start to increase with a delay $\delta t_{on}^{TL} \approx 9$ h with respect to the increase of Prec. According to Liu and Zipser (2005), only less than 5 % of OPFs reach the TL, so other processes in addition to deep convection govern the ice diurnal cycle in the TL over ocean, impacting the delay between the onset of ice injection t_{on}^{TL} and the onset of the convection t_{on}. After t_{on}^{TL}, IWC takes around 13 h to reach a maximum at $t_{end}^{TL} \sim$ 19:00–20:00 LT.

Table 2 presents the magnitude of diurnal variation of ice, that is to say, the amount of ice injected into the UT and the TL estimated using the model presented in Sect. 4.2 from the MLS and TRMM measurements (ΔIWC^{B}) and the magnitude of diurnal variation of ice measured by SMILES (ΔpIWP and ΔIWC_{SMILES}) over the six study zones and during DJF 2009–2010. ΔIWC^{UT} and ΔIWC^{TL} are close to $\Delta pIWP_{SMILES}$ and ΔIWC_{SMILES}, respectively (with differences between 0.02 and 0.28 mg m^{-3}). Thus, during the ENSO period of DJF 2009–2010, the amount of ice injected into the UT (ΔIWC^{UT}) is about 2.06–2.34 mg m^{-3} over land and 1.20–1.22 mg m^{-3} over ocean and into the TL (ΔIWC^{TL}) is about 0.26–0.31 mg m^{-3} over land and 0.13–0.22 mg m^{-3} over ocean. NOAA Interpolated Outgoing Longwave Radiation (OLR) during DJF 2009–2010 is lower over land (mean OLR between 195 and 215 W m^{-2}, not shown) than over ocean (between 235 and 270 W m^{-2}), which is consistent with the more intense land convective activity compared to that of oceans.

In summary, our method based on the correlation between Prec from the TRMM and IWC from the MLS during the growing stage of the convection (presented in Sect. 4.1) allows the amount of ice injected into the UT and the TL (ΔIWC^{B}) to be estimated and has been validated with the SMILES measurements over land and ocean. These results confirm that the diurnal cycle of Prec can be used as a proxy for deep convection reaching the UT and the TL during the growing stage of the deep convection. The analyses of SMILES data also suggest a good correlation of IWC^{UT} and Prec during the dissipating stage of the convection in the UT over land.

4.3 Amount of ice injected into the austral convective UT

Using the method presented in the previous section, 13 years of MLS and TRMM observations are analysed. Table 3 presents the time of the beginning of the IWC injection in the UT (t_{on}^{UT}), the duration of the IWC injection ($\Delta t^{UT} = t_{end} - t_{on}^{UT}$), the minimum value of IWC before the beginning of the IWC injection (IWC_{min}^{UT}), and the amount of ice injected into the UT (equivalent to the amplitude of the IWC diurnal cycle, $\Delta IWC^{UT} = IWC_{max}^{UT} - IWC_{min}^{UT}$).

Over land, t_{on}^{UT} is found during the morning at 08:00–09:00 LT whatever the land zone. However, Δt^{UT} is longer over MariCont-L than SouthAm and SouthAfr ($\Delta t^{UT} =$ 8, 7,and 7 h, respectively). Furthermore, IWC_{min}^{UT} is lower over the MariCont-L than over SouthAm and SouthAfr ($IWC_{min}^{UT} = 1.04$, 1.65, and 1.33 mg m^{-3}, respectively), but ΔIWC^{UT} is greater over the MariCont-L than over SouthAm and SouthAfr ($\Delta IWC^{UT} = 3.34$, 1.99, and 2.86 mg m^{-3}, respectively).

Over ocean, t_{on}^{UT} is found during the evening at 17:00–18:00 LT. Δt^{UT} is much longer over MariCont-O than over IndOc and PacOc ($\Delta t^{UT} = 11$, 9, and 9 h, respectively). However IWC_{min}^{UT} is greater over MariCont-O than over IndOc and PacOc ($IWC_{min}^{UT} = 1.62$, 1.01, and 1.46 mg m^{-3}, respectively), and ΔIWC^{UT} over MariCont-O is also greater than ΔIWC^{UT} over PacOc and IndOc ($\Delta IWC^{UT} = 0.91$, 0.46, and 0.43 mg m^{-3}, respectively).

Thus, the convective growing stage is quicker over land (7 h) than over ocean (10 h). These results are consistent with a previous study by Takahashi and Luo (2014), showing that the lifetime of the mature stage of the deep convection is between 6 and 12 h after the onset of the deep convection considering the Northern and Southern Hemisphere over the tropics. Furthermore, while the estimated means of IWC_{min}^{UT} over land and ocean are very close (1.34 and 1.36 mg m^{-3}, respectively), the means of the land and ocean ΔIWC^{UT} show great differences (2.73 and 0.60 mg m^{-3}, respectively). Thus, the ice minima are of similar amplitudes over land and ocean in the UT, but the amount of ice injected into the UT is about 4 times greater over land than over ocean. These results also show that the MariCont region is a region with a greater amount of ice injection in the UT compared to other tropical deep convective areas.

4.4 Amount of ice injected into the austral convective TL

From the method presented previously and the results from the SMILES instruments (Fig. 11), Table 4 presents t_{on}^{TL},

Table 2. Differences between the amount of ice water content (IWC) estimated by the TRMM and the MLS injected into the upper troposphere (UT) and the tropopause layer (TL) (ΔIWC^{UT} and ΔIWC^{TL}, respectively), and partial ice water path (pIWP) measured by SMILES in the UT ($\Delta pIWP_{SMILES}$) and IWC measured by SMILES in the TL (ΔIWC_{SMILES}), during the period DJF 2009–2010, and their differences ($\Delta IWC^{UT} - \Delta pIWP_{SMILES}$ and $\Delta IWC^{TL} - \Delta IWC_{SMILES}$, in the UT and the TL, respectively). The averages over the land and ocean zones (μ (Lands ZonesTropics) and μ (Oceans ZonesTropics), respectively) are also presented.

		UT			TL		
		ΔIWC^{UT} ($mg\,m^{-3}$)	$\Delta pIWP_{SMILES}$ ($mg\,m^{-3}$)	$\Delta IWC^{UT} - \Delta pIWP_{SMILES}$ ($mg\,m^{-3}$)	ΔIWC^{TL} ($mg\,m^{-3}$)	ΔIWC_{SMILES} ($mg\,m^{-3}$)	$\Delta IWC^{TL} - \Delta IWC_{SMILES}$ ($mg\,m^{-3}$)
Land	SouthAm	2.1	2.8	−0.7	0.34	0.29	+0.05
	SouthAfr	1.5	1.8	−0.3	0.23	0.27	−0.04
	MariCont-L	2.5	2.3	+0.2	0.35	0.23	+0.12
Ocean	IndOc	1.1	1.0	+0.1	0.34	0.09	+0.15
	PacOc	1.0	1.6	−0.5	0.21	0.24	−0.03
	MariCont-O	0.5	1.0	−0.6	0.10	0.08	+0.02
	μ (Lands ZonesTropics)	2.1	2.3	−0.3	0.31	0.26	+0.05
	μ (Oceans ZonesTropics)	1.2	1.2	+0.0	0.22	0.13	+0.09

Table 3. Time of the onset of the ice injection in the tropical upper troposphere (UT), (t_{on}^{UT}), duration of the injection of ice in the UT (Δt^{UT}), minimum amount of ice in the UT (IWC_{min}^{UT}), and amount of ice injected into the UT (ΔIWC^{UT}) as a function of the six study zones and averaged over the land and ocean zones (μ (Lands ZonesTropics) and μ (Oceans ZonesTropics), respectively) during DJF from 2004 to 2017. The bold values highlight the most important injection of ice and the associated regions.

Region	t_{on}^{UT} (LT)	Δt^{UT} (h)	IWC_{on}^{UT} ($mg\,m^{-3}$)	ΔIWC^{UT} ($mg\,m^{-3}$)
SouthAm	08:00–09:00	7	1.6	2.0
SouthAfr	08:00–09:00	7	1.3	2.9
MariCont-L	08:00–09:00	8	1.0	**3.3**
IndOc	17:00–18:00	9	1.0	0.4
PacOc	17:00–18:00	9	1.5	0.5
MariCont-O	17:00–18:00	11	1.6	**0.9**
μ (Lands ZonesTropics)	08:00–09:00	7	1.3	2.7
μ (Oceans ZonesTropics)	17:00–18:00	10	**1.4**	0.6

Δt^{TL}, IWC_{min}^{TL}, and ΔIWC^{TL} with respect to time for ice to be injected into the TL after the onset of deep convection, δt^{TL}, over the different study zones. We propose to use $\delta t^{TL} = 0$ to 3 h in order to always keep δt^{TL} shorter than $t_{on} - t_x$, where x is selected during the growing phase ($x = D$ over land and $x = N$ over ocean) in order to perform a sensitivity study of our results.

Over land, for all t_{on}^{TL}, the period of injection (Δt^{TL}) is longer over MariCont-L than over SouthAm and SouthAfr ($\Delta t^{TL} = 8$, 7, and 7 h, respectively). Depending on the δt^{TL} (between 0 and 3 h), Δt^{TL} can be between 7 and 8 and 4 and 5 h. ΔIWC^{TL} is greater over MariCont-L than over SouthAm and SouthAfr for all the δt^{TL}($\Delta IWC^{TL} \sim 0.56$–0.42, 0.26–0.13, and 0.40–0.24 $mg\,m^{-3}$, respectively). As observed in the short time period study with SMILES, the injection of ice over MariCont-L is the most intense over tropics. Furthermore, the smaller the δt^{TL}, the longer the Δt^{TL} and the greater the ΔIWC^{TL}.

Over ocean, as observed with the SMILES measurements, t_{on}^{TL} cannot be estimated with our method. However, our method is able to estimate Δt^{TL}, IWC_{min}^{TL}, and ΔIWC^{TL} as a function of δt^{TL} (as demonstrated in Sect. 4.1). Over MariCont-O, ice injection into the TL is longer than over IndOc and PacOc ($\Delta t^{TL} = 8$–11, 6–9, and 6–9 h, respectively). The amount of ice injected over MariCont-O is greater than over IndOc and PacOc ($\Delta IWC^{TL} = 0.16$–0.19, 0.09–0.10, 0.08–0.09 $mg\,m^{-3}$, respectively). Furthermore, the ice background in the TL is also greater over MariCont-O than over IndOc and PacOc ($IWC_{min}^{TL} \sim 0.34$–0.37, 0.24–0.26, 0.29–0.30 $mg\,m^{-3}$, respectively). Thus, while the diurnal cycle of Prec over MariCont-O is the weakest, the diurnal cycle of ice over MariCont-O would have the highest values.

Table 4. As a function of the delay ($\delta t = 0$, 1, 2, or 3 h) between the beginning of the Prec onset and the IWC onset in the tropical tropopause layer (TL): duration of the injection of ice in the TL (Δt^{TL}), minimum amount of ice in the TL ($\mathrm{IWC}^{\mathrm{TL}}_{\mathrm{min}}$), and amount of ice injected into the TL ($\Delta\mathrm{IWC}^{\mathrm{TL}}$) as a function of the six study zones and averaged over the land and ocean zones (μ (Lands ZonesTropics) and μ (Oceans ZonesTropics), respectively) during DJF from 2004 to 2017. The bold values highlight the most important $\mathrm{IWC}^{\mathrm{TL}}_{\mathrm{min}}$ and $\Delta\mathrm{IWC}^{\mathrm{TL}}$ and the associated regions.

Zones	$\delta t = 0$ h			$\delta t = 1$ h			$\delta t = 2$ h			$\delta t = 3$ h		
	Δt^{TL} (h)	$IWC^{\mathrm{TL}}_{\mathrm{min}}$ (mg m^{-3})	$\Delta\mathrm{IWC}^{\mathrm{TL}}$ (mg m^{-3})	Δt^{TL} (h)	$IWC^{\mathrm{TL}}_{\mathrm{min}}$ (mg m^{-3})	$\Delta\mathrm{IWC}^{\mathrm{TL}}$ (mg m^{-3})	Δt^{TL} (h)	$IWC^{\mathrm{TL}}_{\mathrm{min}}$ (mg m^{-3})	$\Delta\mathrm{IWC}^{\mathrm{TL}}$ (mg m^{-3})	Δt^{TL} (h)	$\mathrm{IWC}^{\mathrm{TL}}_{\mathrm{min}}$ (mg m^{-3})	$\Delta\mathrm{IWC}^{\mathrm{TL}}$ (mg m^{-3})
SouthAm	7	0.22	0.26	6	0.23	0.25	5	0.28	0.20	4	0.35	0.13
SouthAfr	7	0.19	0.40	6	0.21	0.38	5	0.26	0.33	4	0.35	0.24
MariCont-L	8	0.17	**0.56**	7	0.19	**0.55**	6	0.23	**0.50**	5	0.32	**0.42**
IndOc	9	0.24	0.10	8	0.24	0.10	7	0.25	0.09	6	0.26	0.09
PacOc	9	0.29	0.09	8	0.29	0.09	7	0.29	0.09	6	0.30	0.08
MariCont-O	11	**0.34**	**0.19**	10	**0.35**	**0.18**	9	**0.36**	**0.17**	8	**0.37**	**0.16**
μ (Lands ZonesTropics)	7	0.19	0.41	6	0.21	0.39	5	0.26	0.34	4	0.34	0.26
μ (Oceans ZonesTropics)	10	0.29	0.13	9	0.29	0.12	8	0.30	0.12	7	0.31	0.11

Table 5. Difference d between ice water content measured by the MLS during the decreasing phase (IWC_x) and ice water content estimated at the same hour ($\mathrm{IWC}(x)$) in the upper troposphere (UT) and the tropopause layer (TL) (where x = day or night as a function of the timing of the decreasing phase of the ice diurnal cycle).

	Zones	d in the UT (mg m^{-3})	d in the TL (mg m^{-3})
Land	SouthAm	+0.48 (+23 %)	−0.08 (−20 %)
	SouthAfr	+0.44 (+20 %)	−0.07 (−18 %)
	MariCont-L	−0.09 (−3 %)	−0.09 (−14 %)
Ocean	IndOc	0.17 (−21 %)	−0.02 (−7 %)
	PacOc	−0.20 (−10 %)	+0.03 (+9 %)
	MariCont-O	−0.47 (−26 %)	−0.04 (−8 %)

As expected from the SMILES measurements, the MariCont region presents the largest ice injection in the TL. While the IWC background over MariCont-O is the largest, the injection of IWC over MariCont-L is the most important.

5 Discussion on the processes driving the decreasing phase of the IWC diurnal cycle

The previous section has shown that the growing phase of the diurnal cycle of deep convection in the tropics impacts on the growing phase of diurnal cycle of ice in the UT and the TL. In this section, the convective processes impacting the decreasing phase of the ice diurnal cycle in the UT and the TL are discussed. The decreasing phase of the diurnal cycle of ice in the UT and the TL represents the diurnal loss of ice. This loss can be caused by several processes, including sedimentation, downdraft convective processes during the dissipating stage, sublimation into water vapour, or horizontal advection and mixing. Quantifying the processes impacting the diurnal cycle of ice can help to quantify the amount of water that stays in the UT and TL, the part that falls down to the surface, and the part that is advected up to the LS at the temporal diurnal scale.

In this section, the comparison between the value of IWC measured by the MLS during the decreasing phase (IWC_x) at (x = day or night) and IWC estimated at the same t_x ($\mathrm{IWC}(t_x)$) is discussed. If $\mathrm{IWC}_x \sim \mathrm{IWC}(t_x)$, our model based on Prec evolution is a good predictive tool to consider that convective processes (as represented by Prec) control the decreasing phase of the ice diurnal cycle. Otherwise, non-convective processes also need to be investigated to explain the ice diurnal cycle. Table 5 presents the difference d ($d = \mathrm{IWC}(t_x) - \mathrm{IWC}_x$) in the UT and the TL.

Over land in the UT, d is positive and less than 23 % over SouthAm and SouthAfr and close to zero over the MariCont-L. The fact that the amount of Prec over SouthAm and SouthAfr is greater than required to explain IWC suggests that a significant fraction of the convection is shallow and

does not reach the UT. In contrast, over the MariCont-L, the diurnal cycle of Prec is very similar to the diurnal cycle of IWC, suggesting that the convective activity over this region brings a large amount of ice all over the 24 h. In the TL, d is found between $-14\,\%$ and $-20\,\%$, implying that the ice decreases more slowly than Prec.

Over ocean in the UT, d is negative down to $-26\,\%$, showing that the ice stay longer in the UT compared to the Prec decreasing phase. In the TL, d varies between $+9$ and -7, showing low differences d at this level.

In summary, the method presented in the present paper allows the diurnal cycle of ice in the UT and the TL to be estimated within 26 % over the six tropical zones and to within 14 % over the MariCont-L region.

6 Conclusion and perspectives

To quantify the amount of ice injected into the tropical upper troposphere (UT) and the tropopause layer (TL) and the processes linked to the ice diurnal variation, it is important to better understand the amount of total water in these layers and the amount of water entering into the LS. The information given by the MLS on the diurnal cycle of ice water content (IWC) in the UT and the TL and the method comparing the two measurements per day (Liu and Zipser, 2005; Carminati et al., 2014) are too limited to estimate the ice variability in these layers. Thus, the present study starts to assume that the diurnal cycle in ice is related to the diurnal cycle in precipitation (for which there are TRMM data with much better time resolution) in the austral convective tropics. The strong relationship between precipitation (Prec) measured by the TRMM and IWC measured by the MLS in the UT and the TL is shown in the study. As the MLS measures IWC only twice a day, at 01:30 (night) and 13:30 LT (day), we have proposed a simple model based on the diurnal cycle of Prec to estimate the diurnal cycle of IWC in the UT and in the TL. The method is validated using the short period of DJF 2009–2010 of ice measurement from the SMILES instrument in the troposphere and the TL.

Because of the strong space correlation between Prec and IWC, we show that Prec can be used as a proxy for deep convection reaching the UT and the TL during the growing stage of convection in order to bring ice into the UT and the TL. The method proposed in the study allows us to estimate (1) the diurnal cycle of ice into the UT and the TL and (2) the difference between the maximum and the minimum in the diurnal cycle of ice in these layers, namely the amount of ice injected by deep convection. Our method suggests that deep convection is the most important process in the austral convective tropics driving the diurnal increase of ice in these layers. Other processes may play a minor role, such as the decrease of the temperature in the TTL, increasing the saturation ratio and allowing the crystal nucleation and growth, or ice being brought into the UT and TL by horizontal advection.

The amount of ice injected into the UT ($2.73\,\mathrm{mg\,m^{-3}}$ over land and $0.60\,\mathrm{mg\,m^{-3}}$ over ocean) is found to be much higher than the amount of ice injected into the TL (0.26–$0.41\,\mathrm{mg\,m^{-3}}$ over land and 0.11–$0.13\,\mathrm{mg\,m^{-3}}$ over ocean). Furthermore, the study highlights the importance of separating the land of the Maritime Continent (MariCont-L) from the ocean of the Maritime Continent (MariCont-O) to better understand the ice diurnal cycle in the UT and the TL over the complex and strong convective region of the Maritime Continent. It has been shown that the injection of ice over the MariCont-L into the UT and the TL ($\Delta\mathrm{IWC}^{\mathrm{UT}} = 3.34\,\mathrm{mg\,m^{-3}}$, $\Delta\mathrm{IWC}^{\mathrm{TL}} = 0.56$–$0.42\,\mathrm{mg\,m^{-3}}$) is the greatest in the tropics. This injection of ice has a strong importance for the amount of ice entering into the LS and for feeding what has been called the "stratospheric fountain" (Newell and Gould-Stewart, 1981) observed over the MariCont region.

The decreasing phase of the ice diurnal cycle is also evaluated with Prec and discussed. While it is difficult to quantify the impact of other processes than convective processes on the diurnal cycle of ice in the UT and the TL, we are able to establish that deep convection impacts the depletion of ice during the decreasing phase of the ice diurnal cycle (from Table 5: 97 % in the UT over the MariCont and $\sim 80\,\%$ in averaged UT and TL over other regions). Thus, Prec is also considered to be a good proxy for the decreasing phase of the convection, especially over the MariCont-L region in the UT (to within 3 %, according to Table 5), and convective processes are the main processes impacting the decreasing phase of the diurnal cycle of ice. Furthermore, our study has shown that the estimated diurnal variation of ice is the largest in the regions (identified by the TRMM) where the diurnal variation in temperature is also the largest, although horizontal transport may play a role, but it cannot be quantified using our methodology.

In summary, while the importance of deep convective processes and large-scale three-dimensional circulation processes for the ice and water injection up to the UT, TL, and LS are still debated, this study shows that the ice diurnal cycle in the UT and the TL is mainly governed by vertical processes linked to the convective activity that are much stronger than other processes, such as horizontal mixing, sublimation, and sedimentation.

Although it is beyond the scope of the present paper, some potentially new results might be achievable using our method, e.g. the part of ice sublimating during deep convection and the impact of intra-seasonal variability such as ENSO and the Madden–Jullian Oscillation (MJO) on the ice diurnal cycle. In fact, ENSO and MJO have a strong influence on the tropical deep convection and injection of moisture into the TTL (Gettelman and Forster, 2002; Wong and Dessler, 2007) and are associated to the cold anomalies near the TTL, especially over the Maritime Continent region

(Zhang, 2013). We are expecting a strong impact on the diurnal ice injection timing and duration in the TL. The processes impacting the ice injection into the UT and the TL over the Maritime Continent regions at a local scale will be studied in a forthcoming paper.

Data availability. The observational datasets are available from the following websites: https://trmm.gsfc.nasa.gov/publications_dir/publications.html (last access: 1 January 2019, Prec from TRMM), https://disc.gsfc.nasa.gov/datasets?age=1&keywords=ML2IWC_004 (last access: 1 January 2018, IWC from MLS), ftp://mls.jpl.nasa.gov/pub/outgoing/smiles (last access: 1 December 2018, IWC and pIWC from SMILES), and https://www.esrl.noaa.gov/psd/cgi-bin/db_search/DBSearch.pl?Variable=Tropopause+Pressure&group=0&submit=Search (last access: 1 January 2019, tropopause pressure from NCEP).

Appendix A: List of abbreviations and acronyms and their meanings

CPT	cold point tropopause
DJF	December, January, February
IndOc	Indian Ocean
IWC	ice water content
LS	lower stratosphere
LT	local time
MariCont	Maritime Continent
MariCont-L	Maritime Continent land
MariCont-O	Maritime Continent ocean
MLS	Microwave Limb Sounder
Prec	precipitation
pIWP	partial ice water path
PacOc	Pacific Ocean
RHI	relative humidity with respect to ice
SouthAm	South America
SouthAfr	South Africa
TEMP	temperature
TL	tropopause layer
TRMM	Tropical Rain Measuring Mission
TST	troposphere to stratosphere transport
TTL	tropical tropopause layer
UT	upper troposphere
WV	water vapour

Author contributions. IAD analysed the data, formulated the model used to combine MLS and TRMM data, and took primary responsibility for writing the paper. PR and PH contributed to the design of the study, the interpretation of the results, and the writing of the paper. FC provided advice on MLS data processing, TD contributed to discussion of the overall results, and both FC and TD provided comments on the paper.

Competing interests. The authors declare that they have no conflict of interest.

Acknowledgements. Our study takes place within the Turbulence Effects on Active Species in Atmosphere (TEASAO; http://www.legos.obs-mip.fr/projets/axes-transverses-processus/teasao, last access: 30 April 2019) project. We thank the National Center for Scientific Research (CNRS) and the Excellence Initiative (Idex) of Toulouse, France (TEASAO project, Peter Haynes, Attractivity Chair), for funding this study.

We would like to thank the teams that have provided the MLS data (https://disc.gsfc.nasa.gov/datasets/ML2IWC_V004, last access: 1 January 2018), the TRMM data (https://pmm.nasa.gov/data-access/downloads/trmm, last access: 1 January 2019), and the SMILES data (https://mls.jpl.nasa.gov/data/smiles, last access: 1 December 2018).

Review statement. This paper was edited by Rolf Müller and reviewed by three anonymous referees.

References

Alcala, C. M. and Dessler, A. E.: Observations of deep convection in the tropics using the Tropical Rainfall Measuring Mission (TRMM) precipitation radar, J. Geophys. Res., 107, 4792, https://doi.org/10.1029/2002JD002457, 2002.

Allison, T., Fuelberg, H., and Heath, N.: Simulations of Vertical Water Vapor Transport for TC Ingrid (2013), J. Geophys. Res.-Atmos., 123, 8255–5282, https://doi.org/10.1029/2018JD028334, 2018.

Avery, M. A., Davis, S. M., Rosenlof, K. H., Ye, H., and Dessler, A. E.: Large anomalies in lower stratospheric water vapour and ice during the 2015–2016 El Nino, Nat. Geosci., 10, 405–409, https://doi.org/10.1038/ngeo2961, 2017.

Beucher, F.: Manuel de météorologie tropicale: des alizés au cyclone tropical, Météo-France, Paris, France, 2010.

Birner, T. and Charlesworth, E. J.: On the relative importance of radiative and dynamical heating for tropical tropopause temperatures, J. Geophys. Res.-Atmos., 122, 6782–6787, https://doi.org/10.1002/2016JD026445, 2017.

Carminati, F., Ricaud, P., Pommereau, J.-P., Rivière, E., Khaykin, S., Attié, J.-L., and Warner, J.: Impact of tropical land convection on the water vapour budget in the tropical tropopause layer, Atmos. Chem. Phys., 14, 6195–6211, https://doi.org/10.5194/acp-14-6195-2014, 2014.

Chen, S. S. and Houze, R. A.: Diurnal variation and life-cycle of deep convective systems over the tropical Pacific warm pool, Q. J. Roy. Meteor. Soc., 123, 357–388, 1997.

Corti, T., Luo, B. P., Fu, Q., Vömel, H., and Peter, T.: The impact of cirrus clouds on tropical troposphere-to-stratosphere transport, Atmos. Chem. Phys., 6, 2539–2547, https://doi.org/10.5194/acp-6-2539-2006, 2006.

Dauhut, T., Chaboureau, J.-P., Escobar, J., and Mascart, P.: Large-eddy simulations of Hector the convector making the stratosphere wetter, Atmos. Sci. Lett., 16, 135–140, https://doi.org/10.1002/asl2.534, 2015.

Dauhut, T., Chaboureau, J., Mascart, P., and Pauluis, O.: The Atmospheric Overturning Induced by Hector the Convector, J. Atmos. Sci., 74, 3271–3284, https://doi.org/10.1175/JAS-D-17-0035.1, 2017.

Fueglistaler, S., Dessler, A. E., Dunkerton, T. J., Folkins, I., Fu, Q., and Mote, P. W.: Tropical tropopause layer, Rev. Geophys., 47, RG1004, https://doi.org/10.1029/2008RG000267, 2009.

Gettelman, A. and Forster, P. M. de F.: A Climatology of the Tropical Tropopause Layer, J. Meteorol. Soc. Jpn. Ser II, 80, 911–924, https://doi.org/10.2151/jmsj.80.911, 2002.

Hartmann, D. L., Holton, J. R., and Fu, Q.: The heat balance of the tropical tropopause, cirrus, and stratospheric dehydration. Geophys. Res. Lett., 28, 1969–1972, 2001.

Holton, J. R. and Gettelman, A.: Horizontal transport and the dehydration of the stratosphere, Geophys. Res. Lett., 28, 2799–2802, https://doi.org/10.1029/2001GL013148, 2001.

Jensen, E. J., Toon, O. B., Pfisher, L., and Selkirk, H. B.: Dehydration of the upper troposphere and lower stratosphere by subvisible cirrus clouds near the tropical tropopause, Geophys. Res. Lett., 23, 825–828, https://doi.org/10.1029/96GL00722, 1996.

Jensen, E. J., Smith, J. B., Pfister, L., Pittman, J. V., Weinstock, E. M., Sayres, D. S., Herman, R. L., Troy, R. F., Rosenlof, K., Thompson, T. L., Fridlind, A. M., Hudson, P. K., Cziczo, D. J., Heymsfield, A. J., Schmitt, C., and Wilson, J. C.: Ice supersaturations exceeding 100 % at the cold tropical tropopause: implications for cirrus formation and dehydration, Atmos. Chem. Phys., 5, 851–862, https://doi.org/10.5194/acp-5-851-2005, 2005.

Jiang, J. H., Su, H., Zhai, C., Janice Shen, T., Wu, T., Zhang, J., Cole, J. N., von Salzen, K., Donner, L. J., Seman, C., Del Genio, A., Nazarenko, L. S., Dufresne, J., Watanabe, M., Morcrette, C., Koshiro, T., Kawai, H., Gettelman, A., Millán, L., Read, W. G., Livesey, N. J., Kasai, Y., and Shiotani, M.: Evaluating the Diurnal Cycle of Upper-Tropospheric Ice Clouds in Climate Models Using SMILES Observations, J. Atmos. Sci., 72, 1022–1044, https://doi.org/10.1175/JAS-D-14-0124.1, 2015.

Khaykin, S., Pommereau, J.-P., Korshunov, L., Yushkov, V., Nielsen, J., Larsen, N., Christensen, T., Garnier, A., Lukyanov, A., and Williams, E.: Hydration of the lower stratosphere by ice crystal geysers over land convective systems, Atmos. Chem. Phys., 9, 2275–2287, https://doi.org/10.5194/acp-9-2275-2009, 2009.

Khaykin, S. M., Pommereau, J.-P., and Hauchecorne, A.: Impact of land convection on temperature diurnal variation in the tropical lower stratosphere inferred from COSMIC GPS radio occultations, Atmos. Chem. Phys., 13, 6391–6402, https://doi.org/10.5194/acp-13-6391-2013, 2013.

Kim, J. and Son, S.-W.: Tropical Cold-Point Tropopause: Climatology, Seasonal Cycle, and Intraseasonal Variability Derived from

COSMIC GPS Radio Occultation Measurements, J. Climate, 25, 5343–5360, https://doi.org/10.1175/JCLI-D-11-00554.1, 2012.

Lee, K.-O., Dauhut, T., Chaboureau, J.-P., Khaykin, S., Krämer, M., and Rolf, C.: Convective hydration in the tropical tropopause layer during the StratoClim aircraft campaign: Pathway of an observed hydration patch, Atmos. Chem. Phys. Discuss., https://doi.org/10.5194/acp-2018-1114, in review, 2018.

Liu, C. and Zipser, E. J.: Global distribution of convection penetrating the tropical tropopause, J. Geophys. Res.-Atmos., 110, D23104, https://doi.org/10.1029/2005JD006063, 2005.

Liu, C. and Zipser, E. J.: The global distribution of largest, deepest, and most intense precipitation systems, Geophys. Res. Lett., 42, 3591–3595, https://doi.org/10.1002/2015GL063776, 2015.

Liu, C., Zipser, E., Garrett, T., Jiang, J. H., and Su, H.: How do the water vapor and carbon monoxide "tape recorders" start near the tropical tropopause?, Geophys. Res. Lett., 34, L09804, https://doi.org/10.1029/2006GL029234, 2007.

Livesey, N. J., Read, W. G., and Wagner, P. A.: Earth Observing System (EOS) Aura Microwave Limb Sounder (MLS) version 4.2x Level 2 data quality and description document. Jet Propulsion Laboratory Tech. Rep. JPL, available at: https://mls.jpl.nasa.gov/data/v4-2_data_quality_document.pdf (last access: 7 May 2019), 2017.

Mehta, S. K., Krishna Murthy, B. V., Narayana Rao, D., Venkat Ratnam, M., Parameswaran, K., Rajeev, K., Suresh Raju, C., and Kusuma, G. R.: Identification of tropical convective tropopause and its association with cold point tropopause, J. Geophys. Res., 113, D00B04, https://doi.org/10.1029/2007JD009625, 2008.

Millán, L., Read, W., Kasai, Y., Lambert, A., Livesey, N., Mendrok, J., Sagawa, H., Sano, T., Shiotani, M., and Wu, D. L.: SMILES ice cloud products, J. Geophys. Res.-Atmos., 118, 6468–6477, https://doi.org/10.1002/jgrd.50322, 2013.

Nesbitt, S. W., Zipser, E. J., and Cecil, D. J.: A Census of Precipitation Features in the Tropics Using TRMM: Radar, Ice Scattering, and Lightning Observations, J. Climate, 13, 4087–4106, https://doi.org/10.1175/1520-0442(2000)013<4087:ACOPFI>2.0.CO;2, 2000.

Newell, R. E. and Gould-Stewart, S.: A Stratospheric Fountain?, J. Atmos. Sci., 38, 2789–2796, https://doi.org/10.1175/1520-0469(1981)038<2789:ASF>2.0.CO;2, 1981.

Pereira, L. G. and Rutledge, S. A.: Diurnal Cycle of Shallow and Deep Convection for a Tropical Land and an Ocean Environment and Its Relationship to Synoptic Wind Regimes, Mon. Weather Rev., 134, 2688–2701, https://doi.org/10.1175/MWR3181.1, 2006.

Peter, T., Marcolli, C., Spichtinger, P., Corti, T., Baker, M. B., and Koop, T.: When dry air is too humid, Science, 314, 1399–1402, 2006.

Pommereau, J.-P.: Troposphere-to-stratosphere transport in the tropics, Comptes Rendus Geoscience, 342, 331–338, https://doi.org/10.1016/j.crte.2009.10.015, 2010.

Randel, W. J. and Jensen, E. J.: Physical processes in the tropical tropopause layer and their role in a changing climate, Nat. Geosci., 6, 169–176, https://doi.org/10.1038/ngeo1733, 2013.

Schoeberl, M. R., Jensen, E. J., Pfister, L., Ueyama, R., Avery, M., and Dessler, A. E.: Convective hydration of the upper troposphere and lower stratosphere, J. Geophys. Res.-Atmos., 123, 4583–4593, https://doi.org/10.1029/2018JD028286, 2018.

Soden, B. J., Held, I. M., Colman, R., Shell, K. M., Kiehl, J. T., and Shields, C. A.: Quantifying Climate Feedbacks Using Radiative Kernels, J. Climate, 21, 3504–3520, https://doi.org/10.1175/2007JCLI2110.1, 2008.

Solomon, S., Rosenlof, K. H., Portmann, R. W., Daniel, J. S., Davis, S. M., Sanford, T. J., and Plattner, G. K.: Contributions of stratospheric water vapor to decadal changes in the rate of global warming, Science, 327, 1219–1223, https://doi.org/10.1029/1999RG900008, 2010.

Stuart-Menteth, A. C., Robinson, I. S., and Challenor, P. G.: A global study of diurnal warming using satellite-derived sea surface temperature, J. Geophys. Res.-Oceans, 108, 951–953, 2003.

Suneeth, K. V., Das, S. S., and Das, S. K.: Diurnal variability of the global tropical tropopause: results inferred from COSMIC observations, Clim. Dynam., 49, 3277–3292, https://doi.org/10.1007/s00382-016-3512-x, 2017.

Takahashi, H. and Luo, Z. J.: Characterizing tropical overshooting deep convection from joint analysis of CloudSat and geostationary satellite observations, J. Geophys. Res.-Atmos., 119, 112–121, https://doi.org/10.1002/2013JD020972, 2014.

Ueyama, R., Jensen, E. J., Pfister, L., and Kim, J.-E.: Dynamical, convective, and microphysical control on wintertime distributions of water vapour and clouds in the tropical tropopause layer, J. Geophys. Res.-Atmos., 120, 2015JD023318, https://doi.org/10.1002/2015JD023318, 2015.

Wong, S. and Dessler, A., E.: Regulation of H2O an CO in tropical tropopause layer by the Madden-Julian oscillation, J. Geophys. Res., 112, D14305, https://doi.org/10.1029/2006JD007940, 2007.

Wright, J. S., Fu, R., Fueglistaler, S., Liu, Y. S., and Zhang, Y.: The influence of summertime convection over Southeast Asia on water vapor in the tropical stratosphere, J. Geophys. Res., 116, D12302, https://doi.org/10.1029/2010JD015416, 2011.

Yang, G.-Y. and Slingo, J.: The diurnal cycle in the tropics, Mon. Weather Rev., 129, 784–801, https://doi.org/10.1175/1520-0493(2001)129<0784:TDCITT>2.0.CO;2, 2001.

Zhang, C.: Madden–Julian Oscillation: Bridging Weather and Climate, B. Am. Meteorol. Soc., 94, 1849–1870, https://doi.org/10.1175/BAMS-D-12-00026.1, 2013.

Zhou, C., Dessler, A. E., Zelinka, M. D., Yang, P., and Wang, T.: Cirrus feedback on interannual climate fluctuations, Geophys. Res. Lett., 41, 9166–9173, https://doi.org/10.1002/2014GL062095, 2014.

4.2 Total amount of ice injected into the UT over the tropics

From the model presented on Dion et al. (2019) that is able to estimate the amount of ice injected into the TTL, we have estimate the total amount of ice injected up to the UT over the tropical convective zones during the austral convective seasons at $2° \times 2°$ horizontal resolution to 2.2 g m^{-3}. Considering that the tropical convective zones studied in Dion et al. (2019) are the main areas of injection of ice in the tropics, this value can be interpreted as the total amount of ice injected over the whole tropics. Thus, evens if consequently the ΔIWC mean can be calculated to 0.06 mg m^{-3} per $2° \times 2°$ pixel in the tropics, the importance to study ΔIWC at local scale instead of the global scale will be highlighted in next chapters. For instance, it will be show that ΔIWC over some $2° \times 2°$ pixels observed over the MariCont region, reaches 20 mg m^{-3} (see Chapter 5). Finally, we have estimated that 70% of ΔIWC comes from lands (SouthAm, SouthAfr and MariCont land), and 30% of ΔIWC comes from ocean (PacOce, IndOce, MariCont ocean).

4.3 Chapter summary

The study presented in this chapter is based on (Dion et al., 2019). A model combining datasets from MLS and TRMM space-borne instruments has been developed to estimate the amount of ice injected from deep convection up to the UT (146 hPa) and the TL (100 hPa) over convective areas in the tropics and during the austral convective seasons. The comparison between the convective areas including South America, South Africa, the Maritime Continent land and sea, Indian Ocean and Pacific Ocean has shown that the Maritime Continent is the tropical area where maximum of ice is injected up to the TTL over land (3.3 and 0.56 mg

m^{-3} of ice injected up to the UT and the TL respectively) and over ocean (0.9 and 0.19 mg m^{-3} of ice injected up to the UT and the TL, respectively). The Chapter 5 is then focused on the Maritime Continent region and, in order to better understand the impact of the deep convection on the amount of ice injected up to the TTL at small scale over individual sea and island of this region.

Chapter 5

Ice injected into the TTL over the Maritime Continent

The present chapter dealt with the second study of this thesis focused on the amount of ice injected up to the TTL by deep convection over some specific islands and seas of the MariCont region by trying to answers to the question: what are the processes over the MariCont that lead to the injection of ice up to the TTL and produce the largest amount of ice injected up to the TTL in the tropics?

Processes at small scales over the Maricont impacting the amount of ice injected into the TTL are identified and discussed in this chapter. The same method using MLS and TRMM intruments presented in the previous chapter is used. However, because of the smaller study zones considered in this study (from 1 pixel to an average of $\sim$ 20 pixels of $2^\circ \times 2^\circ$ per study zone), the present study proposes to improve the precision of the results by adding further information from the TRMM-LIS Flash datasets.

This study has been recently (September 2020) revised to Atmospheric Chemistry and Physics for Discussion (ACPD): Dion, I. A., Dallet, C., Ricaud, P., Haynes, P., Carminati, F., and Dauhut, T. (2020) Ice injected up to the Tropopause by Deep

Convection – Part 2: over the Maritime Continent.

5.1 Article-2: Ice injected into the tropopause by deep convection – Part 2: Over the Maritime Continent

5.2 Abstract

The amount of ice injected into the tropical tropopause layer has a strong radiative impact on climate. Results presented in a companion paper (Part I) have used the amplitude of the diurnal cycle of ice water content (IWC) as an estimate of ice injection by deep convection and shown that the Maritime Continent (MariCont) region provides the largest injection to the upper troposphere (UT, 146 hPa) and to the tropopause level (TL, 100 hPa). This study focuses on the MariCont region and extends that approach to assess the processes, the areas and the diurnal amount and duration of ice injected over islands and over seas during the austral convective season. The model presented in the companion paper is again used to estimate the amount of ice injected (ΔIWC) by combining ice water content (IWC) measured twice a day by the Microwave Limb Sounder (MLS; Version 4.2) from 2004 to 2017, and precipitation (Prec) measurements from the Tropical Rainfall Measurement Mission (TRMM; Version 007) averaged at high temporal resolution (1 hour). The horizontal distribution of ΔIWC estimated from Prec (ΔIWC^{Prec}) is presented at $2^\circ \times 2^\circ$ horizontal resolution over the MariCont. ΔIWC is also evaluated by using the number of lightning events (Flash) from the TRMM-LIS instrument (Lightning Imaging Sensor, from 2004 to 2015 at 1-h and $0.25^\circ \times 0.25^\circ$ resolution). ΔIWC^{Prec} and ΔIWC estimated from Flash (ΔIWC^{Flash}) are

compared to ΔIWC estimated from the ERA5 reanalyses (ΔIWC^{ERA5}) with the vertical resolution degraded to that of MLS observations ($\left\langle \Delta IWC^{ERA5} \right\rangle$). Our study shows that the diurnal cycles of Prec and Flash are consistent with each other in phase over land but different over offshore and coastal areas of the MariCont. The observational ΔIWC range between ΔIWC^{Prec} and ΔIWC^{Flash}, interpreted as the uncertainty of our model in estimating the amount of ice injected, is smaller over land (where the two estimates agree to within 6 to 22%) than over ocean (where absolute relative differences are between 6 and 71%) in the UT and TL. The impact of the MLS vertical resolution on the estimation of ΔIWC is greater in the TL (difference between ΔIWC^{ERA5} and $\left\langle \Delta IWC^{ERA5} \right\rangle$ of 32 to 139 %) than in the UT (difference of 9 to 33%). Considering all the methods, in the UT estimates of ΔIWC span 4.2 to 10.0 mg m^{-3} over land and 0.4 to 4.4 mg m^{-3} over sea, and in the TL estimates of ΔIWC span 0.5 to 3.9 mg m^{-3} over land and 0.1 to 0.7 mg m^{-3} over sea. Considering estimates of ΔIWC from all the methods, ΔIWC is estimated in the UT between 4.2 and 10.0 mg m^{-3} over land, and between 0.3 and 4.4 mg m^{-3} over sea, and, in the TL, between 0.5 and 3.7 mg m^{-3} over land and between 0.1 and 0.7 mg m^{-3} over sea. Finally, based on IWC from MLS and ERA5, Prec and Flash, this study highlights that 1) at both levels, ΔIWC estimated over land is more than twice that estimated over sea, and 2) small islands with high topography present the largest ΔIWC (e.g., Java Island, with values of 7.7 to 9.5 mg m^{-3} in the UT).

5.3 Introduction

The tropical tropopause layer (TTL) is widely recognised as a region of great importance for the climate system. The water vapour (WV) and ice cirrus clouds in this region have a strong radiative effect (Stephens and Greenwald, 1991, e.g.).

Furthermore the partitioning between WV and ice in the TTL is a consequence of dehydration processes taking place there control the global distribution of stratospheric water vapour, with implications for climate (e.g. Forster and Shine 1997) and for stratospheric ozone chemistry (Stenke and Grewe, 2005). WV and ice crystals are transported up to the tropopause layer by two main processes: a three-dimensional large-scale slow process (300-m month $^{-1}$), and a small-scale fast convective process (diurnal timescale) (e.g. Fueglistaler et al., 2009a; Randel and Jensen, 2013). Many studies have already shown the impact of convective processes on the hydration of the atmospheric layers from the upper troposphere (UT) to the lower stratosphere (LS) (Liu and Zipser, 2005; Jensen et al., 2007; Dauhut et al., 2018; Dion et al., 2019, e.g.). However, although within the tropical UT and LS the vertical distribution of water vapour is constrained by temperature, the transport of total water (WV and ice) by convection is still poorly quantified. The vertical distribution of water vapour in those layers is constrained by thermal conditions of the CPT (Randel et al., 2006a). Dion et al. (2019) have shown that air masses transported up to 146 hPa in the UT and up to 100 hPa in the tropopause layer (TL) have ice to total water ratios of more than 50% and 70%, respectively, and that ice in the UT is strongly spatially correlated with the diurnal increases of deep convection, while WV is not. Dion et al. (2019) hence focused on the ice phase of total water to estimate the diurnal amount of ice injected into the UT and the TL over convective tropical areas, showing that it is larger over land than over ocean, with maxima over land of the Maritime Continent (MariCont), the region including Indonesian islands. The present study is focusing on the MariCont region in order to gain further understanding small-scale processes impacting the diurnal injection of ice up to the TL.

The method used by Dion et al. (2019) to estimate convective injection of to the UT and TL was via estimation of the amplitude of the diurnal cycle of ice us-

ing twice daily (at 01:30 and 13:30 local time) Ice Water Content (IWC) from the Microwave Limb Sounder (MLS) instrument and the full diurnal cycle of precipitation (Prec) measured by the Tropical Rainfall Measurement Mission (TRMM) instrument (at one hour resolution). The method first focuses on the increasing phase of the diurnal cycle of Prec (peak to peak from the diurnal Prec minimum to the diurnal Prec maximum) and shows that the increasing phase of Prec is consistent in time and in amplitude with the increasing phase of the diurnal cycle of deep convection, over tropical convective zones and during convective season. The amount of ice (ΔIWC) injected into the UT and the TL is estimated by relating IWC measured by MLS during the growing phase of the deep convection to the increasing phase of the diurnal cycle of Prec. Dion et al. (2019) conclude that deep convection over the MariCont region is the main process impacting the increasing phase of the diurnal cycle of ice in those layers.

The MariCont region is one of the main convective centers in the tropics, with the wettest troposphere and the coldest and driest tropopause (Ramage, 1968; Sherwood, 2000; Hatsushika and Yamazaki, 2001). Yang and Slingo (2001) have shown that, over the Indonesian area, the phase of the convective activity diurnal cycle drifts from land to coastlines and to offshore areas. Even though those authors have done a comprehensive study of the diurnal cycle of precipitation and convection over the MariCont, the diurnal cycle of ice injected by deep convection up to the TL over this region is still not well understood. Millán et al. (2013) have tentatively evaluated the upper tropospheric diurnal cycle of ice from Superconducting Submillimeter-Wave Limb-Emission Sounder (SMILES) measurements over the period 2009-2010 but without differentiating land and sea over the MariCont, which caused their analysis to show little diurnal variation over that region. Dion et al. (2019) have 1) highlighted that the MariCont must be considered as two separate areas: the MariCont land (MariCont_L) and the MariCont ocean

(MariCont_O), with two distinct diurnal cycles of the Prec and 2) estimated the amount of ice injected in the UT and the TL. Over these two domains, it has also been shown that convective processes are stronger over MariCont_L than over MariCont_O. Consequently, the amount of ice injected in the UT and the TL is greater over MariCont_L than over MariCont_O.

Building upon the results of Dion et al. (2019), the present study aims to improve their methodology by i) studying smaller study zones and by distinguishing between islands and sea within the MariCont, ii) comparing the sensitivity of our model to different proxies of deep convection and iii) comparing the amount of ice injected in the UT and the TL inferred by our model to that of ERA5 reanalyses. Based on space-borne observations and meteorological reanalyses, ΔIWC is assessed at a horizontal resolution of $2^\circ \times 2^\circ$ over 5 islands (Sumatra, Borneo, Java, Sulawesi and New Guinea) and 5 seas (West Sumatra Sea, Java Sea, China Sea, North Australia Sea, and Bismarck Sea) of the MariCont during convective season (December, January and February, hereafter DJF) from 2004 to 2017. Consistently with Dion et al., (2019), ΔIWC will be first estimated from Prec measured by TRMM-3B42. An alternative estimate of ΔIWC based on the number of flashes (Flash) detected by the TRMM Lightning Imaging Sensor (TRMM-LIS), an other proxy for deep convection as shown by Liu and Zipser (2008), is also provided. Finally, we will use IWC calculated by the ERA5 reanalyses from 2005 to 2016 to estimate ΔIWC in the UT and the TL over each study zone and compare it to ΔIWC estimated from Prec and Flash.

The observational datasets used in our study are presented in Sect. 2. Methodology is reviewed in Sect. 3. The amount of ice (ΔIWC) injected up to the TL estimated from Prec is evaluated in Sect. 4. Diurnal cycles of Prec and Flash are compared to each other over different areas of the MariCont in Sect. 5. Results of the estimated ΔIWC injected up to the UT and the TL over five islands and five

seas of the MariCont are presented and compared with the ERA5 reanalyses in Sect. 6. Results are discussed in Sect. 7, and conclusions are drawn in Sect. 8. This paper contains many abbreviations and acronyms. To facilitate reading, they are compiled in the Acronyms list.

5.4 Datasets

This section presents the instruments and the reanalyses used for this study.

5.4.1 MLS Ice Water Content

The Microwave Limb Sounder (MLS) was launched on NASA's Earth Observing System Aura platform in 2004 (Waters et al., 2006). MLS follows a sun-synchronous near-polar orbit, obtaining daily global coverage. Ascending (northbound) portions of the orbit cross the equator at 13:30 local time (LT); descending portions of the orbit cross the equator at 01:30 LT. Among other products, MLS provides measurements of ice water content (IWC^{MLS}, mg m^{-3}). Although optimal estimation is used to retrieve almost all other MLS products, a cloud-induced radiance technique is used to derive IWC^{MLS} (Wu et al., 2008, 2009). Here we use version 4.2 IWC data, filtered following the recommendations of the MLS team described by Livesey et al. (2018a). We select IWC^{MLS} during all austral convective seasons DJF between 2004 and 2017. MLS data processing provides IWC^{MLS} at 6 levels in the UTLS (82, 100, 121, 146, 177 and 215 hPa). We have chosen to study only two of the available levels: 146 hPa as representative of the lower part of the TTL (named UT for upper troposphere) and 100 hPa as representative of tropopause which lies in the middle of the TTL (named TL for tropopause level). Note that the level at 82 hPa, representing the Lower Stratosphere, would have been also very interesting to study but do not provide enough

significant measurements of IWC to achieve acceptable signal-to noise ratio. The resolution of IWC^{MLS} (horizontal along the path, horizontal perpendicular to the path, vertical) measured at 146 and 100 hPa is 300×7×4 km and 200×7×5 km, respectively. In our study, we consider 13 years of MLS data, which allows the IWC^{MLS} measurements to be averaged in bins of 2° (about 220 km) zonal and meridional extent, over all study zones. The valid IWC range is 0.02–50.0 mg m^{-3} at 100 hPa and 0.1–50.0 mg m^{-3} at 146 hPa (Livesey et al., 2018). Typical single-profile precisions (i.e. random noise) are 0.10 mg m^{-3} at 100 hPa and 0.20–0.35 mg m^{-3} at 146 hPa, and the accuracy (i.e. systematic error) is 100 % for values less than 10 mg m^{-3} at both levels. The fact that our study is based on 13-year averages of all observations within each 2° × 2° bin implies that the uncertainty on the averages due to measurement precision is drastically reduced. On the other hand, the systematic error on the averages will be unchanged. But our analysis, based on the methodology developed in Dion et al. (2019), relies on a differential method to highlight the amplitude of the diurnal cycle of IWC that is expected to be the amount of ice injected in the TL and/or the UT. By considering the difference between the maximum and the minimum of IWC obtained within 24 hours, the associated systematic error dramatically decreases. This supposes that the systematic errors are of the same order of magnitude within each temporal bin within 24 hours.

5.4.2 TRMM-3B42 Precipitation

The Tropical Rainfall Measurement Mission (TRMM) was launched in 1997 and provided measurements of precipitation until 2015. The TRMM satellite carried five instruments, three of which (PR, TMI, VIRS) formed a complementary sensor suite for rainfall. TRMM had an almost circular orbit at 350 km altitude performing a complete revolution in one and a half hour.

The 3B42 algorithm product (TRMM-3B42) (version V7) is a multi-satellite precipitation analysis, created to estimate the precipitation and extends the precipitation product through 2019. The analysis merges microwave and infrared spaceborne observations and included TRMM measurements from 1997 to 2015 (Huffman et al., 2007, 2010, 2018). Precipitation from TRMM-3B42 (Prec) are provided at a 0.25° ($\sim$ 29.2 km) horizontal resolution, extending from 50° S to 50° N (https://pmm.nasa.gov/data-access/downloads/trmm, last access: April 2019). Details of the binning methodology of TRMM-3B42 are provided by Huffman and Bolvin (2018). The precipitation estimates do not distinguish between stratiform and convective precipitation and the implications of this will be discussed later. Work is currently underway with NASA funding to develop more appropriate estimators for random error, and to introduce estimates of bias error (Huffman and Bolvin, 2018). In our study, Prec from TRMM-3B42 was selected over the austral convective seasons (DJF) from 2004 to 2017 and at each location was binned into 1-hour intervals according to local time (LT). This was possible because of the combinaison between the precessing orbit of the TRMM satellite and the precipitation analysis from the other satellites included into TRMM-3B42 long duration (13 years). Finally for each 1-hour interval of LT the data was averaged to a horizontal grid of 2° $\times$2 ° to be compared to IWC^{MLS}.

5.4.3 TRMM-LIS number of Flashes

The Lightning Imaging Sensor (LIS) aboard of the TRMM satellite measures several parameters related to lightning, including the number of flashes within a given time period. Details are given in Christian et al. (2000), including how the raw measurements are processed to estimate the number of flashes (Flash), subject to a detection efficiency of 69% at noon to 88% at night (lower during the day because of background illumination). The observation range of the sensor is between 38°

N and 38° S. The instrument detects lightning with storm-scale resolution of 3-6 km (3 km at nadir, 6 km at limb) over a large region (550×550 km) of the Earth's surface. The LIS instruments obtained measurements between 1 January 1998 and 8 April 2015. To be consistent with the other parts of our study, we used the measurements only for DJF from 2004-2015. As LIS is on the TRMM platform, the measurements can be binned in 1-hour intervals of LT to obtain a full 24-hr diurnal cycle. The measurements could be further binned at either 0.25° × 0.25° or at 2° × 2° horizontal resolution to allow comparison with Prec from TRMM-3B42.

5.4.4 ERA5 Ice Water Content

The European Centre for Medium-range Weather Forecasts (ECMWF) Reanalysis 5, known as ERA5, replaces the ERA- Interim reanalyses as the fifth generation of the ECMWF reanalysis providing global climate and weather for the past decades (from 1979) (Hersbach, 2018). ERA5 provides hourly estimates for a large number of atmospheric, ocean and land surface quantities and covers the Earth on a 30 km grid with 137 levels from the surface up to a height of 80 km. Reanalyses such as ERA5 combine a large number of observations (space-borne, air-borne, and ground-based) with short-range forecasts. Our study uses the specific cloud ice water content (mass of condensate / mass of moist air) (IWC^{ERA5}) as representative of non-precipitating ice. Precipitating ice, classified as snow water, is also provided by ERA5 but not used in this study because it is of little relevance to convectively injected ice in the TTL. No direct observations of atmospheric ice content are provided to the ERA5 process, and IWC^{ERA5} is primarily determined within the forecast model by changes in the analysed temperature (and at low levels, humidity) which is mostly driven by the assimilation of temperature-sensitive radiances from satellite instruments. These determine IWC^{ERA5} through the model microphysics which allows ice supersaturation with respect to ice (100-

150% in relative humidity) but not with respect to liquid water. Although microwave radiances at 183 GHz which are sensitive to atmospheric scattering induced by ice particles (Geer et al., 2017) are assimilated, clouds and precipitation are not used as control variables in the 4D- Var assimilation system and cannot be adjusted independently in the analysis (Geer et al., 2017). Furthermore whilst the modeled microwave radiances data are mainly sensitive to the larger ice particles such as those in the cores of deep convection (Geer et al., 2017), the sensitivity to cirrus clouds in ERA5 is strongly dependent on microphysical assumptions on the shape and size of the cirrus particles. Observations that affect the tropospheric stability or humidity, or the synoptic situation, can affect the upper level ice cloud indirectly, e.g. by changing the intensity of the convection will change the amount of outflow cirrus generated (Geer et al., 2017). A recent study of cloud ice observed by satellites and generated by re-analysis datasets (Duncan and Eriksson, 2018) has found that ERA5 is able to capture both seasonal and diurnal variability in cloud ice water but exhibits noisier and higher amplitude diurnal variability than borne out by multi-satellite estimates.

The present study uses the IWC^{ERA5} at 100 and 150 hPa averaged over DJF from 2005 to 2016 with one-hour temporal resolution. IWC^{ERA5} is compared to the amount of ice injected in the UT and the TL as estimated by the model developed in Dion et al. (2019) and in the present study. IWC^{ERA5} have been degraded along the vertical at 100 and 150 hPa ($\left\langle \Delta IWC^{ERA5} \right\rangle$) consistently with the MLS vertical resolution of IWC^{MLS} (5 and 4 km at 100 and 146 hPa, respectively) using a box function (see section 5.9.2). IWC^{ERA5} and $\left\langle \Delta IWC^{ERA5} \right\rangle$ will be both considered in this study. IWC^{ERA5}, initially provided in kg kg^{-1}, has been converted into mg m^{-3} using the temperature provided by ERA5 in order to be compared with IWC^{MLS}.

5.5 Methodology

This section summarizes the method developed by Dion et al. (2019) to estimate ΔIWC, the amount of ice injected into the UT and the TL. Dion et al. (2019) have presented a model relating Prec (as proxy of deep convection) from TRMM to IWC^{MLS} over tropical convective areas during austral convective season DJF. The IWC^{MLS} value measured by MLS during the growing phase of the convection (at x = 01:30 LT or 13:30 LT) is compared to the Prec value at the same time x in order to define the correlation coefficient (C) between Prec and IWC^{MLS}, as follows:

$$C = \frac{IWC_x^{MLS}}{Prec_x} \tag{5.1}$$

The diurnal cycle of IWC estimated ($IWC^{est}(t)$) can be calculated by using C applied to the diurnal cycle of Prec ($Prec(t)$), where t is the time, as follows:

$$IWC^{est}(t) = Prec(t) \times C \tag{5.2}$$

The amount of IWC injected up to the UT or the TL (ΔIWC^{Prec}) is defined by the difference between the maximum of IWC^{est} (IWC$^{est}_{max}$) and its minimum (IWC$^{est}_{min}$).

$$\Delta IWC^{Prec} = C \times (Prec_{max} - Prec_{min}) = IWC^{est}_{max} - IWC^{est}_{min} \tag{5.3}$$

where $Prec_{max}$ and $Prec_{min}$ are the diurnal maximum and minimum of Prec, respectively. Figure 5.1 illustrates the relationship between the diurnal cycle of Prec and the two MLS measurements at 01:30 and 13:30 LT. The growing phase of the convection is defined as the period of increase in precipitation from $Prec_{min}$ to

$Prec_{max}$. The amplitude of the diurnal cycle is defined by the difference between $Prec_{max}$ and $Prec_{min}$. In Fig. 1, because the growing phase of the convection illustrated is happening during the afternoon, only the MLS measurement at 13:30 LT is used in the calculation of ΔIWC. IWC at 01:30 LT is not used in that case.

5.6 Horizontal distribution of ΔIWC estimated from Prec over the MariCont

5.6.1 Prec from TRMM related to IWC from MLS

In order to identify the main regions of injection of ice in the TL over the MariCont, Figure 5.2 presents different parameters associated with this region: a) the name of the main islands and seas over the MariCont, b) the elevation (http://www.soda-pro.com/web-services/altitude/srtm-in-a-tile, last access: June 2019), c) the daily mean of Prec at 0.25° × 0.25° horizontal resolution, d) the hour of the diurnal maxima of Prec at 0.25° × 0.25° horizontal resolution, and e) the daily mean ($\bar{IWC} = (IWC_{01:30} + IWC_{13:30}) \times 0.5$) of IWC^{MLS} at 146 hPa at 2° × 2° horizontal resolution. Several points need to be highlighted. Daily means of Prec over land and coastal regions are higher than over oceans (Fig. 5.2c). Regions where the daily mean of Prec is maximum are usually surrounding the highest elevation over land (e.g. over New Guinea) and near coastal regions (North West of Borneo in the China Sea and southern Sumatra in the Java Sea) (Fig. 5.2b and c). The times of the maxima of Prec are over land during the evening (18:00-00:00 LT), over coast during the night-morning (00:00-06:00 TL) and over sea during the morning-noon and even evening depending on the sea considered (09:00-12:00 LT and 15:00-00:00 LT). These differences may be related to the diurnal variation of the land/sea breeze over the course of 24 hours. The

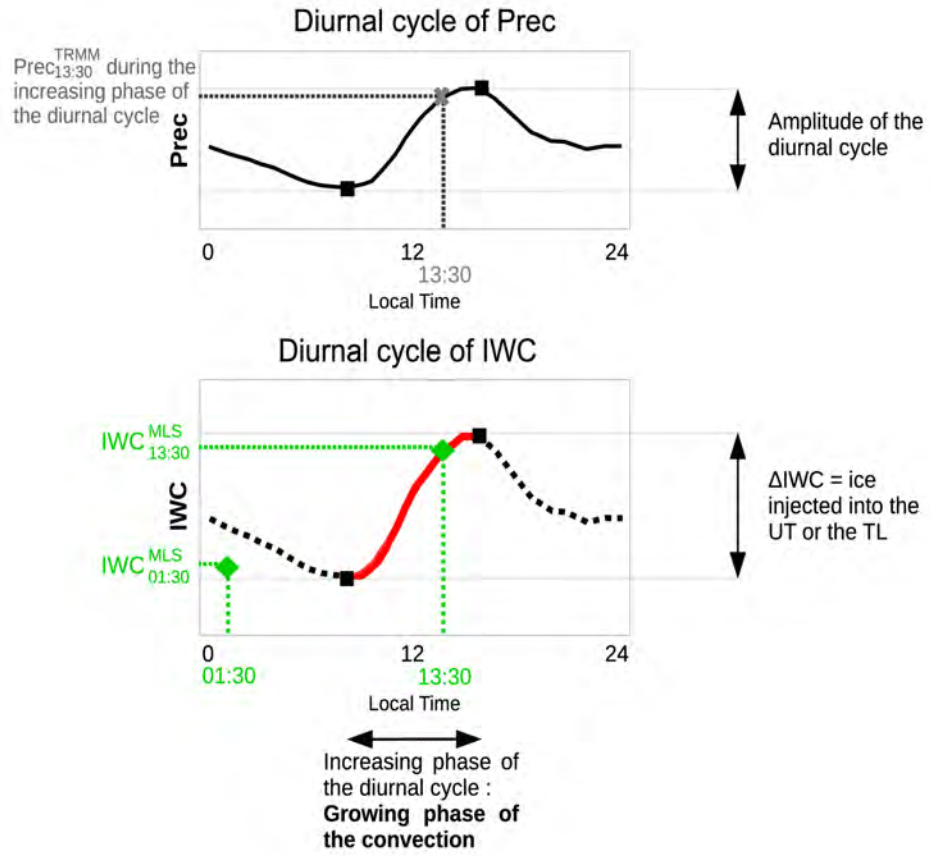

Figure 5.1 – Illustration of the model developed in Dion et al. (2019) to estimate the amount of ice (ΔIWC) injected into the UT or the TL. Diurnal cycle of a proxy of deep convection (Prec) (a), diurnal cycle of ice water content (IWC) estimated from diurnal cycle of the proxy of deep convection (b). In red line, the increasing phase of the diurnal cycle. In black dashed line, the decreasing phase of the diurnal cycle. The green diamonds are the two IWC^{MLS} measurements from MLS. Grey thick cross represents the measurement of Prec during the growing phase of the convection ($Prec_x$), used in the model. Maximum and minimum of the diurnal cycles are represented by black squares. Amplitude of the diurnal cycle is defined by the differences between the maximum and the minimum of the cycle.

sea breeze during the day favours land convection at the end of the day when land surface temperature is higher than oceanic surface temperature. During the night,

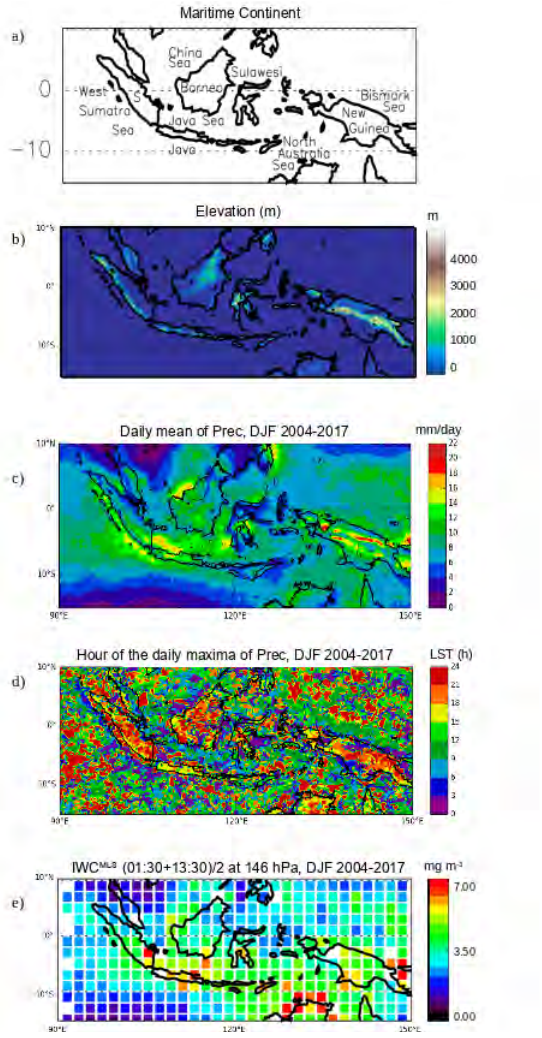

Figure 5.2 – Main islands and seas of the MariCont (S is for Sumatra) (a), elevation from Solar Radiation Data (SoDa) (b); daily mean of Prec obtained from TRMM analysis over the Maritime Continent, averaged over the period of DJF 2004-2017 (c), hour (local solar time (LST)) of the diurnal maxima of Prec over the MariCont (d); daily mean (01:30 LT + 13:30 LT)/2 of IWC^{MLS} at 146 hPa from MLS over the MariCont averaged over the period of DJF 2004-2017 (e). Observations are presented with a horizontal resolution of $0.25° \times 0.25°$ (b, c and d) and $2° \times 2°$ (e).

the coastline sea surface temperature rises above the land surface temperature, and the land breeze systematically favours the development of convection over coasts. These observations are consistent with results presented by Qian (2008), who ex-

plained that high precipitation is mainly concentrated over land in the MariCont because of the strong sea-breeze convergence, but also because of the combination with the mountain–valley winds and cumulus merging processes. Amplitudes of the diurnal cycles of Prec over the MariCont will be detailed as a function of island and sea in section 5.7. The location of the largest concentration of IWC^{MLS} (3.5 – 5.0 mg m^{-3}, Fig. 5.2e) is consistent with that of Prec ($\sim$ 12 – 16 mm day^{-1}) over the West Sumatra Sea, and over the South of Sumatra island. However, over North Australia seas (including the Timor Sea and the Arafura Sea), we observed large differences between Prec low values (4 – 8 mm day^{-1}) and IWC^{MLS} large concentrations (4 – 7 mg m^{-3}).

5.6.2 Convective processes compared to IWC measurements

Although TRMM horizontal resolution is 0.25° × 0.25°, we require information at the same resolution as IWC^{MLS}. The diurnal cycle of Prec obtained from TRMM analysis, can be used for each 2° × 2° pixel to deduce the duration of the increasing phase of Prec and hence the duration of the growing phase of the convection. From the diurnal cycle of Prec in TRMM analysis, the duration of the increasing phase of Prec can be known for each 2° × 2° pixel. The duration of the growing phase of the convection can then be defined from Prec over each pixel. Figures 3a and b present the anomaly (deviation from the mean) of Prec in TRMM-3B42 over the MariCont for the pixels where convection is in the growing phase at 01:30 LT and 13:30 LT, respectively. Anomalies are calculated relative to the average computed over the entire MariCont region. Thus, red colors show regions that are experiencing the growing phase of convection and whose Prec value is greater than the overall MariCont mean at the respective time (01:30 LT or 13:30 LT), whereas blue colors show those regions where there is little precipitation compared to the overall MariCont mean during the growing phase of convection. Pixels can be

represented in the panels for both local times when: 1) the onset of the convection is before 01:30 LT and the end is after 13:30 LT, or 2) the onset of the convection is before 13:30 LT and the end is after 01:30 LT. The gray color denotes pixels for which convection is not ongoing at 01:30 LT nor at 13:30 LT. Similar anomalies of IWC^{MLS} over the MariCont are shown in Figs. 3c and d, over pixels when the convection is in the growing phase at 01:30 LT and 13:30 LT, respectively. Note that, within each $2^\circ \times 2^\circ$ pixel, at least 60 measurements of Prec or IWC^{MLS} at 13:30 LT or 01:30 LT over the period 2004-2017 have been selected for the average.

The Prec anomaly at 01:30 LT and 13:30 LT varies between -0.15 and +0.15 mm h^{-1}. The IWC^{MLS} anomaly at 13:30 LT and 01:30 LT varies between -3 and +3 mg m^{-3}. At 13:30 LT, the growing phase of the convection is found mainly over land. At 13:30 LT, over land, the strongest Prec and IWC^{MLS} anomalies (+0.15 mm h^{-1} and +2.50 mg m^{-3}, respectively) are found over the Java island, and northern Australia for IWC^{MLS}. At 01:30 LT, the growing phase of the convection is found mainly over sea (while the pixels of the land are mostly gray), with maxima of Prec and IWC^{MLS} anomalies over coastlines and seas close to coasts such as the Java Sea and the Bismarck Sea. Three types of regions can be distinguished from Fig. 5.3: i) regions where Prec and IWC^{MLS} anomalies have the same sign (positive or negative either at 01:30 LT or 13:30 LT) (e.g. over Java, Borneo, Sumatra, Java Sea and coast of Borneo or the China Sea); ii) regions where Prec anomaly is positive and IWC^{MLS} anomaly is negative (e.g. over West Sumatra Sea); and iii) regions where Prec anomaly is negative and IWC^{MLS} anomaly is positive (e.g. over the North Australia Sea at 01:30 LT). Convective processes associated to these three types of regions over islands and seas of the MariCont are discussed in Sect. 6.

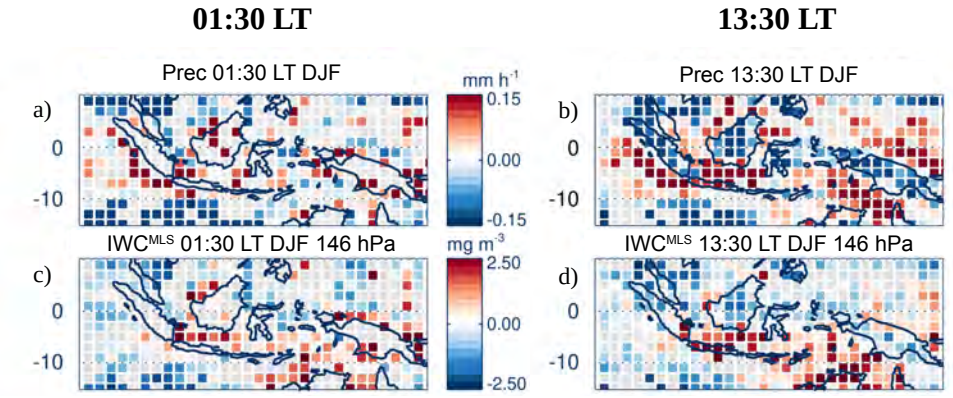

Figure 5.3 – Anomaly (deviation from the mean) of Prec (a-b) and Ice Water Content (IWC^{MLS}) at 146 hPa (c-d), at 01:30 LT (left) and at 13:30 LT (right) over pixels where 01:30 LT and 13:30 LT are during the growing phase of the convection, respectively, averaged over the period of DJF 2004-2017. The gray color denotes pixels for which convection is not ongoing.

5.6.3 Horizontal distribution of ice injected into the UT and TL estimated from Prec

From the model developed in Dion et al. (2019) based on Prec from TRMM–3B42 and IWC from MLS and synthesized in section 2.4, we can calculate the amount of IWC injected (ΔIWC) at 146 hPa (UT, Figure 5.4a) and at 100 hPa (TL, Figure 5.4b) by deep convection over the MariCont. In the UT, the amount of IWC injected over land is on average larger (> 10 – 20 mg m^{-3}) than over seas (< 15 mg m^{-3}). Southern Sumatra, Sulawesi, northern New Guinea and northern Australia present the largest amounts of ΔIWC over land (15 – 20 mg m^{-3}). Java Sea, China Sea and Bismarck Sea present the largest amounts of ΔIWC over seas (7 – 15 mg m^{-3}). West Sumatra Sea and North Australia Sea present low values of ΔIWC (< 2 mg m^{-3}). We can note that the anomalies of Prec and IWC during the growing phase over North Australia Sea at 13:30 LT are positive (> 0.2 mm h^{-1}, Fig. 5.3b and > 2.5 mg m^{-3}, Fig. 5.3d, respectively). In the TL, the

maxima (up to 3.0 mg m^{-3}) and minima (down to 0.2 – 0.3 mg m^{-3}) of ΔIWC are located within the same pixels as in the UT, although 3 to 6 times lower than in the UT. The decrease of ΔIWC with altitude is larger over land (by a factor 6) than over sea (by a factor 3). We can note that the similar pattern between the two layers comes from the diurnal cycle of Prec in the calculation of ΔIWC at 146 and 100 hPa. The differences in the magnitudes of the ΔIWC values at 100 and 146 hPa arise from the different amounts of IWC measured by MLS at those two levels. That is, similar ΔIWC patterns are expected between the two levels because, according to the model developed in Dion et al. (2019), deep convection is the main process transporting ice into the UT and the TL during the growing phase of the convection. Convective processes associated to land and sea are further discussed in Sect. 6.

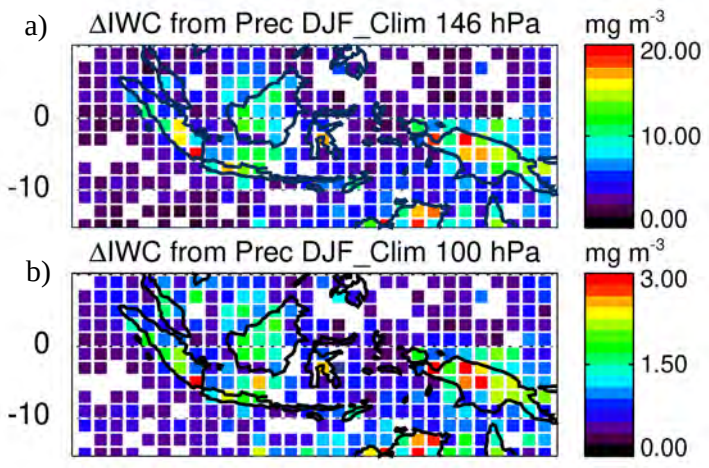

Figure 5.4 – Daily amount of ice injected (ΔIWC) up to the UT (a) and up to the TL (b) estimated from Prec, averaged during DJF 2004-2017.

In order to understand better the role of deep convection in determining the largest values of ΔIWC per pixel, isolated pixels selected in Fig. 4a are presented separately in Figure 5.5a and f. This Figure shows the diurnal cycles of Prec in four pixels selected for their large ΔIWC in the UT (larger than 15 mg m^{-3}, Fig.

5.5b, c, d, e), and the diurnal cycle of Prec in four pixels selected for their low ΔIWC in the UT (but large enough to observe the diurnal cycles of IWC between 2.0 and 5.0 mg m^{-3}, Fig. 5.5g, h, i, j). Pixels with low values of ΔIWC over land (Fig. 5.5g, h and i) present small amplitude of diurnal cycles of Prec ($\sim$ +0.5 mm h^{-1}), with maxima between 15:00 LT and 20:00 LT and minima around 11:00 LT.

The pixel with low value of ΔIWC over sea (Fig. 5.5j) shows an almost null amplitude of the diurnal cycle of Prec, with low values of Prec all day long ($\sim$ 0.25 mm h^{-1}). Pixels with large values of ΔIWC over land (Fig. 5.5b, c, d, e) show longer duration of the increasing phase of the diurnal cycle (from $\sim$ 09:00 LT to 20:00 – 00:00 LT) than the increasing phase of Prec diurnal cycle over pixels with low values of ΔIWC (from 10:00 LT to 15:00 – 19:00 LT). More precisely, pixels labeled 1 and 2 over New Guinea (Fig. 5.5d and e) and the pixel over southern Sumatra (Fig. 5.5c) show amplitude of diurnal cycle of Prec reaching 1.0 mm h^{-1}, while the pixel over North Australia (Fig. 5.5b) shows lower amplitude of diurnal cycle of Prec (0.5 mm h^{-1}).

IWC^{MLS} during the growing phase of deep convection and the diurnal cycle of IWC estimated from Prec are also shown on Fig. 5.5. For pixels with large values of ΔIWC, IWC^{MLS} is between 4.5 and 5.7 mg m^{-3} over North Australia, South Sumatra and New Guinea 1. For pixels with low values of ΔIWC, IWC^{MLS} is found between 1.9 and 4.7 mg m^{-3}. To summarize, large values of ΔIWC are observed over land in combination with i) longer growing phase of deep convection (> 9 hours) and/or ii) large diurnal amplitude of Prec (> 0.5 mm h^{-1}). However, as IWC^{MLS} ranges overlap for the high and low ΔIWC, no definitive conclusion about the relationship between IWC^{MLS} and ΔIWC can be drawn.

In the next section, we estimate ΔIWC using another proxy of deep convection, namely Flash measurements from LIS.

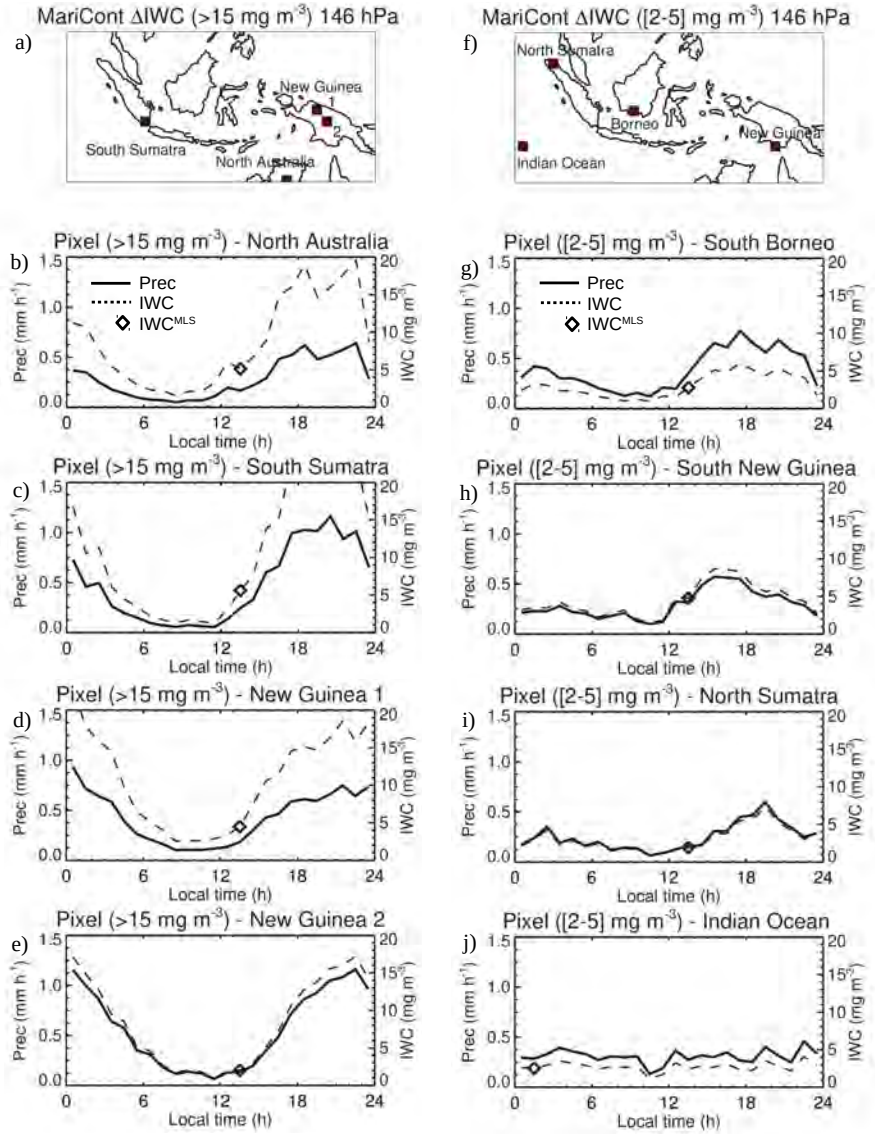

Figure 5.5 – a) and f) Location of 2° × 2° pixels where ΔIWC have been found higher than 15 mg m^{-3} (in Fig. 4) and where ΔIWC have been found between 2 and 5 mg m^{-3} (in Fig. 4), respectively. Diurnal cycle of Prec (solid line): (b, c, d, e) over 4 pixels where ΔIWC have been found higher than 15 mg m^{-3} (in Fig. 4), (g, h, i, j) over 4 pixels where ΔIWC have been found between 2 and 5 mg m^{-3} (in Fig. 4), during DJF 2004-2017. The diamond represents IWC^{MLS} during the increasing phase of the convection. The dashed line is the diurnal cycle of IWC estimated from the diurnal cycle of Prec and from IWC^{MLS}.

5.7 Relationship between diurnal cycle of Prec and Flash over MariCont land and sea

Lightning is created in cumulonimbus clouds when the electric potential energy difference is large between the base and the top of the cloud. Lightning can appear at the advanced stage of the growing phase of the convection and during the mature phase of the convection. For these reasons, in this section, we use Flash measured from LIS during DJF 2004-2015 as another proxy of deep convection in order to estimate ΔIWC (ΔIWC^{Flash}) and check the consistency with ΔIWC obtained with Prec (ΔIWC^{Prec}).

5.7.1 Flash distribution over the MariCont

Figure 5.6a shows the daily mean of Flash in DJF 2004-2015 at 0.25° × 0.25° horizontal resolution. Over land, Flash can reach a maximum of 10^{-1} flashes day^{-1} per pixel while, over seas, Flash takes smaller values ($\sim 10^{-3}$ flashes day^{-1} per pixel). When compared to the distribution of Prec (Fig. 5.2c), maxima of Flash are found over similar regions as maxima of Prec (Java, East of Sulawesi coast, Sumatra and northern Australia). Over Borneo and New Guinea, coastlines show larger values of Flash ($\sim 10^{-2}$ flashes day^{-1}) than inland ($\sim 10^{-3}$ flashes day^{-1}). Differences between Flash and Prec distributions are found over North Australia Sea, with relatively large number of Flash (>10^{-2} flashes day^{-1}) compared to low Prec (4 – 10 mm day^{-1}) (Fig. 5.2c), and over several inland regions of New Guinea where the number of Flash is relatively low ($\sim 10^{-2}$– 10^{-3} flashes day^{-1}) while Prec is high ($\sim$14 – 20 mm day^{-1}). Figure 5.6b shows the hour of the Flash maxima. Over land, the maximum of Flash is between 15:00 LT and 19:00 LT, slightly earlier than the maximum of Prec (Fig. 5.2d) observed between 16:00 LT and 24:00 LT. Coastal regions show similar hours of maximum of Prec and Flash,

i.e between 00:00 LT and 04:00 LT although, over the West Sumatra Coast, diurnal maxima of both Prec and Flash happen 1–4 hours earlier (from 23:00-24:00 LT) than those of other coasts.

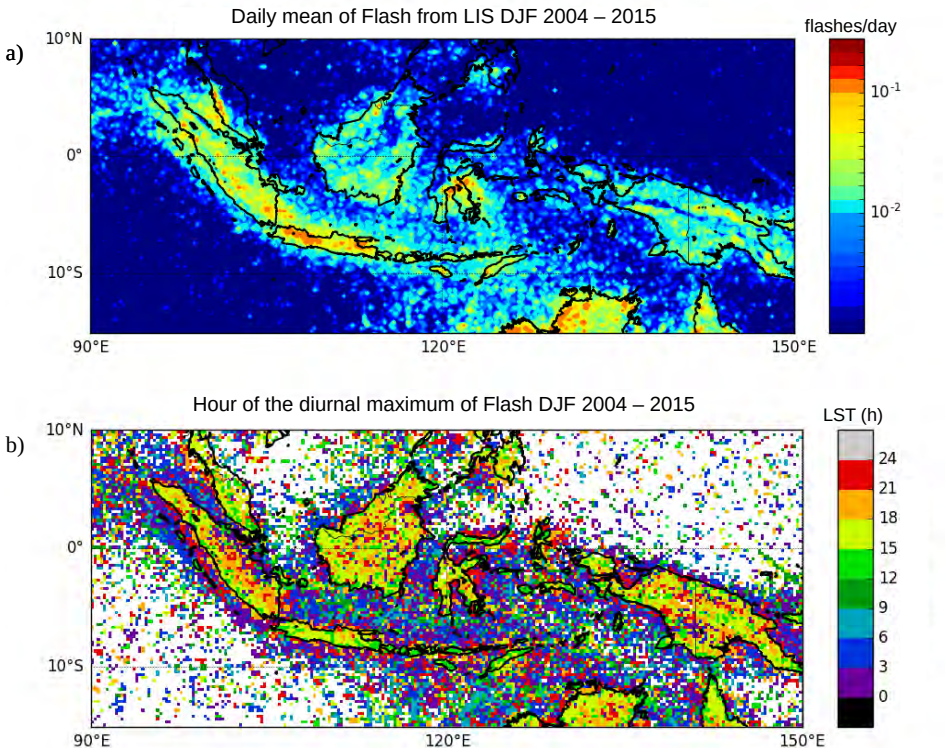

Figure 5.6 – Daily mean of Flash measured by LIS averaged over the period DJF 2004-2015 (a); Hour (local solar time (LST)) of the diurnal maximum of Flash (b).

5.7.2 Prec and Flash diurnal cycles over the MariCont

This section compares the diurnal cycle of Flash with the diurnal cycle of Prec in order to assess the potential for Flash to be used as a proxy of deep convection over land and sea of the MariCont. Diurnal cycles of Prec and Flash over the MariCont land, coastline and offshore (MariCont_L, MariCont_C, MariCont_O, respectively) are shown in Figs. 5.7a–c, respectively. Within

each 0.25° × 0.25° pixel, ocean/land/coast filters were applied from the Solar Radiation Data (SoDa, `http://www.soda-pro.com/web-services/altitude/srtm-in-a-tile`). Each pixel is designated as either land or sea. Then MariCont_C is the region defined by sea pixels that are within 5 pixels of a land pixel. This choice of 5 pixels was made after consideration of some sensitivity tests in order to have the best compromise between a high signal-to-noise ratio and a good representation of the coastal region. The MariCont_O is the average of all offshore pixels defined as sea pixels excluding 10 pixels (2000 km) over the sea from the land, thus coastline pixels are excluded as well as all the coastal influences. MariCont_L is the average over all land pixels.

Over land, during the growing phase of the convection, Prec and Flash start to increase at the same time (10:00 LT – 12:00 LT) but Flash reaches a maximum earlier (15:00 LT – 16:00 LT) than Prec (17:00 LT – 18:00 LT). This is consistent with the finding of Liu and Zipser (2008) over the whole tropics. The different timing of the maxima could come from the fact that in the dissipating stage of the convection the number of flashes decreases whilst the precipitation remains relatively high. Combining our results with the ones presented in Dion et al. (2019), Flash and Prec can be considered as good proxies of deep convection during the growing phase of the convection over the MariCont_L.

Over coastlines (Fig. 5.7b), the Prec diurnal cycle is delayed by about +2 to 7 h with respect to the Flash diurnal cycle. Prec minimum is around 18:00 LT while Flash minimum is around 11:30 LT. Maxima of Prec and Flash are found around 04:00 LT and 02:00 LT, respectively. This means that the increasing phase of Flash is 2-3 h longer than that of Prec. These results are consistent with the work of Mori et al. (2004) showing a diurnal maximum of precipitation in the early morning between 02:00 LT and 03:00 LT and a diurnal minimum of precipitation between 11:00 LT and 21:00 LT, over coastal zones of Sumatra. According to

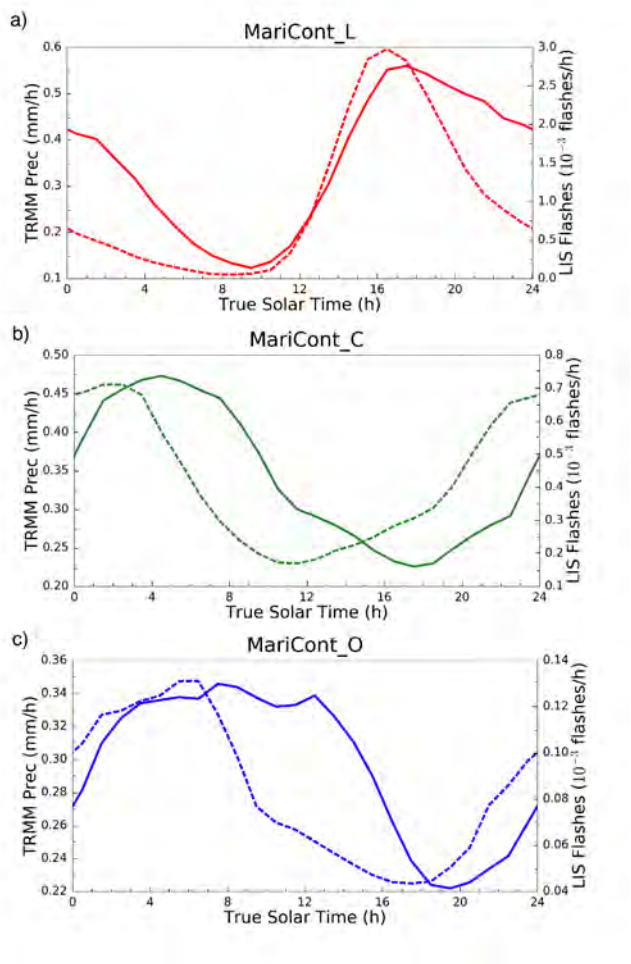

Figure 5.7 – Diurnal cycle of Prec (solid line) and diurnal cycle of Flash (dashed line) over MariCont_L (a), MariCont_C (b) and MariCont_O (c).

Petersen and Rutledge (2001) and Mori et al. (2004), coastal zones are areas where precipitation results more from convective activity than from stratiform activity and the amplitude of diurnal maximum of Prec decreases with the distance from the coastline.

Over offshore areas (Fig. 5.7c), minima of diurnal cycle of Prec and diurnal cycle of Flash are reached in the late afternoon, between 16:00 LT and 17:00 LT (Flash) and 17:00 LT and 18:00 LT (Prec), whilst maxima of diurnal cycle of

Prec and Flash are reached in the early morning, between 06:00 LT and 07:00 LT (Flash) and around 08:00 LT – 09:00 LT (Prec). Results over offshore areas are consistent with diurnal cycle of Flash and Prec calculated by Liu and Zipser (2008) over the whole tropical ocean, showing the increasing phase of the diurnal cycle of Flash starting 1–2 hours before the increasing phase of the diurnal cycle of Prec.

The time interval between the maximum and minimum of Prec is always longer than that for Flash. The period after the maximum of Prec is likely more representative of stratiform rainfall than deep convective rainfall. Consistent with that picture, model results from Love et al. (2011) have shown the suppression of deep convection over the offshore area west of Sumatra from the early afternoon due to a downwelling wavefront characterized by deep warm anomalies around noon. According to the authors, later in the afternoon, gravity waves are forced by the stratiform heating profile and propagate slowly offshore. They also highlighted that the diurnal cycle of the offshore convection responds strongly to the gravity wave forcing at the horizontal scale of 4 km. To summarize, diurnal cycles of Prec and Flash show that:

i) over land, Flash increases proportionally with Prec during the growing phase of the convection,

ii) over coastlines, Flash increasing phase is more than 6–7 hours ahead of Prec increasing phase,

iii) over offshore areas, Flash increasing phase is about 1–2 hours ahead of Prec increasing phase.

In section 5.9, we investigate whether this time difference impacts the estimation of ΔIWC over land, coasts, and offshore areas.

5.7.3 Prec and Flash diurnal cycles and small-scale processes

In this subsection, we study the diurnal cycle of Prec and Flash at 0.25° × 0.25° resolution over areas of deep convective activity over the MariCont. In line with the distribution of large values of Prec (Fig. 5.2), IWC^{MLS} (Fig. 5.3) and ΔIWC (Fig. 5.4), we have selected five islands and five seas over the MariCont. Diurnal cycles of Prec and Flash are presented over land for a) Java, b) Borneo, c) New Guinea, d) Sulawesi and e) Sumatra as shown in Figure 5.8 and over sea for the a) Java Sea, b) North Australia Sea (NAusSea), c) Bismarck Sea, d) West Sumatra Sea (WSumSea) and e) China Sea as shown in Figure 5.9. Diurnal cycles of IWC from ERA5 (IWC^{ERA5}) are also presented in Figs. 8 and 9 and will be discussed in Section 6.

Over land, the amplitude of the diurnal cycle of Prec is the largest over Java (Fig. 5.8a), consistent with Qian (2008), with a maximum reaching 1 mm h^{-1}, while, over the other areas, maxima are between 0.4 and 0.6 mm h^{-1}. Furthermore, over Java, the duration of the increasing phase in the diurnal cycle of Prec is 6 h, consistent with that of Flash, whereas elsewhere the duration of the increasing phase is longer in Prec than in Flash by 1–2 h. The particularity of Java is related to the increasing phase of the diurnal cycle of Prec (6 h), which is faster than over all the other land areas considered in our study (7 – 8 h). The strong and rapid convective growing phase measured over Java might be explained by the fact that the island is narrow with high mountains (up to ∼ 2000 m altitude, as shown in Fig. 2b) reaching the coast. The topography promotes the growth of intense and rapid convective activity. The convection starts around 09:00 LT, rapidly elevating warm air up to the top of the mountains. Around 15:00 LT, air masses cooled at higher altitudes are transported to the sea, favoring the dissipating stage of the convection. Like Java, Sulawesi is a small island with high topography. However, the amplitude of the diurnal cycle of Prec and Flash is not as strong as

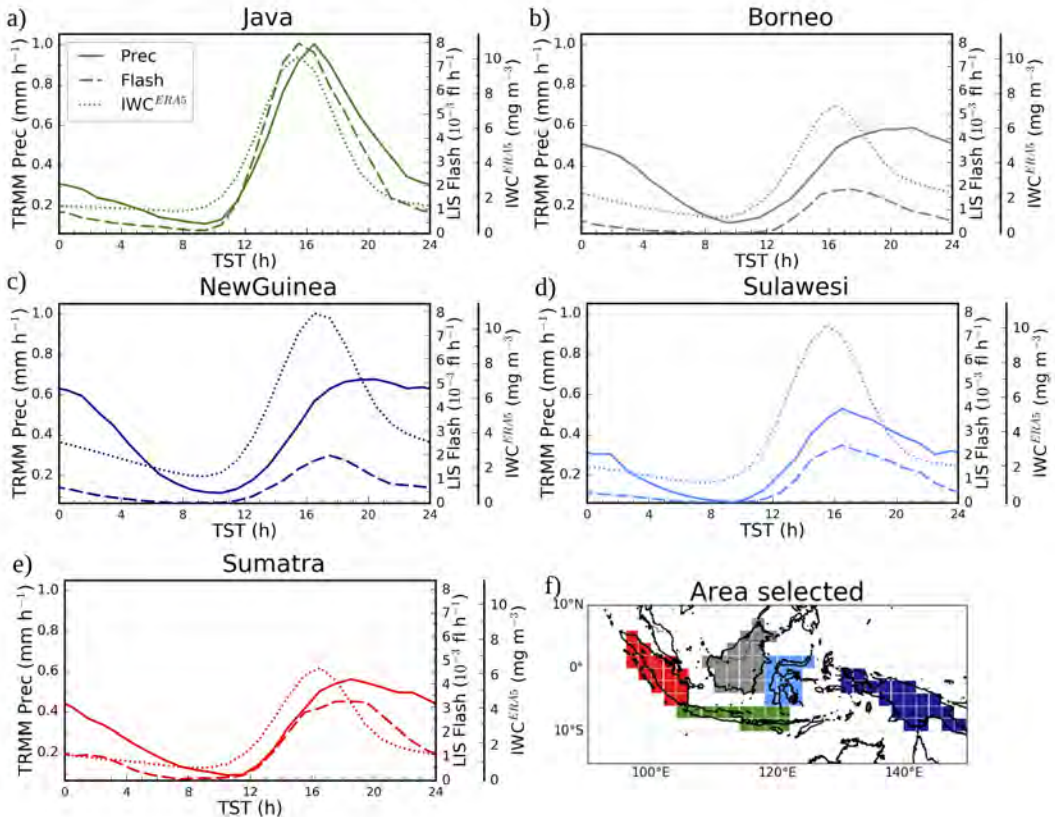

Figure 5.8 – Diurnal cycles of Prec (solid line), Flash (dashed line) and IWC^{ERA5} from ERA5 at 150 hPa (dotted line) over MariCont islands: Java (a), Borneo (b), New Guinea (c), Sulawesi (d) and Sumatra (e) and map of the study zones over land (f).

over Java. Other islands, such as Borneo, New Guinea and Sumatra, have high mountains but also large lowland areas. Mountains promote deep convection at the beginning of the afternoon while lowlands help maintain the convective activity through shallow convection and stratiform rainfall (Nesbitt and Zipser, 2003; Qian, 2008). Deep and shallow convection are then mixed during the slow dissipating phase of the convection (from $\sim$ 16:00 LT to 08:00 LT). However, because Flash are observed only in deep convective clouds, the decreasing phase of Flash diurnal cycles decreases more rapidly than the decreasing phase of Prec. The diurnal maxima of Prec found separately over the 5 islands of the MariCont (at 0.25°

$\times$ 0.25° resolution) are much higher than the diurnal maxima of Prec found over broad tropical land regions (South America, South Africa and MariCont_L, at 2° $\times$ 2° resolution) from Dion et al. (2019): $\sim$ 0.6 – 1.0 mm h^{-1} and $\sim$ 0.4 mm h^{-1}, respectively. However, the duration of the increasing phase of the diurnal cycle of Prec is consistent with the one calculated over tropical land by Dion et al. (2019).

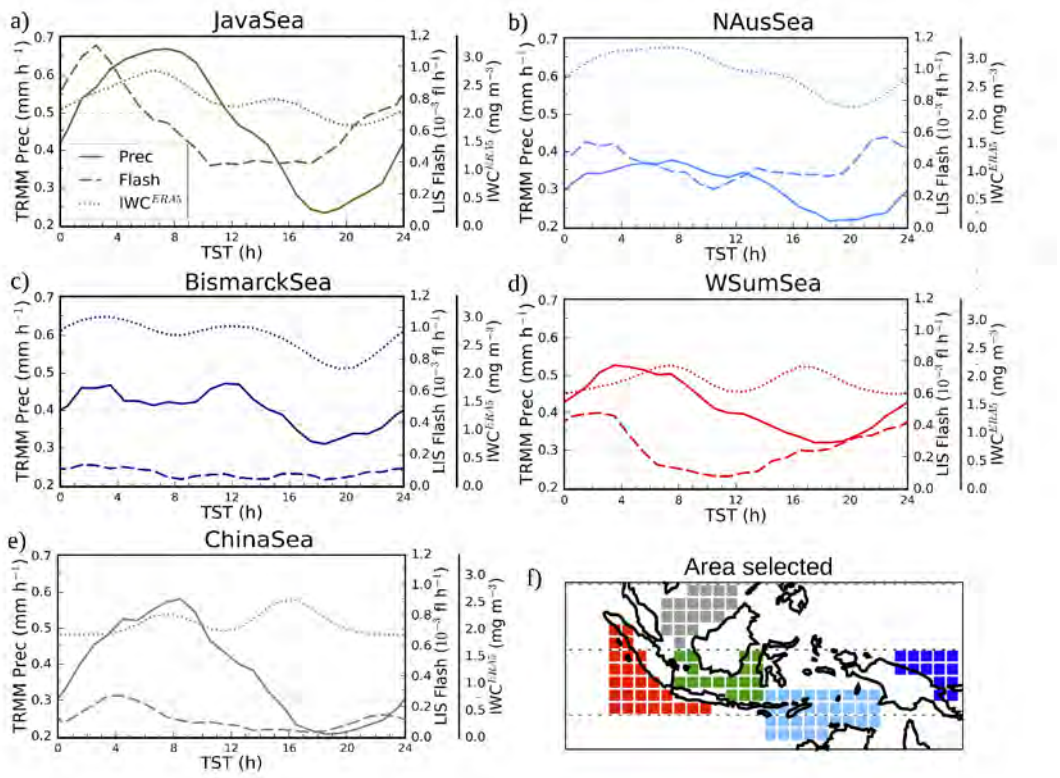

Figure 5.9 – Diurnal cycles of Prec (solid line), Flash (dashed line) and IWC^{ERA5} from ERA5 at 150 hPa (dotted line) over MariCont seas: Java Sea (a), North Australia Sea (NAusSea) (b), Bismarck Sea (c), West Sumatra Sea (WSumSea) (d), China Sea (e) and map of the study zones over sea (f).

Over sea, the five selected areas (Fig. 5.9a–e) show a diurnal cycle of Prec and Flash similar to that of either coastline or offshore areas depending on the region considered. The diurnal cycle of Prec and Flash over Java Sea is similar to the one

over coastlines (Fig. 5.7b). Java Sea (Fig. 5.9a), an area mainly surrounded by coasts, shows the largest diurnal maximum of Prec ($\sim$ 0.7 mm h^{-1}) and Flash ($\sim$ 1.1 10^{-3} flashes h^{-1}) with the longest growing phase. In this area, land and sea breezes observed in coastal areas impact the diurnal cycle of the convection (Qian, 2008). Over Java Sea, Prec is strongly impacted by land breezes from Borneo and Java islands (Qian, 2008), explaining why Prec and Flash reach largest values during the early morning. By contrast, NAusSea, Bismarck Sea and WSumSea (Figs. 5.9b, c and d, respectively), which are large regions on which coastal influences are likely to be weak, show small amplitude of the diurnal cycle. In our analysis, these three study zones are the areas including the most offshore pixels. Java Sea and WSumSea present a similar diurnal cycle of Prec and Flash, with Flash growing phase starting about 4 h earlier than that of Prec. China Sea also shows a diurnal maximum of Flash shifted by about 4 hours before the diurnal maximum of Prec, but the time of the diurnal minimum of Prec and Flash is similar. Over China Sea and Bismarck Sea, the diurnal cycle of Flash shows a weak amplitude with maxima reaching only 0.1 - 0.2 10^{-3} flashes h^{-1}. Furthermore, over Bismarck Sea, while the diurnal minimum in Prec is around 18:00 LT, there are several local minima in Flash (08:00, 14:00 and 18:00 LT). Over NAusSea, the diurnal minimum of Prec is delayed by more than 7 hours compared to the diurnal minimum of Flash.

To summarize, over islands, Flash and Prec convective increasing phases start at the same time and increase similarly but the diurnal maximum of Flash is reached 1–2 hours before the diurnal maximum of Prec. Over seas, the duration of the convective increasing phase and the amplitude of the diurnal cycles are not always similar depending on the area considered. The diurnal cycle of Flash over Java Sea and West Sumatra Sea is 4 hours ahead of the diurnal cycle of Prec, and over North Australia Sea, it is more than 7 hours ahead. China Sea and Bismarck

Sea present the same time of the onset of the Flash and Prec increasing phase. In Section 7, we estimate ΔIWC over the 5 selected island and sea areas from Prec and Flash as a proxy of deep convection.

5.8 Horizontal distribution of IWC from ERA5 reanalyses

The ERA5 reanalysis provides hourly IWC at 150 and 100 hPa (IWC^{ERA5}). The diurnal cycle of IWC^{ERA5} over the MariCont will be used to calculate ΔIWC^{ERA5} in order to support the horizontal distributions and the amount of ice injected in the UT and the TL deduced from our model combining IWC^{MLS} and TRMM-3B42 Prec or IWC^{MLS} and LIS flash. In assessing the consistency or lack thereof in the comparisons between ΔIWC^{ERA5} and both ΔIWC^{Prec} and ΔIWC^{Flash}, it should be kept in mind that IWC^{ERA5} data quality has not yet been fully evaluated. Figures 5.10a, b, c and d present the daily mean and the hour of the diurnal maxima of IWC^{ERA5} at 150 and 100 hPa. In the UT, the daily mean of IWC^{ERA5} shows a horizontal distribution over the MariCont consistent with that of IWC^{MLS} (Fig. 5.2e), except over New Guinea, where IWC^{ERA5} (exceeding 6.4 mg m^{-3}) is much stronger than IWC^{MLS} ($\sim$ 4.0 mg m^{-3}). The highest amount of IWC^{ERA5} is located over the New Guinea mountain chain and over the West coast of North Australia (exceeding 6.4 mg m^{-3} in the UT and 1.0 mg m^{-3} in the TL). Over islands in the UT and the TL, the time of the IWC^{ERA5} diurnal maximum is found between 12:00 LT and 15:00 LT over Sulawesi and New Guinea and between 15:00 LT and 21:00 LT over Sumatra, Borneo and Java, which is close to the hour of the diurnal maximum of Flash over islands (Fig. 5.6). Over sea, in the UT and the TL, the time of the IWC^{ERA5} diurnal maximum is found between 06:00 LT and 09:00 LT over West Sumatra Sea, Java Sea, North Australia Sea, between

06:00 LT and 12:00 LT over China Sea and between 00:00 LT and 03:00 LT over Bismarck Sea. There are no significant differences between the hour of the maximum of IWC^{ERA5} in the UT and in the TL.

The diurnal cycles of IWC^{ERA5} at 150 hPa are presented in Figs. 5.8 and 5.9 over the selection of islands and seas of the MariCont together with the diurnal cycles of Prec and Flash. Over islands (Fig. 5.8), the maximum of the diurnal cycle of IWC^{ERA5} is found between 16:00 LT and 17:00 LT, consistent with the diurnal cycle of Prec and Flash. The durations of the increasing phase of the diurnal cycles of Prec, Flash and IWC^{ERA5} are all consistent to each other (6 – 8 h). Over sea (Fig. 5.9), the maximum of the diurnal cycle of IWC^{ERA5} is mainly found between 07:00 LT and 10:00 LT over Java Sea and North Australia Sea, consistent with the diurnal cycle of Prec, and a second peak is found around 16:00 LT. Thus, the duration of the increasing phase of the diurnal cycles of IWC^{ERA5} is consistent with the one of Prec over these two sea study zones (about 10 hours), but not with the one of Flash. Over Bismarck Sea, the diurnal maxima of IWC^{ERA5} are found at 04:00 LT with a second peak later at noon. Over West Sumatra Sea, two diurnal maxima are found at 08:00 LT and 17:00 LT. Over China Sea, the diurnal maximum of IWC^{ERA5} is found at 16:00 LT with a second peak at 08:00 LT. These differences in the timing of the maximum of the diurnal cycle of Prec, Flash and IWC^{ERA5} observed at small-scale over sea of the MariCont are not well understood. However, these differences do not affect the calculation of the ΔIWC^{Prec}, ΔIWC^{Flash} or ΔIWC^{ERA5}, because only the magnitude of the diurnal cycle (max-min) matters for the calculation of ΔIWC.

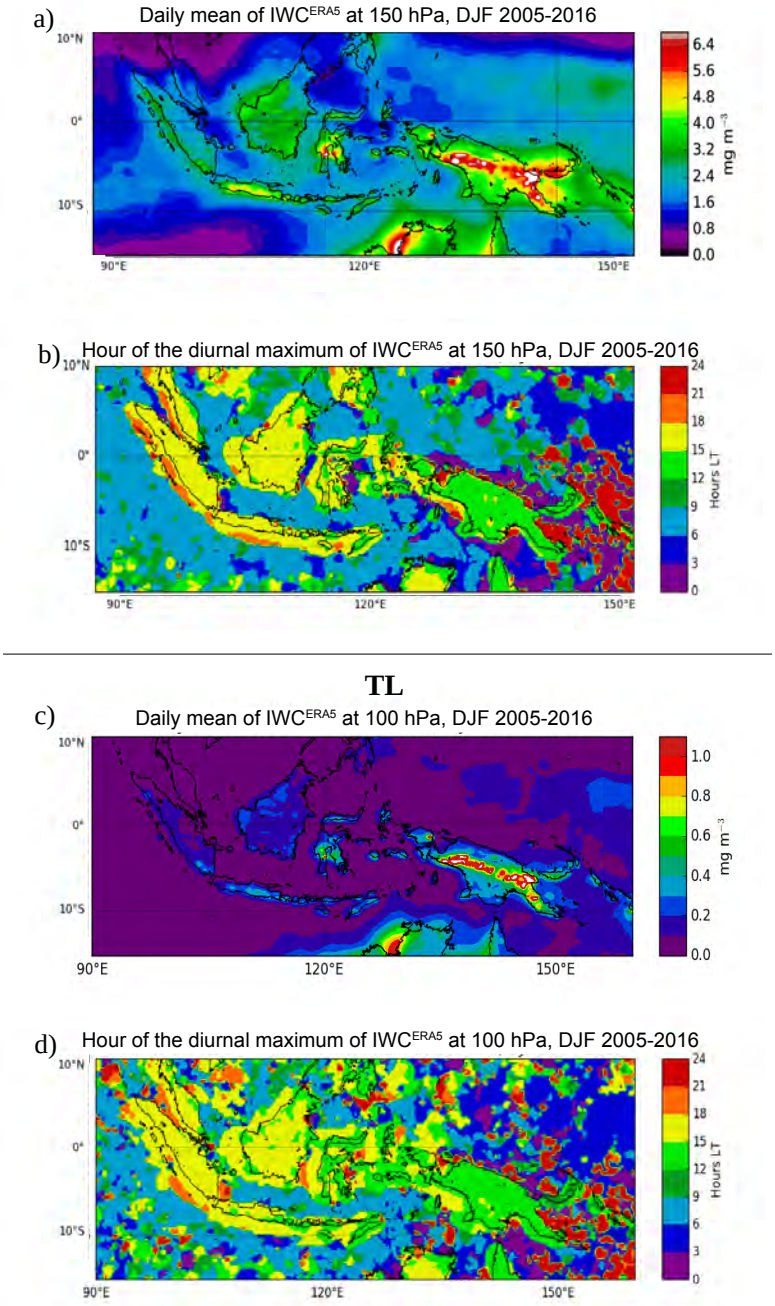

Figure 5.10 – Daily mean of IWC^{ERA5} averaged over the period DJF 2005-2016 at 150 hPa (a) and at 100 hPa (c); Time (hour, local time (LT)) of the diurnal maximum of IWC^{ERA5} at 150 hPa (b) and at 100 hPa (d).

5.9 Ice injected over a selection of island and sea areas

Figure 5.11 synthesizes ΔIWC deduced from observations and reanalysis in the UT and the TL over the 5 islands and 5 seas of the MariCont studied in the previous section.

5.9.1 ΔIWC deduced from observations

Eqs. (1-3) are used to calculate ΔIWC from Prec (ΔIWC^{Prec}) and from Flash (ΔIWC^{Flash}). As presented in the previous section, Prec and Flash can be used as two proxies of deep convection, although differences in their diurnal cycles may depend on the region considered. The observational ΔIWC range calculated between ΔIWC^{Prec} and ΔIWC^{Flash} provides a quantitative characterisation of the uncertainty in our model. In the following we will consider the relative difference, expressed as a percentage, between between ΔIWC^{Prec} and ΔIWC^{Flash} as:

$$r^{Prec-Flash} = 100 \times \frac{\Delta IWC^{Prec} - \Delta IWC^{Flash}}{(\Delta IWC^{Prec} + \Delta IWC^{Flash}) \times 0.5} \tag{5.4}$$

In the UT (Fig. 5.11a), over islands, ΔIWC calculated over Sumatra, Borneo, Sulawesi and New Guinea varies from 4.9 to 7.1 mg m^{-3} whereas, over Java, ΔIWC reaches 8.1–8.7 mg m^{-3}. ΔIWC^{Flash} is generally greater than ΔIWC^{Prec} by less than 1.4 mg m^{-3} (with $r^{Prec-Flash}$ ranging from -6 to -22% over the study zones) for all the islands, except for Java where ΔIWC^{Prec} is larger than ΔIWC^{Flash} by 0.7 mg m^{-3} ($r^{Prec-Flash}$ = 7.1%). Over sea, ΔIWC varies from 1.1 to 4.4 mg m^{-3}. ΔIWC^{Flash} is greater than ΔIWC^{Prec} by 0.6 to 2.3 mg m^{-3} ($r^{Prec-Flash}$ = -35 to -71%), except for Java Sea, where ΔIWC^{Prec} is greater than ΔIWC^{Flash} by 0.2 mg m^{-3} ($r^{Prec-Flash}$ = 6%). Over North Australia Sea

and West Sumatra Sea, ΔIWC^{Flash} is more than twice as large as ΔIWC^{Prec} ($r^{Prec-Flash}$ = -63% and -71%, respectively).

In the TL (Fig. 5.11b), the observational ΔIWC range is found between 0.7 and 1.3 mg m^{-3} over islands and between 0.2 and 0.7 mg m^{-3} over seas. The same conclusions apply to the observational ΔIWC range calculated between ΔIWC^{Prec} and ΔIWC^{Flash} in the TL as in the UT, with differences less than 0.4 mg m^{-3}.

To summarize, independently of the proxies used for the calculation of ΔIWC, and for both UT and TL, Java island shows the largest injection of ice over the MariCont. The minimum value of the observational ΔIWC range over Java island is larger than the maximum value of the observational ΔIWC range of other land study zones by more than 1.0 mg m^{-3} in the UT and more than 0.3 mg m^{-3} in the TL. Furthermore, it has been shown that both proxies can be used in our model, with more confidence over land: ΔIWC^{Prec} and ΔIWC^{Flash} are more consistent to each other, both in the UT and in the TL, over islands (relative difference $r^{Prec-Flash}$=-6 to -22 %) than over seas ($r^{Prec-Flash}$ = +6 to -71 %). The larger difference over seas is probably due to the larger contribution from stratiform precipitation to Prec over sea.

5.9.2 ΔIWC deduced from reanalyses

ΔIWC from ERA5 ($\Delta\text{IWC}^{ERA5}_{z_0}$) is calculated in the UT and the TL (z_0 = 150 and 100 hPa, respectively) as the max–min difference in the amplitude of the diurnal cycle. We can use the IWC^{ERA5} to assess the impact of the vertical resolution of the MLS measurements on the observationally-derived ΔIWC estimates. According to Wu et al. (2008), estimates of IWC derived from MLS represent spatially-averaged quantities within a volume that can be approximated by a box of $\sim 300\times7\times4$ km^3 near the pointing tangent height. In order to com-

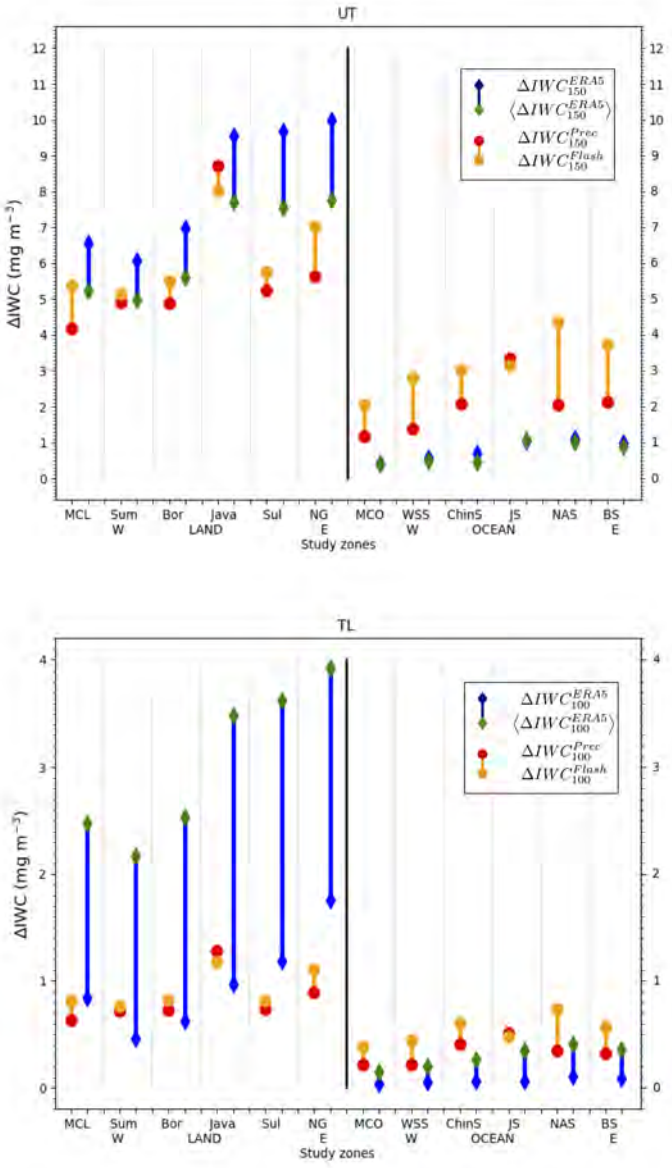

Figure 5.11 – Top: ΔIWC (mg m^{-3}) estimated from Prec (red) and Flash (orange) at 146 hPa and ΔIWC estimated from ERA5 at the level 150 hPa and at the level 150 hPa degraded in the vertical, over islands and seas of the MariCont: MariCont_L (MCL) and MariCont_O (MCO); from West (W) to East (E) over land, Sumatra (Sum), Borneo (Bor), Java, Sulawesi (Sul) and New Guinea (NG); and over seas, West Sumatra Sea (WSS), China Sea (ChinS), Java Sea (JS), North Australia Sea (NAS) and Sea (BS). Bottom: Same as in top but for 100 hPa.

pare IWC^{MLS} and IWC^{ERA5}, two steps were taken: 1) the horizontal resolution of ERA5 was degraded from 0.25°×0.25° to 2°×2° (∼ 200 km×200 km), and 2) the vertical resolution of ERA5 was degraded by convolving the vertical profiles of IWC^{ERA5} with a box function whose width is 5 and 4 km at 100 and 146 hPa, respectively. The ERA5 amount of ice injected at z_0 = 146 and 100 hPa with degraded vertical resolution ($\left\langle \Delta IWC^{ERA5}_{z_0} \right\rangle$) is thus calculated from $\left\langle IWC^{ERA5}_{z_0} \right\rangle$. In the following we consider the difference $r^{ERA5-\langle ERA5\rangle}$ between ΔIWC^{ERA5} and $\left\langle \Delta IWC^{ERA5} \right\rangle$ as:

$$r^{ERA5-\langle ERA5\rangle} = 100 \times \frac{\Delta IWC^{ERA5} - \left\langle \Delta IWC^{ERA5} \right\rangle}{(\Delta IWC^{ERA5} + \langle \Delta IWC^{ERA5} \rangle) \times 0.5} \tag{5.5}$$

Figure 5.11 shows $\Delta IWC^{ERA5}_{z_0}$ and $\left\langle \Delta IWC^{ERA5}_{z_0} \right\rangle$ at z_0 = 150 and 100 hPa, over the island and the sea study zones. In the UT (Fig. 5.11a), over islands, ΔIWC^{ERA5}_{150} and $\left\langle \Delta IWC^{ERA5}_{150} \right\rangle$ calculated over Sumatra and Borneo vary from 4.9 to 7.0 mg m^{-3} ($r^{ERA5-\langle ERA5\rangle}$ ranges from 20 to 22 %) whilst ΔIWC^{ERA5}_{150} and $\left\langle \Delta IWC^{ERA5}_{150} \right\rangle$ over Java, Sulawesi and New Guinea reach 7.5–10.0 mg m^{-3} ($r^{ERA5-\langle ERA5\rangle}$ = 21 to 24 %). Over sea, ΔIWC^{ERA5}_{150} and $\left\langle \Delta IWC^{ERA5}_{150} \right\rangle$ vary from 0.35 to 1.1 mg m^{-3} ($r^{ERA5-\langle ERA5\rangle}$ = 9 to 33 %). Over island and sea, ΔIWC^{ERA5}_{150} is greater than $\left\langle \Delta IWC^{ERA5}_{150} \right\rangle$. The small differences between ΔIWC^{ERA5}_{150} and $\left\langle \Delta IWC^{ERA5}_{150} \right\rangle$ over island and sea in the UT support the fact that the vertical resolution at 150 hPa has a low impact on the estimated ΔIWC.

In the TL, over land, ΔIWC^{ERA5}_{100} and $\left\langle \Delta IWC^{ERA5}_{100} \right\rangle$ vary from 0.5 to 3.9 mg m^{-3} ($r^{ERA5-\langle ERA5\rangle}$ = -32 to -138%) with $\left\langle \Delta IWC^{ERA5}_{100} \right\rangle$ being larger than ΔIWC^{ERA5}_{100} by as much as 2.5 mg m^{-3} over some islands. Over sea, ΔIWC^{ERA5}_{100} and $\left\langle \Delta IWC^{ERA5}_{100} \right\rangle$ vary from 0.05 to 0.4 mg m^{-3} ($r^{ERA5-\langle ERA5\rangle}$ = -85 to -139%) with ΔIWC^{ERA5}_{100} lower than $\left\langle \Delta IWC^{ERA5}_{100} \right\rangle$ by as much as 0.3 mg m^{-3}. The

large differences between ΔIWC_{100}^{ERA5} and $\left\langle \Delta IWC_{100}^{ERA5} \right\rangle$ over island and sea in the TL support the fact that the vertical resolution at 100 hPa has a high impact on the estimation of ΔIWC.

5.9.3 Synthesis

The comparison between the observational ΔIWC range and the reanalysis ΔIWC range is presented in Fig. 5.11. In the UT, over land, observation and reanalysis ΔIWC ranges agree to within 0.1 to 1.0 mg m^{-3}, which highlights the robustness of our model over land, except over Sulawesi and New Guinea, where the observational and the reanalysis ΔIWC ranges differ by at least 1.7 and 0.7 mg m^{-3}, respectively. Over sea, the observational ΔIWC range is systematically greater than that of the reanalysis by ∼1.0–2.2 mg m^{-3}, with systematically larger estimates derived from observations than from the reanalysis. The consistency between observational and reanalysis ΔIWC ranges is calculated as the minimum value of the higher range minus the maximum value of the lower range divided by the mean of these two values. In the UT, observational and reanalysis ΔIWC estimates are found to be consistent over land, where the relative differences between their ranges are less than 25%, but inconsistent over sea, where differences are 62–96%. In the TL, the relative differences between the observational and reanalysis ΔIWC ranges are 0–49% over land and 0–28% over sea. In the following, we define the total range covering the observational and reanalysis ΔIWC estimates, r^{Total}, as the maximum value of the higher range minus the minimum value of the lower range divided by the mean of these two values. In the UT, the observational and reanalysis ΔIWC estimates span 4.2 to 10.0 mg m^{-3} (with r^{Total} values from 20 to 57%) over land and 0.4 to 4.4 mg m^{-3} (with r^{Total} values from 107 to 156%) over sea. In the TL, the observational and reanalysis ΔIWC estimates span 0.5 to 3.9 mg m^{-3} (with r^{Total} values from 88 to 134%) over land and 0.1 to 0.7 mg m^{-3}

(with r^{Total} values of 142 to 160%) over sea.

Amounts of ice injected deduced from observations and reanalysis are consistent (i.e., the relative differences between their respective ranges are less than 49%) over land in the UT and over land and sea in the TL but inconsistent over sea in the UT (where differences are as large as 96%). However, the impact of the vertical resolution on the estimation of ΔIWC is much larger in the TL than in the UT (r^{Total} is larger in the TL than in the UT). At both levels, observational and reanalyses ΔIWC estimated over land is more than twice as large as ΔIWC estimated over sea. At any considered level, although Java has shown the largest values of ΔIWC form observations compared to other study zones, the reanalysis ΔIWC range shows that Sulawesi and New Guinea may also reach high values of ΔIWC, similar to those seen over Java. However, as the ERA5 IWC data have yet to be extensively validated, it is also possible that the reanalysis overestimates IWC in these regions.

5.10 Discussion on small-scale convective processes impacting ΔIWC over a selection of areas

Our results have shown that, in all the datasets used, Java island and Java Sea are the two areas with the largest amount of ice injected up to the UT and the TL over the MariCont land and sea, respectively. In this section, processes impacting ΔIWC in the different study zones are discussed.

5.10.1 Java island, Sulawesi and New Guinea

Sulawesi, New Guinea and particularly Java island have been shown as the areas of the largest ΔIWC in the UT and TL. Qian (2008) have used high resolution

observations and regional climate model simulations to show the three main processes impacting the diurnal cycle of rainfall over the Java island. The main process explaining the rapid and strong peak of Prec during the afternoon over Java (Fig. 5.8a) is the sea-breeze convergence around midnight. This convergence caused by sea-breeze phenomenon increases the deep convective activity and impacts the diurnal cycle of Prec and the IWC injected up to the TL by amplifying their quantities. The second process is the mountain-valley wind converging toward the mountain peaks, reinforcing the convergence and the precipitation. The land breeze becomes minor compared to the mountain-valley breeze and this process is amplified with the mountain altitude. As shown in Fig. 5.2b, New Guinea has the highest mountain chain of the MariCont. The third process shown by Qian (2008) is precipitation that is amplified by the cumulus merging processes, which are more important over small islands such as Java (or Sulawesi) than over large islands such as Borneo or Sumatra. Another process is the interaction between sea-breeze and precipitation-driven cold pools that generates lines of strong horizontal moisture convergence (Dauhut et al., 2016). Thus, IWC increases proportionally with Prec, consistent with the results from Dion et al. (2019), and rapid convergence combined with deep convection transports elevated amounts of IWC at 13:30 LT (Fig. 5.3), producing high ΔIWC during the growing phase of the convection (Fig. 5.4 and Fig. 5.11) over Java Island.

5.10.2 West Sumatra Sea

In section 5.6.2, it has been shown that the West Sumatra Sea is an area with positive anomaly of Prec during the growing phase of the convection but negative anomaly of IWC, which differs from other places. These results suggest that Prec is representative not only of convective precipitation but also of stratiform precipitation. The diurnal cycle of stratiform and convective precipitation over

West Sumatra Sea has been studied by Mori et al. (2004) using 3 years of TRMM precipitation radar (PR) datasets, following the 2A23 Algorithm (Awaka, 1998). Mori et al. (2004) have shown that rainfall over Sumatra is characterized by convective activity with a diurnal maximum between 15:00 LT and 22:00 LT while, over the West Sumatra Sea, the rainfall type is convective and stratiform, with a diurnal maximum during the early morning (as observed in Fig. 5.9). Furthermore, their analyses have shown a strong diurnal cycle of 200-hPa wind, humidity and stability, consistent with the PR over West Sumatra Sea and Sumatra Island. Stratiform and convective clouds are both at the origin of heavy rainfall in the tropics (Houze and Betts, 1981; Nesbitt and Zipser, 2003) and in the West Sumatra Sea, but stratiform clouds are mid-altitude clouds in the troposphere and do not transport ice up to the tropopause. Thus, over the West Sumatra Sea, ΔIWC calculated from Prec is possibly overestimated because Prec includes a non-negligible amount of stratiform precipitation over this area.

5.10.3 North Australia Sea and seas with nearby islands

The comparisons between Figs. 2c and 6a have shown strong daily mean of Flash (10^{-2} –10^{-1} flashes day^{-1}) but low daily mean of Prec (2.0 – 8.0 mm day^{-1}) over the North Australia Sea. Additionally, Fig. 11 shows that the strongest differences between ΔIWC^{Prec} and ΔIWC^{Flash} are found over the North Australia Sea, with ΔIWC^{Flash} greater than ΔIWC^{Prec} by 2.3 mg m^{-3} in the UT ($r^{Prec-Flash}$ = ∼-71%) and by 0.4 mg m^{-3} in the TL ($r^{Prec-Flash}$ = - 75%). These results imply that the variability range in our model is too large, highlighting the difficulty of estimating ΔIWC over this study zone. Furthermore, as for Java Sea or Bismarck Sea, North Australia Sea is surrounded by several islands. According to the study from Pope et al. (2008), the cloud size is the largest during the afternoon over the North Australia land, during the night over North Australia coastline and during

the early morning over the North Australia sea. These results suggest that deep convective activity moves from the land to the sea during the night. Over the North Australia Sea, it seems that the deep convective clouds are mainly composed of storms with lightning but precipitation is weak or does not reach the surface before evaporating.

5.11 Conclusions

The present study has combined observations of ice water content (IWC) measured by the Microwave Limb Sounder (MLS), precipitation (Prec) from the algorithm 3B42 of the Tropical Rainfall Measurement Mission (TRMM), the number of flashes (Flash) from the Lightning Imaging Sensor (LIS) on board of TRMM with IWC provided by the ERA5 reanalyses in order to estimate the amount of ice injected (ΔIWC) in the upper troposphere (UT) and the tropopause level (TL) over the MariCont, from the method proposed in a companion paper (Dion et al., 2019). The study is focused on the austral convective season of DJF from 2004 to 2017. In the model used (Dion et al., 2019), Prec is considered as a proxy of deep convection injecting ice (ΔIWC^{Prec}) in the UT and the TL. ΔIWC^{Prec} is firstly calculated by the correlation between the growing phase of the diurnal cycle of Prec from TRMM-3B42 (binned at 1-hour resolution over the diurnal cycle) and the value of IWC measured by MLS (IWC^{MLS}, provided at the temporal resolution of 2 observations in local time per day) during the growing phase of the diurnal cycle of Prec. While Dion et al. (2019) have calculated ΔIWC^{Prec} over large convective study zones in the tropics, we show the spatial distribution of ΔIWC^{Prec} in the UT and the TL at $2^\circ \times 2^\circ$ horizontal resolution over the MariCont, highlighting local areas of strong injection of ice up to 20 mg m^{-3} in the UT and up to 3 mg m^{-3} in the TL. ΔIWC injected in the UT and the TL has also been

evaluated by using another proxy of deep convection: Flash measured by TRMM-LIS. Diurnal cycle of Flash has been compared to diurnal cycle of Prec, showing consistencies in 1) the spatial distribution of Flash and Prec over the MariCont (maxima of Prec and Flash located over land and coastline), and 2) their diurnal cycles over land (similar onset and duration of the diurnal cycle increasing phase). Differences have been mainly observed over sea and coastline areas, with the onset of the diurnal cycle increasing phase of Prec delayed by several hours depending on the considered area (from 2 to 7 h) compared to Flash. ΔIWC calculated by using Flash as a proxy of deep convection (ΔIWC^{Flash}) is compared to ΔIWC^{Prec} over five islands and five seas of the MariCont. Over each study zone, the range of values between ΔIWC^{Prec} and ΔIWC^{Flash}, the observational ΔIWC range, allows us to characterize the uncertainty of our model. ΔIWC is also estimated from IWC provided by the ERA5 reanalyses (ΔIWC^{ERA5} and IWC^{ERA5}, respectively) at 150 and 100 hPa over the study zones. We have also degraded the vertical resolution of IWC^{ERA5} to be consistent with that of IWC^{MLS} observations: 4 km at 146 hPa and 5 km at 100 hPa. The ΔIWC ranges calculated from observations and reanalyses were evaluated over the selected study zones (island and sea).

With the study of ΔIWC^{Prec}, results show that the largest amounts of ice injected in the UT and TL per $2^\circ \times 2^\circ$ pixels are related to i) an amplitude of Prec diurnal cycle larger than 0.5 mm h^{-1} and ii) a duration of the growing phase of the convection longer than 9 hours. ΔIWC^{Prec} is typically smaller than ΔIWC^{Flash}, with the two estimates disagreeing by –6 to –22 % over land and +6 to –71% over sea. The larger differences between ΔIWC^{Prec} and ΔIWC^{Flash} over sea might be due to the combination of the presence of stratiform precipitation included in Prec and the very low values of Flash over seas ($<10^{-2}$ flashes day^{-1}). The diurnal cycle of IWC^{ERA5} at 150 hPa is more consistent with that of Prec and Flash over

land than over ocean. Finally, ΔIWC estimated from observations has been shown to be consistent with ΔIWC estimated from reanalysis to within 25% over land in the UT, to within 49 % over land in the TL and to within 28 % over sea in the TL, but inconsistent over sea in the UT, where relative differences are as large as 96 %. Thus, considering the combination of the observational and reanalysis ΔIWC ranges, the total ΔIWC range has been found in the UT to be between 4.2 and 10.0 mg m^{-3} over land and between 0.4 and 4.4 mg m^{-3} over sea and, in the TL, between 0.5 and 3.9 mg m^{-3} over land and between 0.1 and 0.7 mg m^{-3} over sea. The impact of the vertical resolution on the estimation of ΔIWC has been found to be greater in the TL than in the UT.

The study at small scale over islands and seas of the MariCont has shown that ΔIWC from ERA5, Prec and Flash in the UT agree to within 0.1 – 1.0 mg m^{-3} over MariCont_L, Sumatra, Borneo and Java, with the largest values obtained over Java Island. Based on observations, Java Island presents the largest amount of ice in the UT and the TL (with the minimum value of the observational ΔIWC range over Java island being larger than the maximum value of the observational ΔIWC range of other land study zones by more than 1.0 mg m^{-3} in the UT and than 0.3 mg m^{-3} in the TL). Based on the reanalysis, New Guinea and Sulawesi reach similar ranges of ice injection in the UT and even larger ranges of values in the TL than Java Island, although it must be kept in mind that ERA5 IWC data have not yet been evaluated. Processes related to the strongest amount of ΔIWC injected into the UT and the TL have been identified as the combination of sea-breeze, mountain-valley breeze and merged cumulus, accentuated over small islands with high topography such as Java or Sulawesi.

5.12 *Author contribution.*

IAD analysed the data, formulated the model and the method combining MLS, TRMM and LIS data and took primary responsibility for writing the paper. CD has treated the LIS data, provided the Figures with Flash datasets, gave advices on data processing and contributed to the Prec and Flash comparative analysis. PR strongly contributed to the design of the study, the interpretation of the results and the writing of the paper. PR, FC, PH and TD provided comments on the paper and contributed to its writing.

5.13 *Acknowledgement.*

We thank the National Center for Scientific Research (CNRS) and the Excellence Initiative (Idex) of Toulouse, France to fund this study and the project called Turbulence Effects on Active Species in Atmosphere (TEASAO – http://www.legos.obs-mip.fr/projets/axes-transverses-processus/teasao, last access: May 2020, Peter Haynes Chair of Attractivy). We would like to thank the teams that have provided the MLS data (https://disc.gsfc.nasa.gov/datasets?page=1&keywords=ML2IWC_004, last access: May 2020), the TRMM data (https://pmm.nasa.gov/data-access/downloads/trmm), the LIS data (https://ghrc.nsstc.nasa.gov/lightning/data/data_lis_trmm.html, last access: May 2020) and the ERA5 Reanalysis data (https://cds.climate.copernicus.eu/cdsapp#!/dataset/reanalysis-era5-pressure-levels-monthly-means?tab=form, last access: May 2020). We would like to thank both reviewers for their helpful comments and especially Michelle Santee for the many very detailed comments she provided that were invaluable in improving the study.

5.14 *Data availability.*

The observational datasets are available from the following websites: https://disc.gsfc.nasa.gov/datasets?age=1&keywords=ML2IWC_004 (last access: 1 January 2018, IWC from MLS), https://trmm.gsfc.nasa.gov/publications_dir/publications.html (last access: 1 January 2019, Prec from TRMM-3B42), https://ghrc.nsstc.nasa.gov/lightning/data/data_lis__trmm.html (last access: 1 January 2019, Flash from TRMM-LIS), https://cds.climate.copernicus.eu/cdsapp#!/dataset/reanalysis-era5-pressure-levels-monthly-means?tab=form (last access: July 2019, IWC from ERA5), and https://www.esrl.noaa.gov/psd/thredds/catalog/Datasets/ncep/catalog.html (last access : 17 June 2019, Wind from NOAA).

Chapter 6

Impact of large-scale oscillations on the ice injected in the TTL over the Maritime Continent

This chapter deals with the impact of different oscillations (**MJO** and **La Niña**) on the ice injected into the TTL over the Maritime Continent in comparison with the amount of ice injected during the austral convective season of **DJF**.

6.1 Context

Weather and climate over the MariCont region follow an annual cycle with strongest convective activity during the **DJF** season (Zhang et al., 2016). However, intra-seasonal and inter-annual oscillations have also strong impacts on the MariCont convective activity, particularly the Madden Julian Oscillation (**MJO**) and the El Niño Southern Oscillation (ENSO). ENSO and **MJO** definitions have been detailed and illustrated in chapter 2. **MJO** and ENSO are large-scale intra-seasonal and inter-annual convective activities and are associated with cold and

warm anomalies near the tropopause and rapid phenomena of convective overshoot systems, transporting WV and ice into high altitudes in the troposphere. The **MJO** episodes have a lifetime of about 80 days and are moving Eastward through the MariCont, propagating strong wet convective activity preceded and followed by particularly dry and suppressed convective activity. Eight phases of the **MJO** are defined by the location of the deep convective activity crossing Eastward the MariCont (Wheeler and Hendon, 2004). ENSO is divided into cold, warm and neutral episodes with a duration of one to few months, distinguished by the inhibition or the amplification of the convective activity over some tropical areas. The warmer and wetter period of ENSO over the MariCont region is called **La Niña**, but this episode is rather similar to the neutral conditions of the ENSO over this region. Because **MJO** and ENSO complex responses on weather and climate are erratic and still not well understood, numerical models are limited to produce and forecast **MJO** and ENSO.

In this study, the daily amount of ice injected (ΔIWC) into the UT over the MariCont, averaged from 2004 to 2017, is studied for three strong convective processes occurring during i) the austral convective season of **DJF**, ii) the **DJF** seasons not including the **MJO** episodes nor the **La Niña** episodes, iii) the **La Niña** episodes not including the **DJF** season nor the **MJO** episodes and iv) the **MJO** active phase episodes over the MariCont not including austral convective season of **DJF** nor the **La Niña** episodes. The same method, using precipitation from TRMM-3B42 (Prec) and IWC from MLS (IWC^{MLS}), as presented in Dion et al. (2019) and in Chapter 5, is used to estimate ΔIWC (ΔIWC^{Prec}) over five islands and five seas of the MariCont. The non-precipitating ice (MRI) concentration simulated from the atmospheric non-hydrostatic regional model Meso-NH during the **MJO** period from 23 to the 30 November 2011 (presented in Chapter 3) is used to estimate ΔIWC ($\Delta\text{IWC}^{Meso-NH}$). The goal of this study is to assess

the impact of different oscillations (**MJO** and **La Niña**) on the amount of ice injected up to the UT, at small scales over islands and seas of the MariCont, and to check whether it significantly differs from the amount of ice injected during the **DJF** austral summer convective season.

Datasets used are recalled in section 6.2.1, the study zones are defined in section 6.2.2 and the methodology is presented in section 6.2.3. The difference in deep convective processes between the four study processes (**DJF_Clim, DJF, La Niña** and **MJO**) is studied though the comparison of the diurnal cycle of Prec over MariCont island and seas in section 6.3. Prec and IWC^{MLS} measured during the growing phase of the convection are compared for each study process over the MariCont at the 2° × 2° horizontal resolution in section 6.4. Finally, ΔIWC^{Prec} is studied for the four study convective processes in section 6.5 and compared to ΔIWC$^{Meso-NH}$ over the island and sea study zones. Synthesis and discussions are drawn in section 6.6.

6.2 Datasets, study zones and methodology

6.2.1 Datasets

In this study, the same datasets (IWC from MLS (IWC^{MLS}) and precipitation from TRMM-3B43 (Prec)) already presented in Chapter 3, Chapter 4 and Chapter 5) are used from 2004 to 2017 at 2°×2°horizontal resolution.

The Meso-scale Meso-NH model is a model able to provide high enough horizontal and vertical resolution to study processes at the convective scale. Details on the simulation used and on Meso-NH are presented in Chapter 3, section 3.3.2. The non-precipitating ice (MRI) is calculated from Meso-NH (Lafore et al., 1997; Lac et al., 2018), version 5-1 during the period from 23 to 30 November 2011. The period selected for the study corresponds to the passage of the **MJO** over the

Indian Ocean and MariCont region (Kuznetsova et al., 2019). The simulated **MJO** period has been shown to be in active convective phase (wet air circulation) over the Indian Ocean and West part of the MariCont (from 90°E to 120°E, including West Sumatra Sea and Sumatra, Java Sea and Java, China Sea and Borneo), and in suppressed convective phase (dry air circulation) over the East part of the MariCont (from 120°E to 160°E, including Sulawesi, North Australia Sea and Land, New Guinea and Bismark Sea) (Kuznetsova et al., 2019). Figure 6.1 shows the Hovmöller diagram of the precipitation averaged for the band of 7.5° S–7.5° N over the Indian ocean (50° E – 90° E) and MariCont (90° E – 150° E) during the simulated study period.

6.2.2 Study zones

Five island and five sea study zones are chosen for their strong convective activities (see Chapter 5): Sumatra, Java, Borneo, Sulawesi, New Guinea islands and the West Sumatra Sea, Java Sea, China Sea, North Australia Sea and Bismark Sea. As in Chapter 4 and 5, each 2° × 2° pixel is land/ocean filtered by using the Solar Radiation Data (SoDa, `http://www.soda-pro.com/web-services/altitude/srtm-in-a-tile`), providing a TIFF image with values from the SRTM (Shuttle Radar Topography Mission) Digital Elevation Model.

6.2.3 Methodology

The model developed in Chapter 4 (Dion et al., 2019) is used. In this study, tropical deep convective activities are separated in four processes and compared to one inhibited convective process (Table 6.1).

The climatology of deep convective activity during the austral convective sea-

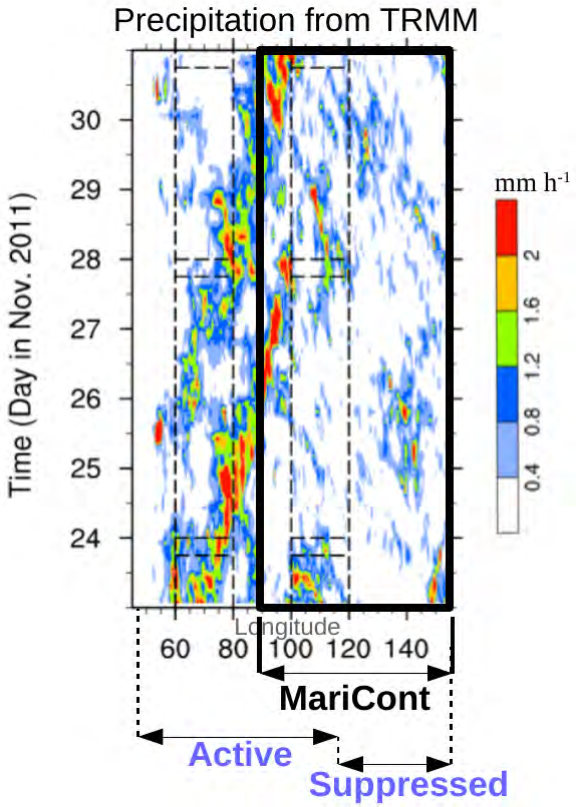

Figure 6.1 – Figure 2a from Kuznetsova et al. (2019). Hovmöller diagram of the precipitation from 24 to 30 November 2011, averaged over the region of 7.5° S–7.5° N for (a) TRMM. The vertical dashed lines show the studied longitudinal domains defining a part of the Indian Ocean, 60°–80°E, and a part of the Maritime Continent, 100° –120° E, according to the Kuznetsova et al. (2019) study. The horizontal lines show the time periods chosen for the analyses of the different **MJO** phases for the Kuznetsova et al. (2019) study. The back box has been added to the figure to identify the domain used in our study definded the MariCont. The domain when the MJO has been observed in active and suppressed phases have been noted by arrows.

son of **DJF** has been chosen consistently with Dion et al. (2019): labelled as **DJF_Clim**. Since, during the climatological period of **DJF**, some large-scale oscillations may have occurred, we have selected **DJF** season excluding the **MJO** (active and suppressed phases) and **La Niña** episodes in order to study pure deep convective activity not impacted by large-scale oscillations: labelled as **DJF**.

The large-scale convective processes forced by the **La Niña** large-scale oscillations are studied excluding the **DJF** and the **MJO** (active and suppressed phases) periods: labelled as **La Niña**. The **La Niña** index used in this study comes from the NOAA National Weather Service – Climate Prediction Center, `https://origin.cpc.ncep.noaa.gov/products/analysis_monitoring/ensostuff/ONI_v5.php`, last access: June 2019), based on a threshold of +/- 0.5°C for the Oceanic Niño Index (ONI) (3-month running mean of ERSST.v5 SST anomalies in the Niño 3.4 region (5°N-5°S, 120°-170°W)), and centred on 30-year base periods updated every 5 years. The ONI index has been chosen as a function of the Barnston et al., 1997 results showing that the Nino 3.4 index would be the more general index impacting the global Pacific Ocean.

The large-scale convective processes forced by the MJO large-scale oscillations in active phase over the MariCont are studied by excluding all the **DJF** and **La Niña** periods: labelled as **MJO active in MariCont**. The selection of the **MJO active in MariCont** over the study zone considered varies as a function of the studied islands and seas. The two phases the most representative of the strongest convective activity during **MJO** over each study zone have been chosen consistently with the composites of intra-seasonal (30-90 days) anomalies in TRMM precipitation during November-April of 1998-2012 based on the real-time multivariate **MJO** index studied by Zhang et al. (2013) (presented in Figure 2.16, Chapter 2). Java, Borneo, Sumatra, Java Sea and MariCont_L are studied during the phases 3 and 4 of the **MJO**, while New Guinea, Sulawesi, West Sumatra Sea, China Sea, North Australia Sea and MariCont_O are studied during the phases 4 and 5 of the **MJO**. Thus, **MJO active in MariCont** convective processes are an average of the **MJO** events during the phases 3 and 4 and the phases 4 and 5, as a function of the study zones considered. **MJO** index used in this study is from the National Center for Environ-

Process	Study period	Label	Number of days
Climatology of deep convective activity	All days of the DJF season from 2004 to 2017	**DJF_Clim**	1180
Pure deep convective activity not impacted by large-scale oscillations	All days of the DJF season from 2004 to 2017, excluding days during La Niña and MJO.	**DJF**	680
Large-scale oscillation: La Nina	All days of La Niña episodes whatever the season from 2004 to 2017, except the DJF season, and the days during MJO episodes.	**La Nina**	300
Large-scale oscillation: active phase of the MJO	All days of the MJO episodes in active phase over the MariCont, whatever the season from 2004 to 2017, excepted the DJF season, and the days during La Niña episodes.	**MJO active in MariCont**	222 (phases 4 and 5) 227 (phases 3 and 4)
Large-scale oscillation: suppressed phase of the MJO	From the 23 to the 30 November 2011	**MJO suppressed in MariCont**	8

Table 6.1 – Definition of the five study processes evaluated over the MariCont impacting on ice injected into the TTL.

mental Prediction analyses (NCEP, `http://www.bom.gov.au/climate/mjo/graphics/rmm.74toRealtime.txt`, last access: June 2019). The **MJO active in MariCont** studied with the Meso-NH simulation only concerns the West part of the MariCont as observed in Fig. 6.1.

The suppressed phase of the MJO is only studied from the Meso-NH simulation: labelled **MJO suppressed in MariCont**. Processes during this period will be used to be compared to processes during the **MJO active in MariCont** from the observations and from the Meso-NH simulation results (in section 6.5.2).

The number of days used in our study differs for each study period: 1180 days are used in **DJF_Clim**, 680 days in **DJF**, 300 days in **La Niña**, 222 and 227 days in the **MJO active in MariCont** considering the phases 4 – 5, and the phases 3 – 4, respectively, and 8 days simulated from Meso-NH in **MJO suppressed in MariCont**.

6.3 Diurnal cycle of Prec over the Maritime Continent: comparison between the study periods

In order to study the convective activity sensitivity as a function of the four deep convective study periods (**DJF_Clim**, **DJF**, **La Niña**, **MJO active in MariCont**) and as a function of the geographical characteristics (land, coast, mountain chains and sea) over the MariCont region, this section evaluates the diurnal cycles of Prec (previously used as a proxy a deep convection) over land (Figure 6.2) and over sea (Figure 6.3).

Over land, the diurnal cycles of Prec during **DJF**, **DJF_Clim** and **MJO active in MariCont** have similar amplitude and phase over Sulawesi and New Guinea. The diurnal cycle of Prec during **La Niña** over these two islands presents the lowest diurnal maxima of Prec. Over Borneo, Sumatra and the MariCont_L, the diurnal cycle of Prec during **MJO active in MariCont**, presents higher diurnal maxima (about + 0.1 mm h^{-1}) than diurnal cycle of Prec during **La Niña** and **DJF**. Java is the only island showing strong differences between the four deep convective study processes. Over Java, diurnal maxima of Prec during **MJO active in MariCont** and **La Niña** are lower than during **DJF** (by about -0.4 mm h^{-1}). Maxima of the diurnal cycle of Prec over Java during the **MJO active in MariCont** and **La Niña** are similar to diurnal maxima of Prec of others islands (about 0.6 mm h^{-1}). Regarding the phase of the diurnal cycle, whatever the period, the phase of the four diurnal cycles is similar for each island.

Over sea, the diurnal cycles of Prec considering the four study deep convective periods and the six study zones are similar to each other but the amplitude of the diurnal cycle of Prec varies as a function of the processes considered. The highest amplitude of the diurnal cycle of Prec are found for **DJF** or **MJO active in MariCont** as a function of the study zone considered. Over Bismark Sea and

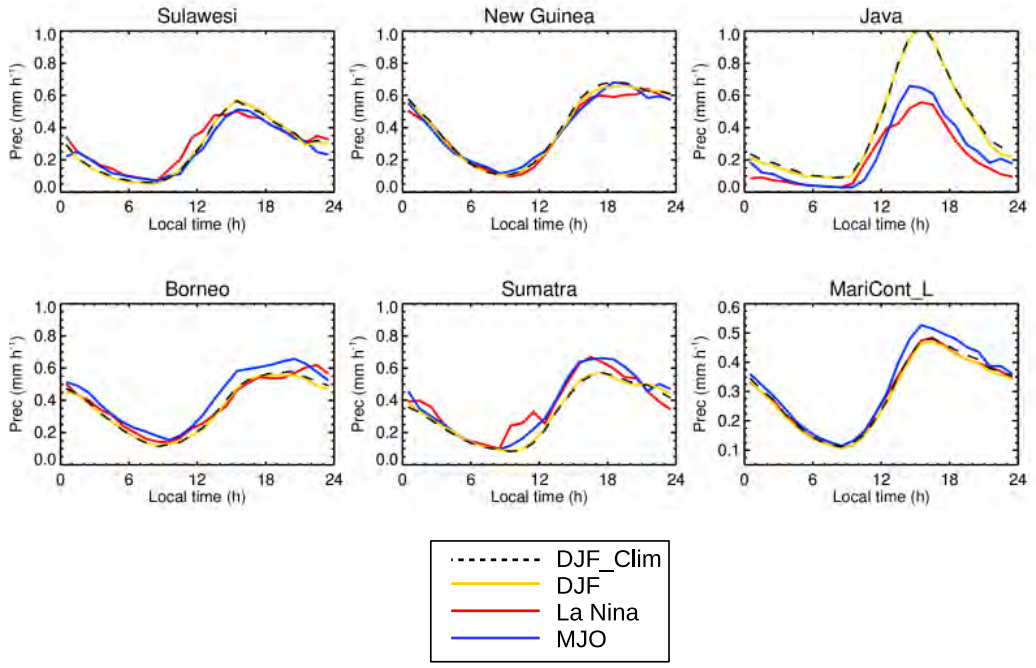

Figure 6.2 – Diurnal cycles of Prec over MariCont island study zones, during **DJF**, **DJF_Clim**, **MJO active in MariCont** and **La Niña** (2004-2017). 2-h running averages.

the MariCont_O, the diurnal cycles of Prec during the **MJO active in MariCont** shows the strongest concentration of Prec (about 0.1 – 0.2 mm h^{-1} higher than during **DJF** or **La Niña**). Java Sea and North Australia Sea present the two lowest amplitude of the diurnal cycle of Prec during the **MJO active in MariCont** and **La Niña** (about 0.1 – 0.2 mm h^{-1} lower than during the **DJF** and **DJF_Clim**). During **DJF** and **DJF_Clim**, the amplitude of the diurnal cycle of Prec over Java Sea and China Sea is the strongest with a peak-to-peak between 0.2 to 0.6 mm h^{-1} over China Sea and between 0.3 to 0.7 mm h^{-1} over Java Sea compared to a peak-to-peak between $\sim$ 0.4 and 0.5 mm h^{-1} over Bismark Sea and West Sumatra Sea.

To sum up, over land, the diurnal cycle of Prec is weakly impacted by the

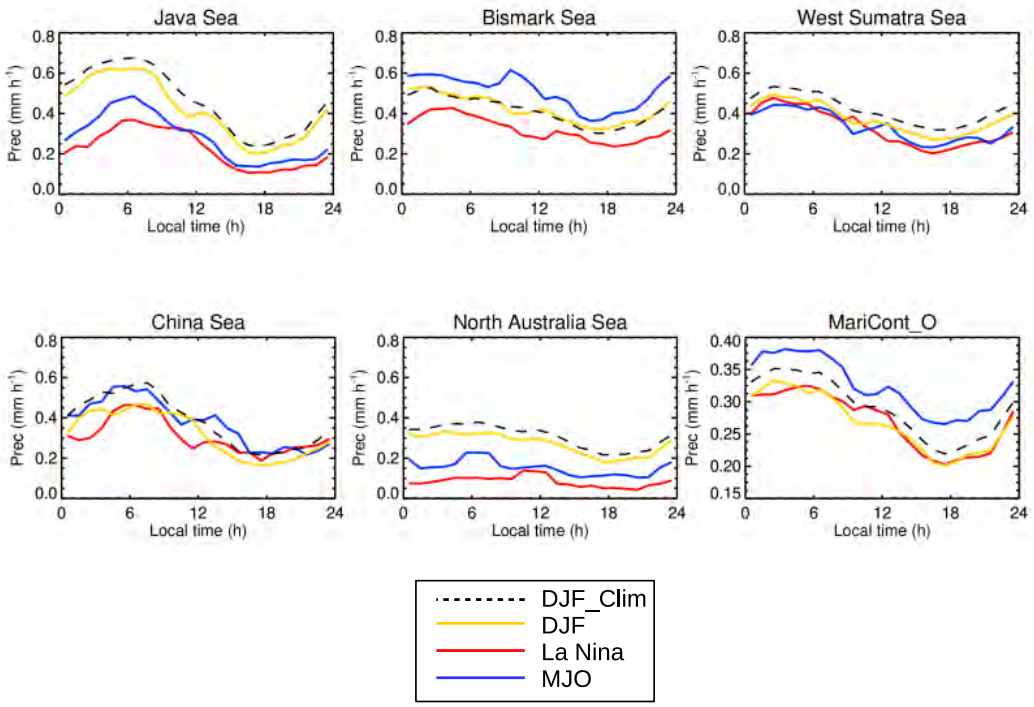

Figure 6.3 – Diurnal cycles of Prec over MariCont sea study zones, during **DJF**, **DJF_Clim**, **MJO active in MariCont** and **La Niña** (2004-2017). 2-h running averages.

large-scale oscillations compared to the diurnal cycle of Prec during pure deep convective activity (**DJF**), except over Java island. Over sea, the diurnal cycle of Prec during **La Niña** is always lower than the diurnal cycle of Prec during **DJF**, **DJF_Clim** and **MJO active in MariCont**, while the diurnal cycle of Prec during **MJO active in MariCont** is composed by the largest values of Prec over the MariCont_O (larger by 0.5 to 1.0 mm h^{-1} than for the other study processes).

6.4 Horizontal distribution of Prec and IWC^{MLS} measured at 01:30 LT and 13:30 LT

6.4.1 Prec during the increasing phase of the convection

Since IWC^{MLS} are measured at 01:30 LT and 13:30 LT, the calculation of the amount of ice injected (ΔIWC^{Prec}) up to the UT and the TL from the method presented in Dion et al. (2019) needs to consider Prec in time coincidence with MLS observations during the increasing phase of the deep convection. Figure 6.4 shows Prec from TRMM at 01:30 LT and 13:30 LT selected during the increasing phase of the convection for **DJF_Clim**, **DJF**, **La Niña** and **MJO active in MariCont**.

At 01:30 LT, pixels where Prec are in the increasing phase of the convection are mainly found over sea. In **DJF_Clim** and **DJF**, Prec are between 0.40 and 0.75 mm h^{-1} on average. Over coastal areas, Prec reach the highest values around 0.75 mm h^{-1}. During **La Niña** and **MJO active in MariCont**, a North-South gradient is observed with higher values (greater than 0.50 mm h^{-1}) in the North than in the South because of the impact of the boreal convective season (JJA) included in **La Niña** and the **MJO active in MariCont** periods. We will verify in section 6.4.2 whether this North-South gradient is also present in the IWC measurements.

At 13:30 LT, pixels where Prec are in the increasing phase of the convection are mainly found over land. In **DJF_Clim** and **DJF**, Prec are lower than 0.35 mm h^{-1} over land, except over Java and coastal pixels and south of Borneo where Prec reach $\sim$ 0.50 mm h^{-1}. During **MJO active in MariCont** and **La Niña**, Prec can reach 0.50 mm h^{-1} over land and 0.75 mm h^{-1} over sea. The impact of the boreal convective season of JJA is also observed at 13:30 LT over land and sea during the **MJO active in MariCont** and **La Niña** in the northern hemisphere.

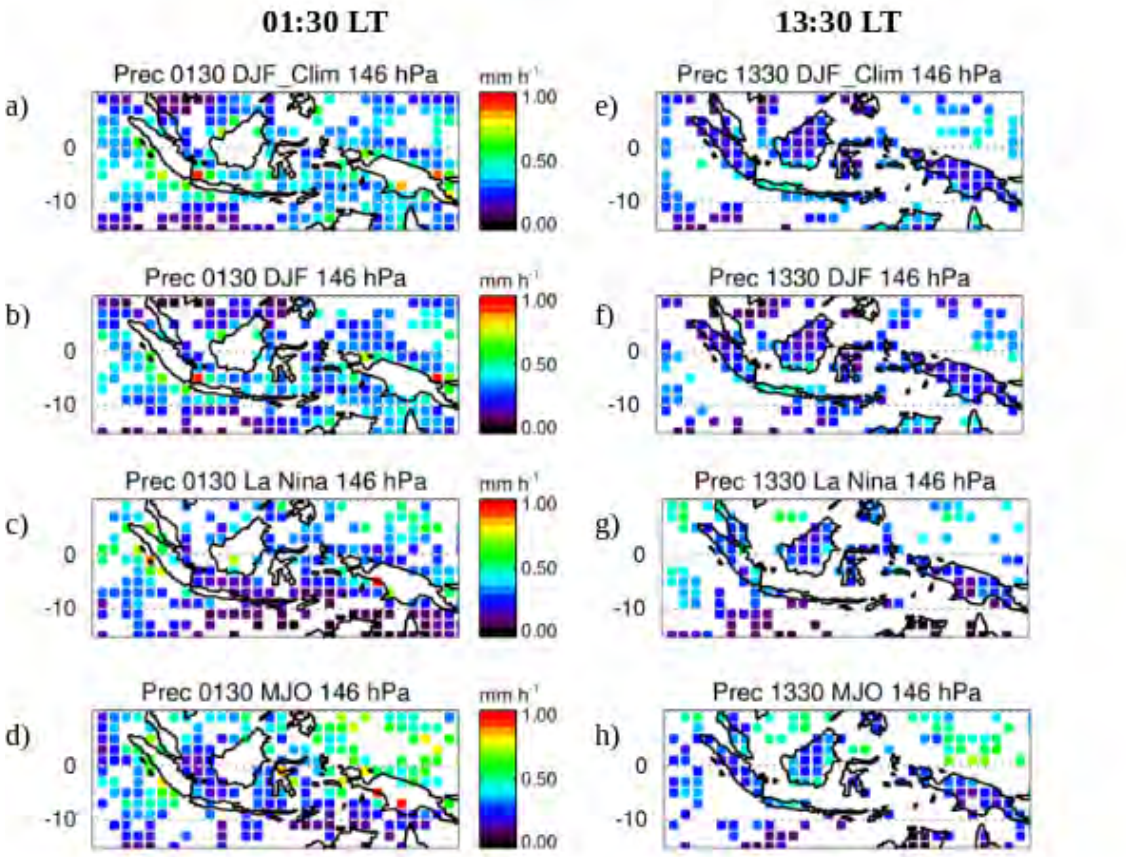

Figure 6.4 – Prec at 0130 LT (left) and at 1330 LT (right) over pixels where 0130 LT and 1330 LT are respectively during the increasing phase of the convection, for (a) **DJF_Clim**, (b) **DJF**, (c) **La Niña**, and (d) **MJO active in MariCont**, averaged over the period 2004-2017.

6.4.2 IWC^{MLS} in the UT during the increasing phase of the convection

In order to estimate ΔIWC^{Prec}, only IWC^{MLS} measured by MLS during the increasing phase of the convection are used in the model developed in Dion et al. (2019). Figure 6.5 shows IWC^{MLS} at 01:30 LT and 13:30 LT over pixels when the deep convective activity is in the increasing phase at 01:30 LT and 13:30 LT, respectively for **DJF_Clim**, **DJF**, **La Niña** and **MJO active in MariCont**.

At 01:30 LT, IWC^{MLS} in the increasing phase of the convection are, as for Prec, mainly found over sea. During **DJF_Clim** and **DJF**, IWC^{MLS} in coastal regions can reach high values of $\sim$ 5.0 mg m^{-3} (Java Sea, North Australia Sea, Bismark Sea, and China Sea) with a number of pixels reaching 5.0 mg m^{-3} higher in **DJF_Clim** than in **DJF**. During **La Niña**, while the diurnal cycle of Prec has not shown particularly low values of Prec over sea (Fig. 6.4), IWC^{MLS} values at 01:30 LT are very low (lower than 0.75 mg m^{-3}). Thus, Prec observed at 01:30 LT over seas would not inject ice up to 146 hPa, except in very local areas near the coasts. During the **MJO active in MariCont**, the number of pixels available is significantly reduced and no conclusion can be drawn.

At 13:30 LT, pixels where IWC^{MLS} in the increasing phase of the convection are, as for Prec, mainly found over land. During **DJF_Clim**, IWC^{MLS} over South of Sumatra, Java, south coast of Borneo, North of Australia and North and South coastal part of New Guinea reach 5.0 mg m^{-3} per pixel. Over islands and seas, IWC^{MLS} is between 1.0 and 3.0 mg.m^{-3} per pixel, except the sea north of the New Guinea where there are many islands. In general, over the Maricont, for **DJF_Clim**, **DJF** and **La Niña**, IWC^{MLS} at 13:30 LT are consistent to each other.

To sum up, at 01:30 LT and 13:30 LT during the increasing phase of the convection, it has been shown low differences in the horizontal distribution of Prec between each study period. Only the impact of the JJA convective period during **La Niña** and the **MJO active in MariCont** has been highlighted in the Prec observations but not present in the IWC^{MLS} horizontal distribution. Strong differences in IWC^{MLS} horizontal distribution have been observed at 01:30 LT over sea for **La Niña**, with very low values of IWC^{MLS} compared to the other study processes, but have not been observed in the Prec horizontal distribution at 01:30 LT for **La Niña**.

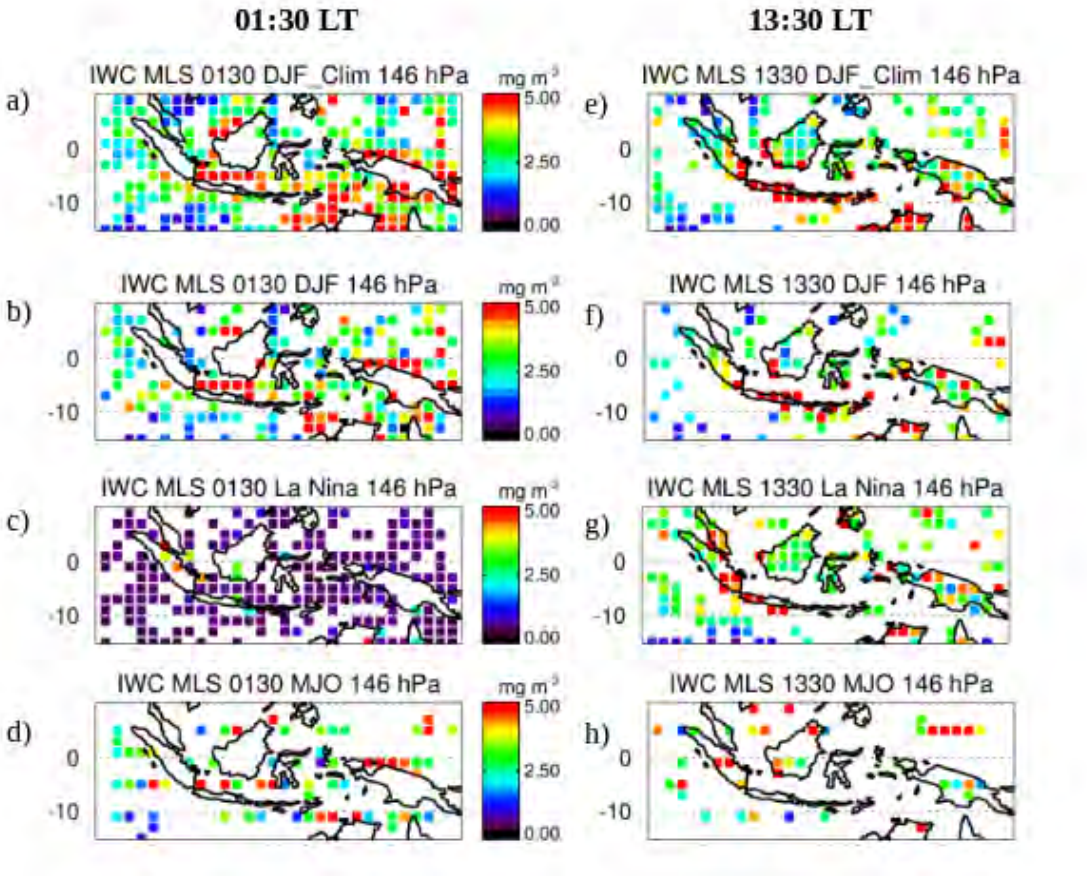

Figure 6.5 – IWC^{MLS} at 0130 LT (left) and at 1330 LT (right) over pixels where 0130 LT and 1330 LT are respectively during the increasing phase of the convection, for (a) **DJF_Clim**, (b) **DJF**, (c) **La Niña**, and (d) **MJO active in MariCont**, averaged over the period 2004-2017.

6.5 ΔIWC injected in the UT during DJF, MJO active in MariCont and La Niña

In this section, we estimate ΔIWC from Prec measured by TRMM and IWC^{MLS} (ΔIWC^{Prec}) and from MRI simulated from Meso-NH ($\Delta IWC^{Meso-NH}$).

6.5.1 Horizontal distribution of ΔIWC^{Prec}

ΔIWC^{Prec} at 146 hPa (UT) over the MariCont for **DJF_Clim**, **DJF**, **La Niña** and **MJO active in MariCont** processes are shown in Figure 6.6a, b, c and d, respectively. During the **DJF_Clim** period, as it as been shown in Chapter 5, ΔIWC^{Prec} reaches large values between 10 and 20 mg m^{-3} per pixel, over land pixels. During **DJF**, ΔIWC^{Prec} reaches values between 10 and 20 mg m^{-3} per pixel over land and also over sea (as in China Sea and Bismark Sea). During **La Niña**, ΔIWC^{Prec} reaches values larger than 17 mg m^{-3} per pixel over almost all the land pixels while, over sea pixels, ΔIWC^{Prec} is negligible (< 0.1 mg m^{-3}). During the **MJO active in MariCont**, less pixels are available than for the other study processes. Over land pixels, ΔIWC^{Prec} is between 10 and 20 mg m^{-3} while, over sea pixels ΔIWC^{Prec} is lower than 10 mg m^{-3}, except over North Australia Sea, Java Sea, China Sea, and Bismark Sea where ΔIWC^{Prec} reaches values between 10 and 20 mg m^{-3}.

Differences in ΔIWC^{Prec} between **DJF** and **DJF_Clim**, **La Niña** and **DJF** and between **MJO active in MariCont** and **DJF** are presented in Fig. 6.6e, f and g, respectively, in order to compare the impact of the large-scale oscillations on ΔIWC^{Prec} to the impact of the austral convective activity on ΔIWC^{Prec} for **DJF**. Firstly, the differences between ΔIWC^{Prec} for **DJF** and for **DJF_Clim** highlight the impact of the large-scale processes during the **DJF** season. Fig.6.6e shows larger ΔIWC^{Prec} for **DJF_Clim** than for **DJF** over sea (reaching 4 mg m^{-3} of differences), excepted over North Australia Sea where ΔIWC^{Prec} for **DJF_Clim** is lower by about 4 mg m^{-3} than ΔIWC^{Prec} for **DJF**. **La Niña** and the **MJO active in MariCont** processes during the **DJF** season tend to decrease the ΔIWC^{Prec} values, except over North Australia Sea, and Arafura Sea where **La Niña** and the **MJO active in MariCont** processes force ΔIWC^{Prec} to increase during **DJF**. Secondly, differences between ΔIWC^{Prec} for **La Niña** and for **DJF** highlight the

impact of the large-scale **La Niña** processes on ΔIWC^{Prec} compared to the austral deep convective activity of **DJF**. Fig. 6.6f shows that **La Niña** oscillation tends to reduce ΔIWC^{Prec} over sea and to increase ΔIWC^{Prec} over land compared to the **DJF** season (by about $\sim$ 4 mg m^{-3}). Differences between ΔIWC^{Prec} for the **MJO active in MariCont** and for **DJF** highlight the impact of the large-scale **MJO active in MariCont** processes on ΔIWC^{Prec} compared to the austral deep convective activity during **DJF**. Fig. 6.6g shows that the **MJO active in MariCont** processes tend to increase the ΔIWC^{Prec} in the UT over land and sea of the Maricont, compared to deep convection on the **DJF** season.

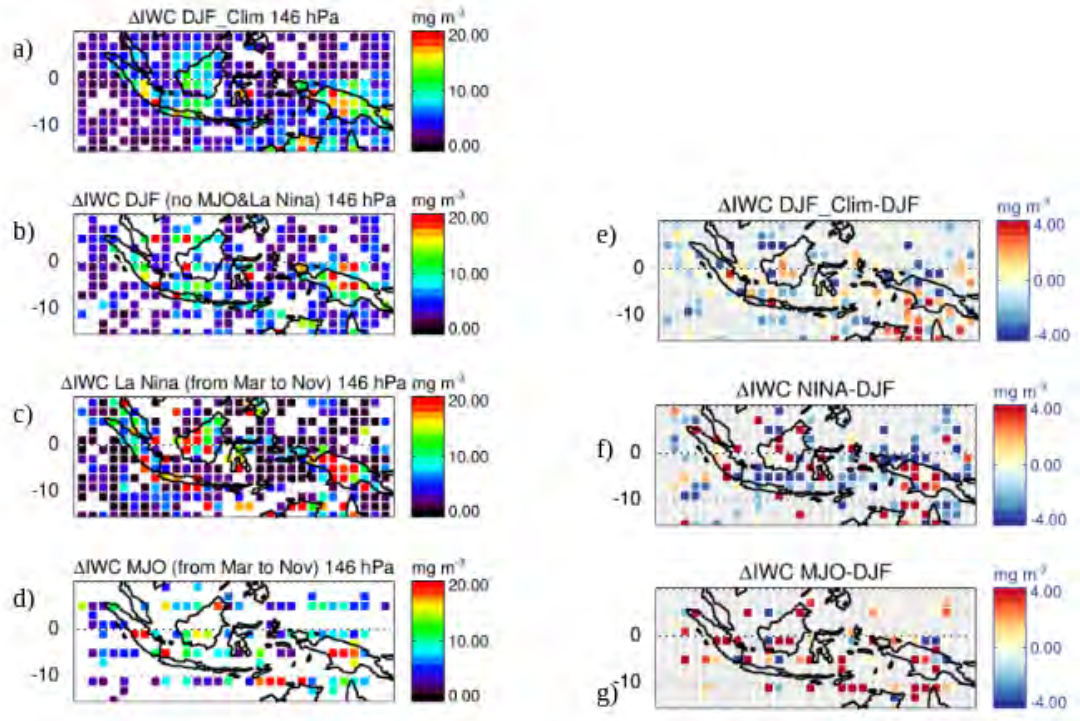

Figure 6.6 – ΔIWC^{Prec} during (a) **DJF_Clim**, (b) **DJF** (c) **La Niña**, and (d) **MJO active in MariCont**, and the difference between ΔIWC^{Prec} during **DJF_Clim** and **DJF** (e), between **La Niña** and **DJF** (f) and between **MJO active in MariCont** and **DJF** (g), averaged over the period 2004-2017. White means no data in ą b, c and d and grey means no data in e, f and g.

The study of ΔIWC^{Prec} at 2° × 2° horizontal resolution during the four study deep convective periods is limited because of the low number of pixel available. In order to quantify the amount of ice injected into the TTL over different regions (land and sea) and to consider different processes (**DJF_Clim**, **DJF La Niña** and **MJO active in MariCont**), we calculate ΔIWC^{Prec} on island and sea study zones in subsection 6.5.2 and 6.5.3.

6.5.2 ΔIWC during MJO over island and sea of the MariCont

In this section, MRI at 146 hPa from Meso-NH ($IWC^{Meso-NH}$) over 8 days of **MJO active in MariCont** and **MJO suppressed in MariCont** (as defined in Figure 6.1) are compared to each other and to the climatology of IWC^{MLS} during 13 years of **MJO active in MariCont**.

Figure 6.7 illustrates the daily mean of $IWC^{Meso-NH}$ at 146 hPa over the simulation zone, averaged from 23 to 30 November 2011. This Figure can be compared with Fig. 5.2 showing the daily mean of IWC^{MLS} at 146 hPa and with Fig. 5.10 showing the daily mean IWC^{ERA5} at 146 hPa (Chapter 5). In Fig. 6.7, larger daily mean values are shown over the coasts in West of Sumatra, South of Borneo and North of Australia and over the New Guinea mountain chain while, in Fig. 5.10, larger daily mean values have been shown mainly over land. Furthermore, in Fig. 6.7, larger daily mean of $IWC^{Meso-NH}$ can be observed over the Indian Ocean ($\sim$ 70° – 90°) than over the Maricont region (90° – 150°). These results are consitent with the study of Kuznetsova et al. (2019) showing that the MJO episodes during the simulated period is in active phase over the Indian Ocean and West of MariCont and in suppressed phase over the East of MariCont, producing a drying of the lower to middle troposphere (shown previously in Fig. 6.1).

Diurnal cycle of $IWC^{Meso-NH}$ is provided with one hour temporal resolution. Thus, $IWC^{Meso-NH}$ is used to estimate ΔIWC at 146 hPa ($\Delta IWC^{Meso-NH}$) from

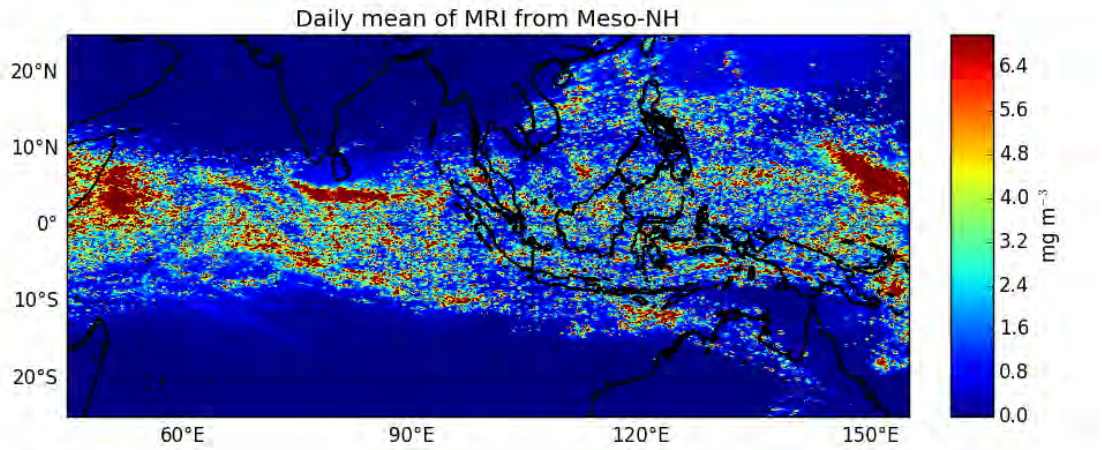

Figure 6.7 – Daily mean of $IWC^{Meso-NH}$ (MRI) at 146 hPa, 23 to 30 November 2011

the method proposed in Dion et al. (2019), over the island and sea study zones. $\Delta IWC^{Meso-NH}$ is shown in Figure 6.8 and compared to ΔIWC^{Prec} for the four study deep convective processes over the land and sea study zones.

Over West study zones (Sumatra, West Sumatra Sean and Java Sea), $\Delta IWC^{Meso-NH}$ and ΔIWC^{Prec} present very similar within 0.5 mg m^{-3} of differences. This result show similar values ΔIWC of during the **MJO active in MariCont** periods. In contrast, over East part of the MariCont (New Guinea, North Australia Sea, Bismark Sea), $\Delta IWC^{Meso-NH}$ is always lower than ΔIWC^{Prec} within about 2 mg m^{-3}. This result highlighting the impact of the MJO suppressed in MariCont over the MariCont with dry convective processes compared to the **MJO active in Maricont** with wet deep convective processes. Furthermore, $\Delta IWC^{Meso-NH}$ follows the same evolution over island and sea than all of ΔIWC^{Prec} study processes (**DJF_Clim**, **DJF**, **La Niña** and **MJO active in MariCont**), with differences less than 1.0 mg m^{-3}, except over New Guinea and over

North Australia Sea where $\Delta IWC^{Meso-NH}$ are lower than all the ΔIWC^{Prec} study processes by more than 2 mg m^{-3}.

6.5.3 ΔIWC^{Prec} during the study periods over island and sea of the MariCont

In this section, ΔIWC^{Prec} estimated for the four study deep convective processes on island and sea study zones are presented in Figure 6.8. Results from Chapter 5 have been added to Fig. 6.8 as references on ΔIWC for **DJF_Clim**. Numbers of pixel per study zone considered on the calculation of ΔIWC^{Prec} is detailed Table 6.2.

Number of pixels used per zone in the calculation of ΔIWC

	MCO	Sum	Bor	Java	Sul	NG	MCO	WSS	ChinS	JS	NAS	BS
DJF_Clim	86	9	19	4	8	18	323	27	19	15	32	14
DJF	53	8	11	4	4	13	257	17	4	15	23	11
La Nina	85	9	4	4	8	18	323	25	11	15	32	14
MJO active in MariCont	20	4	6	1	0	5	127	7	3	8	4	9
MJO suppressed in MariCont	86	9	19	4	8	18	323	27	19	15	32	14

Table 6.2 – Number of pixels of 2° × 2° used per study zone in the calculation of ΔIWC estimated from space-borne observations.

For **DJF_Clim**, as observed in Chapter 5, Java presents the largest value of ΔIWC^{Prec} (reaching 9 mg m^{-3}) compared to other islands and seas (between 4 and 7 mg m^{-3}). ΔIWC^{Prec} for **DJF** is consistent to within 0.5 mg m^{-3} with the observational range of ΔIWC established from Prec and Flash over mainly islands and seas. Although the number of pixels considered per zones and per study processes is different, ΔIWC^{Prec} estimated for the four study deep convective processes is about 1 mg m^{-3} except over Sulawesi. Thus, the impact of **La Niña**

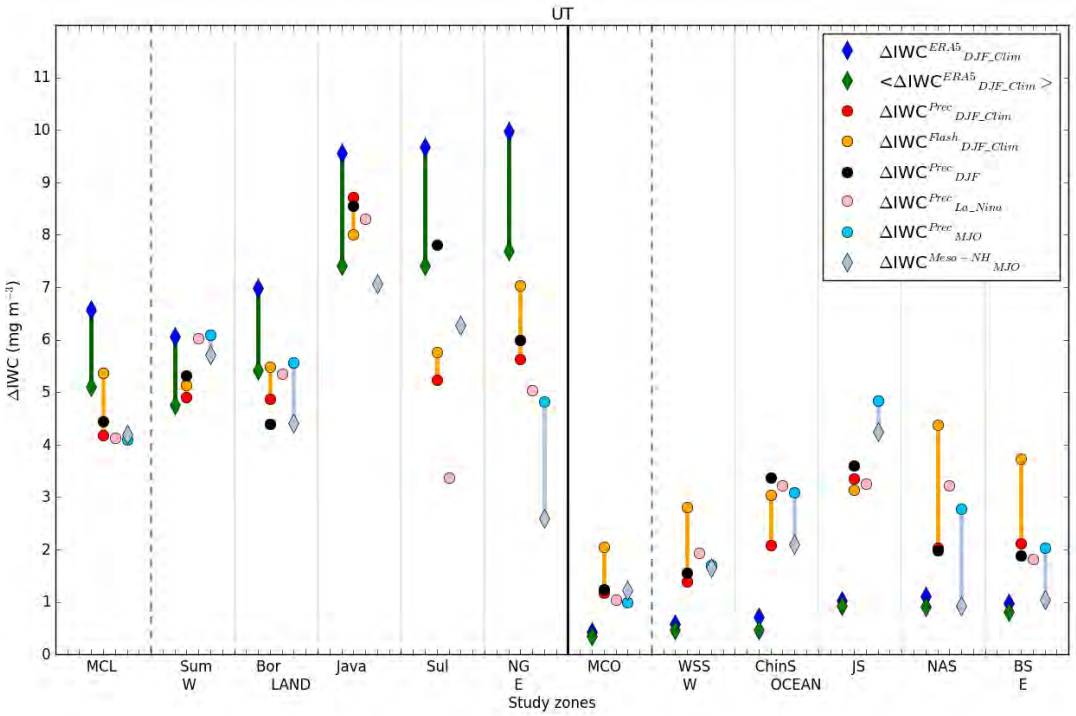

Figure 6.8 – ΔIWC^{Prec} at 146 hPa during **DJF_Clim**, **DJF**, **MJO active in MariCont** and **La Niña** at 146 hPa, ΔIWC^{Flash} at 146 hPa during **DJF_Clim**, ΔIWC^{ERA5} and $\left\langle \Delta IWC_{150}^{ERA5} \right\rangle$ at 150 hPa during **DJF_Clim**, and ΔIWC$^{Meso-NH}$ at 146 hPa during the **MJO suppressed in MariCont** episode from 23 to 30 november of 2011, in mg m^{-3}, over islands and seas of the MariCont: MariCont_L (MCL) and MariCont_O (MCO); from West (W) to East (E) over land, Sumatra (Sum), Borneo (Bor), Java, Sulawesi (Sul) and New Guinea (NG); and over seas, West Sumatra Coast (WSS), China Sea (ChinS), Java Sea (JS), North Australia Sea (NAS) and Bismark Sea (BS). To facilitate the reading, ΔIWC^{Prec} and ΔIWC^{Flash} for **DJF_Clim** are compared to ΔIWC^{Prec} for **DJF** over the same x-axis coordinates, as well as ΔIWC$^{Meso-NH}$ for the **MJO suppressed in MariCont**and ΔIWC^{Prec} for the **MJO active in MariCont** processes. Observational results are represented by a circle and model results are represented by a diamond.

and the **MJO active in MariCont** on the convective processes in **DJF** is negligeable at the horizontal scale of island and sea. Furthermore, Java island shows also the largest amount of ΔIWC^{Prec} for **La Niña** over land. ΔIWC estimated

for the four study deep convective processes present the similar variabilities for island and sea. The exceptions are over Java Sea, China Sea and North Australia Sea, where ΔIWC^{Prec} for **La Niña** show very similar values ($\sim$ 3 mg m^{-3}) while ΔIWC^{Prec} for the **MJO active in MariCont** vary within 1 mg m^{-1} between this three study zones. Furthermore, the Sulawesi island is the only study zone where **La Niña** convective processes decrease ΔIWC^{Prec} values by about 2 mg m^{-3}.

6.6 Synthesis and discussion

Several points are summarised in this section.

Firstly, the phase of the diurnal cycle of Prec is the same whatever the deep convective processes considered (**DJF_Clim, DJF, MJO active in MariCont and La Niña**), while the amplitude can change as a function of the local study zones, especially over sea or over Java island and sea.

Secondly, while Prec measured at 01:30 LT and 13:30 LT during the growing phase of the convection is consistent whatever the study processes considered, the IWC^{MLS} measured at 01:30 LT and 13:30 LT show large differences in **La Niña** at 01:30 LT over sea, compared to the other study processes (with IWC^{MLS} lower than 0.75 mg m^{-3} in **La Niña** and IWC^{MLS} between 1.5 to 5 mg m^{-3} during the other study processes).

Thirdly, the amount of ice injected up to the UT and estimated from Prec (ΔIWC^{Prec}) has been evaluated at 2° $\times$ 2° horizontal resolution. During **La Niña**, over land, ΔIWC^{Prec} has shown a larger number of pixel (almost all the land areas) reaching the strongest ΔIWC^{Prec} values (5 mg m^{-3}) compared to the other study periods. However, during **La Niña**, over sea, ΔIWC^{Prec} is less than for the **DJF** season.

Finally, ΔIWC has been calculated over the land and sea study zones as a

function of several convective conditions. Whatever the convective study processes considered, the differences in the ΔIWC^{Prec} calculated have been found in a range lower than 1 mg m^{-3}, excepted over Sulawesi where ΔIWC^{Prec} calculated for **La Niña** is lower by 2 mg m^{-3} than ΔIWC^{Prec} for **DJF_Clim** and by 4.5 mg m^{-3} than ΔIWC^{Prec} for the **DJF**, highlighting the strong impact of the **La Niña** processes over the Sulawesi island, especially during **DJF**. Excepted for Sulawesi, the low differences between the four study convective processes may be explained by the impact of the JJA boreal summer convective season included into **La Niña** and **MJO active in MariCont** study processes (particularly over study zones in the Northern hemisphere, such as Sumatra, China Sea and Borneo).

The comparison between **DJF_Clim** and **DJF** has highlighted the impact of **La Niña** and **MJO active in MariCont** during the **DJF** season. At the $2^\circ \times 2^\circ$ horizontal resolution, our study has shown that **La Niña** and the **MJO active in MariCont** tend to decrease ΔIWC^{Prec} values during **DJF** over sea pixels and tend to increase ΔIWC^{Prec} within 4 mg m^{-3} per pixel over some pixels near the North Australia coast and sea, Borneo and Java. This impact is harder to observe over the land and sea study zones, showing lower differences (within 1 mg m^{-3}) because of the larger area considered (including up to 32 pixels).

The study of **La Niña** convective processes at $2^\circ \times 2^\circ$ horizontal resolution has shown that **La Niña** convective processes tend to increase ΔIWC^{Prec} over land but decrease ΔIWC^{Prec} over sea compared to the **DJF** deep convective processes. This impact is not observed in the calculation of ΔIWC^{Prec} at larger horizontal scale over land and sea study zones.

The study of the MJO convective processes has firstly shown that ΔIWC^{Prec} impacted by **MJO active in MariCont** convective processes at $2^\circ \times 2^\circ$ horizontal resolution increases within 4 mg m^{-3} per pixels compared to ΔIWC^{Prec} impacted by the **DJF** deep convection. Secondly, ΔIWC^{Prec} during active phase of the MJO

has also been compared to $\Delta IWC^{Meso-NH}$ estimated from the simulation of MRI during 8 days during **MJO active in MariCont** and **MJO suppressed in MariCont** periods over different study zones. ΔIWC estimated from observations and from the Meso-NH simulation during active phases of the MJO have shown similar value within 0.5 mg m^{-3}. In contrast, the comparison between ΔIWC^{Prec} during the **MJO active in MariCont** and $\Delta IWC^{Meso-NH}$ during a **MJO suppressed in MariCont** has highlighted the impact of the dry convective processes during the **MJO suppressed in MariCont**, reducing ΔIWC within 2 mg m^{-3} compared to the wet convective processes during the **MJO active in MariCont**.

6.7 *Acknowledgement*

We thank the National Center for Scientific Research (CNRS) and the Excellence Initiative (Idex) of Toulouse, France to fund this study and the project called Turbulence Effects on Active Species in Atmosphere (TEASAO – http://www.legos.obs-mip.fr/projets/axes-transverses-processus/teasao, Peter Haynes Chair of Attractivy). We would like to thank the teams that have provided the MLS data (https://disc.gsfc.nasa.gov/datasets/ML2IWC_V004, last access: June 2019), the TRMM data (https://pmm.nasa.gov/data-access/downloads/trmm), the LIS data (https://ghrc.nsstc.nasa.gov/lightning/data/data_lis_trmm.html, last access: June 2019), the ERA5 Reanalysis data (https://cds.climate.copernicus.eu/cdsapp/dataset/reanalysis-era5, last access: June 2019), and Meso-NH simulations (provided by J.P. Chaboureau from the Laboratoire d'Aerologie, Toulouse)

Chapter 7

Further works: Application of the methodology to the Asian monsoon region

The methodology developed in this thesis to estimate the amount of ice injected in the TTL has been applied to the Asian area where it is known that the Asian monsoon and its associated anticyclone are efficient meteorological processes to transport air masses from the surface to the UTLS (Randel et al., 2010). The study has been performed within a Master 2 intership by C. Dallet under the supervision of P. Ricaud and myself. All the Figures presented in this chapter are taken from the Master 2 internship report of C. Dallet. The interpretations and analysis of the study composing this chapter has been done by myself, in collaboration with P. Ricaud and C. Dallet.

7.1 Introduction

The Asian monsoon is a large-scale meteorological phenomenon appearing yearly over the Asian continent and playing an important role in the climate and circulation in the Northern Hemisphere. It is characterized by persistent deep convection reaching the UT and even the LS, followed by a strong anticyclonic circulation (Hoskins and Rodwell, 1995; Gettelman et al., 2004b) in the UT. Different studies focusing on the tropopause hydration and on the UT to LS exchanges have shown important concentration of WV in the UTLS over Asia during the Asian monsoon period in JJA (Gettelman et al., 2004b; Park et al., 2007; James et al., 2008; Randel et al., 2010; Su et al., 2011). The recent Strato-Clim campaign has provided airborne measurements over the Asian monsoon area in order to produce more reliable projections of climate change and stratospheric ozone by improving the understanding of key processes in the UT and Stratosphere. Based on the Strato-Clim campaign, Lee et al. (2018) have shown the strong effect of the overshoot on the moistening LS. Tissier and Legras (2016) have also shown that the overshoot processes can be fast enough to sublimate ice into water vapour when crossing the cold point. However, while the impact of the deep convection combined with the Asian monsoon anticyclone (AMA) on the tropopause humidity has been intensively studied, quantifying the amount of ice injected up to the tropopause by deep convection during the Asian monsoon remains challenging because various processes are involved (dynamical, physical and radiative).

The method developed in this thesis and in Dion et al. (2019) has been then used to quantify the amount of ice injected up to the UT over the Asian continent during the Asian monsoon period. These quantities will be compared to the amount of ice injected into the tropopause from deep convective processes over the tropics and the MariCont during DJF (presented in previous chapters).

7.2 Instruments and methodology

The same datasets presented in Chapters 3 to 6 have been used in this study that will be briefly presented. Based on the model developed in this thesis, Prec from TRMM-3B42 averaged between 2004 and 2017 and to Flash from TRMM-LIS averaged between 2005 and 2015 are combined with IWC from MLS to estimate ΔIWC^{Prec} and ΔIWC^{Flash} over Asia. Similarly, IWC^{ERA5} provided with one hour temporal resolution from ERA5 reanalysis and averaged from 2005 to 2017, has been used to estimate ΔIWC^{ERA5} over Asia.

Because it has been shown that the impact of the Asian monsoon on the transport of WV up to the UTLS occurs during the boreal convective season (July-September according toGettelman et al. (2004b) and July-August according to Randel et al. (2006a)), the present study focuses on the three month boreal summer season of June, July and August (JJA).

7.3 Horizontal distributions of Prec, Flash and IWC over Asia

7.3.1 Horizontal distributions

The Asian study zone have been defined from 4°N to 38°N and 65°E to 125°E. One particularity of this region is the high elevation composed by the Himalaya mountains and the Tibetan Plateau (h > 5000 m above mean sea level) (Figure 7.1 top). The daily means of Prec and Flash are presented in Figure 7.1 bottom left and right respectively, with a horizontal resolution of 0.25° × 0.25°. Large Prec and Flash are found over areas of low elevations. The horizontal distribution of Prec and Flash present consistencies with maxima over the Eastern part of India, Vietnam and Southern border of Himalaya where altitudes are lower than 2500 m.

However, Prec and Flash presents inconsistencies over: 1) Pakistan where Prec is very low (< 0.1 mm day^{-1}) and Flashs reach maximum values over Asia ($\sim$ 10 flash day^{-1}), and 2) the Bay of Bengal where Prec is very high ($\sim$ 22 mm day^{-1}) and Flash is very low (< 10^{-1} flash day^{-1}).

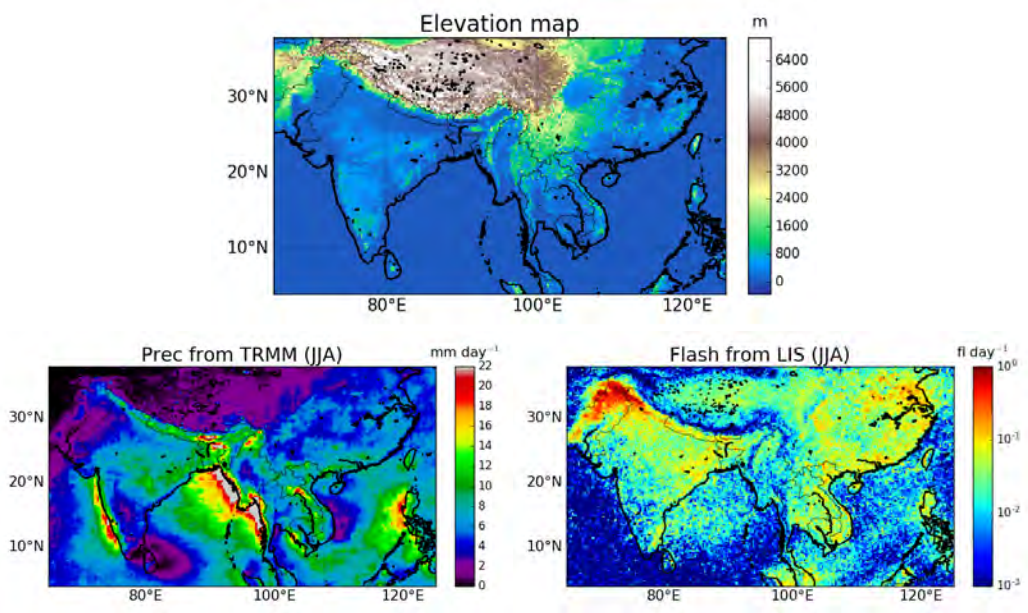

Figure 7.1 – Elevation (m) from Solar Radiation Data (SoDa) over Asia (top); daily mean of Prec (mm h^{-1}) measured by TRMM over Asia, averaged over the period of 2004-2017 (middle), daily mean of Flash (flashes per day (fl day^{-1})) measured by TRMM over Asia, averaged over the period of 2004-2015 (bottom).

The horizontal distributions of IWC^{MLS} at 146 hPa over Asia is presented at 01:30 LT and 13:30 LT in Figure 7.2. IWC^{MLS} is found larger at 13:30 LT than at 01:30 LT, mainly over Eastern India and the Bay of Bengal reaching values larger than 5 mg m^{-3}. The geopotential lines and wind direction at 150 hPa are also presented in Figure 7.2 to highlight the presence of the AMA. According to the strong daily mean of Prec observed in the Eastern Bay of Bengal, it can be suggest that the strong values of IWC at 13:30 LT observed over the Bay of Bengal can come from the transport westward of air masses following the geopotential lines

and strong winds. Indeed, if we except the North Pakistan zone, the maxima of IWC^{MLS} appear to be spatially correlated with the maxima of Prec and Flash. Furthermore, the AMA is not fully filled by ice as it is for instance by medium and long lived species as CO, O_3 or some polluted species from biomass burning (Randel et al., 2010). It might be that the lifetime of ice in the UT over this region is so short (< 12 hours) that the horizontal transport within the AMA cannot redistribute ice.

The horizontal distribution of IWC^{ERA5} over Asia is presented at 01:30 LT and 13:30 LT in Figure 7.3 left and right, respectively. First of all, at 01:30 LT, the horizontal distribution of IWC^{ERA5} is consistent with the horizontal distribution of IWC^{MLS}, with maxima in Eastern India and Bay of Bengal. At 13:30 LT, although IWC^{ERA5} and IWC^{MLS} show maxima over Eastern Indian and Bay of Bengal, IWC^{ERA5} are much larger than IWC^{MLS} over the Himalaya, Tibet, West of China (Yunnan and Sichuan China provinces) and the Myanmar (IWC^{ERA5} > 8 mg m $^{-3}$ and IWC^{MLS} < 2 mg m $^{-3}$).

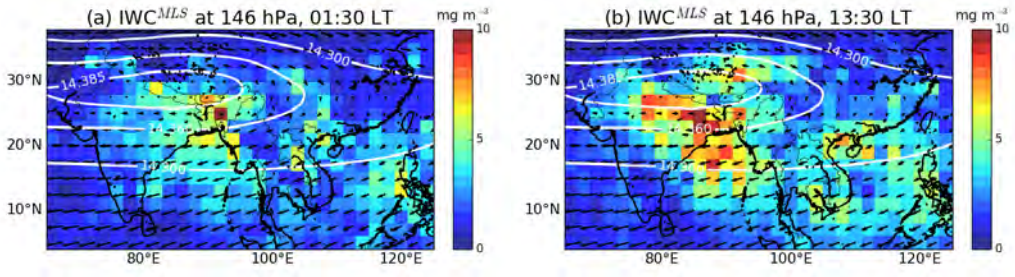

Figure 7.2 – IWC^{MLS} at 01:30 LT (left) and IWC^{MLS} at 13:30 LT (right) at 146 hPa from MLS. White contours are the geopotential height (from NOAA) dataset at 14.30 km, 14.39 km and 14.60 km at 150 hPa. Black arrows illustrate the wind direction (from NOAA dataset).

From Figures 7.1 – 7.3, eight Asian study zones have been chosen as a function of the land/ocean contrast, the topography, the convective areas defined as areas with maxima of Prec or Flash, and maxima of IWC. The study zones are presented

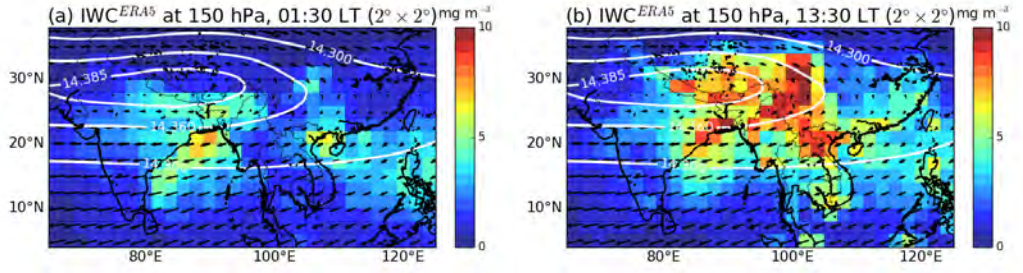

Figure 7.3 – IWC^{MLS} at 01:30 LT (left) IWC^{MLS} at 13:30 LT (right) at 150 hPa from ERA5.

in Figure 7.4 and have been chosen as follow:

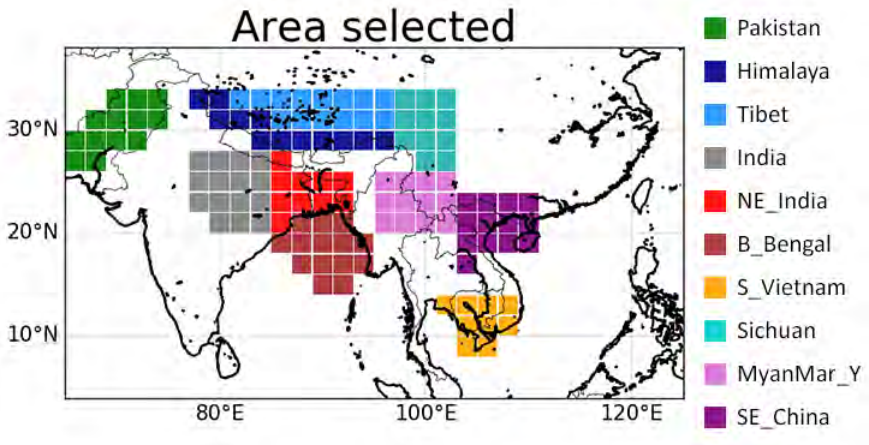

Figure 7.4 – Selected Study zones over Asia.

Pakistan: the largest daily mean of Flash (reaching 10 flashes per day). **Himalaya** and **Tibet**: the highest altitudes (higher than 4000 m) found over the Asian study zones. **India**: low altitude, high IWC at 13:30 LT and high daily mean of Flash and Prec. **NE_India**: (North East of India) the largest IWC^{MLS} values over land at 13:30 LT. **B_Bengal**: (Bay of Bengal) the largest IWC^{MLS} values over ocean at 13:30 LT and because it is one of the most intense precipitation area with more than 22 mm.day^{-1}. **S_Vietnam**: (South of Vietnam) high IWC^{ERA5} values at 13:30 LT ($\sim$ 7 mg m^{-3}) and strong Flash values ($\sim 10^{-1}$ flashes

per day). **Sichuan**: (province of China) altitude higher than 2000 m and high differences between IWC^{MLS} and IWC^{ERA5} at 13:30 LT. **Myanmar_Y**: (Myanmar and the Yunnan province of China), altitude lower than 2000 m and high differences between IWC^{MLS} and IWC^{ERA5}. **SE_China**: (South East of China) high IWC values at 01:30 LT and 13:30 LT (between 5.0 and 7.5 mg m^{-3} according to MLS and ERA5) and large Prec and Flash values ($\sim$ 10 mm h^{-1} and $\sim 10^{-1}$ flashes per day, respectively). Each study zone selected includes between 9 to 17 pixels of $2^\circ \times 2^\circ$ per zone.

7.4 Diurnal cycle of Prec and Flash over the Asian study zones

To evaluate Prec and Flash as good proxy of deep convection over Asia and during the Asian monsoon, and to better understand the impact of the convection on ΔIWC up to the UT, the diurnal cycles of Prec and Flash are compared to each other over the Asian study zones in Figure 7.5.

The diurnal cycles of Prec and Flash present similar duration of their increasing phase over NE_India, India, Sichuan, Myanmar_Y, Pakistan, Tibet, Himalaya, SE_China, and Vietnam ($\sim$ 6 hours) but differences over B_Bengal, the only one ocean study zone ($\sim$ 10 hours for Flash and $\sim$ 15 hours for Prec). While B_Bengal shows the largest diurnal maximum of Prec (reaching 0.9 mm day^{-1}) compared to all the other study zones ($\sim$ 0.5 mm day^{-1} on average), the diurnal maximum of Flash over B_Bengal is the lowest (lower than 0.5 10^{-3} Flash day^{-1}) compared to all the other study zones ($\sim$ 6 10^{-3} Flash day^{-1} on average). Conversely, the Pakistan study zone shows the largest diurnal maxima of Flash with strong Flash during the all night and in early morning (reaching 11 10^{-3} Flash per day), while Prec over this study zone are very low (lower than 0.1 mm h^{-1}) all over the diurnal cycle

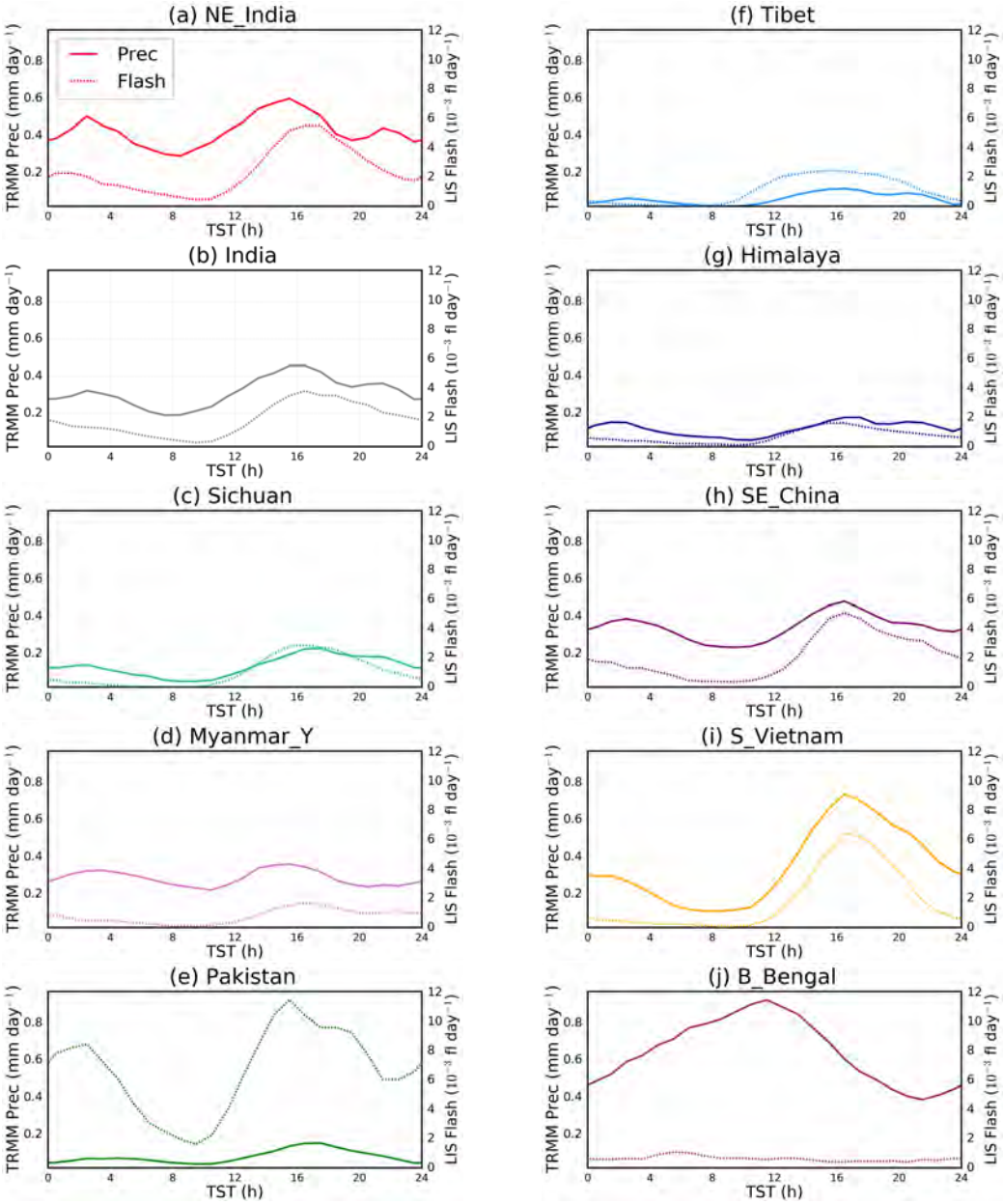

Figure 7.5 – Diurnal cycle of Prec (solid line), diurnal cycle of Flash (dashed line), over Asian region: (a) North East India (NE_India), (b) India, (c) Sichuan, (d) Myanmar and Yunnan provinces (Myanmar_Y), (e) Pakistan, (f) Tibet, (g) Himalaya, (h) South East China (SE_China), (i) South Vietnam (S_Vietnam), (j) Bay of Bengal (B_Bengal).

of Prec. High altitude areas such as Tibet, Himalaya, Myanmar_Y and Sichuan presents low diurnal maxima of Prec and Flash ($\sim$ 0.2 mm day^{-1} and $\sim$ 2 flash day^{-1}, respectively) compared to other areas.

Note that it can be observed that Prec diurnal cycles present one main maximum during the afternoon and one or two secondary maxima during the evening and the morning. This secondary maximum was not observed over South America, South Africa nor MariCont lands in previous studies (Chapter 4 to 6), while the diurnal cycle of Flash shows only one the diurnal maximum during the afternoon.

To sum up, our study over Asia reveal i) large amounts of Flash not associated to high Prec not high IWC over Pakistan, probably associated to "dry" convection not transporting ice up to the UTLS, ii) high Prec combined with almost no Flash but high IWC at 01:30 LT and 13:30 LT, found over the only one ocean study zone of the B_Bengal, iii) low Prec and Flash over high altitudes study zones, probably associated to weak convective processes transporting low amount of ice up to the UTLS and iv) consistencies in the increasing phase of Prec and Flash over the land study zones with low elevations (NE_India, India, Pakistan, S_Vietnam and SE_China). Over these areas, both Prec and Flash can be used as proxy of deep convection.

7.5 Diurnal cycle of IWC over the Asian study zones

The diurnal cycles of IWC^{Prec} and IWC^{Flash} are estimated from the model proposed by Dion et al. (2019) and compared to the diurnal cycle of IWC^{ERA5} and to the two daily IWC^{MLS} MLS measurements over each study zone (Figure 7.6).

Over NE_India, India, SE_China and S_Vietnam, maxima of IWC^{Flash} are found larger than that of IWC^{Prec} and that of IWC^{ERA5} by about 4 mg m^{-3}. How-

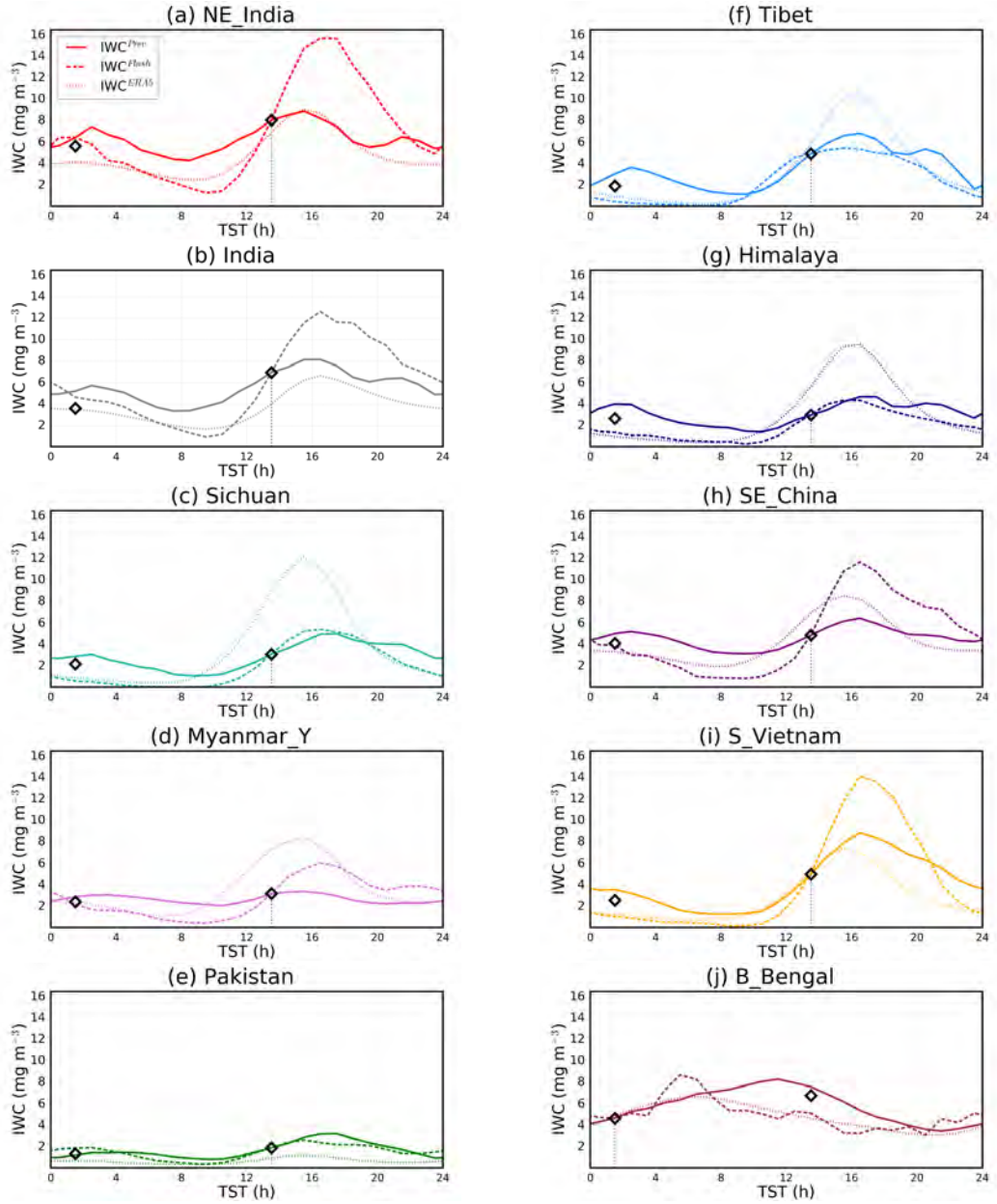

Figure 7.6 – Diurnal cycle of IWC^{Prec} (solid line), diurnal cycle of IWC^{Flash} (dashed line), diurnal cycle of IWC^{ERA5} from ERA5 at 150 hPa (dotted line) and the two daily IWC measurements from MLS (diamond) over Asian region: (a) North East India (NE_India), (b) India, (c) Sichuan, (d) Myanmar and Yunnan provinces (Myanmar_Y), (e) Pakistan, (f) Tibet, (g) Himalaya, (h) South East China (SE_China), (i) South Vietnam (S_Vietnam), (j) Bay of Bengal (B_Bengal).

ever, whatever the area considered in the UT, on average, the duration of the increasing phase of IWC^{ERA5} is closer to that of IWC^{Flash} than that of IWC^{Prec}. Furthermore, the diurnal cycle of IWC^{ERA5} presents maxima lower than that of IWC^{Prec} and IWC^{Flash} over India, Pakistan and S_Vietnam (by less than 2 mg m^{-3}) and greater than that IWC^{Prec} and IWC^{Flash} over Tibet, Himalaya, Sichuan and Myanmar_Y (by more than 4 mg m^{-3}).

During the growing phase of the diurnal cycle of IWC, the diurnal maximum of IWC^{ERA5} has been shown consistencies with IWC^{Prec}, IWC^{Flash} and IWC^{MLS} at 13:30 LT over NE_India, S_Vietnam and Tibet. Over Tibet, Himalaya and SE_China, IWC^{ERA5} at 13:30 LT is overestimated compare to IWC^{MLS} at 13:30 LT (within 1.5 mg m^{-3}), and the diurnal maxima of IWC^{ERA5} is overestimated compare to the diurnal maxima of IWC^{Prec} and IWC^{Flash} (within 5 mg m^{-3}). During the decreasing phase of the diurnal cycle, as highlighted in Dion et al. (2019), the IWC^{MLS} measurement can be considered to evaluate the consistencies between our estimations of the diurnal cycle of IWC and the measure of IWC^{MLS}. Over Pakistan, SE_China and Myanmar_Y, IWC^{MLS} during the decreasing phase of the diurnal cycle is close to IWC^{Prec} or IWC^{Flash} during the decreasing phase of the diurnal cycle within less than 0.2 mg m^{-3}. However, over NE_India, India, S_Vietnam, Sichuan, Himalaya and Tibet, IWC^{MLS} during the decreasing phase of the diurnal cycle is distanced from IWC^{Prec} at 01:30 LT and IWC^{Flash} at 01:30 LT by about 1.0 mg m^{-3}. Over B_Bengal, IWC^{MLS} at 13:30 LT during the decreasing phase of the diurnal cycle is found closer to IWC^{Prec} at 13:30 LT within 0.5 mg m^{-3} than to IWC^{Flash} at 13:30 LT.

Due to the proximity of the IWC^{MLS} measurement during the decreasing phase of the diurnal cycle of IWC, it is shown how Flash and Prec are two good proxies of deep convection transporting ice up to the UT.

7.6 Horizontal distribution of ΔIWC over Asia

ΔIWC has been calculated from IWC^{Prec} (ΔIWC^{Prec}) and from IWC^{ERA5} (ΔIWC^{ERA5}) using the model proposed in Dion et al. (2019). The horizontal distributions of ΔIWC^{Prec} and ΔIWC^{ERA5} (Figure 7.7) show maxima over Tibet ($\sim$ 20°N - 90°W, reaching 16 mg m $^{-3}$ in the core of the AMA), North-East India, Gulf of Bengal, the western part of the S_Vietnam and the North-East part of the AMA over the North of China.

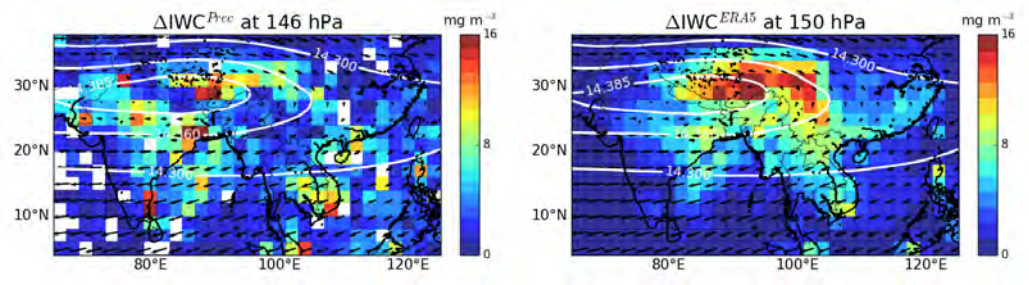

Figure 7.7 – ΔIWC^{Prec} (left) ΔIWC^{ERA5} (right) at 146 and 150 hPa, respectively and at 2° $\times$ 2° horizontal resolution.

Large differences between ΔIWC^{Prec} and ΔIWC^{ERA5} are mainly found in the two provinces of Sichuan and Yunnan in South West of China ($\sim$ 97°E – 107°E, 21°N 34°N), where ΔIWC^{Prec} are low (< 4 mg m^{-3}) and ΔIWC^{ERA5} are high (> 8 mg m^{-3}). Some isolated pixels present also high values of ΔIWC^{Prec} over South of India and in Pakistan and can be interpreted as isolated anomalies. Note that ΔIWC^{Flash} has not been presented because of the to poor signal-to-noise ratio of Flash measured during the increasing phase of the convection studied at the 2° $\times$ 2°.

7.7 ΔIWC over Asian study zones

ΔIWC^{Prec}, ΔIWC estimated from Flash (ΔIWC^{Flash}) and ΔIWC^{ERA5} in the UT have been calculated over the eight study zones and presented in Figure 7.8.

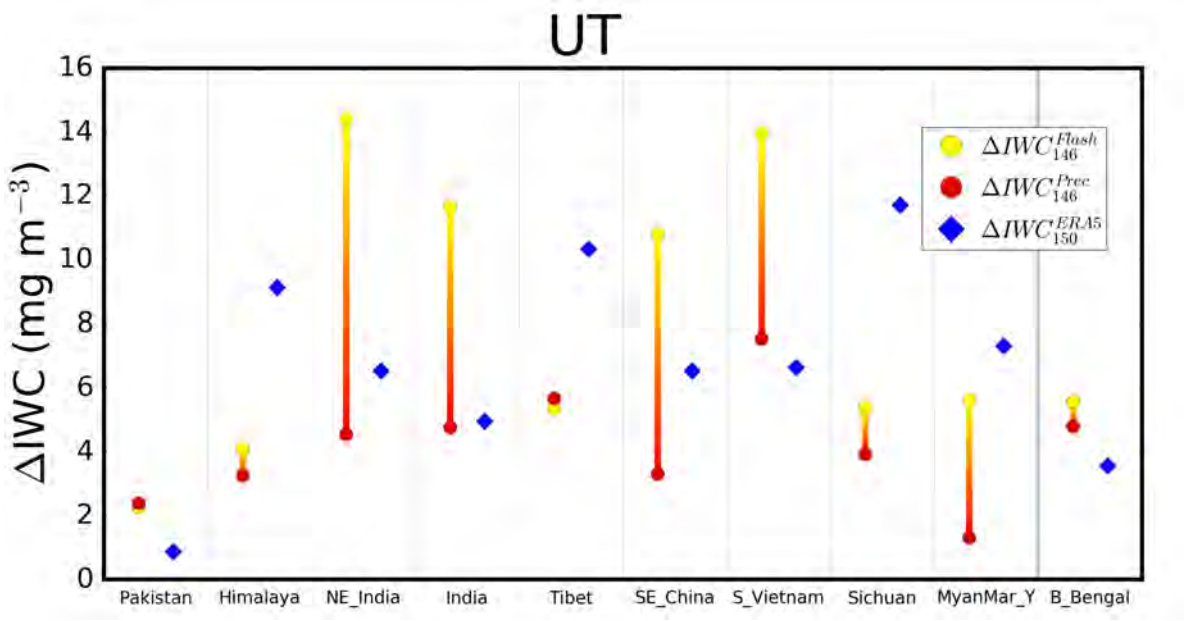

Figure 7.8 – ΔIWC (mg m^{-3}) estimated from Prec (red) and Flash (orange) at 146 hPa and ΔIWC estimated from ERA5 at the level 150 hPa over the Asian study zones.

In the UT, ΔIWC^{Prec} and ΔIWC^{Flash} are very similar over Pakistan, Himalaya, Tibet, Sichuan and B_Bengal (within 0.7 mg m^{-3}) while ΔIWC^{Flash} is much larger than ΔIWC^{Prec} over NE_India, India, SE_China and S_Vietnam (> 8 mg m^{-3} per). Over NE_India, India and SE_China, ΔIWC^{ERA5} are consistencies with the range of variation of ΔIWC estimated from observations. It appears that the results are consistent with results previously obtained over land of the MariCont (between 4 and 9 in the UT), presented in Chapter 5.

Differences between ΔIWC^{ERA5} and the observational range of variation of ΔIWC are lower than 1 mg m^{-3} over NE_India, India, Myanmar_Y and SE_China,

larger than 1 mg m^{-3} over Pakistan, S_Vietnam and B_Bengal and larger than 5 mg m^{-3} over the high altitudes study zones of Himalaya, Tibet and Sichuan. These differences can be assume by:

i) the limit of the model developed by Dion et al. (2019) regarding the consistencies between Prec, Flash and IWC in the UT, particularly over high altitudes areas (Himalaya, Tibet and Sichuan),

ii) the limit of the vertical resolution in ERA5. Indeed, it can be note that the overestimation of IWC_{150}^{ERA5} can comes from the fact that IWC_{150}^{ERA5} has been studied without having considered the same vertical distribution as the IWC^{MLS} averaging kernels (as it has been proposed in the study presented in Chapter 5). (Further works based on the C. Dallet intership, not presented here, have studied the ΔIWC_{150}^{ERA5} in the UT convolved as a function of the IWC_{150}^{MLS} vertical resolution ($\left\langle \Delta IWC_{150}^{ERA5} \right\rangle$), and have shown lower values of $\left\langle \Delta IWC_{150}^{ERA5} \right\rangle$ than ΔIWC_{150}^{ERA5} (by about -2 mg m^{-3}), showing more consistencies with ΔIWC estimated from Prec and Flash over high altitude study zones).

iii) the limit in the observation, particularly over high altitude areas.

7.8 Synthesis

The present study intended to assess the amount of ice injected in the UT during the Asian monsoon period. The model proposed in Dion et al. (2019) has been used for the first time during the JJA convective season and over the Asian region (4°N to 38°N and 65°E to 125°E). It has been shown that the horizontal distributions of Prec and Flash over the Asian study zone are not fully consistent all together, showing some large differences as e.g. over Pakistan or Tibet where Prec are low (< 2 mm day^{-1}) and Flash are high (> 10^{-1} Flash day^{-1}). IWC^{MLS} and IWC^{ERA5} at 13:30 LT over Asia have been shown to be higher than

IWC^{MLS} and IWC^{ERA5} at 01:30 LT (even over the ocean area of the Bay of Bengal) with IWC^{ERA5} at 13:30 LT overestimating IWC^{MLS} over Himalaya, Tibet and the two China provinces of Sichuan and Yunnan of China. The horizontal distributions of ΔIWC^{ERA5} and ΔIWC^{Prec} have shown maxima of ΔIWC^{ERA5} higher than ΔIWC^{Prec} by $\sim$ 15 mg m^{-3} over Tibet, Myanmar and the two China provinces of Sichuan and Yunnan. The comparison between the diurnal cycles of Prec and Flash has shown that same duration and hour of the onset of the increasing phase of the diurnal cycle for all the study zones except over Pakistan and B_Bengal study zones. The diurnal cycles of IWC^{Prec} and IWC^{Flash} show similar or stronger diurnal maxima for IWC^{Flash} than for IWC^{Prec} depending of the study zone considered. Whatever the study zone considered, both diurnal cycles were found to be consistent with the value of IWC^{MLS} during the decreasing phase of the cycle within 1 mg m^{-3}. The diurnal maximum of IWC^{ERA5} has been shown consistencies with IWC^{Prec}, IWC^{Flash} and IWC^{MLS} at 13:30 LT over NE_India, S_Vietnam and Tibet. However, the diurnal maximum of IWC^{ERA5} has been shown underestimated compare to that of IWC^{Prec}, IWC^{Flash} and IWC^{MLS} over India, Pakistan, B_Bengal and S_Vietnam. The diurnal maximum of IWC^{ERA5} has been shown overestimated compared to that of IWC^{Prec}, IWC^{Flash} and IWC^{MLS} over Tibet and Himalaya.

Finally, ΔIWC estimated in the UT over the Asian study zones have shown values of the same order of magnitude as ΔIWC estimated in the UT over the tropical lands (including lands of MariCont) during convective periods (DJF, MJO and La Nina) (Chapter 4, 5 and 6). The model developed in Dion et al. (2019) has been successfully applied to estimate the amount of ice injected in the UT by deep convective processes over Asia and during the Asian monsoon period and has provided the first horizontal distribution of the ice injected in the UT over this area, showing an overall consistencies between observations and reanalysis with

a systematic difference over elevated domains like Himalayas, Tibet Plateau and the Chinese province of Sichuan.

7.9 *Author contribution.*

IAD formulated the model and the method combining MLS, TRMM and LIS data and wrote this chapter. CD has treated the LIS data, analysed all the data and made the Figures with the contribution of PR and IAD. PR contributed to the design of the study and the interpretation of the results. The comparative analysis has been done together with IAD, CD and PR.

Chapter 8

Conclusions and perspectives

8.1 Conclusions (English)

8.1.1 Issues and motivations: the TTL a transition layer between the troposphere and the stratosphere

The tropical tropopause layer (TTL), defined by the layer between the level of maximum convective outflow (10-12 km, 200 hPa) and the cold point tropopause (CPT) temperature (16-17 km, 100 hPa) (Gettelman and Fothers, 2002; Mehta et al., 2008; Birner and Charlesworth, 2017) is a key atmospheric layer controlling the troposphere-stratosphere exchanges of air masses. The water budget in the TTL, composed by water vapour and ice, is known to have strong radiative impact on climate at global scale. However, temporal and spatial multi-scales processes impacting the TTL temperature, altitude and atmospheric compounds, and controlling the water budget into this layer, are still difficult to understand, and have motivated the research studies of this thesis.

It is known that slow (few meters per month) and large-scale phenomena are combined to rapid (kilometres per day) and local-scale processes of deep con-

vection to transport air masses composed of water vapour and ice up to the TTL. These processes control the hydration and dehydration of the upper troposphere to the lower stratosphere (Corti et al., 2006; Adler and Mack, 1986; Danielsen, 1982; Dessler, 2002; Fueglistaler et al., 2009b). At the convective system scale, the cloud related processes such as ascent of air masses (turbulent mixing) and processes at the cloud tops (overshoots) are the main actors of the convective transport from the boundary layer to the lower stratosphere (Folkins et al., 2006; Fueglistaler et al., 2009b). However, these processes are difficult to study from space-borne observations and it is thus a challenge to quantify the impact of these processes on the water budget into the TTL.

8.1.2 Objectives and strategy

The present thesis has been focused on the impact of the tropical deep convection on the water budget into the TTL, with an emphasis on the solid phase of water. The goal has been to estimate the amount of ice injected up to the TTL from deep convection over convective region and during convective periods.

For that, this thesis benefited from useful scientist community's tools available for the study of tropical deep convection and water budget (space-borne measurements and models). However, few satellite data are able to provide ice and water vapour at the altitudes of the TTL. The MLS instruments on board the Aura platform is the only instrument able to provide ice water content (IWC) and water vapour (WV) in the TTL during a long time series (from 2004 to 2017). However, MLS measures IWC observations at only two local times a day in the tropics, at 01:30 LT and 13:30 LT. For this reason, this thesis has combined the IWC measurements of MLS at two local times with the 1-h temporal resolution observations of the convective activity based on precipitation (Prec) and on the number of flashes from lightning (Flash) from TRMM observations to develop a model

able to estimate the amount of ice injected up to the TTL by deep convection.

The study of the water budget in the TTL has been evaluated from results of our model and from observations provided by MLS such as the water vapour (WV), relative humidity and temperature from MLS. Observations have been studied at the 2°× 2° horizontal resolution ($\sim$ 200 $\times$ 200 km) in the tropics, allowing to study the impact of meso-scale processes on the ice injected up to the TTL in order to distinguish land to ocean areas.

8.1.3 Method used

The method combines the study of deep convection and water budget in the TTL. To study deep convection, we have selected convective study zones during convective periods. To study the water budget in the TTL, we have highlighted the key role of the solid phase compared to gas phase of water in the UT (at 146 hPa) and the tropopause level (TL, at 100 hPa) over convective regions by showing that: i) the amount of IWC compared to the amount of total water (IWC + WV) is larger than 70% in the UT and larger than 50% in the TL, and ii) IWC in the UT is highly spatially correlated with Prec (Pearson linear correlation coefficient R $\sim$ 0.7) while WV is not (R $\sim$ 0.2).

For these reasons, the model developed in this thesis focuses on the growing phase of the deep convection development and its impact on the amount of ice injected up to the TTL. Because MLS provides data of IWC at only two local times in the diurnal cycle, the model estimates the increasing phase of the diurnal cycle of IWC from a linear relationship between IWC measured by MLS during the growing phase of the deep convection, and diurnal cycle of Prec or Flash from TRMM in the UT and the TL. The model has defined the amount of ice injected up to the UT and the TL (named ΔIWC) as the difference between the maximum and the minimum of ice in its diurnal cycle. ΔIWC has been calculated and compared

over several study zones in the tropics and has been compared to other datasets during the austral convective season of December, January and February (DJF) within the period from 2004 to 2017.

8.1.4 Validation

To validate the amount of ice injected into the TTL by our model, we have used IWC data measured by the SMILES instrument on board the ISS (ftp://mls.data/jpl.nasa.gov/pub/outgoing/smiles) with 1-h temporal resolution during December 2009 to February 2010. ΔIWC estimated by our model from Prec as proxy of deep convection (named ΔIWC^{Prec}) has also been compared to ΔIWC estimated from Flash as proxy of deep convection (named ΔIWC^{Flash}), establishing a variability range of ΔIWC from space-borne observational datasets. To evaluate the variability range of ΔIWC, we have calculated ΔIWC from IWC provided by the meteorological ERA5 reanalyses (https://%20cds.climate.copernicus.eu/cdsapp#%21/dataset/reanalysis-era5-pressure-levels-monthly-means?tab=form) and from ice provided by the meso-scale Meso-NH model (Lafore et al., 1997; Lac et al., 2018) at the 1-h temporal resolution.

The increasing phase of the diurnal cycles of IWC estimated from our model has been shown very consistent with that of the diurnal cycle of IWC measured by SMILES. ΔIWC estimated from our model and ΔIWC estimated from SMILES have shown consistencies within 0.7 mg m^{-3} in the UT and within 0.15 mg m^{-3} in the TL. Furthermore, ΔIWC estimated from ERA5 reanalysis have been shown to be consistent with ΔIWC estimated from our model over land study zones and under-estimated values of ΔIWC compared to that of our model over ocean study zones in the UT (by $\sim$ -1 mg m^{-3}) .

8.1.5 Main results of the thesis

This thesis is separated into **four main studies** based on the following subjects: 1) austral convective areas in the **tropics**, 2) the **Maritime Continent** region, 3) the intra-seasonal and inter-annual **oscillations** over the Maritime Continent region, and 4) the **Asian Monsoon** area.

• 1) The model has been developed and used to estimate ΔIWC from IWC and Prec during the austral convective season of DJF from 2004 to 2017 and over the main austral convective areas in the tropics: South America, South Africa, Indian Ocean, Pacific Ocean and the land and the sea of the Maritime Continent region (named MariCont). ΔIWC has been estimated, in the UT, in a range of 2 – 3 mg m^{-3} over land and 0.4 – 0.9 mg m^{-3} over ocean, and in the TL, in a range of 0.13 – 0.56 mg m^{-3} over land and 0.09 – 0.19 mg m^{-3} over ocean. The land of the MariCont have been shown to be the convective region with the highest amount of ice injected up to the UT and the TL (higher by more than 0.3 mg m^{-3} in the UT and the TL compared to all the other regions). The MariCont region is composed of many islands and seas, and our study has highlighted the importance to separate this region into two sub-regions: the MariCont land (MariCont_L) and the MariCont ocean (MariCont_O), providing two different diurnal cycles of Prec, and thus of the deep convection, impacting differentially ΔIWC over land and over ocean. The ice budget in the TTL over the whole tropics has been calculated to be 2.2 g m^{-3} in the UT during DJF, with 70% of IWC injected over land and 30% over ocean.

• 2) Due to the strongest ΔIWC observed over the MariCont, the thesis has focused on this region to study ΔIWC at 2°$\times$ 2° horizontal resolution over selected islands and seas. ΔIWC has been observed reaching 10 to 20 mg m^{-3} per 2°$\times$ 2° pixel over land. The variatibility range of ΔIWC estimated from space-borne observations based on ΔIWC^{Prec} and ΔIWC^{Flash} has been compared to the vari-

ability range of ΔIWC estimated from the ERA5 meteorological reanalyses in the UT (resp. TL) and vertically degraded taking in account the vertical resolution of MLS observations in the UT (resp. TL). The observational and reanalysis variability ranges of ΔIWC have been found to be, in the UT, between 4.17 and 9.97 mg m^{-3} over island and between 0.35 and 4.37 mg m^{-3} over sea, and, in the TL, between 0.63 and 3.65 mg m^{-3} over island and between 0.04 and 0.74 mg m^{-3} over sea. The Java island has been found to be the area of the largest ΔIWC in the UT (7.89 – 8.72 mg m^{-3}) whatever the datasets considered. The diurnal cycles of Flash and Prec have been studied separately over island, sea, and coastal areas to assess the role of the different processes implied in the ΔIWC variabilities. Processes involved in the initiation of the deep convection have been discussed and pre-existing surface conditions such as orography, mesoscale breezes induced by the hot-dry/cold-wet contrast at the surface, density currents, coastal regions were highlighted as a function of each study zone. Tiny islands with high mountains falling into the sea, such as the Java Island, have been pinpointed as ideal areas to generate deep convection and transport the largest amounts of ice up to the TTL.

- 3) Because the MariCont region is a region strongly impacted by intra-seasonal and inter-annual large-scale oscillations, we have studied the impact of the Madden-Julian Oscillation (MJO) and La Niña Oscillation on the processes related to the development of the deep convection life cycle and on the amount of ice injected up to the TTL. Four study processes have been compared: deep convective processes during the austral convective season of DJF (named DJF_Clim) that is consistent with the previous studies, the impact of the active phase of the Madden-Julian Oscillations not including DJF neither La Niña periods (named MJO), the impact of the La Niña oscillations not including DJF neither MJO (named La Niña) and deep convective processes during the DJF period not including MJO neither La Niña (named DJF). Ice datasets simulated from the meso-

scale model Meso-NH during a MJO suppressed phase over the MariCont have also been used to estimate ΔIWC. Whatever the oscillations considered, ΔIWC over land have been shown more than twice higher than ΔIWC over sea in the UT and in the TL. La Niña processes tend to increase ΔIWC (within 4 mg m^{-3} per pixel) over land and decrease ΔIWC (within - 4 mg m^{-3} per pixel) over sea compared to the pure deep convective processes during DJF. The MJO suppressed phase reduces ΔIWC within 2 mg m^{-3} compared to the MJO active phase.

- 4) Because the method proposed in this study have shown consistencies with space-borne observations, model and reanalysis allowing to estimate ΔIWC over convective areas at several horizontal scales, we have extended the use of this model to the Asian region during the Asian monsoon period (June, July and August, JJA) from 2004 to 2017 to estimate ΔIWC and to improve knowledges on the impact of deep convection on the water budget in the TTL over this region. The same methodology as used in the previous studies has been applied in a study based on the master 2 internship by C. Dallet, supervised by P. Ricaud and myself combining ΔIWC from MLS, TRMM-3B42, TRMM-LIS and ERA5 over different areas of Asia. The diurnal cycle of IWC from ERA5 have been shown to be underestimated (by $\sim$ 0.5 mg m^{-3}) compared to the diurnal cycles of IWC estimated from Prec and Flash, excepted over areas of high altitudes (higher than 2000 m) where the diurnal cycle of IWC from ERA5 was overestimated (by $\sim$ 1 mg m^{-3}) compared to the diurnal cycle of IWC estimated from Prec and Flash. It has been shown that IWC estimated from Prec and Flash at 01:30 LT and 13:30 LT agreed with the IWC measurement of MLS during the decreasing phase of the IWC diurnal cycle. Whatever the datasets used, ΔIWC shown maxima on the Tibetan Plateau, the North-East India, the Bay of Bengal and over the two Chinese provinces of Shishuan and Yunnan. The variation range of ΔIWC estimated from ERA5, Prec and Flash has been found to be of the same order of

magnitude as the one calculated in the UT and the TL over the land and sea of the MariCont region.

To conclude, in this thesis, we have developed a **model** able to estimate the amount of ice injected by deep convection over convective area and during convective periods. The land of the **MariCont** region has been shown to be the region of strongest ΔIWC in the tropics. Over this region, the **Java Island** has been highlighted as the area with the strongest ΔIWC. La Niña and the MJO, known as two main large-scale oscillations impacting the convective activity over the MariCont, have produced **ΔIWC consistent** with values estimated during the DJF season. The model has also been used in the extra-tropics over Asia during deep convective activities occurring in the Asian Monsoon anticyclones in JJA. ΔIWC over Asia has been shown as strong as ΔIWC over the MariCont in DJF. This thesis has highlighted the **land/ocean contrast** in ΔIWC with values more than twice larger over land than over ocean in the UT and in the TL. Finally, the **vertical distribution** of ΔIWC in the TTL has shown a gradient of - 6 mg m^{-3} between the UT and the TL over land compared to a gradient of - 2 mg m^{-3} between the UT and the TL over ocean.

8.2 Perspectives (English)

Based on the model developed and the scientific results obtained in the thesis, some new perspectives can be drawn to study of: 1) the tropical **deep convection**, 2) the **diurnal cycle** of the total **water budget** in the TTL, 3) the amount of ice injected to the **lower stratosphere** (LS), and 4) the impact of **large-scale oscillation** on the injection of ice in the TTL.

8.2.1 Tropical deep convection from space-borne observations

This thesis has used Prec and Flash as proxies of deep convection over convective areas and convective periods to establish the variability range of the estimated ΔIWC. However, some differences in the diurnal cycles of these two proxies are still not well understood and our study has not been able to determine which of the two variables is the best proxy of deep convection. For that, other parameters related to Prec and Flash could be considered to evaluate the deep convective activity: i) the strength of the convection could be evaluated by the intensity of Prec or the vertical wind speed impacting on the air masses transport into the cloud, or ii) the altitude reached by the convective clouds could be evaluated for instance from the cloud top height by using the outgoing longwave radiation (OLR) measuring the brightness temperature. These pieces of information could be used to filter the Prec and Flash datasets and improve the accuracy of the results and the knowledge on the deep convective life cycle.

8.2.2 Diurnal cycle of water budget in TTL

The thesis has shown the impact of the growing phase of the deep convection on the injection of ice into the TTL. However, once the mature phase of the deep convection is reached, processes impacting the amount of ice in the TTL are still not well understood. Thus, while this thesis has shown the essential role of convective processes impacting the amount of ice into the TTL during the increasing phase of the convection, it can be suggested that other processes (such as the sublimation of ice, the vertical advection of ice or the ice falling for instance) can compete with convective processes during the decreasing phase of the convection. Many studies have shown that the increasing phase of the diurnal cycle of WV is delayed compared to the increasing phase of the diurnal cycle of ice (Carminati

et al., 2014; Dauhut et al., 2015), suggesting that the amount of WV in the TTL increases with the beginning of the ice sublimation processes.

Some observations have been done in this thesis about the decreasing phase of the diurnal cycle of ice in the TTL, by the comparative study between the amount of IWC measured by MLS during the decreasing phase of the convection and the estimated value of IWC at the same hour. Strong differences ($\sim$ 20 %) between the two values have been shown over South America, South Africa, and Ocean areas while low differences ($\sim$ 3 %) have been found over the MariCont. During the decreasing phase of the convection, the consistency between the estimated and the measured IWC values tends to suggest that convective processes also impact ice and its associated diurnal cycle in the TTL. However, this thesis has not validated this assumption.

Several ways could be followed to validate this assumption and to study the full diurnal cycle of water budget into the TTL. Five points combining further information related to the water budget in the TTL can be proposed as follow:
1) The study of the relationship between the vertical distribution of the diurnal cycle of **temperature** and vertical distribution of the estimated diurnal cycle of ice (by the comparison between results in the UT and in the TL). The diurnal cycle of temperature in the TTL can be provided by the temperature datasets covering several years available from the joint COSMIC mission between the National Aeronautics and Space Administration (NASA) and National Space Organization (NSPO) of Taiwan, based on the limb viewing radio occultation technique.
2) The relationship between the **altitude** of the TTL and the amount of ice injected up to the TTL as a function of the horizontal distribution in the tropics. Note that the altitude of the TTL can also be provided by the COSMIC mission over a long time series.
3) The height and pressure of the cloud top as well as the location of the over-

shooting top have already been processed from the high horizontal and temporal resolutions space-borne observations of the Japanese geostationary satellite **Himawari-8** focused over of the MariCont region, by the Met Office Satellite Imagery Applications Group and Satellite Data Processing Systems. This information can be useful to improve our understanding of the deep convective activity life cycle over this region.

4) A longer time series (reaching $\sim$ 20 years) of IWC, WV, temperature and relative humidity with respect to ice measurements from MLS could increase the signal-to-noise ratio and improve the estimation of ΔIWC, especially in the study of the intra-seasonal and inter-annual oscillations, where the MJO and La Nina periods have shown a weak number of days between 2004 to 2017.

5) The comparison between the two daily MLS measurements of water vapour with the diurnal cycle (1-h resolution) of the tropospheric specific humidity (kg kg^{-1}) and with the specific cloud liquid water content (kg kg^{-1}) provided by the meteorological ERA5 reanalyses and with the water vapour mixing ratio (ppmv) in the TTL simulated by the Meso-NH model. The method could be used firstly to study this comparison over areas where ΔIWC estimated from ERA5 has been shown to be consistent with ΔIWC estimated from observations, and secondly over areas where it has been found inconsistencies.

8.2.3 Ice injection up to the lower stratosphere

Because the TTL controls the troposphere to stratosphere exchanges, the studies performed in this thesis can be used as a step toward the understanding of the total water budget variabilities up to the lower stratosphere, particularly through the **overshoots** processes.

IWC from MLS in the stratosphere still provides a too low signal-to-noise ratio to be studied. However, WV from MLS can be studied in the lower stratosphere

(LS, higher than 82 hPa). An interesting way to study the water budget into the LS from MLS observations would be, firstly, to understand the relationship between IWC and WV into the TTL and, secondly, to observe differences in the Day-Night signal of WV between the TTL and the LS.

Application of the work in the context of stratospheric hydration

Recent work, following a collaboration between T. Dauhut and V. Noël and myself, has highlighted how the fraction of tropical clouds evolves above the tropopause during the day. From Lidar space-borne observations, it has been shown that a relationship between the diurnal cycle of stratospheric clouds and the diurnal cycle of the deep convective activity (Dauhut et al., 2020). From this study, authors have suggested a 3-hour delay between the diurnal cycle of very deep convection and the stratospheric cloud fraction. These results are consistent with the assumptions presented in Dion et al. (2019). However, the ice and WV ratios of the stratospheric cloud fraction measured are not detailed.

8.2.4 Impact of large-scale oscillation of the ice injected into the TTL

The large differences observed in this thesis between ΔIWC measured during the MJO active and suppressed phases can be explained either by the differences in convective process considered in these two MJO phases or by a bias of the model vs the observations induced by the time and space data sampling. In order to perform the model/observations comparison, the same phase of the MJO should be compared. However, since the model proposed in this thesis to estimate ΔIWC from observations works only for convective periods and over convective regions, it would be not possible to study the suppressed phase of the MJO (due to low

precipitation and low lightning during this period). But, it would be interesting to use the Meso-NH model during periods of deep convection (MJO in active phase, but also DJF and La Niña) to compare the calculated ΔIWC with those presented in this thesis.

8.2.5 Integration of the results into current research projects

The three campaigns presented in this subsection are strongly related to the scientific issues developed in this thesis and could provide useful information to better understand the impact of the deep convection on the water budget in the UTLS.

Over the Maritime Continent

This thesis has been performed in parallel to the recent international campaign focused on various climatological and meteorological processes over the MariCont region from 2017 to 2019. This campaign is called the Year of the Maritime Continent (YMC, http://www.jamstec.go.jp/ymc/, last access: May 2019) and integrates observations and modelling, bridging research and operation, and outreach and capacity building, to better understand weather-climate systems. The goal of YMC is to improve the understanding and prediction of local multi-scale variability of the MariCont weather-climate systems. Thus, many campaigns and modelling activities drawn during the YMC would provide data to improve our understanding of the tropopause humidity variabilities over this strong deep convective region.

Over the Asia monsoon region

The Strato-Clim (Stratospheric and upper tropospheric processes for better climate predictions, http://www.stratoclim.org/, last access: August 2019) project (2013 - 2018) is a collaborative research project with the aim to produce more

reliable projections of climate change and stratospheric ozone by improving the understanding of key processes in the Upper Troposphere and Stratosphere. Studies presented in this thesis, providing water budget informations in the TTL, are fully related to this project with recent measurement campaigns carried out in the Asian monsoon region were dedicated to understand the troposphere-stratosphere exchanges.

The futur ACCLIP (Asian summer monsoon chemical and Climate impact, https://www2.acom.ucar.edu/acclip, last access: August 2019) project (July-August 2020) aims to investigate the impacts of Asian gas and aerosol emissions on global chemistry and climate via the linkage of Asian Summer Monsoon (ASM) convection and associated large-scale dynamics. Thus, studies on convective activity during the Asian monsoon are expected and could help the understanding of the horizontal and vertical distributions and amounts of ice in the UTLS.

Conclusions et perspectives

8.3 Conclusions (Français)

8.3.1 Enjeux et motivations : la TTL, une couche de transition entre la troposphère et la stratosphère

La tropopause tropicale (TTL pour tropical tropopause layer en anglais) est définie par la couche entre le niveau d'écoulement convectif maximal (vers 10-12 km, $\sim$ 200 hPa) et le point froid de la température (vers 16-17 km, $\sim$ 100 hPa) (Gettelman and Fothers, 2002; Mehta et al., 2008; Birner and Charlesworth, 2017). La TTL est une couche atmosphérique clé contrôlant les échanges de masses d'air entre la troposphère et la stratosphère. Le bilan hydrique de la TTL, composé de vapeur d'eau et de glace, est connu pour avoir un fort impact radiatif sur le climat à l'échelle mondiale. Cependant, les processus spatiaux temporels de multi-échelles ayant un impact sur la température de la TTL, son altitude, sa composition chimique, et contrôlant le bilan hydrique dans cette couche, sont encore difficiles à comprendre et ont motivé les recherches de cette thèse.

On sait que les phénomènes lents (de quelques mètres par mois) et de grande échelle sont combinés à des processus rapides (de l'ordre du kilomètre par jour) et locaux de convection profonde pour transporter les masses d'air composées de vapeur d'eau et de glace jusqu'à la TTL. Ces processus contrôlent l'hydratation et

la déshydratation de la haute troposphère vers la basse stratosphère (Corti et al., 2006; Adler and Mack, 1986; Danielsen, 1982; Dessler, 2002; Fueglistaler et al., 2009b). A l'échelle des systèmes convectifs, les processus liés à la formation des nuages convectifs profonds tels que l'ascension des masses d'air (par le mélange turbulent) et les processus au sommet des nuages (comme les percées nuageuses) sont les principaux acteurs du transport convectif de la couche limite vers la basse stratosphère (Folkins et al., 2006; Fueglistaler et al., 2009b). Cependant, ces processus sont difficiles à étudier à partir d'observations et il est donc difficile de quantifier l'impact de ces processus sur le bilan hydrique dans la TTL.

8.3.2 Objectifs et stratégie

La thèse s'est concentrée sur l'impact de la convection profonde tropicale sur le bilan hydrique dans la TTL, avec un accent particulier sur la phase solide de l'eau. L'objectif était d'estimer la quantité de glace injectée jusqu'à la TTL par convection profonde dans les régions convectives et pendant les périodes convectives.

Pour cela, cette thèse a bénéficié d'outils utilisés par la communauté scientifique et disponibles pour l'étude de la convection profonde tropicale et du bilan hydrique (mesures spatiales et modèles). Toutefois, peu d'instrument satellitaires sont capable de mesurer les quantités de glace et de vapeur d'eau aux altitudes de la TTL. L'instrument MLS à bord de la plate-forme Aura est le seul instrument capable de mesurer les concentrations en eau glacée (IWC) et de vapeur d'eau (WV) dans la TTL pendant une longue série temporelle (de 2004 à 2017). Cependant, les observations de IWC mesurées par MLS ne sont fournies qu'à deux heures locales par jour sous les tropiques, à 01:30 heure locale (LT pour local time en anglais) et 13:30 LT. Pour cette raison, cette thèse a combiné les deux mesures quotidiennes en heures locales de IWC de MLS avec des observations de l'activité convective à bien meilleure résolution temporelle, basées sur les précipitations (Prec) et sur le

nombre d'éclairs lors d'événements orageux (Flash) fournis par les observations du satellite TRMM pour développer un modèle capable d'estimer la quantité de glace injectée jusqu'à la TTL par convection profonde.

L'étude du bilan hydrique dans la TTL a été évaluée à partir des résultats de notre modèle et des observations fournies par MLS telles que la vapeur d'eau (WV), l'humidité relative et la température. Les observations ont été étudiées à la résolution horizontale de $2° \times 2°$ ($\sim 200 \times 200$ km) sous les tropiques, permettant d'étudier l'impact des processus de méso-échelle sur la glace injectée jusqu'à la TTL en y distinguant les zones terrestres et océaniques.

8.3.3 Méthode utilisée

La méthode combine l'étude de la convection profonde et du bilan hydrique dans la TTL. Pour étudier la convection profonde, nous avons sélectionné des zones d'étude convective pendant les périodes convectives. Pour étudier le bilan hydrique dans le TTL, nous avons mis en évidence le rôle important de la phase solide par rapport à la phase gazeuse de l'eau dans l'UT (à 146 hPa) et au niveau de la tropopause (TL pour tropopause layer, à 100 hPa) en montrant que : i) la quantité de IWC par rapport à la quantité d'eau totale (IWC + WV) est supérieure à 70% dans l'UT et à 50% dans la TL, et que ii) IWC dans l'UT est fortement spatialement corrélée avec Prec (coefficient de corrélation linéaire de Pearson, R $\sim$ 0.7) alors que la WV ne l'est pas (R $\sim$ 0.2).

Pour ces raisons, le modèle développé dans cette thèse se concentre sur la phase croissante du développement de la convection profonde et sur son impact sur la quantité de glace injectée jusqu'à la TTL. Comme l'instrument MLS ne fournit IWC qu'à deux heures locales par cycle diurne, le modèle estime la phase croissante du cycle diurne de IWC à partir d'une relation linéaire entre IWC mesurée par MLS pendant la phase croissante de la convection profonde et le

cycle diurne de Prec ou de Flash fournis par TRMM dans l'UT et dans la TL. Le modèle a défini la quantité de glace injectée jusqu'à l'UT et la TL (appelée ΔIWC) comme la différence entre le maximum et le minimum de glace dans son cycle diurne. ΔIWC a été calculée et comparée sur plusieurs zones d'étude sous les tropiques et a été comparée à d'autres jeux de données pendant la saison convective australe de décembre, janvier et février (DJF) au cours de la période allant de 2004 à 2017.

8.3.4 Validation

Pour valider la quantité de glace injectée dans la TTL estimée par notre modèle, nous avons utilisé les données de IWC mesurées par l'instrument SMILES à bord de l'ISS (`ftp://mls.data/jpl.nasa.gov/pub/outgoing/smiles`, dernier accès: août 2019) avec une résolution temporelle de 1 heure entre décembre 2009 et février 2010. ΔIWC estimée par notre modèle à partir de Prec comme approximation de la convection profonde (nommé ΔIWC^{Prec}) a également été comparée à ΔIWC estimée à partir de Flash comme approximation de la convection profonde (nommé ΔIWC^{Flash}), établissant la plage de variabilité de ΔIWC à partir des jeux de données d'observations spatiales. Pour évaluer la plage de variabilité de ΔIWC, nous avons calculé ΔIWC à partir de IWC fourni par les réanalyses météorologiques de ERA5 (`https://%20cds.climat.copernicus.eu/cdsapp#%21/dataset/reanalysis-era5-pressure-levels-monthly-means?tab=form`, dernier accès: août 2019) et de la glace fournie par le modèle de méso-échelle Meso-NH (Lafore et al., 1997; Lac et al., 2018) à la résolution temporelle de 1-h.

La phase croissante des cycles diurnes de IWC estimée à partir de notre modèle s'est révélée très cohérente avec celle du cycle diurne de IWC mesurée par

SMILES. En effet, ΔIWC estimée par de notre modèle et ΔIWC estimée par SMILES ont montré des cohérences de l'ordre de 0,7 mg m^{-3} dans l'UT et de 0,15 mg m^{-3} dans la TL. De plus, l'estimation de ΔIWC estimée à partir des réanalyses de ERA5 s'est avérée conforme aux estimations de ΔIWC estimée par notre modèle sur les zones d'étude terrestres mais ont montré des valeurs de ΔIWC sous-estimées par rapport à celles estimées par notre modèle sur les zones d'étude océaniques (par $\sim$ -1 mg m^{-3}).

8.3.5 Résultats principaux de la thèse

Cette thèse est séparée en **quatre études principales** basées sur les thématiques suivantes : 1) les zones convectives australes dans la région des **tropiques**, 2) la région du **Continent Maritime**, 3) les **oscillations** intra-saisonnière et inter-annuelle sur la région du Continent Maritime, et 4) la région de **la mousson Asiatique**.

• 1) Le modèle a été développé et utilisé pour estimer ΔIWC à partir de IWC et Prec pendant la saison convective australe de DJF de 2004 à 2017 et sur les principales zones convectives australes des tropiques : l'Amérique du Sud, l'Afrique du Sud, l'Océan Indien, l'Océan Pacifique et les terres et mers de la région du Continent Maritime (appelée MariCont). ΔIWC a été estimé, dans l'UT, à 2 – 3 mg m^{-3} sur terre et 0,4 – 0,9 mg m^{-3} sur mer, et dans la TL, à 0,13 – 0,56 mg m^{-3} sur terre et 0,09 – 0,19 mg m^{-3} sur mer. Les terres du MariCont se sont avérées être la région convective ayant la plus grande quantité de glace injectée jusqu'à l'UT et la TL (avec des valeurs de ΔIWC de plus de 0,3 mg m^{-3} dans l'UT et la TL par rapport aux autres régions étudiées). La région du MariCont est composée de nombreuses îles et mers, et notre étude a souligné l'importance de séparer cette région en deux sous-régions : les terres du MariCont (MariCont_L) et les mers du MariCont (MariCont_O), fournissant deux cycles diurnes différents de Prec, et

donc de la convection profonde, ayant un impact different sur ΔIWC estimé sur les terres et sur les océans. Le bilan de la glace dans la TTL sur l'ensemble des tropiques a été quantifié à 2,2 g m^{-3} dans l'UT en DJF, avec 70% de IWC injectée sur les terres et 30% sur mer.

• 2) En raison des plus fortes quantités de ΔIWC observées sur le MariCont, la thèse s'est concentrée sur cette région pour étudier ΔIWC à la résolution horizontale de $2^\circ \times 2^\circ$ sur certaines îles et mers. On a observé que ΔIWC pouvait atteindre jusqu'à 10 à 20 mg m^{-3} par pixel de $2^\circ \times 2^\circ$ sur les terres. La plage de variabilité de ΔIWC estimée à partir d'observations spatiales basées sur ΔIWC^{Prec} et ΔIWC^{Flash} a été comparée à celle de ΔIWC estimée à partir des réanalyses météorologiques de ERA5 dans l'UT (respectivement la TL) et verticalement dégradée en prenant en compte la résolution verticale des observations de MLS dans l'UT (respectivement la TL). Les plages de variabilité de ΔIWC établies à partir des observations et des réanalyses se situent, dans l'UT, entre 4,17 et 9,97 mg m^{-3} sur les îles et entre 0,35 et 4,37 mg m^{-3} sur les mers, et, dans la TL, entre 0,63 et 3,65 mg m^{-3} sur les îles et entre 0,04 et 0,74 mg m^{-3} sur les mers. L'île de Java s'est avérée être la zone de plus grande ΔIWC dans l'UT (7,89 – 8,72 mg m^{-3}) quel que soit le jeu de données considérées. Les cycles diurnes des Flash et Prec ont été étudiés séparément sur les zones insulaires, maritimes et côtières pour évaluer le rôle des différents processus impliqués dans les variabilités de ΔIWC. Les processus impliqués dans le déclenchement de la convection profonde ont été discutés et les conditions de surface préexistantes telles que l'orographie, les brises de mésoéchelles induites par le contraste chaud-sec/froid-humide de surface, les courants de densité et les régions côtières ont été soulignés en fonction de chaque zone étudiée. De petites îles avec de hautes montagnes tombant dans la mer, comme l'île de Java, ont été identifiées comme des zones idéales pour générer une convection profonde et transporter les plus grandes quantités de glace

jusqu'à la TTL.

• 3) Comme la région du MariCont est une région fortement touchée par les oscillations intra-saisonnières et inter-annuelles de grande échelle, nous avons étudié l'impact de l'oscillation de Madden-Julian (MJO) et de La Niña sur les processus liés au développement du cycle de vie de la convection profonde et sur l'injection de glace jusqu'à la TTL. Quatre processus d'étude ont été comparés : i) les processus convectifs profonds pendant la saison convective australe de DJF (appelés DJF_Clim) qui sont cohérents avec les études précédentes, ii) l'impact de la phase active des oscillations de MJO sans inclure les périodes de DJF ni de La Niña (appelé MJO), iii) l'impact des oscillations de La Niña sans inclure les périodes de DJF ni de MJO (appelé La Niña) et iv) les processus convectifs profonds durant les périodes de DJF sans inclure les périodes de MJO ni de La Niña (nommé DJF). Les données de glace simulées à partir du modèle de méso-échelle Meso-NH, pendant une phase inhibée de la MJO sur le MariCont ont également été utilisées pour estimer ΔIWC. Quelles que soient les périodes considérées, on a montré que ΔIWC sur terre était plus de deux fois supérieures à ΔIWC sur mer dans l'UT et la TL. Les processus durant La Niña ont tendance à augmenter ΔIWC (dans les limites de 4 mg m^{-3} par pixel) sur terre et à diminuer ΔIWC (dans les limites de -4 mg m^{-3} par pixel) sur mer par rapport aux processus convectifs purs de convection profonde observés en DJF. La phase inhibée de la MJO réduit ΔIWC de 2 mg m^{-3} par rapport à la phase active de la MJO.

• 4) Parce que la méthode proposée dans cette étude a montré des cohérences dans les valeurs de ΔIWC estimées à partir des observations spatiales, du modèle et des réanalyses sur des zones convectives à plusieurs échelles horizontales, nous avons étendu l'utilisation de ce modèle à la région asiatique pendant la mousson asiatique (juin, juillet et août, JJA) de 2004 à 2017 pour estimer ΔIWC et pour améliorer la connaissance sur l'impact de la convection profonde sur le bi-

lan hydrique de la TTL. La même méthodologie que celle utilisée dans les études précédentes a été appliquée dans une étude basée sur le stage de Master 2 de C. Dallet, supervisé par P. Ricaud et moi-même combinant ΔIWC de MLS, Prec and Flash de TRMM et IWC de ERA5 sur différentes régions d'Asie. On a montré que le maximum diurne de IWC dans le cycle diurne de IWC fourni par ERA5 était sous-estimé (par $\sim$ -0.5 mg m^{-3}) par rapport aux maxima diurnes de IWC estimés à partir de Prec et Flash, sauf dans les zones de hautes altitudes (> 2000 m) où le cycle diurne de IWC fourni par ERA5 a été montré sur-estimé (de l'ordre de $\sim$ 1 mg m^{-3}) par rapport à celui de IWC estimé à partir de Prec et Flash. Il a été montré que IWC estimé à partir de Prec et Flash à 01:30 LT et 13:30 LT est en accord avec IWC mesuré par MLS pendant la phase décroissante du cycle diurne de IWC. Quels que soient les jeux de données utilisés, ΔIWC est maximum sur le plateau tibétain, le nord-est de l'Inde, la baie du Bengale et sur les deux provinces chinoises du Shishuan et Yunnan. La plage de variabilité de ΔIWC estimée à partir de ERA5, Prec et Flash est du même ordre de grandeur que celle calculée dans l'UT et la TL sur la terre et la mer de la région du MariCont.

Pour conclure, dans cette thèse, nous avons développé un modèle capable d'estimer la quantité de glace injectée par convection profonde sur les régions convectives tropicales et pendant les périodes convectives. La région du **MariCont** s'est avérée être la région de plus forte ΔIWC sous les tropiques. Dans cette région, l'île de **Java** a été mise en évidence comme étant la zone où ΔIWC est la plus forte. La Niña et la MJO, connues pour être deux oscillations de grande échelle ayant un impact sur l'activité convective au-dessus du MariCont, ont montré des valeurs de **ΔIWC cohérentes** avec les valeurs estimées pendant la saison DJF. Le modèle a également été utilisé dans les régions extra-tropicales au-dessus de l'Asie au cours d'activités convectives profondes durant l'anticyclone de la

mousson asiatique en JJA. ΔIWC sur l'Asie s'est montré aussi fort que ΔIWC sur le MariCont en DJF. Cette thèse a mis en évidence le **contraste terre/océan** dans les valeurs de ΔIWC avec des valeurs plus de deux fois supérieures sur terre que sur mer dans l'UT et la TL. Enfin, la **distribution verticale** de ΔIWC dans la TTL a montré un gradient de -6 mg m^{-3} entre l'UT et la TL sur terre comparé à un gradient de -2 mg m^{-3} entre l'UT et la TL sur mer.

8.4 Perspectives (Français)

Sur la base du modèle développé et des résultats scientifiques obtenus dans le cadre de la thèse, de nouvelles perspectives peuvent être proposées pour l'étude : 1) de la convection profonde tropicale, 2) du **cycle diurne** du **bilan de l'eau** total dans la TTL, 3) de la quantité de glace injectée jusqu'à la **basse stratosphère** (LS), et 4) de l'impact des **l'oscillation de grande échelle** sur l'injection de glace dans la TTL.

8.4.1 Convection profonde tropicale à partir d'observations spatiales

Cette thèse a utilisé Prec et Flash comme approximations de la convection profonde sur les zones convectives et les périodes convectives pour établir un intervalle de variabilité de ΔIWC. Cependant, certaines différences dans les cycles diurnes de ces deux variables ne sont pas encore bien comprises et notre étude n'a pas été en mesure de déterminer laquelle des deux variables est la meilleure pour étudier la convection profonde tropicale. Pour cela, d'autres paramètres liés à Prec et Flash pourraient être pris en compte pour évaluer l'activité convective profonde : i) l'intensité de la convection pourrait être évaluée par l'intensité de Prec ou la vitesse verticale du vent affectant le transport des masses d'air dans le nuage (bien

qu'encore difficile à mesurer), ou ii) l'altitude atteinte par les nuages convectifs pourrait être estimée par exemple par la hauteur des nuages en utilisant le rayonnement (OLR) qui mesure la température de brillance au sommet des nuages. Ces informations pourraient être utilisées pour filtrer les jeux de données de Prec et Flash et améliorer la précision des estimations de ΔIWC et nos connaissances sur le cycle de vie de la convection profonde.

8.4.2 Cycle diurne du bilan hydrique dans la TTL

La thèse a montré l'impact de la phase de croissance de la convection profonde sur l'injection de glace dans la TTL. Cependant, une fois que la phase mature de la convection profonde est atteinte, les processus ayant un impact sur la quantité de glace dans la TTL ne sont pas encore bien compris. Ainsi, bien que cette thèse ait montré que les processus convectifs sont les principaux processus impactant l'injection de glace dans la TTL, on peut suggérer que d'autres processus (comme la sublimation de la glace, l'advection verticale de la glace ou la sédimentation de la glace par exemple) peuvent concurrencer les processus convectifs pendant la phase décroissante de la convection. Par exemple, de nombreuses études ont montré que la phase croissante du cycle diurne de la WV est retardée par rapport à la phase croissante du cycle diurne de la glace (Carminati et al., 2014; Dauhut et al., 2015), ce qui suggère que la quantité de WV dans la TTL augmente avec le début du processus de sublimation de la glace.

Quelques observations ont été faites dans cette thèse sur la phase décroissante du cycle diurne de la glace dans la TTL, de par l'étude comparative entre la quantité de IWC mesurée par MLS pendant la phase décroissante de la convection et la valeur estimée de IWC à la même heure. De fortes différences ($\sim$ 20 %) entre les deux valeurs ont été observées en Amérique du Sud, en Afrique du Sud et dans les zones océaniques convectives, tandis que de faibles différences ($\sim$ 3 %) ont été

observées dans la zone du MariCont. Pendant la phase décroissante de la convection, la cohérence entre les valeurs de IWC estimées et mesurées tend à suggérer que les processus convectifs ont également un impact important sur la glace et sur son cycle diurne dans la TTL.

Plusieurs possibilités peuvent être suggérées pour valider cette hypothèse et étudier le cycle diurne complet du bilan de l'eau dans la TTL. Cinq points combinant des informations complémentaires relatives au bilan de l'eau dans la TTL peuvent être proposés comme suit :
1) L'étude de la relation entre la distribution verticale du cycle diurne de la **température** et la distribution verticale du cycle diurne de IWC estimée (de par la comparaison des résultats dans l'UT et dans la TL). Le cycle diurne de la température dans la TTL peut être étudié à partir des jeux de données de températures fournis par la mission COSMIC (conjointe entre la National Aeronautics and Space Administration (NASA) et la National Space Organization (NSPO) de Taiwan), couvrant plusieurs années disponibles.
2) La relation entre l'**altitude** de la TTL et la quantité de glace injectée jusqu'à la TTL en fonction de la distribution horizontale sous les tropiques. Notez que l'altitude de la TTL peut aussi être fournie par la mission COSMIC sur une longue série temporelle.
3) La hauteur et la pression du sommet des nuages ainsi que localisation des percées nuageuses ont été traitées à partir des observations spatiales à haute résolution horizontale et temporelle du satellite géostationnaire japonais **Himawari-8** centrées sur la région du MariCont, par le Met Office Satellite Imagery Applications Group and Satellite Data Processing Systems. Ces informations peuvent être utiles pour améliorer notre compréhension du cycle de vie de l'activité convective profonde dans cette région d'injection de glace jusqu'à la LS.
4) Une série chronologique plus longue (atteignant $\sim$ 20 ans) de mesures de IWC,

WV, température et humidité relative fournie par l'instrument MLS pourrait augmenter le rapport signal/bruit et améliorer l'estimation de ΔIWC, surtout dans l'étude des oscillations intra-saisonnières et inter-annuelles.
5) La comparaison entre les deux mesures quotidiennes en heure locale de WV par MLS et le cycle diurne à haute résolution temporelle (1-h) de l'humidité spécifique dans la troposphere (kg kg^{-1}) et de la teneur spécifique en eau liquide dans le nuage (kg kg^{-1}) fournie par les analyses météorologiques de ERA5 ainsi que le rapport de mélange de vapeur d'eau (ppmv) dans la TTL simulé par le modèle Meso-NH. La méthode pourrait d'abord être utilisée pour étudier cette comparaison sur des domaines où il a été démontré que ΔIWC estimé à partir de ERA5 est cohérent avec ΔIWC estimé à partir des observations, et ensuite sur des domaines où il a été constaté des incohérences.

8.4.3 Injection de la glace jusqu'à la basse stratosphère

Comme la TTL contrôle les échanges entre la troposphère et la stratosphère, les études réalisées dans le cadre de cette thèse peuvent être utilisées comme une étape vers la compréhension des variabilités du bilan hydrique total jusqu'à la basse stratosphère.

Cependant, IWC mesurée par MLS dans la stratosphère fournit encore un rapport signal/bruit trop faible pour être étudié. En revanche, la WV mesurée par MLS peut être étudiée dans la basse stratosphère (LS, supérieure à 82 hPa). Ainsi, une façon intéressante d'étudier le bilan hydrique dans la LS à partir des observations de MLS serait, premièrement, de comprendre la relation entre IWC et WV dans la TTL (à 100 hPa) et, deuxièmement, d'observer les différences dans le signal Jour-Nuit de la WV entre la TTL et la LS.

Application des travaux dans le contexte de l'hydratation stratosphérique

De récents travaux, suite à une collaboration avec T. Dauhut, V. Noël et moi-même, ont mis en avant la façon dont la fraction des nuages tropicaux évolue au-dessus de la tropopause au cours de la journée. Il a été étudié, à partir des observations spatiales d'instrument lidar, la relation entre le cycle diurne des nuages stratosphériques et le cycle diurne de l'activité convective profonde (Dauhut et al., 2020). D'après cette étude, les auteurs ont suggéré un délai de trois heures entre le cycle diurne de la convection très profonde et la fraction stratosphérique des nuages. Ces résultats sont cohérents avec les hypothèses soumises dans Dion et al. (2019). Cependant, les ratios de glace et de vapeur d'eau de la fraction de nuage stratosphérique mesurés dans cette étude ne sont pas détaillés.

8.4.4 Impact de l'oscillation à grande échelle de la glace injectée dans le TTL

Les grandes différences observées dans cette thèse entre la phase active et la phase inhibée de la MJO peuvent s'expliquer soit par les différences des processus convectifs considérées dans les deux phases de la MJO, soit par un biais du modèle par rapport aux observations induites par les données temporelles et spatiales choisies. Afin d'effectuer la comparaison modèle/observations, il faudrait ainsi comparer la même phase de la MJO. Cependant, comme le modèle proposé dans cette thèse pour estimer ΔIWC à partir des observations ne fonctionne que pour les périodes convectives et sur les régions convectives, il ne serait pas possible d'étudier la phase inhibée de la MJO (en raison des faibles précipitations et du faible nombre d'éclairs durant cette période). En revanche, il serait intéressant d'utiliser le modèle Meso-NH pendant les périodes de convection profonde (MJO en phase active, mais aussi durant DJF et La Niña) pour comparer le ΔIWC calculé avec

ceux présentés dans cette thèse.

8.4.5 Intégration des résultats dans les projets de recherche actuels

Les trois campagnes présentées dans cette sous-section sont étroitement liées aux questions scientifiques développées dans cette thèse et pourraient fournir des informations utiles pour mieux comprendre l'impact de la convection profonde sur le bilan hydrique dans l' UTLS.

Sur le Continent Maritime

Cette thèse a été développée parallèlement à la récente et actuelle campagne internationale sur les divers processus climatologiques et météorologiques dans la région du MariCont, qui s'est effectuée entre 2017 et 2019. Cette campagne s'intitule l'Année du Continent Maritime (YMC pour "Year of the Maritime Continent", http://www.jamstec.go.jp/ymc/, dernier accès : mai 2019) et intègre des observations et modélisation, reliant la recherche et l'exploitation de données afin de mieux comprendre les systèmes météorologiques et climatiques de cette région. L'objectif du YMC est d'améliorer la compréhension et la prévision de la variabilité locale et de multi-échelles des systèmes météorologiques et climatiques du MariCont. Ainsi, de nombreuses campagnes menées au cours du YMC fourniraient des données éventuellement disponibles pour améliorer la compréhension des variabilités de l'humidité de la tropopause dans cette région de forte activité convective.

Sur la région Asiatique

Le projet Strato-Clim (Stratospheric and upper tropospheric processes for better climate predictions, http://www.stratoclim.org/, dernier accès : août 2019) (2013 - 2018) est un projet de recherche se concentrant sur les thématiques du changement climatique et de l'ozone stratosphérique en améliorant la compréhension des processus clés impactant la haute troposphère et la stratosphère. Les études présentées dans cette thèse, qui fournissent des informations sur le bilan hydrique dans la TTL, sont pleinement liées à ce projet, notamment par le fait que de récentes campagnes de mesure dans le cadre du projet Strato-Clim ont été menées en Asie ayant pour but de comprendre les échanges troposphère-stratosphère durant l'anticyclone de la mousson asiatique.

Le futur projet ACCLIP (Asian summer monsoon chemical and Climate impact, https://www2.acom.ucar.edu/acclip, dernier accès : août 2019) (juillet-août 2020) vise à étudier les impacts des émissions asiatiques de gaz et d'aérosols sur la chimie et le climat à l'échelle globale via les relations entre la convection profonde durant les périodes de la mousson asiatique et la dynamique à grande échelle. Ainsi, les futures études sur l'activité convective pendant la mousson asiatique pourraient aider à la compréhension des distributions horizontales et verticales des quantités de glace dans l'UTLS.

Bibliography

J. P. D. Abbatt and M. J. Molina. The heterogeneous reaction of hocl+ hcl → cl2+ h2o on ice and nitric acid trihydrate: Reaction probabilities and stratospheric implications. *Geophysical research letters*, 19(5):461–464, 1992.

R. F. Adler and R. A. Mack. Thunderstorm cloud top dynamics as inferred from satellite observations and a cloud top parcel model. *Journal of the atmospheric sciences*, 43(18):1945–1960, 1986.

P. K. Aggarwal, U. Romatschke, L. Araguas-Araguas, D. Belachew, F. J. Longstaffe, P. Berg, Co. Schumacher, and A. Funk. Proportions of convective and stratiform precipitation revealed in water isotope ratios. *Nature Geoscience*, 9(8):624, 2016.

C. M. Alcala and A. E. Dessler. Observations of deep convection in the tropics using the tropical rainfall measuring mission (trmm) precipitation radar. *Journal of Geophysical Research: Atmospheres*, 107(D24):AAC–17, 2002.

T. Allison, H. Fuelberg, and N. Heath. Simulations of vertical water vapor transport for tc ingrid (2013). *Journal of Geophysical Research: Atmospheres*, 123(15):8255–8282, 2018. doi: 10.1029/2018JD028334. URL https://agupubs.onlinelibrary.wiley.com/doi/abs/10.1029/2018JD028334.

M. G. Atticks and G. D. Robinson. Some features of the structure of the tropical tropopause. *Quarterly Journal of the Royal Meteorological Society*, 109(460): 295–308, 1983.

M. A. Avery, S. M. Davis, K. H. Rosenlof, and A. E. Ye, H. ansd Dessler. Large anomalies in lower stratospheric water vapour and ice during the 2015–2016 el niño. *Nature Geoscience*, 10:405, 2014. doi: 10.1038/ngeo2961. URL `https://doi.org/10.1038/ngeo2961`.

K. Bedka, J. Brunner, R. Dworak, W. Feltz, J. Otkin, and T. Greenwald. Objective satellite-based detection of overshooting tops using infrared window channel brightness temperature gradients. *Journal of Applied Meteorology and Climatology*, 49(2):181–202, 2010.

F. A. Berson. Circulation and energy balance in a tropical monsoon. *Tellus*, 13 (4):472–485, 1961.

F. Beucher. *Manuel de météorologie tropicale: des alizés au cyclone tropical*. Météo-France, 2010.

T. Birner. Fine-scale structure of the extratropical tropopause region. *Journal of Geophysical Research: Atmospheres*, 111(D4), 2006. doi: 10.1029/2005JD006301. URL `https://agupubs.onlinelibrary.wiley.com/doi/abs/10.1029/2005JD006301`.

T. Birner and E. J. Charlesworth. On the relative importance of radiative and dynamical heating for tropical tropopause temperatures. *Journal of Geophysical Research: Atmospheres*, 122(13):6782–6797, 2017.

T. Birner, A. Dörnbrack, and U. Schumann. How sharp is the tropopause at midlatitudes? *Geophysical Research Letters*, 29(14):45–1–45–4, 2002. doi:

10.1029/2002GL015142. URL https://agupubs.onlinelibrary.wiley.com/doi/abs/10.1029/2002GL015142.

S. Bony, B. Stevens, D. M. W. Frierson, C. Jakob, M. Kageyama, R. Pincus, T. G. Shepherd, S. C. Sherwood, Pier S. Siebesma, A., A. H. Sobel, et al. Clouds, circulation and climate sensitivity. *Nature Geoscience*, 8(4):261, 2015.

A. W. Brewer. Evidence for a world circulation provided by the measurements of helium and water vapour distribution in the stratosphere. *Quarterly Journal of the Royal Meteorological Society*, 75(326):351–363, 1949.

N. Butchart. The brewer-dobson circulation. *Reviews of geophysics*, 52(2):157–184, 2014.

F. Cairo. Atmospheric thermodynamics. In *Thermodynamics-Interaction Studies-Solids, Liquids and Gases*. IntechOpen, 2011.

W. Cantrell and A. Heymsfield. Production of ice in tropospheric clouds: A review. *Bulletin of the American Meteorological Society*, 86(6):795–808, 2005.

F. Carminati, P. Ricaud, J.-P. Pommereau, E. Rivière, S. Khaykin, J.-L. Attié, and J. Warner. Impact of tropical land convection on the water vapour budget in the tropical tropopause layer. *Atmos. Chem. Phys.*, 14(12):6195–6211, 2014. doi: 10.5194/acp-14-6195-2014.

J-P. Chaboureau, J-P. Cammas, J. Duron, P. J. Mascart, N. M. Sitnikov, and H-J. Voessing. A numerical study of tropical cross-tropopause transport by convective overshoots. *Atmospheric Chemistry and Physics*, 7(7):1731–1740, 2007.

D. D. Churchill and Robert A. Houze, Jr. Development and structure of winter monsoon cloud clusters on 10 december 1978. *Journal of the atmospheric sciences*, 41(6):933–960, 1984.

T. Corti, B. P. Luo, T. Peter, H. Vömel, and Q. Fu. Mean radiative energy balance and vertical mass fluxes in the equatorial upper troposphere and lower stratosphere. *Geophysical Research Letters*, 32(6), 2005. doi: 10.1029/2004GL021889. URL `https://agupubs.onlinelibrary.wiley.com/doi/abs/10.1029/2004GL021889`.

T. Corti, B. P. Luo, Q. Fu, H. Vömel, and T. Peter. The impact of cirrus clouds on tropical troposphere-to-stratosphere transport. *Atmospheric Chemistry and Physics*, 6(9):2539–2547, 2006.

T. Corti, B. P. Luo, M. De Reus, D. Brunner, F. Cairo, M. J. Mahoney, G. Martucci, R. Matthey, V. Mitev, F. H. Dos Santos, et al. Unprecedented evidence for deep convection hydrating the tropical stratosphere. *Geophysical Research Letters*, 35(10), 2008.

S. K. Cox and K. T. Griffith. Estimates of radiative divergence during phase iii of the garp atlantic tropical experiment: Part ii. analysis of phase iii results. *Journal of the Atmospheric Sciences*, 36(4):586–601, 1979.

A. Dai. Global precipitation and thunderstorm frequencies. part ii: Diurnal variations. *Journal of Climate*, 14(6):1112–1128, 2001.

E. F. Danielsen. The laminar structure of the atmosphere and its relation to the concept of a tropopause. *Archiv für Meteorologie, Geophysik und Bioklimatologie, Serie A*, 11(3):293–332, 1959.

E. F. Danielsen. A dehydration mechanism for the stratosphere. *Geophysical Research Letters*, 9(6):605–608, 1982.

E. F. Danielsen. In situ evidence of rapid, vertical, irreversible transport of lower tropospheric air into the lower tropical stratosphere by convective cloud turrets

and by larger-scale upwelling in tropical cyclones. *Journal of Geophysical Research: Atmospheres*, 98(D5):8665–8681, 1993.

E. F. Danielsen, R. S. Hipskind, S. E. Gaines, G. W. Sachse, G. L. Gregory, and G. F. Hill. Three-dimensional analysis of potential vorticity associated with tropopause folds and observed variations of ozone and carbon monoxide. *Journal of Geophysical Research: Atmospheres*, 92(D2):2103–2111, 1987.

T. Dauhut. *Hector the convector, the epitome of the tropical convection that hydrates the stratosphere*. Theses, Université Paul Sabatier - Toulouse III, November 2016. URL `https://tel.archives-ouvertes.fr/tel-01760663`.

T. Dauhut, J.-P. Chaboureau, J. Escobar, and P. Mascart. Large-eddy simulations of hector the convector making the stratosphere wetter. *Atmospheric Science Letters*, 16(2):135–140, 2015.

T. Dauhut, J.-P. Chaboureau, J. Escobar, and P. Mascart. Giga-les of hector the convector and its two tallest updrafts up to the stratosphere. *Journal of the Atmospheric Sciences*, 73(12):5041–5060, 2016.

T. Dauhut, J.-P. Chaboureau, P. Mascart, and T. Lane. The overshoots that hydrate the stratosphere in the tropics. In *EGU General Assembly Conference Abstracts*, volume 20, page 9149, 2018.

T. Dauhut, V. Noel, and I-A Dion. Diurnal cycle of clouds extending above the tropical tropopause observed by spaceborne lidar. *Atmospheric Chemistry and Physics*, 20:3921–3929, 2020.

A. E. Dessler. The effect of deep, tropical convection on the tropical tropopause layer. *Journal of Geophysical Research: Atmospheres*, 107(D3):ACH–6, 2002.

A. Devasthale and S. Fueglistaler. A climatological perspective of deep convection penetrating the ttl during the indian summer monsoon from the avhrr and modis instruments. *Atmospheric Chemistry and Physics*, 10(10):4573–4582, 2010.

T. Dinh, D. R. Durran, and T. Ackerman. Cirrus and water vapor transport in the tropical tropopause layer–part 1: A specific case modeling study. *Atmospheric Chemistry and Physics*, 12(20):9799–9815, 2012.

I.-A. Dion, P. Ricaud, P. Haynes, F. Carminati, and T. Dauhut. Ice injected into the tropopause by deep convection–part 1: In the austral convective tropics. *Atmospheric Chemistry and Physics*, 19(9):6459–6479, 2019.

I.-A. Dion, C. Dallet, P. Ricaud, F. Carminati, T. Dauhut, and P. Haynes. Ice injected into the tropopause by deep convection – part 2: Over the maritime continent. *Atmospheric Chemistry and Physics, in review*, 2020.

G. M. B. Dobson, D. N. Harrison, and J. Lawrence. Measurements of the amount of ozone in the earth's atmosphere and its relation to other geophysical conditions.—part iii. *Proceedings of the Royal Society of London. Series A, Containing Papers of a Mathematical and Physical Character*, 122(790):456–486, 1929.

J. Dudhia. Numerical study of convection observed during the winter monsoon experiment using a mesoscale two-dimensional model. *Journal of the atmospheric sciences*, 46(20):3077–3107, 1989.

I. Folkins and R. V Martin. The vertical structure of tropical convection and its impact on the budgets of water vapor and ozone. *Journal of the atmospheric sciences*, 62(5):1560–1573, 2005.

I. Folkins, M. Loewenstein, J. Podolske, S. J. Oltmans, and M. Proffitt. A barrier to vertical mixing at 14 km in the tropics: Evidence from ozonesondes and

aircraft measurements. *Journal of Geophysical Research: Atmospheres*, 104 (D18):22095–22102, 1999.

I. Folkins, P. Bernath, C. Boone, G. Lesins, N. Livesey, A. M. Thompson, K. Walker, and J. C. Witte. Seasonal cycles of o3, co, and convective outflow at the tropical tropopause. *Geophysical Research Letters*, 33(16), 2006.

W. Frey, R. Schofield, P. Hoor, D. Kunkel, F. Ravegnani, A. Ulanovsky, S. Viciani, F. D'amato, and T. P. Lane. The impact of overshooting deep convection on local transport and mixing in the tropical upper troposphere/lower stratosphere (utls). 2015.

Q. Fu, Y. Hu, and Q. Yang. Identifying the top of the tropical tropopause layer from vertical mass flux analysis and calipso lidar cloud observations. *Geophysical Research Letters*, 34(14), 2007.

S. Fueglistaler, A. E. Dessler, T. J. Dunkerton, I. Folkins, Q. Fu, and P. W. Mote. Tropical tropopause layer. *Reviews of Geophysics*, 47(1), 2009a. doi: 10.1029/2008RG000267. URL `https://agupubs.onlinelibrary.wiley.com/doi/abs/10.1029/2008RG000267`.

S. Fueglistaler, A. E. Dessler, T. J. Dunkerton, I. Folkins, Q. Fu, and P. W. Mote. Tropical tropopause layer. *Reviews of Geophysics*, 47(1), 2009b.

R. R. Garcia, D. R. Marsh, D. E. Kinnison, B. A. Boville, and F. Sassi. Simulation of secular trends in the middle atmosphere, 1950–2003. *Journal of Geophysical Research: Atmospheres*, 112(D9), 2007.

J.-F. Gayet, J. Ovarlez, V. Shcherbakov, J. Ström, U. Schumann, A. Minikin, F. Auriol, A. Petzold, and M. Monier. Cirrus cloud microphysical and optical properties at southern and northern midlatitudes during the inca experiment. *Journal of Geophysical Research: Atmospheres*, 109(D20), 2004.

A. J. Geer, K. Lonitz, P. Weston, M. Kazumori, K. Okamoto, Y. Zhu, E. H. Liu, A. Collard, W. Bell, S. Migliorini, et al. All-sky satellite data assimilation at operational weather forecasting centres. *Quarterly Journal of the Royal Meteorological Society*, 144(713):1191–1217, 2018.

A. Gettelman and Fothers. A climatology of the tropical tropopause layer. *Journal of the Meteorological Society of Japan. Ser. II*, 80(4B):911–924, 2002.

A. Gettelman, J. R. Holton, and A. R. Douglass. Simulations of water vapor in the lower stratosphere and upper troposphere. *Journal of Geophysical Research: Atmospheres*, 105(D7):9003–9023, 2000.

A. Gettelman, P. M. de F. Forster, M. Fujiwara, Q. Fu, Ho. Vömel, L. K. Gohar, C. Johanson, and M. Ammerman. Radiation balance of the tropical tropopause layer. *Journal of Geophysical Research: Atmospheres*, 109(D7), 2004a.

A. Gettelman, D. E. Kinnison, T. J. Dunkerton, and G. P. Brasseur. Impact of monsoon circulations on the upper troposphere and lower stratosphere. *Journal of Geophysical Research: Atmospheres*, 109(D22), 2004b.

A. Gettelman, M. I Hegglin, S.-W. Son, J. Kim, M. Fujiwara, T. Birner, S. Kremser, M. Rex, J. A. Añel, H. Akiyoshi, et al. Multimodel assessment of the upper troposphere and lower stratosphere: Tropics and global trends. *Journal of Geophysical Research: Atmospheres*, 115(D3), 2010.

J. Gottschalck, P. E. Roundy, Carl J., A. Vintzileos, and C. Zhang. Large-scale atmospheric and oceanic conditions during the 2011–12 dynamo field campaign. *Monthly Weather Review*, 141(12):4173–4196, 2013.

R. G. Graversen, P. L. Langen, and T. Mauritsen. Polar amplification in ccsm4: Contributions from the lapse rate and surface albedo feedbacks. *Journal of*

Climate, 27(12):4433–4450, 2014. doi: 10.1175/JCLI-D-13-00551.1. URL https://doi.org/10.1175/JCLI-D-13-00551.1.

W. M. Gray and Robert W. Jacobson J. Diurnal variation of deep cumulus convection. *Monthly Weather Review*, 105(9):1171–1188, 1977.

D. P. Grosvenor, T. W. Choularton, H. Coe, and G. Held. A study of the effect of overshooting deep convection on the water content of the ttl and lower stratosphere from cloud resolving model simulations. *Atmospheric Chemistry and Physics*, 7(18):4977–5002, 2007.

A. Guharay, D. Nath, P. Pant, B. Pande, J. M. Russell III, and K. Pandey. Observation of semiannual and annual oscillation in equatorial middle atmospheric long term temperature pattern. 2009.

S. C. Hardiman, I. A. Boutle, A. C. Bushell, N. Butchart, M. J. P. Cullen, P. R. Field, K. Furtado, J. C. Manners, S. F. Milton, C. Morcrette, F. M. O'Connor, B. J. Shipway, C. Smith, D. N. Walters, M. R. Willett, K. D. Williams, N. Wood, N. L. Abraham, J. Keeble, A. C. Maycock, J. Thuburn, and M. T. Woodhouse. Processes controlling tropical tropopause temperature and stratospheric water vapor in climate models. *Journal of Climate*, 28(16):6516–6535, 2015. doi: 10.1175/JCLI-D-15-0075.1. URL https://doi.org/10.1175/JCLI-D-15-0075.1.

D. L Hartmann, J. R. Holton, and Q. Fu. The heat balance of the tropical tropopause, cirrus, and stratospheric dehydration. *Geophysical research letters*, 28(10):1969–1972, 2001.

M. E. E. Hassim and T. P. Lane. A model study on the influence of overshooting convection on ttl water vapour. *Atmospheric Chemistry and Physics*, 10(20):

9833–9849, 2010. doi: 10.5194/acp-10-9833-2010. URL https://www.atmos-chem-phys.net/10/9833/2010/.

H. Hatsushika and K. Yamazaki. Interannual variations of temperature and vertical motion at the tropical tropopause associated with enso. *Geophysical research letters*, 28(15):2891–2894, 2001.

P. Haynes and E. Shuckburgh. Effective diffusivity as a diagnostic of atmospheric transport: 2. troposphere and lower stratosphere. *Journal of Geophysical Research: Atmospheres*, 105(D18):22795–22810, 2000.

H. Hersbach. *Operational global reanalysis: progress, future directions and synergies with NWP*. European Centre for Medium Range Weather Forecasts, 2018.

T. Heus and H. J. J. Jonker. Subsiding shells around shallow cumulus clouds. *Journal of the Atmospheric Sciences*, 65(3):1003–1018, 2008. doi: 10.1175/2007JAS2322.1. URL https://doi.org/10.1175/2007JAS2322.1.

T. Heus, H. J. J. Jonker, Harry EA Van den Akker, Eric J Griffith, Michal Koutek, and Frits H Post. A statistical approach to the life cycle analysis of cumulus clouds selected in a virtual reality environment. *Journal of Geophysical Research: Atmospheres*, 114(D6), 2009.

M. P. Hoerling, T. K. Schaack, and A. J. Lenzen. Global objective tropopause analysis. *Monthly Weather Review*, 119(8):1816–1831, 1991.

K. P. Hoinka. Statistics of the global tropopause pressure. *Monthly Weather Review*, 126(12):3303–3325, 1998. doi: 10.1175/1520-0493(1998)126<3303:SOTGTP>2.0.CO;2. URL https://doi.org/10.1175/1520-0493(1998)126<3303:SOTGTP>2.0.CO;2.

J. R. Holton. Synoptic-scale motions i: quasi-geostrophic analysis. *An introduction to dynamic meteorology, 4th edn. Elsevier Academic Press, Amsterdam*, pages 139–176, 2004.

J. R. Holton and A. Gettelman. Horizontal transport and the dehydration of the stratosphere. *Geophysical Research Letters*, 28(14):2799–2802, 2001.

J. R. Holton, P. H. Haynes, M. E. McIntyre, A. R. Douglass, R. B. Rood, and L. Pfister. Stratosphere-troposphere exchange. *Reviews of geophysics*, 33(4): 403–439, 1995.

Brian J Hoskins and Mark J Rodwell. A model of the asian summer monsoon. part i: The global scale. *Journal of the Atmospheric Sciences*, 52(9):1329–1340, 1995.

R. A. Houze and A. K. Betts. Convection in gate. *Reviews of Geophysics*, 19(4): 541–576, 1981.

G. J. Huffman. The transition in multi-satellite products from trmm to gpm (tmpa to imerg). *Version 161025*, page 5, 2016.

G. J. Huffman, D. T. Bolvin, E. J. Nelkin, D. B. Wolff, R. F. Adler, G. Gu, Y. Hong, K. P. Bowman, and E. F. Stocker. The trmm multisatellite precipitation analysis (tmpa): Quasi-global, multiyear, combined-sensor precipitation estimates at fine scales. *Journal of hydrometeorology*, 8(1):38–55, 2007.

G. J. Huffman, R. F. Adler, D. T. Bolvin, and E. J. Nelkin. The trmm multi-satellite precipitation analysis (tmpa) in satellite rainfall applications for surface hydrology. *Springer, Dordrecht*, pages 3–22, 2010.

G. J. Huffman, R. F. Adler, D. T. Bolvin, and E. J. Nelkin. Real-time trmm multi-satellite precipitation analysis data set documentation. *Available online: URL*

https://gpm.nasa.gov/sites/default/files/document_files/3B4XRT_doc_V7_180426.pdf, 2018.

D. F. Hurst, S. J. Oltmans, H. Vömel, K. H. Rosenlof, S. M. Davis, E. A. Ray, E. G. Hall, and A. F. Jordan. Stratospheric water vapor trends over boulder, colorado: Analysis of the 30 year boulder record. *Journal of Geophysical Research: Atmospheres*, 116(D2), 2011.

Y. Inai, T. Shibata, M. Fujiwara, F. Hasebe, and H. Vömel. High supersaturation inside cirrus in well-developed tropical tropopause layer over indonesia. *Geophysical Research Letters*, 39(20), 2012.

A. R. Jain, S. S. Das, T. K. Mandal, and A. P. Mitra. Observations of extremely low tropopause temperature over the indian tropical region during monsoon and postmonsoon months: Possible implications. *Journal of Geophysical Research: Atmospheres*, 111(D7), 2006.

R. James, M. Bonazzola, B. Legras, K. Surbled, and S. Fueglistaler. Water vapor transport and dehydration above convective outflow during asian monsoon. *Geophysical Research Letters*, 35(20), 2008.

E. J. Jensen, A. S. Ackerman, and J. A Smith. Can overshooting convection dehydrate the tropical tropopause layer? *Journal of Geophysical Research: Atmospheres*, 112(D11), 2007.

E. J. Jensen, L. Pfister, and T. P. Bui. Physical processes controlling ice concentrations in cold cirrus near the tropical tropopause. *Journal of Geophysical Research: Atmospheres*, 117(D11), 2012.

E. J. Jensen, G. Diskin, R. P. Lawson, S. Lance, T. P. Bui, D. Hlavka, M. McGill, L. Pfister, O. B Toon, and R. Gao. Ice nucleation and dehydration in the tropical

tropopause layer. *Proceedings of the National Academy of Sciences*, 110(6): 2041–2046, 2013.

H. Jiang, C. Liu, and E. J. Zipser. A trmm-based tropical cyclone cloud and precipitation feature database. *Journal of Applied Meteorology and Climatology*, 50(6):1255–1274, 2011.

J. H. Jiang, H. Su, C. Zhai, S. T. Janice, T. Wu, J. Zhang, et al. Evaluating the diurnal cycle of upper-tropospheric ice clouds in climate models using smiles observations. *Journal of the Atmospheric Sciences*, 72(3):1022–1044, 2015a.

J. H. Jiang, H. Su, C. Zhai, T. Janice, S., T. Wu, J. Zhang, J. N. S. Cole, K.t von Salzen, L. J. Donner, C. Seman, A. Del Genio, Larissa S. Nazarenko, J.-L. Dufresne, M. Watanabe, C. Morcrette, T. Koshiro, H. Kawai, A. Gettelman, L. Millán, W. G. Read, N. J. Livesey, Y. Kasai, and Ma Shiotani. Evaluating the diurnal cycle of upper-tropospheric ice clouds in climate models using smiles observations. *Journal of the Atmospheric Sciences*, 72(3):1022–1044, 2015b. doi: 10.1175/JAS-D-14-0124.1. URL `https://doi.org/10.1175/JAS-D-14-0124.1`.

R. H. Johnson, T. M. Rickenbach, Steven A. Rutledge, P. E. Ciesielski, and W. H. Schubert. Trimodal characteristics of tropical convection. *Journal of climate*, 12(8):2397–2418, 1999.

T. D. Keenan, B. Ferrier, and J. Simpson. Development and structure of a maritime continent thunderstorm. *Meteorology and Atmospheric Physics*, 53(3-4):185–222, 1994.

M. Khairoutdinov and D. Randall. High-resolution simulation of shallow-to-deep convection transition over land. *Journal of the atmospheric sciences*, 63(12): 3421–3436, 2006.

S. M. Khaykin, J.-P. Pommereau, and A. Hauchecorne. Impact of land convection on temperature diurnal variation in the tropical lower stratosphere inferred from cosmic gps radio occultations. *Atmospheric Chemistry and Physics*, 13(13): 6391–6402, 2013.

K. Kikuchi and B. Wang. Diurnal precipitation regimes in the global tropics. *Journal of Climate*, 21(11):2680–2696, 2008.

D. E. Kingsmill. Convection initiation associated with a sea-breeze front, a gust front, and their collision. *Monthly weather review*, 123(10):2913–2933, 1995.

A. F. Krueger and J. S. Winston. A comparison of the flow over the tropics during two contrasting circulation regimes. *Journal of the Atmospheric Sciences*, 31 (2):358–370, 1974.

D. Kuznetsova, T. Dauhut, and J.-P. Chaboureau. The three atmospheric circulations over the indian ocean and the maritime continent and their modulation by the passage of the mjo. *Journal of the Atmospheric Sciences*, 76(2):517–531, 2019.

C. Lac, J.-P Chaboureau, V. Masson, P. Pinty, P. Tulet, J. Escobar, M. Leriche, C. Barthe, B. Aouizerats, C. Augros, et al. Overview of the meso-nh model version 5.4 and its applications. *Geoscientific Model Development*, 11:1929–1969, 2018.

L. Lacher, U. Lohmann, Y. Boose, A. Zipori, E. Herrmann, N. Bukowiecki, M. Steinbacher, and Z. A. Kanji. The horizontal ice nucleation chamber (hinc): Inp measurements at conditions relevant for mixed-phase clouds at the high altitude research station jungfraujoch. *Atmospheric Chemistry and Physics*, 17 (24):15199–15224, 2017.

L. Lacher, P. J. DeMott, E. J. T. Levin, K. J. Suski, Y. Boose, A. Zipori, E. Herrmann, N. Bukowiecki, M. Steinbacher, E. Gute, et al. Background free-tropospheric ice nucleating particle concentrations at mixed-phase cloud conditions. *Journal of Geophysical Research: Atmospheres*, 123(18):10–506, 2018.

J.-P. Lafore, J. Stein, N. Asencio, P. Bougeault, V. Ducrocq, J. Duron, C. Fischer, P. Héreil, P. Mascart, V. Masson, et al. The meso-nh atmospheric simulation system. part i: Adiabatic formulation and control simulations. In *Annales Geophysicae*, volume 16, pages 90–109. Springer, 1997.

K.-O. Lee, T. Dauhut, J.-P. Chaboureau, S. Khaykin, M. Krämer, and C. Rolf. Convective hydration in the tropical tropopause layer during the strato-clim aircraft campaign: Pathway of an observed hydration patch. *Atmospheric Chemistry and Physics Discussions*, 2018:1–31, 2018. doi: 10.5194/acp-2018-1114. URL `https://www.atmos-chem-phys-discuss.net/acp-2018-1114/`.

J.-L. Lin. The double-itcz problem in ipcc ar4 coupled gcms: Ocean–atmosphere feedback analysis. *Journal of Climate*, 20(18):4497–4525, 2007.

C. Liu and E. J. Zipser. Global distribution of convection penetrating the tropical tropopause. *Journal of Geophysical Research: Atmospheres*, 110(D23), 2005.

C. Liu and E. J. Zipser. Implications of the day versus night differences of water vapor, carbon monoxide, and thin cloud observations near the tropical tropopause. *Journal of Geophysical Research: Atmospheres*, 114(D9), 2009.

Chuntao Liu and Edward J. Zipser. Diurnal cycles of precipitation, clouds, and lightning in the tropics from 9 years of trmm observations. *Geophysical Research Letters*, 35(4), 2008. doi: 10.1029/2007GL032437.

URL https://agupubs.onlinelibrary.wiley.com/doi/abs/10.1029/2007GL032437.

X. M. Liu, E. D. Rivière, V. Marécal, G. Durry, A. Hamdouni, J. Arteta, and S. Khaykin. Stratospheric water vapour budget and convection overshooting the tropopause: modelling study from scout-amma. *Atmospheric Chemistry and Physics*, 10(17):8267–8286, 2010.

N. J. Livesey, W. G. Read, and P. A. Wagner. Earth observing system (eos) aura microwave limb sounder (mls) version 4.2x level 2 data quality and description document. *Jet Propulsion Laboratory Tech. Rep. JPL,*, JPL D-33509 Rev. D: 91109–8099, 2018a.

N. J. Livesey, W. G. Read, P. A. Wagner, L. Froidevaux, A. Lambert, G. L. Manney, L. F. Millán, H. C. Pumphrey, M. L. Santee, M. J. Schwartz, et al. Earth observing system (eos), aura microwave limb sounder (mls), version 4.2 x level 2 data quality and description document, version 4.2 x-3.0, d-33509. *Jet Propulsion Laboratory, California Institute of Technology, Pasadena, California, available at: https://mls. jpl. nasa. gov/data/datadocs. php, last access*, 7, 2018b.

B. S. Love, A. J. Matthews, and G. M. S. Lister. The diurnal cycle of precipitation over the maritime continent in a high-resolution atmospheric model. *Quarterly Journal of the Royal Meteorological Society*, 137(657):934–947, 2011.

F. H. Ludlam and R. S. Scorer. Reviews of modern meteorology—10 convection in the atmosphere. *Quarterly Journal of the Royal Meteorological Society*, 79 (341):317–341, 1953.

Z. Luo, G. Y. Liu, and G. L. Stephens. Cloudsat adding new insight into tropical penetrating convection. *Geophysical Research Letters*, 35(19), 2008.

E. Martins, V. Noel, and H. Chepfer. Properties of cirrus and subvisible cirrus from nighttime cloud-aerosol lidar with orthogonal polarization (caliop), related to atmospheric dynamics and water vapor. *Journal of Geophysical Research: Atmospheres*, 116(D2), 2011.

A. C. Maycock, M. M. Joshi, K. P. Shine, and A. A. Scaife. The circulation response to idealized changes in stratospheric water vapor. *Journal of Climate*, 26(2):545–561, 2013.

C. J. McGee and S. C. van den Heever. Latent heating and mixing due to entrainment in tropical deep convection. *Journal of the Atmospheric Sciences*, 71(2): 816–832, 2014.

S. K. Mehta, B. V. Murthy, D. N. Rao, M. V. Ratnam, K. Parameswaran, K. Rajeev, C. S. Raju, and K. G. Rao. Identification of tropical convective tropopause and its association with cold point tropopause. *Journal of Geophysical Research: Atmospheres*, 113(D7), 2008.

L. Millán, W. Read, Y. Kasai, A. Lambert, N. Livesey, J. Mendrok, H. Sagawa, T. Sano, M. Shiotani, and D. L. Wu. Smiles ice cloud products. *Journal of Geophysical Research: Atmospheres*, 118(12):6468–6477, 2013.

K. Mohanakumar. *Stratosphere troposphere interactions: an introduction*. Springer Science & Business Media, 2008.

S. Mori, H. Jun-Ichi, Y. I. Tauhid, M. D. Yamanaka, N. Okamoto, F. Murata, N. Sakurai, H. Hashiguchi, and T. Sribimawati. Diurnal land–sea rainfall peak migration over sumatera island, indonesian maritime continent, observed by trmm satellite and intensive rawinsonde soundings. *Monthly Weather Review*, 132(8):2021–2039, 2004.

B. R. Morton. Buoyant plumes in a moist atmosphere. *Journal of Fluid Mechanics*, 2(2):127–144, 1957.

S. C. Mossop. Atmospheric ice nuclei. *Zeitschrift für angewandte Mathematik und Physik ZAMP*, 14(5):456–486, 1963.

P. W. Mote, K. H. Rosenlof, M. E. McIntyre, E. S. Carr, J. C. Gille, J. R. Holton, J. S. Kinnersley, H. C. Pumphrey, J. M. Russell III, and J. W. Waters. An atmospheric tape recorder: The imprint of tropical tropopause temperatures on stratospheric water vapor. *Journal of Geophysical Research: Atmospheres*, 101 (D2):3989–4006, 1996.

S. W. Nesbitt and E. J. Zipser. The diurnal cycle of rainfall and convective intensity according to three years of trmm measurements. *Journal of Climate*, 16 (10):1456–1475, 2003.

R. E. Newell and S. Gould-Stewart. A stratospheric fountain? *Journal of the Atmospheric Sciences*, 38(12):2789–2796, 1981.

S. J. Oltmans, H. Vömel, D. J. Hofmann, K. H. Rosenlof, and D. Kley. The increase in stratospheric water vapor from balloonborne, frostpoint hygrometer measurements at washington, dc, and boulder, colorado. *Geophysical Research Letters*, 27(21):3453–3456, 2000.

M. Park, W. J. Randel, A. Gettelman, S. T. Massie, and J. H. Jiang. Transport above the asian summer monsoon anticyclone inferred from aura microwave limb sounder tracers. *Journal of Geophysical Research: Atmospheres*, 112 (D16), 2007.

Swagata Payra, Philippe Ricaud, Rachid Abida, Laaziz El Amraoui, Jean-Luc Attie, Emmanuel Riviere, Fabien Carminati, and Thomas von Clarmann. Evaluation of water vapour assimilation in the tropical upper troposphere and lower

stratosphere by a chemical transport model. *Atmospheric Measurement Techniques*, 9(9):4355–4373, 2016.

T. Peter, C. Marcolli, P. Spichtinger, T. Corti, M. B. Baker, and T. Koop. When dry air is too humid. *Science*, 314(5804):1399–1402, 2006.

W. A. Petersen and S. A. Rutledge. Regional variability in tropical convection: observations from trmm. journal of climate. *Journal of Climate*, 14(17):3566–3586, 2001.

J.-P. Pommereau. Troposphere-to-stratosphere transport in the tropics. *Comptes Rendus Geoscience*, 342(4-5):331–338, 2010.

M. Pope, C. Jakob, and M. J. Reeder. Convective systems of the north australian monsoon. *Journal of Climate*, 21(19):5091–5112, 2008.

B. E. Potter and J. R. Holton. The role of monsoon convection in the dehydration of the lower tropical stratosphere. *Journal of the atmospheric sciences*, 52(8): 1034–1050, 1995.

J.-H. Qian. Why precipitation is mostly concentrated over islands in the maritime continent. *Journal of the Atmospheric Sciences*, 65(4):1428–1441, 2008.

J.-H. Qian, A. W. Robertson, and V. Moron. Interactions among enso, the monsoon, and diurnal cycle in rainfall variability over java, indonesia. *Journal of the Atmospheric Sciences*, 67(11):3509–3524, 2010.

C. S. Ramage. Role of a tropical "maritime continent" in the atmospheric circulation. *Mon. Wea. Rev*, 96(6):365–370, 1968.

D. A. Randall and D. A. Dazlich. Diurnal variability of the hydrologic cycle in a general circulation model. *Journal of the atmospheric sciences*, 48(1):40–62, 1991.

W. J. Randel and F. Wu. A stratospheric ozone profile data set for 1979–2005: Variability, trends, and comparisons with column ozone data. *Journal of Geophysical Research: Atmospheres*, 112(D6), 2007. doi: 10.1029/2006JD007339. URL https://agupubs.onlinelibrary.wiley.com/doi/abs/10.1029/2006JD007339.

W. J. Randel, F. Wu, H. Voemel, G. E. Nedoluha, and P. Forster. Decreases in stratospheric water vapor after 2001: Links to changes in the tropical tropopause and the brewer-dobson circulation. *Journal of Geophysical Research: Atmospheres*, 111(D12), 2006a.

W. J. Randel, F. Wu, H. Vömel, G. E. Nedoluha, and P. Forster. Decreases in stratospheric water vapor after 2001: Links to changes in the tropical tropopause and the brewer-dobson circulation. *Journal of Geophysical Research: Atmospheres*, 111(D12), 2006b. doi: 10.1029/2005JD006744. URL https://agupubs.onlinelibrary.wiley.com/doi/abs/10.1029/2005JD006744.

W. J. Randel, M. Park, L. Emmons, D. Kinnison, P. Bernath, K. A. Walker, C. Boone, and H. Pumphrey. Asian monsoon transport of pollution to the stratosphere. *Science*, 328(5978):611–613, 2010.

William J Randel, Dian J Seidel, and Laura L Pan. Observational characteristics of double tropopauses. *Journal of Geophysical Research: Atmospheres*, 112 (D7), 2007.

W.J. Randel and E.J. Jensen. Physical processes in the tropical tropopause layer and their roles in a changing climate. *Nature Geoscience*, 6:169, 2013. doi: 10.1038/ngeo1733. URL https://doi.org/10.1038/ngeo1733.

C. A. Reddy and L. Vijayan. Annual and semiannual oscillations in the equatorial middle atmospheric winds. *Advances in Space Research*, 13(1):373–376, 1993.

R. J. Reed and E. F. Danielsen. Fronts in the vicinity of the tropopause. *Archiv für Meteorologie, Geophysik und Bioklimatologie, Ser. A, Meteorologie und Geophysik*, 11(1):1–17, 1958.

M Reus, S. Borrmann, A. Bansemer, A. J. Heymsfield, R. Weigel, C. Schiller, V. Mitev, W. Frey, D. Kunkel, A. Kürten, et al. Evidence for ice particles in the tropical stratosphere from in-situ measurements. *Atmospheric Chemistry and Physics*, 9(18):6775–6792, 2009.

T. Rieckh, B. Scherllin-Pirscher, F. Ladstädter, and U. Foelsche. Characteristics of tropopause parameters as observed with gps radio occultation. *Atmospheric Measurement Techniques*, 7(11):3947–3958, 2014.

D. M. Romps and Z. Kuang. Overshooting convection in tropical cyclones. *Geophysical Research Letters*, 36(9), 2009.

W. B. Rossow and C. Pearl. 22-year survey of tropical convection penetrating into the lower stratosphere. *Geophysical research letters*, 34(4), 2007.

M. Scherer, H. Vömel, S. Fueglistaler, S. J. Oltmans, and J. Stähelin. Trends and variability of midlatitude stratospheric water vapour deduced from the re-evaluated boulder balloon series and haloe. *Atmospheric Chemistry and Physics*, 8(5):1391–1402, 2008.

J. Schmetz, S. A. Tjemkes, M. Gube, and L. Van de Berg. Monitoring deep convection and convective overshooting with meteosat. *Advances in Space Research*, 19(3):433–441, 1997.

C. Schumacher, S. N. Stevenson, and C. R. Williams. Vertical motions of the tropical convective cloud spectrum over darwin, australia. *Quarterly Journal of the Royal Meteorological Society*, 141(691):2277–2288, 2015.

D. J. Seidel, R. J. Ross, J. K. Angell, and G. C. Reid. Climatological characteristics of the tropical tropopause as revealed by radiosondes. *Journal of Geophysical Research: Atmospheres*, 106(D8):7857–7878, 2001.

R. B. Seigel, S. C. Van Den Heever, and S. M. Saleeby. Mineral dust indirect effects and cloud radiative feedbacks of a simulated idealized nocturnal squall line. *Atmospheric Chemistry and Physics*, 13(8):4467–4485, 2013.

M. A. Shapiro. Turbulent mixing within tropopause folds as a mechanism for the exchange of chemical constituents between the stratosphere and troposphere. *Journal of the Atmospheric Sciences*, 37(5):994–1004, 1980.

M. A. Shapiro, T. Hampel, and A. J. Krueger. The arctic tropopause fold, mort. *Weather Rev*, 115:454, 1987.

S. C. Sherwood. A stratospheric "drain" over the maritime continent. *Geophysical research letters*, 27(5):677–680, 2000.

S. C. Sherwood and A. E. Dessler. On the control of stratospheric humidity. *Geophysical research letters*, 27(16):2513–2516, 2000.

S. C. Sherwood and A. E. Dessler. A model for transport across the tropical tropopause. *Journal of the Atmospheric Sciences*, 58(7):765–779, 2001.

Steven C Sherwood, Daniel Hernández-Deckers, Maxime Colin, and Francis Robinson. Slippery thermals and the cumulus entrainment paradox. *Journal of the Atmospheric Sciences*, 70(8):2426–2442, 2013.

Brian J Soden, Isaac M Held, Robert Colman, Karen M Shell, Jeffrey T Kiehl, and Christine A Shields. Quantifying climate feedbacks using radiative kernels. *Journal of Climate*, 21(14):3504–3520, 2008.

S. Solomon, R. R Garcia, F. S. Rowland, and D. J. Wuebbles. On the depletion of antarctic ozone. *Nature*, 321(6072):755, 1986.

S. Solomon, K. H. Rosenlof, R. W. Portmann, J. S. Daniel, S. M. Davis, T. J. Sanford, and G.-K. Plattner. Contributions of stratospheric water vapor to decadal changes in the rate of global warming. *Science*, 327(5970):1219–1223, 2010.

S.-W. Son and L. M. Polvani. Dynamical formation of an extra-tropical tropopause inversion layer in a relatively simple general circulation model. *Geophysical Research Letters*, 34(17), 2007.

A. Stenke and V. Grewe. Simulation of stratospheric water vapor trends: impact on stratospheric ozone chemistry. *Atmospheric Chemistry and Physics*, 5(5): 1257–1272, 2005.

G. L. Stephens and T. J. Greenwald. The earth's radiation budget and its relation to atmospheric hydrology: 2. observations of cloud effects. *Journal of Geophysical Research: Atmospheres*, 96(D8):15325–15340, 1991.

G. L. Stephens and P. J. Webster. Clouds and climate: Sensitivity of simple systems. *Journal of the Atmospheric Sciences*, 38(2):235–247, 1981.

J. Ström, B. Strauss, T. Anderson, F. Schröder, J. Heintzenberg, and P. Wendling. In situ observations of the microphysical properties of young cirrus clouds. *Journal of the atmospheric sciences*, 54(21):2542–2553, 1997.

H. Su, J. H. Jiang, X. Liu, J. E. Penner, W. G. Read, S. Massie, M. R. Schoeberl, P. Colarco, N. J. Livesey, and M. L. Santee. Observed increase of ttl temperature

and water vapor in polluted clouds over asia. *Journal of Climate*, 24(11):2728–2736, 2011.

K. V. Suneeth, S. S. Das, and S. K. Das. Diurnal variability of the global tropical tropopause: results inferred from cosmic observations. *Climate dynamics*, 49 (9-10):3277–3292, 2017.

J. Tan, C. Jakob, W. B. Rossow, and G. Tselioudis. Increases in tropical rainfall driven by changes in frequency of organized deep convection. *Nature*, 519 (7544):451, 2015.

W. K. Tao, S. Lang, J. Simpson, C. H. Sui, B. Ferrier, and M. D. Chou. Mechanisms of cloud-radiation interaction in the tropics and midlatitudes. *Journal of the atmospheric sciences*, 53(18):2624–2651, 1996.

E. W. Tian, H. Su, B. Tian, and J. H. Jiang. Interannual variations of water vapor in the tropical upper troposphere and the lower and middle stratosphere and their connections to enso and qbo. *Atmospheric Chemistry and Physics Discussions*, 2018:1–25, 2018. doi: 10.5194/acp-2018-1010. URL `https://www.atmos-chem-phys-discuss.net/acp-2018-1010/`.

A.-S.e Tissier and B. Legras. Convective sources of trajectories traversing the tropical tropopause layer. *Atmospheric Chemistry and Physics*, 16(5):3383–3398, 2016.

Ann-Sophie Tissier. *Transport au niveau de la tropopause tropicale et convection*. PhD thesis, Université Pierre et Marie Curie-Paris VI, 2016.

J. R. Turner. Buoyancy effects in fluids. page 368, 1973.

A. Tzella and B. Legras. A lagrangian view of convective sources for transport of air across the tropical tropopause layer: distribution, times and the radiative

influence of clouds. *Atmospheric Chemistry and Physics*, 11(23):12517–12534, 2011.

R. Ueyama, E. J. Jensen, L. Pfister, and J.-E. Kim. Dynamical, convective, and microphysical control on wintertime distributions of water vapor and clouds in the tropical tropopause layer. *Journal of Geophysical Research: Atmospheres*, 120(19):10–483, 2015.

A. Varble, E. J. Zipser, A. M. Fridlind, P. Zhu, A. S. Ackerman, J.-P. Chaboureau, S. Collis, J. Fan, A. Hill, and B. Shipway. Evaluation of cloud-resolving and limited area model intercomparison simulations using twp-ice observations: 1. deep convective updraft properties. *Journal of Geophysical Research: Atmospheres*, 119(24):13–891, 2014.

Sunita Verma, Divya Prakash, Manish Soni, and Kirpa Ram. Atmospheric aerosols monitoring: Ground and satellite-based instruments. In *Environmental Monitoring and Assessment*. IntechOpen, 2019.

B. Vogel, T. Feck, and J.-U. Grooß. Impact of stratospheric water vapor enhancements caused by ch4 and h2o increase on polar ozone loss. *Journal of Geophysical Research: Atmospheres*, 116(D5), 2011.

R. M. Wakimoto and N. T. Atkins. Observations of the sea-breeze front during cape. part i: Single-doppler, satellite, and cloud photogrammetry analysis. *Monthly weather review*, 122(6):1092–1114, 1994.

Shuguang Wang and Lorenzo M Polvani. Double tropopause formation in idealized baroclinic life cycles: The key role of an initial tropopause inversion layer. *Journal of Geophysical Research: Atmospheres*, 116(D5), 2011.

Joe W Waters, Lucien Froidevaux, Robert S Harwood, Robert F Jarnot, Herbert M Pickett, William G Read, Peter H Siegel, Richard E Cofield, Mark J Filipiak,

Dennis A Flower, et al. The earth observing system microwave limb sounder (eos mls) on the aura satellite. *IEEE Transactions on Geoscience and Remote Sensing*, 44(5):1075–1092, 2006.

P. J Webster and G. L. Stephens. Tropical upper-tropospheric extended clouds: Inferences from winter monex. *Journal of the Atmospheric Sciences*, 37(7): 1521–1541, 1980.

Matthew C Wheeler and Harry H Hendon. An all-season real-time multivariate mjo index: Development of an index for monitoring and prediction. *Monthly Weather Review*, 132(8):1917–1932, 2004.

D. L. Wu, J. H. Jiang, W. G. Read, R. T. Austin, C. P. Davis, A. Lambert, G. L. Stephens, D. G. Vane, and J. W Waters. Validation of the aura mls cloud ice water content measurements. journal of geophysical research: Atmospheres. *Journal of Geophysical Research: Atmospheres*, 113(D15), 2008.

D. L. Wu, R. T. Austin, and M. et al. Deng. Comparisons of global cloud ice from mls, cloudsat, and correlative data sets. *Journal of Geophysical Research: Atmospheres*, 114(D8), 2009.

G.-Y. Yang and J. Slingo. The diurnal cycle in the tropics. *Monthly Weather Review*, 129(4):784–801, 2001. doi: 10.1175/1520-0493(2001)129<0784:TDCITT>2.0.CO;2. URL `https://doi.org/10.1175/1520-0493(2001)129<0784:TDCITT>2.0.CO;2`.

J. Yang, Z. Wang, A. J. Heymsfield, and J. R. French. Characteristics of vertical air motion in isolated convective clouds. *Atmospheric Chemistry and Physics*, 16(15):10159–10173, 2016.

C. Zhang. On the annual cycle in highest, coldest clouds in the tropics. *Journal of climate*, 6(10):1987–1990, 1993.

C. Zhang, J. Gottschalck, E. D. Maloney, M. W. Moncrieff, F. Vitart, D. E. Waliser, B. Wang, and M. C. Wheeler. Cracking the mjo nut. *Geophysical Research Letters*, 40(6):1223–1230, 2013.

T. Zhang, S. Yang, X. Jiang, and P. Zhao. Seasonal–interannual variation and prediction of wet and dry season rainfall over the maritime continent: Roles of enso and monsoon circulation. *Journal of Climate*, 29(10):3675–3695, 2016.

M. Zhao and P. H. Austin. Life cycle of numerically simulated shallow cumulus clouds. part ii: Mixing dynamics. *Journal of the atmospheric sciences*, 62(5): 1291–1310, 2005.

C Zhou, AE Dessler, MD Zelinka, P Yang, and T Wang. Cirrus feedback on interannual climate fluctuations. *Geophysical Research Letters*, 41(24):9166–9173, 2014.

Ice injected into the tropical tropopause layer by deep convection

Thesis of the Toulouse III University - Paul Sabatier

Defended 25/10/2019 at Météo-france, Toulouse, France

Author: Iris-Amata DION

Thesis supervisor: Philippe RICAUD

Co-supervisor of the thesis: Peter HAYNES

Abstract : The Tropical Tropopause (TTL), which delimits the troposphere to the stratosphere, controls the vertical distribution of water vapour and ice clouds with a significant radiative effect on climate. However, the way in which water vapour and ice are transported to the TTL is still poorly understood. Among the major processes identified to control the humidity of the TTL, this thesis focuses on deep convective processes to estimate the quantities of ice injected (ΔIWC) into the TTL. The Microwave Limb Sounder (MLS) spaceborne instrument measured ice water content (IWC) in the upper troposphere (146 hPa) and near the cold point of the TTL (100 hPa) from 2004 to 2017 but with a low temporal resolution at two local times (LT) (01:30 LT and 13:30 LT) per day in the tropics. The instruments on board of the Tropical Rainfall Measuring Mission (TRMM) satellite measured precipitation (Prec) and number of flashes during thunderstorm events (Flash) in the tropics from 2004 to 2015 with a high (1 h) temporal resolution to resolve the diurnal cycle. All data used in our studies are averaged within a horizontal resolution of $2^\circ \times 2^\circ$ and for the southern convective season of December, January and February (DJF).

The thesis proposes a model relating Prec and Flash of TRMM, used as a proxy of deep convection, and the two daily MLS IWC measurements at two local times to estimate ΔIWC in the TTL. ΔIWC has been estimated over several oceanic and continental regions of the tropics (South America, South Africa, South Africa, Pacific Ocean, Indian Ocean and Maritime Continent (MariCont)), showing the highest values in the TTL over the MariCont. Over the MariCont, ΔIWC estimated from Flash and Prec were compared to ΔIWC estimated from IWC provided by ERA5 meteorological reanalyses averaged from 2005 to 2016. All the ΔIWC datasets have been shown to be greater over land than over sea and the Java Island, composed of high mountains, has revealed the most important values of ΔIWC. The impact of large-scale intra-seasonal oscillations (Madden Julian Oscillation (MJO) and La Niña) on ΔIWC in the TTL was studied over the MariCont compared to DJF, separating MJO in active and inhibited phases using the ice provided by the Meso-NH mesoscale model. A complementary study was performed, using the model proposed in this thesis, to assess ΔIWC into the TTL over Asia during the Asian Monsoon, showing values of ΔIWC of the same order of magnitude than that over the MariCont.

Key words: Ice, Water Vapour, Tropical Tropopause Layer, Deep Convection, MLS, TRMM.

Discipline : Ocean, Atmosphere and Continental Surfaces

Research Unit : Centre National de Recherche Météorologiques

Large Scale Meteorology and Climate Team

Glace injectée dans la Tropopause Tropicale par Convection Profonde

Doctorat de l'Université de Toulouse III - Paul Sabatier

Soutenue le 25/10/2019 à Météo-france, Toulouse, France

Auteur : Iris-Amata DION

Directeur de thèse : Philippe RICAUD

Co-directeur de thèse : Peter HAYNES

Résumé : La tropopause tropicale (TTL), délimitant la troposphère de la stratosphère, contrôle la distribution verticale de la vapeur d'eau et des nuages de glace ayant un effet radiatif important sur le climat. Cependant, la façon dont la vapeur d'eau et la glace sont transportées jusqu'à la TTL est encore mal connue. Parmi les processus majeurs identifiés pour contrôler l'humidité de la TTL, cette thèse se focalise sur les processus de convection profonde dans le but d'estimer les quantités de glace injectées (ΔIWC) dans la TTL. L'instrument spatial MLS (Microwave Limb Sounder) a mesuré la teneur en eau glacée (IWC) dans la haute troposphère (146 hPa) et proche du point froid de la TTL (100 hPa), de 2004 à 2017 mais avec une faible résolution temporelle de deux heures locales (LT en anglais) par jour (01:30 LT and 13:30 LT) dans les tropiques. Les instruments du satellite TRMM (Tropical Rainfall Measuring Mission) ont mesuré les précipitations (Prec) et le nombre d'éclairs lors d'évènements orageux (Flash) dans les tropiques de 2004 à 2015 avec une résolution temporelle élevée (1 h) permettant d'établir le cycle diurne. Toutes les données utilisées dans nos études ont une résolution moyenne horizontale de $2^\circ \times 2^\circ$ et sont moyennées sur la saison convective australe de décembre, janvier et février (DJF).

La thèse propose un modèle reliant Prec et Flash de TRMM, utilisés comme approximation de la convection profonde, et les deux mesures journalières en heures locales de IWC de MLS pour estimer ΔIWC dans la TTL. ΔIWC a été estimée sur plusieurs régions océaniques et continentales des tropiques (Amérique du Sud, Afrique du Sud, Ocean Pacifique, Océan Indien et le Continent Maritime (MariCont)), montrant les plus fortes valeurs au-dessus du MariCont. Sur le MariCont, ΔIWC estimée à partir de Flash et Prec ont été comparées à ΔIWC estimé à partir des données de IWC fournis par les réanalyses météorologiques de ERA5 moyennées de 2005 à 2016. Quel que soit le jeu de données utilisé, on a montré que ΔIWC était supérieure sur terre que sur mer et l'île de Java, composée de hauts reliefs, a révelé les plus importantes valeurs de ΔIWC. L'impact des oscillations intrasaisonnières à grande échelle (Oscillation Madden Julien (MJO) et La Niña) sur ΔIWC dans la TTL sur le MariCont a été comparé à DJF, séparant MJO en phases active et inhibée en utilisant la glace fournie par le modèle de méso-échelle méso-NH. Une étude complémentaire a été réalisée, utilisant le modèle proposé dans cette thèse, pour évaluer ΔIWC dans la TTL sur l'Asie durant la mousson asiatique, montrant des valeurs de ΔIWC du même ordre de grandeur que sur le MariCont.

Mots-clés : Glace, Vapeur d'Eau, Tropopause Tropicale, Convection Profonde, MLS, TRMM.

Discipline : Océan, Atmosphère et Surfaces Continentales

Unité de Recherche : Centre National de Recherche Météorologiques

Groupe de Météorologie de Grande Echelle et Climat